Cell cycle functions of gamma-tubulin, cyclins, and E3 ubiquitin ligases in *Aspergillus nidulans*

By

Vitoria Kate Paolillo

Submitted to the graduate degree program in Molecular Biosciences and the Graduate Faculty of the University of Kansas in partial fulfillment of the requirements for the degree of Doctor of Philosophy.

_____
Chairperson – Dr. Berl Oakley

_____
Dr. Mizuki Azuma

_____
Dr. Yoshiaki Azuma

_____
Dr. Truman Christopher Gamblin

_____
Dr. Kristi Neufeld

_____
Dr. Joy Ward

Date Defended: May 21, 2018

The Dissertation Committee for Vitoria Kate Paolillo certifies that this is the approved version of the following dissertation:

Cell cycle functions of gamma-tubulin, cyclins, and E3 ubiquitin ligases in *Aspergillus nidulans*

_____

Chairperson – Dr. Berl Oakley

Date Approved: May 21, 2018

Abstract

In addition to its well-established role in nucleating microtubules at microtubule-organizing centers, γ-tubulin has essential, microtubule-independent functions that are incompletely understood [reviewed in (Oakley *et al.*, 2015)]. Experiments in our lab with the cold-sensitive γ-tubulin mutant *mipA*D159 in the filamentous fungus *Aspergillus nidulans* revealed that γ-tubulin has a role in inactivating the anaphase promoting complex/cyclosome (APC/C) resulting in continuous destruction of cyclin B and failure of nuclei to progress through the cell cycle (Nayak *et al.*, 2010). Deletion of the APC/C co-activator CdhA (the *A. nidulans* Cdh1 homolog) restores cyclin B accumulation and these and other data demonstrate that γ-tubulin plays an important role in inactivating APC/C-CdhA at the G_1/S boundary. However, *cdhA*Δ, *mipA*D159 strains are as cold sensitive as the *mipA*D159 parent, indicating that the cold sensitivity is not due to continuous APC/C-CdhA activity (Edgerton-Morgan and Oakley, 2012).

Although the underlying molecular mechanism(s) by which γ-tubulin regulates CdhA are not yet known, our data do not support a direct interaction between γ-tubulin and CdhA. Instead, we hypothesize that γ-tubulin acts through regulators of CdhA. Proteins involved in Cdh1 inhibition and inactivation have been identified in other organisms but not in *A. nidulans* prior to my work. Thus, the first part of my main project consisted of identifying and characterizing regulators of CdhA. As filamentous fungi are hugely important medically, agriculturally and commercially [reviewed in (Meyer *et al.*, 2016)], it is vital that we understand the cell biology of filamentous fungi to be able to combat fungal pathogens and to maximize their growth for production of desirable products. The second part of my main project was aimed at determining

whether these CdhA regulators are candidates through which γ-tubulin acts to regulate CdhA at the G_1/S transition.

In many organisms, initial Cdh1 inactivation at G_1/S occurs via phosphorylation by cyclin/CDK complexes which then triggers Cdh1 ubiquitination by the Skp1-Cullin1-F-box (SCF) complex. However, cyclins have not been well studied in members of aspergilli, including *A. nidulans.* In chapter 3 of this work, I report my identification of all cyclin domain-containing proteins in *A. nidulans* and establish that this cyclin repertoire is well-conserved in closely and distantly related filamentous ascomycetes. This is significant as the complement of cyclins found in model yeasts (*Saccharomyces cerevisiae, Schizosaccharomyces pombe* and *Candida albicans*) differs considerably from one another and from the great majority of filamentous ascomycetes. Thus, *A. nidulans* is a much better model than these yeasts for studying cyclin function and cell cycle regulation in filamentous fungi.

My phylogenetic analyses reveal there are three *A. nidulans* cyclins that likely carry out cell cycle-related functions ($NimE^{Cyclin\ B}$, PucA, and ClbA). In Chapter 4 of this work, I focus on cyclins PucA and ClbA as they had not been characterized previously. My results reveal that ClbA is not essential, but its destruction is required for mitotic exit. ClbA also appears to function at the G_2/M transition. My experiments further demonstrate that both $NimE^{Cyclin\ B}$ and ClbA play critical roles in chromosomal disjunction. My results also reveal that PucA is the essential cyclin required for CdhA inactivation at the G_1/S transition and that there are no other redundant mechanisms for CdhA inactivation in *A. nidulans.* Finally, my data indicate that PucA function is required for some of the growth limiting effects of two *mipA* mutants, including *mipA*D159, although the mechanism of this interaction is not yet understood.

I have also determined that the SCF complex plays a role in regulating CdhA in *A. nidulans.* In Chapter 5 of this work, I focus on two essential components of the SCF complex, Cullin A (CulA) and SkpA. I have determined their terminal phenotypes via the heterokaryon rescue technique, and I have studied their *in vivo* localization patterns using fluorescent protein fusions I have generated. Interestingly, CulA-GFP strains in a wild-type background are slightly cold sensitive, and CulA-GFP causes strong synthetic growth reduction with *mipA*D159. The strong, synthetic genetic interaction between *mipA*D159 and *culA*-GFP indicates that γ-tubulin and CulA are involved in a common function that is required for growth. Additionally, I have found that the SCF complex in *A. nidulans* has a crucial role in suppressing septation near the hyphal tip, which is essential for rapid tip extension in filamentous fungi.

My study of cell cycle-related cyclins and SCF components in *A. nidulans* provides new insights into the regulation of the cell cycle and growth of filamentous fungi. My phylogenetic cyclin analyses also indicate that *A. nidulans* is a well-suited model compared to popular model yeasts for studying cyclin function and cell cycle regulation in aspergilli and other filamentous fungi. Finally, my data also indicate that PucA and CulA are strong candidates through which γ-tubulin acts to control APC/C-CdhA activity and are worthy of follow-up studies.

Acknowledgements

The opportunity to attend and complete graduate school would not have been possible without the support of numerous individuals. It is my pleasure to acknowledge them here. I must first acknowledge my family, as I would never have considered graduate school without their encouragement and unfaltering confidence in me. My parents Gary and Barbara Paolillo were the first to instill in me a passion for science and creative thinking, and, for that, I can never thank the both of you enough. To my sister Casi Paolillo, thank you for your unwavering support and for letting me vent to you on numerous occasions. To my boyfriend David Vestal, thank you for being my anchor during these six years of graduate school. I cannot thank you enough for your patience, for making me laugh when I am at my most stressed, and for all the times you listened to me go into overly excited, painstaking detail about my experiments and results. Thank you.

To my mentor, Dr. Berl Oakley, thank you for allowing me the opportunity to train as a scientist under your guidance. Your passion for science is contagious, and I appreciate you letting me follow some of my crazy ideas for projects and experiments. My hypotheses were not often correct, but both your expertise and our discussions regarding my results over the years have taught me to keep an open-mind, think critically about my results, and that unexpected results can often be the most interesting results.

I must also thank current and past members of the Oakley lab. First and foremost, I have to thank Dr. Heather Edgerton, who provided the majority of my scientific training my first year in the Oakley Lab. Thank you for your patience and for taking the time to answer all of my questions. To Liz Oakley, thank you for letting me pick your brain when my experiments went awry and for all of your wonderful advice over the years. To Ruth, thank you for all of the jokes

and for providing me the opportunity to laugh, even on the challenging days. Finally, a huge thank you to all of the undergraduate and technicians in the lab over the years; you helped make science fun.

I am also incredibly appreciative of my committee members, Dr. Mizuki Azuma, Dr. Yoshiaki Azuma, Dr. Chris Gamblin, Dr. Kristi Neufeld, and Dr. Joy Ward. Thank you for your guidance, support, constructive criticism, and encouragement during my graduate career. You helped me become a better scientist and to think more critically about my results.

Finally, I must thank all of the graduate students and other individuals at KU that provided me with the opportunity to help organize the first Scientists Exploring non-Academic caReer CHoices (SEARCH) Symposium at KU as well as numerous other workshops, seminars, and programs. I did not initially seek out these opportunities, so I am incredibly grateful to those individuals that gave me a nudge in that direction. These various experiences were extremely important in my own personal professional development and provided me with valuable leadership experience.

Table of Contents

List of Tables

List of Figures

Chapter 1: Introduction

1.1 Microtubules and microtubule-organizing centers

1.1.1 Microtubules

Microtubules are essential and universal components of the eukaryotic cytoskeleton. They are required for chromosomal segregation during nuclear division, intracellular trafficking, providing cellular structure and polarity, and for the creation of specialized structures such as cilia or flagella. As microtubules are a prerequisite for cells to proliferate, they are attractive targets for chemotherapies [reviewed in (Cao *et al.*, 2018; Katsetos and Draber, 2012)].

Microtubules are hollow, tubular polymers that assemble from heterodimers of α-tubulin and β-tubulin (α/β-tubulin). These α/β-tubulin heterodimers associate in a "head-to-tail" fashion that is GTP-dependent to form structures called protofilaments (**Fig. 1.1**). Protofilaments are polar, with α-tubulin at the minus-end (the slow-growing end) and β-tubulin at the plus-end (the highly dynamic end). Lateral interactions between protofilaments are α-α and β-β except for at the seam, the site at which α-tubulin and β-tubulin subunits interact laterally within the microtubule lattice (**Fig. 1.1A**) (Nogales *et al.*, 1999). The lateral interactions between protofilaments generate a left handed, three-start helix (a three rise per turn around the axis) (Mandelkow *et al.*, 1986) (**Fig. 1.1A**). The predominant microtubule structure found in eukaryotes contain 13 of these protofilaments. However, some species contain divergent protofilament numbers, such as the giant 40-protofilament accessory microtubules found in the sperm axoneme of the mantidfly *Mantispa perla* [reviewed in (Chaaban and Brouhard, 2017)].

Microtubules are highly dynamic and switch between phases of growth (microtubule assembly) and shrinkage (microtubule disassembly) (**Fig. 1.1B**), a property that is essential to drive

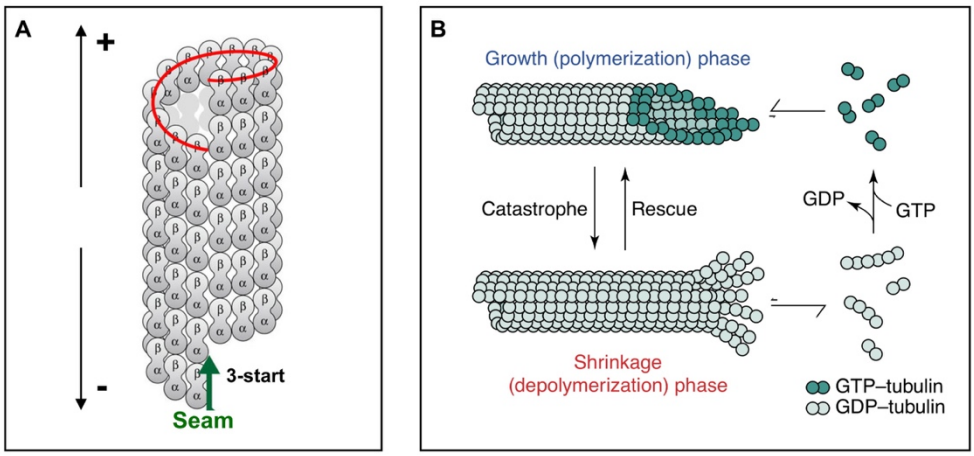

Figure 1.1: Microtubule structure and dynamics

(**A**) The structure of a microtubule consisting of 13 protofilaments. Microtubules polymerize by the addition of α/β-tubulin heterodimers to generate protofilaments. Lateral interactions between protofilaments are α-α and β-β except for at the seam and these interactions generate a left handed, 3-start helix (a three rise per turn around the axis). Microtubules are polar with α-tubulin monomers at the minus-end (the slow-growing end) and β-tubulin monomers at the plus-end (the highly dynamic end). Modified from Katsuki *et al.* (2014). (**B**) Microtubules are assembled in a GTP-dependent fashion, of which the β-tubulin is bound to GTP. This generates a stabilizing cap of GTP-bound tubulin subunits, called a GTP cap. Loss of the GTP-cap causes microtubules to depolymerize with peeling protofilaments, called a catastrophe. Depolymerizing microtubules can switch back to a polymerizing state, called a rescue. Polymerization and depolymerization of microtubules occurs more rapidly at the plus end where β-tubulin is exposed. Modified from Kinoshita *et al.* (2002).

cellular processes. Many factors affect microtubule dynamics *in vivo*, such as structural changes at the plus end (e.g. end tapering), GTP hydrolysis, tubulin isoforms and post-translational modifications, and the binding of microtubule-associated proteins and motor proteins [reviewed in (Aher and Akhmanova, 2018; Akhmanova and Steinmetz, 2015; Martin and Akhmanova, 2018)]. Microtubule formation can occur spontaneously *in vitro* from purified tubulin protein, in the presence of GTP, if the concentration of α-tubulin and β-tubulin exceed a threshold concentration (Weisenberg, 1972). However, under physiological conditions, efficient

microtubule polymerization requires a nucleator. The main microtubule nucleator, γ-tubulin and γ-tubulin ring complexes, will be covered in the following sections.

1.1.2 Microtubule-organizing centers

In the cell, microtubules are typically nucleated from microtubule-organizing centers (MTOCs), which include the centrosome in animal cells and the spindle pole body (SPB) in fungal cells. Centrosomes and SPBs, although structurally different, serve the same functional role to nucleate and organize microtubules [reviewed in (Cuschieri *et al.*, 2007)]. Microtubules are organized such that their minus ends are at the MTOC and their plus ends are located distally from the MTOC, often growing toward the cell periphery. MTOCs require γ-tubulin for microtubule nucleation, which will be discussed in section 1.3 of this chapter.

An electron micrograph and model of a mammalian centrosome is shown in **Fig. 1.2A**. The centrosome is composed of a mother and daughter centriole lying at right angles to one another and are surrounded by a protein matrix known as the pericentriolar matrix (PCM). The PCM harbors proteins important for microtubule nucleation, anchoring, outgrowth, and stabilization in addition to proteins that are important regulators of the cell cycle and its checkpoints. Centriole duplication occurs only once per cell cycle and it occurs in three major stages (**Fig. 1.2B**): (1) centriole disengagement and licensing, (2) biogenesis of a new centriole from the pre-existing centriole, and (3) maturation of centrioles and centrosomes. Centriole duplication is highly regulated as aberrations contribute to various human diseases [reviewed in (Nigg and Holland, 2018; Nigg and Raff, 2009)].

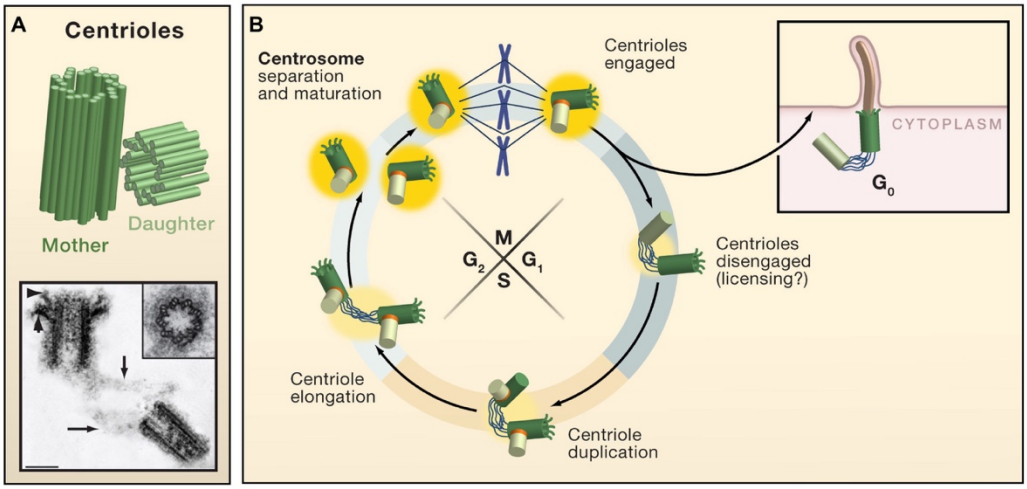

Figure 1.2: Mammalian centrioles form centrosomes and cilia

(A) A mammalian centriole pair is shown schematically (top) and via electron microscopy (bottom). In the EM image, arrowheads point to appendages that allow the older, mother centriole to be distinguished from the daughter centriole. The mother and daughter centrioles are in G_1 and disengaged, although still linked by a fibrous network (arrows). The inset shows a cross-section through the centriole and the nine groups of three microtubules. Scale bar = 0.2 μm. **(B)** A schematic of the centriole duplication cycle in proliferating cells. After mitosis, each daughter cell contains a single pair of disengaged centrioles that are duplicated during S-phase which then gradually elongate during S and G_2. The centrioles organize a pericentriolar matrix (PCM, shown in yellow) to form a centrosome starting in G_1. The PCM houses proteins that nucleate microtubules as well as numerous cell cycle regulatory proteins. Centrosome separation and maturation occurs at the G_2/M transition. In some cells that are not actively proliferating (G_0), a cilium can be assembled from the mother centriole. Modified from Nigg and Raff (2009).

The functional equivalent of the centrosome in fungi is the spindle pole body (SPB). The structure of the fungal SPB has been most thoroughly studied in the budding yeast *Saccharomyces cerevisiae*. The *S. cerevisiae* SPB is embedded in the nuclear membrane, which remains intact during nuclear division, and the SPB is duplicated within its membrane prior to mitosis. It is cylindrical in shape and composed of three plaques that are visible via electron microscopy (**Fig. 1.3A**). The outer plaque faces the cytoplasm while the inner plaque faces the nucleoplasm. Most

of the components of the SPB have been identified in *S. cerevisiae* (**Fig. 1.3B**) [reviewed in (Kilmartin, 2014)].

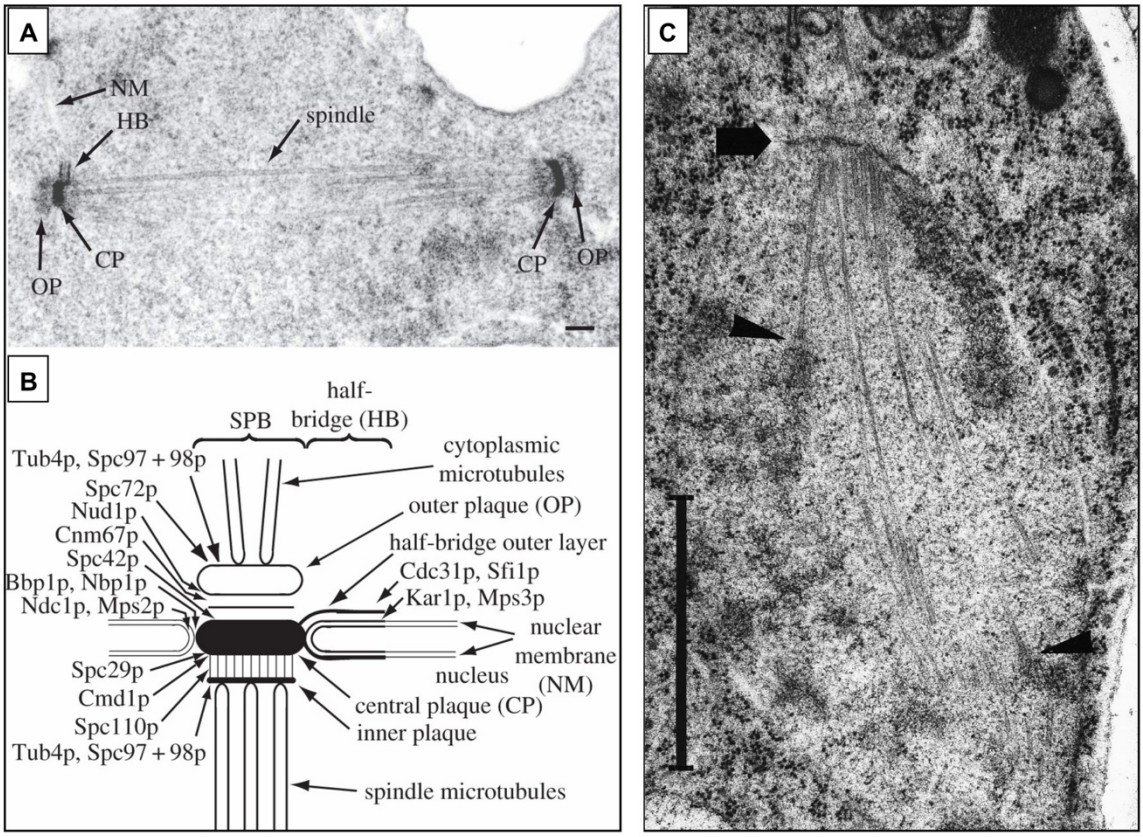

Figure 1.3: Fungal spindle pole bodies

(A) An electron micrograph of a *Saccharomyces cerevisiae* spindle with two spindle-pole bodies (SPBs). The SPBs are embedded in the nuclear membrane (NM) and one can easily visualize the outer plaque (OP), central plaque (CP), and half-bridge (HB). Scale bar = 0.1 μm. **(B)** Schematic of the *S. cerevisiae* SPB. Many of the SPB components have been identified and their localizations to the various parts of the SPB are shown. Tub4p (γ-tubulin) localizes to the outer and inner plaque where it nucleates both cytoplasmic and spindle microtubules. **A** and **B** are modified from Kilmartin (2014). **(C)** A freeze substitution electron micrograph of a SPB and mitotic spindle of *Aspergillus nidulans*. The nuclear membrane embedded SPB is indicated by the arrow. Chromatin is visible as darkly stain fibrous material in the nucleoplasm. Spindle microtubules extend from the inner surface of the SPB into the nucleoplasm. Arrowheads indicate microtubule-kinetochore interactions. Scale bar = 1 μm. The electron micrograph was by Professor I.B. Heath (York University) and published in Jung *et al.* (1998).

The structure of the *A. nidulans* SPB has been studied in less detail, but it is also embedded in the nuclear membrane with its outer surface facing the cytoplasm and its inner surface facing the nucleoplasm (Jung *et al.*, 1998; Oakley and Morris, 1983) (**Fig. 1.3C**). During interphase, cytoplasmic microtubules are nucleated from the outer surface of the SPB (Jung *et al.*, 1998), while tubulin and microtubules are absent from nuclei (Ovechkina *et al.*, 2003). Mitosis in *A. nidulans* is semi-open, so nuclear pore complexes partially disassemble at mitotic onset, but the nuclear membrane remains intact with embedded duplicated SPBs (De Souza *et al.*, 2004). Cytoplasmic microtubules are disassembled at mitotic entry and spindle microtubules are nucleated from the inner surfaces of the duplicated SPBs. As the spindle elongates and cells enter anaphase, astral microtubules nucleated from the outer surface of the SPBs lengthen. In telophase, the spindle microtubules disassemble and the astral microtubules grow to form the interphase cytoplasmic microtubule array (Szewczyk and Oakley, 2011).

Although the role of centrosomes and SPBs as MTOCs is well-established, it is becoming clear that they are multifunctional organelles. For example, the destruction of a centrosome during metaphase generates an acentrosomal daughter cell that arrests in G_1 (Khodjakov and Rieder, 2001). Altogether, it is highly likely that many proteins that localize to the centrosome/SPB are not involved, or at least not exclusively involved, in microtubule organization and function. In fact, many proteins involved in the regulation of the cell cycle localize to centrosomes/SPBs. However, the sheer number of proteins that localize to centrosomes/SPBs make it a challenge to tease apart the multiple functions of these complex structures.

It is also important to note that not all microtubule minus ends are anchored at the centrosome or SPB. In mammalian interphase cells, another major MTOC is the Golgi apparatus, which allows for control of secretory trafficking to and from the Golgi apparatus [reviewed in

(Martin and Akhmanova, 2018)]. Microtubules have also been shown to be nucleated from gamma-tubulin complexes on the sides of existing microtubules in many organisms, including fungi [reviewed in (Oakley *et al.*, 2015)]. Plants, which do not have centrosomes, still have abundant microtubule arrays. Acentrosomal MTOCs called "gametosomes" were recently found to form *de novo* during prophase in the gametophore of the moss *Physcomitrella patens* (Kosetsu *et al.*, 2017). In the fission yeast *Schizosaccharomyces pombe*, MTOCs have been described at the division plane and at the nuclear envelope during interphase. In *A. nidulans*, cytoplasmic microtubules are also nucleated at permanent septum-associated MTOCs (Konzack *et al.*, 2005; Zhang *et al.*, 2017). Importantly, in all of the cases listed above, γ-tubulin and γ-tubulin complexes are required for microtubule nucleation.

1.2 γ-tubulin

1.2.1 Identification

The discovery of γ-tubulin by C. Elizabeth and Berl Oakley (Oakley and Oakley, 1989) came from a genetic screen in the filamentous fungus *Aspergillus nidulans* designed to identify extragenic suppressors of a heat-sensitive β-tubulin mutation, *benA*33 (Weil *et al.*, 1986). Although most of the extragenic suppressors were found to have mutations in the *A. nidulans* α-tubulin gene *tubA*, three of the suppressors mapped to a locus closely linked to the *riboB* gene. This locus was designated *mipA* (for microtubule interacting protein) (Weil *et al.*, 1986). *mipA* was later cloned by chromosome walking from the previously cloned *riboB* gene and sequenced (Oakley and Oakley, 1989; Oakley *et al.*, 1987). Comparisons of the predicted *mipA* product revealed that it was a novel member of the tubulin superfamily of genes with ~30% identities to

α-tubulin and β-tubulin genes from *A. nidulans* as well other diverse organisms. The product of *mipA* was therefore called γ-tubulin (Oakley and Oakley, 1989).

γ-tubulin has since been found to be ubiquitous in eukaryotes. There are between one to three γ-tubulin genes in eukaryotic genomes (Findeisen *et al.*, 2014), and *A. nidulans* has only the one γ-tubulin gene (*mipA*). γ-tubulins are well-conserved across genetically diverse organisms. For example, *A. nidulans* and human γ-tubulins share ~67% identity (Oakley and Akkari, 1999). In fact, our lab determined that human γ-tubulin is functional in *A. nidulans* when *mipA* is deleted (unpublished results), although vegetative growth was decreased. Both human and *Arabidopsis* γ-tubulin have been shown to be functional in *Schizosaccharomyces pombe* cells lacking endogenous γ-tubulin (Horio and Oakley, 2003; Horio *et al.*, 1991).

1.2.2 Initial localization and functional analysis of γ-tubulin

The first localization of γ-tubulin to MTOCs and the discovery that γ-tubulin is essential for microtubule nucleation were both demonstrated by our lab using the model *A. nidulans.* Oakley *et al.* (1990) showed that γ-tubulin localized to interphase and mitotic spindle pole bodies, the major MTOC in fungi (**Fig. 1.4B**). In addition, a lethal *mipA* mutation was analyzed via heterokaryon rescue (see Methods, **2.8**) and found to inhibit nuclear division, reduce cytoplasmic microtubules, and completely abolish the mitotic spindle (Oakley *et al.*, 1990). Following the discovery and initial studies of γ-tubulin in *A. nidulans*, γ-tubulin homologs were shown to localize to MTOCs in other eukaryotes and function as an essential microtubule nucleator (**Fig 1.4A**).

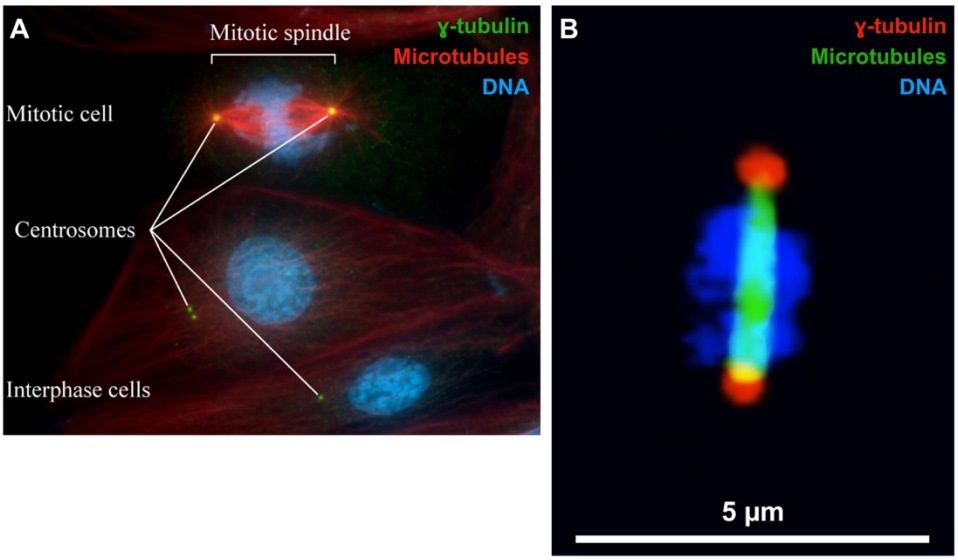

Figure 1.4: γ-tubulin localizes to microtubule-organizing centers in eukaryotes where it nucleates microtubule arrays

(A) Interphase and mitotic microtubule arrays in *Xenopus laevis* kidney epithelial cells. Microtubules are shown in red, DNA shown in blue, and γ-tubulin shown in green. Modified from Wiese and Zheng (2006). **(B)** A 3D projection image of a mitotic *Aspergillus nidulans* nucleus. This image was taken *in vivo* by Dr. Heather Edgerton with the following fluorescently tagged proteins: γ-tubulin-mCherry, GFP-α-tubulin (microtubules), and histone H1-T-Sapphire (DNA marker).

1.2.3 γ-tubulin complexes nucleate microtubules

γ-tubulin associates with other proteins to form structures capable of nucleating microtubules. The canonical ring-shaped structure, called the γ-tubulin ring complex (γ-TuRC), is composed of γ-tubulin, γ-tubulin complex proteins (GCPs), and additional associated proteins (**Fig. 1.5A**). Five of the GCPs (GCP2-6) found in γ-TuRCs are structurally related and contain conserved regions called GRIP (γ-tubulin ring protein) motifs, which mediate binding to γ-tubulin (Guillet *et al.*, 2011) and are involved in the lateral contacts between GCPs. Other core subunits

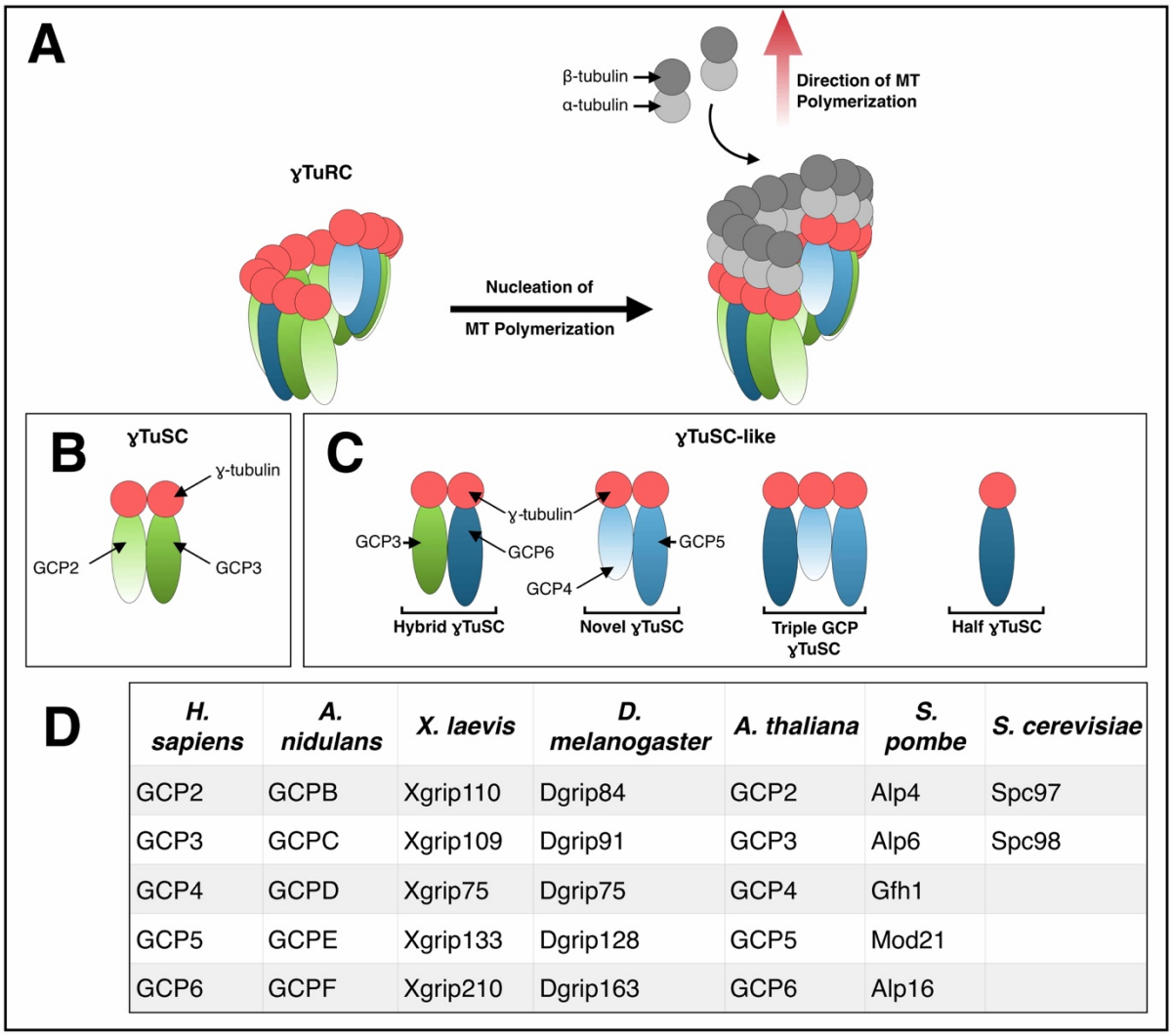

D

H. sapiens	*A. nidulans*	*X. laevis*	*D. melanogaster*	*A. thaliana*	*S. pombe*	*S. cerevisiae*
GCP2	GCPB	Xgrip110	Dgrip84	GCP2	Alp4	Spc97
GCP3	GCPC	Xgrip109	Dgrip91	GCP3	Alp6	Spc98
GCP4	GCPD	Xgrip75	Dgrip75	GCP4	Gfh1	
GCP5	GCPE	Xgrip133	Dgrip128	GCP5	Mod21	
GCP6	GCPF	Xgrip210	Dgrip163	GCP6	Alp16	

Figure 1.5: γ-tubulin complexes in microtubule nucleation

(A) Microtubule nucleation by a γ-tubulin ring complex (γ-TuRC). γ-TuRCs are composed of γ-tubulin complex proteins (GCPs) that each bind γ-tubulin and one another to form a ring-shaped complex. This structure forms a pre-existing nucleus that mimics the plus end of a microtubule and can, thus, nucleate microtubule formation effectively. **(B)** γ-tubulin small complexes (γ-TuSCs) contain GCP2, GCP3, and 2 molecules of γ-tubulin. **(C)** It is possible that γ-tubulin and GCPs may assemble into other γ-TuSC-like structures. (**D**) Designations of GCP homologs that have been well-studied in various organisms. Some organisms, such as *Saccharomyces cerevisiae*, only contain γ-TuSC components and do not contain γ-TuRC-specific GCP4-6. Figure by Tori Paolillo and published in Oakley *et al.* (2015).

of γ-TuRCs include MOZART1 (mitotic spindle-organizing protein associated with a ring of γ-tubulin, or GCP9), MOZART2A/B (GCP8A/B), NEDD1/GCP-WD, Cdk5rap2/Cep215, and NME7. These proteins are predicted to regulate γ-TuRCs by taking part in their recruitment, assembly, and/or activation [reviewed in (Farache *et al.*, 2018)].

γ-tubulin small complexes (γ-TuSCs) are composed of GCP2, GCP3, and 2 molecules of γ-tubulin (**Fig. 1.5B**). The components of γ-TuSCs are conserved in all eukaryotes examined thus far while γ-TuRC-specific GCP4-6 are missing in some organisms, such as the model yeast *Saccharomyces cerevisiae* (**Fig. 1.5D**). In other organisms, such as *A. nidulans*, GCP4-6 are present in the genome but not essential. Thus, the minimal subunit required for microtubule nucleation is the γ-TuSC, although oligomerization of seven γ-TuSCs would be needed to generate the microtubule template [reviewed in (Farache *et al.*, 2018)]. However, γ-TuRCs nucleate microtubules much more effectively than γ-TuSCs *in vitro* (Oegema *et al.*, 1999).

As microtubule nucleation must be carefully controlled in cells, helical γ-tubulin complexes are not enough to initiate the formation of microtubules. These complexes must be recruited to MTOCs, anchored, and activated by effector proteins [reviewed in (Farache *et al.*, 2018)]. A persuasive model for γ-tubulin complex activation involves GCP3. GCP3 contains a hinge region and movement about this hinge could alter the position of its bound γ-tubulin molecule in relation to neighboring γ-tubulins. In the straight hinge position, the γ-tubulins bound to GCP3 are brought into the exact microtubule lattice spacing, which would allow microtubule nucleation to occur (Kollman *et al.*, 2011).

1.2.4 Functions of γ-tubulin beyond microtubule nucleation

The original concept that each protein has a single function has been replaced by the knowledge that many proteins have many functions. To this end, it is becoming increasing clear that γ-tubulin has additional, essential functions beyond microtubule nucleation. During mitosis, γ-tubulin has been shown to regulate microtubule plus-end dynamics, coordinate mitotic events and/or the spindle assembly checkpoint, and control mitotic exit. In interphase, γ-tubulin appears to regulate E2F1-mediated gene expression and forms a complex with Rad51, suggesting a role in the Rad51-mediated DNA damage response. It also promotes the transition from G_1 into S-phase via inactivation of the anaphase promoting complex/cyclosome, which will be discussed in more detail in Chapter 1.5.3. A summary of these functions is reviewed in Oakley *et al.* (2015) and shown in **Figure 1.6**. In all the cases listed above, the molecular mechanisms by which γ-tubulin functions in these various non-nucleation roles are unclear. Teasing apart these various functions is difficult as γ-tubulin is critical for generating the mitotic spindle and thus critical for mitosis. Disruption of mitosis has many consequences and results in many phenotypes, making it difficult to distinguish between nucleation errors and nucleation-independent errors.

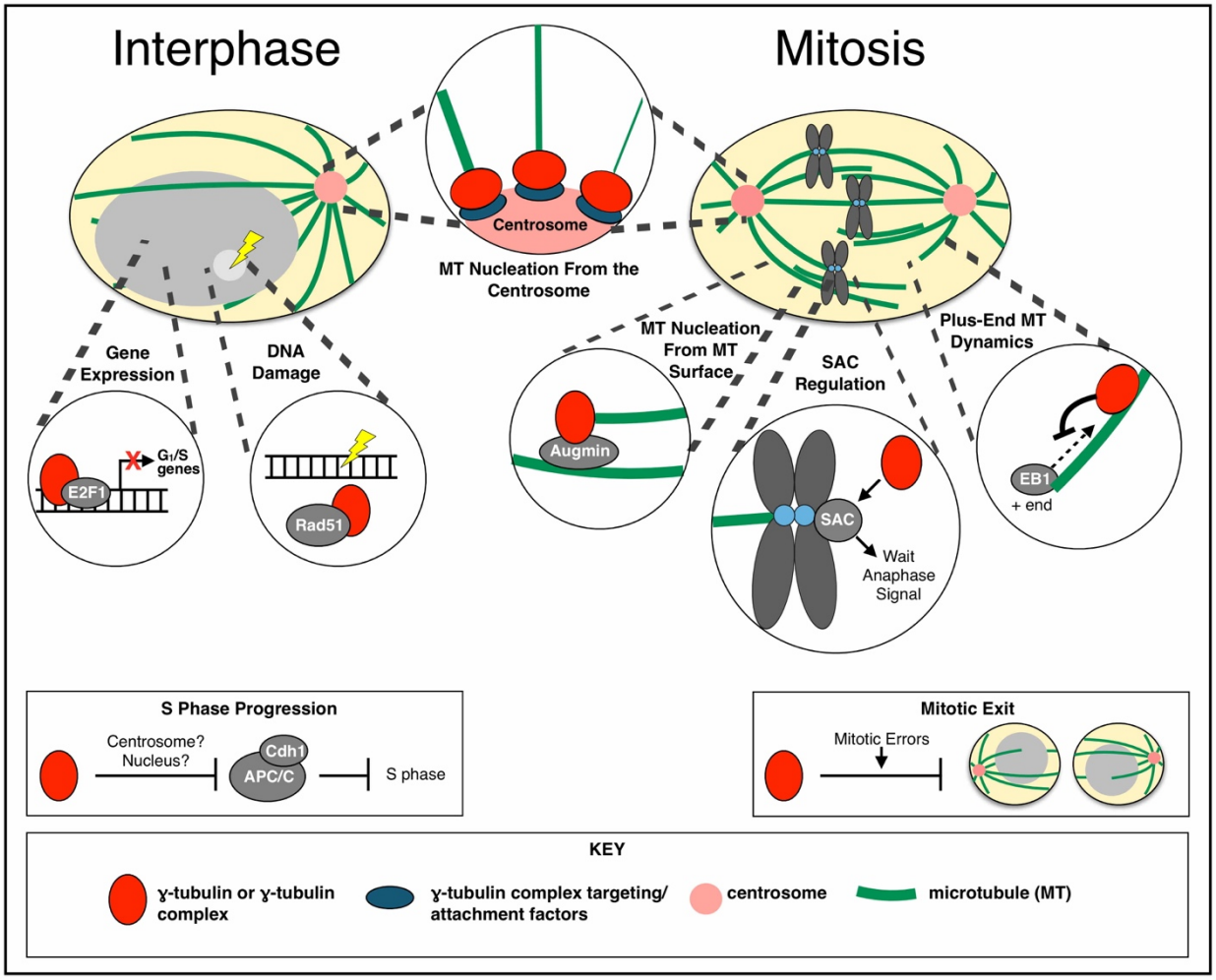

Figure 1.6: Functions of γ-tubulin or γ-tubulin complexes in microtubule nucleation and beyond

In addition to nucleating microtubules from the centrosome, γ-tubulin complexes have been shown to localize to mitotic spindles via augmin complexes and nucleate microtubules from the surface of existing microtubules. In both interphase and mitosis, γ-tubulin has been shown to regulate microtubule plus-end dynamics. γ-tubulin plays a role in the regulation of the spindle assembly checkpoint (SAC) during mitosis and the control of mitotic exit. During interphase, γ-tubulin plays an important role in inactivating Cdh1, an activator of the anaphase-promoting complex/cyclosome (APC/C), which allows proper progression from G_1 into S phase. γ-tubulin also appears to regulate E2F1-mediated gene expression, and it forms a complex with Rad51, suggesting it has a role in the Rad51-mediated DNA damage response. Figure by Tori Paolillo and published in Oakley *et al.* (2015).

1.3 Cell cycle regulation by cyclins and E3 ubiquitin ligases

Progression through the cell cycle is controlled by oscillations in cyclin-dependent kinase (CDK) activity. CDKs become active when bound to their particular cyclin partner but can be rapidly inactivated when their cyclin is degraded. This rapid degradation is essential to drive the cell forward in a sequential and irreversible manner. Importantly, this degradation is regulated primarily by the activity of two E3 ubiquitin ligases, the anaphase promoting complex/cyclosome (APC/C) and the Skp1/Cullin/F-box protein (SCF) complexes, which are structurally similar (**Fig. 1.7**). These complexes are responsible for recognizing cyclins and other cell cycle regulators at

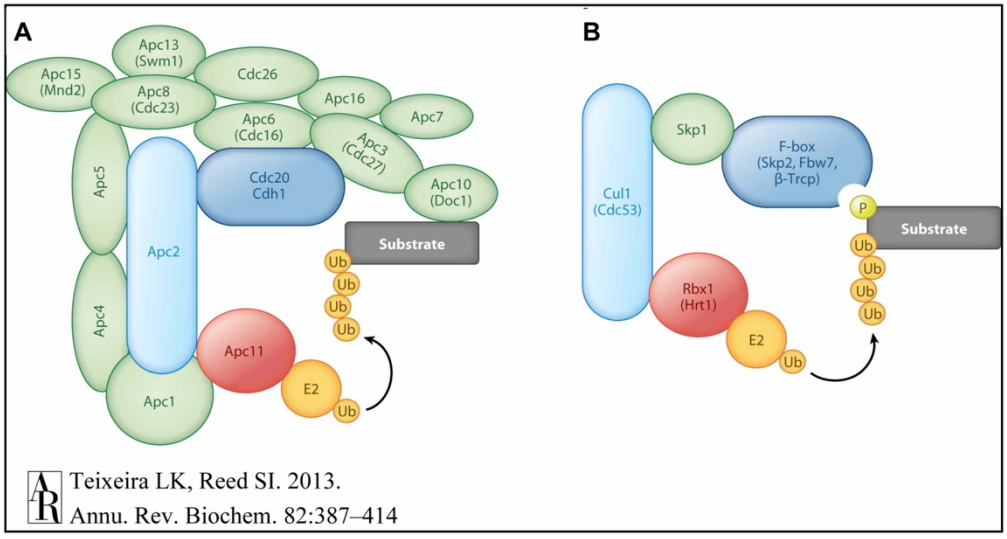

Figure 1.7: Components of the APC/C and SCF E3 ubiquitin ligase complexes
The anaphase promoting complex/cyclosome (APC/C) **(A)** and the skp1/cullin/F-box-containing (SCF) **(B)** complexes are structurally similar. Both have a cullin-like protein (Apc2 in APC/C and Cul1 in SCF, light blue) that serves as the scaffold for the complex and a RING-finger protein (Apc11 in APC/C and Rbx1 in SCF, red) which recruits the E2 enzyme (yellow) that transfers the ubiquitin molecules onto the target substrate. In APC/C complexes, activation and substrate binding and specificity is provided by one of two proteins, Cdc20 or Cdh1 (dark blue). In SCF complexes, substrate binding and specificity is provided by one of many F-box-containing proteins, which recognize their substrates via specific phosphorylated sequences. The APC/C is composed of numerous other proteins that provide molecular scaffold support (green). In SCF complexes, Skp1 (green) recruits F-box proteins to the SCF complex. Figure adapted from Teixeira and Reed (2013).

specific times during the cell cycle and targeting them, through ubiquitination, for degradation via the 26S proteasome. Thus, the regulation of these E3 ligases is critical to ensure proper cell cycle progression and maintain genomic integrity [reviewed in (Teixeira and Reed, 2013)].

Two proteins, Cdc20 and Cdh1, are responsible for the activation of the APC/C and recruitment of substrates during distinct stages of the cell cycle (Visintin *et al.*, 1997). The association of Cdc20 with APC/C is promoted by phosphorylation of APC/C subunits via cyclin B/Cdk1 during prometaphase. The APC/C-Cdc20 is kept inactive, however, by the spindle assembly checkpoint (SAC), which monitors the attachment of spindle microtubules to kinetochores (Hwang *et al.*, 1998). Once the SAC is satisfied, the APC/C can be activated to initiate anaphase. APC/C-Cdc20 typically recognizes substrates that contain a destruction box motif (D-box; amino acid sequences RXXL) (Zur and Brandeis, 2002). Two notable substrates of APC/C-Cdc20 complexes include securin (degradation of securin triggers sister chromatid separation) and cyclin B (degradation of cyclin B is required for mitotic exit). Throughout early mitosis when Cdc20 is active, Cdh1 is prevented from associating with the APC/C by phosphorylation by mitotic cyclin/CDK complexes, notably cyclin B/cdk1 (Jaspersen *et al.*, 1999; Kramer *et al.*, 2000; Zachariae *et al.*, 1998), and through interactions with inhibitory proteins. Inhibitory proteins also keep Cdh1 inactive during S and G_2 phases.

As cells enter anaphase, Cdh1 replaces Cdc20 in APC/C activation. This is, in part, due to the degradation of cyclin B and inactivation of Cdk1; Cdh1 must be dephosphorylated in order to activate the APC/C. APC/C-Cdh1 has a wide range of substrates it targets for degradation, many of which prevent mitotic exit and are responsible for committing the cell to another round of cell division. Cdh1 recognizes these substrates by the presence of a D-box or KEN box. Interestingly, many APC/C-Cdh1 targets are putative oncoproteins found overexpressed in various cancers, and

these include Skp2, cyclin A, polo-like kinase 1 (Plk1), and the Aurora kinases. Concomitant with the overexpression of APC/C-Cdh1 targets, Cdh1 is often found downregulated in cancer (Qiao *et al.*, 2010). Cdh1 is phosphorylated and inactivated at G_1/S via cyclin A/cdk2, cyclin E/cdk2, and Plk1 (Fukushima *et al.*, 2013; Keck *et al.*, 2007; Lau *et al.*, 2013).

While the APC/C is active from anaphase through G_1, the SCF complex is active from late G_1 to mitosis and plays key roles in S-phase entry and mitotic onset. SCF complexes are composed of a core of three invariable components: Skp1 (S-phase kinase-associated protein 1), Cul1 (Cullin 1), and Rbx1 (RING-box protein 1). Cul1 acts as a scaffold protein that binds both Rbx1 and Skp1. Rbx1 recruits the E2 enzyme and Skp1 recruits F-box proteins. F-box proteins are the variable component of the SCF complex and are thus responsible for recruiting substrates in a highly specific manner [reviewed in (Teixeira and Reed, 2013)]. Skp2 and β-TrCP1 are key F-box protein adaptors responsible for the various cell cycle activities of the SCF complex. APC/C-Cdh1 inactivation allows accumulation of Skp2, and SCF-Skp2 activity allows progression through S and G_2 phases. SCF-β-TrCP1 is primarily responsible for mitotic entry but has been shown to trigger Cdh1 ubiquitination at G_1/S (Fukushima *et al.*, 2013). Together, these data present an elegant system by which these two E3 ubiquitin ligases repress one another to govern cell cycle transitions in an efficient manner (**Fig. 1.8**).

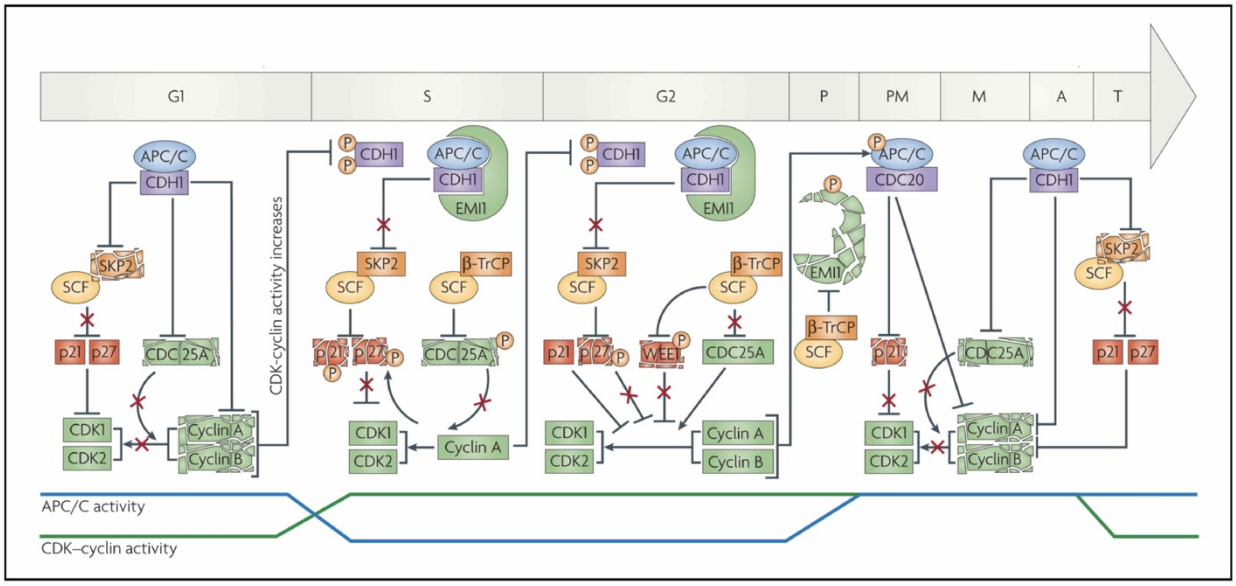

Figure 1.8: Regulation of the cell cycle by cyclins and E3 ubiquitin ligases
Cell cycle progression is regulated by oscillations in cyclin/cyclin-dependent kinase (cyclin/CDK) activity and by protein degradation via the ubiquitin-proteasome pathway. Two major cell cycle regulatory E3 ubiquitin ligases, the anaphase promoting complex/cyclosome (APC/C) and the skp1/cullin/F-box-containing (SCF), are active at different stages of the cell cycle to regulate the degradation of key cell cycle regulatory proteins. APC/C-Cdh1 is active in late mitosis through G_1 to target substrates such as Skp2 (F-box protein for the SCF complex), Cdc25 (phosphatase), and cyclins (such as cyclin A and cyclin B) for degradation. At the G_1/S transition and during interphase, both phosphorylation of Cdh1 via cyclin/CDK complexes and inhibitor binding (Emi1) inhibit APC/C-Cdh1 activity. SCF complexes are active in S-phase through early mitosis and target substrates such as Cdh1 (not shown in figure), CDK inhibitors (p21 and p27), and Wee1 (kinase that inhibits cyclin B) for degradation. Cyclin/CDK activity promotes entry into mitosis and promotes the binding of Cdc20 to APC/C. APC/C-Cdc20 is kept inactive until the spindle assembly checkpoint is satisfied, and then targets substrates for degradation such as securin (which leads to the separation of chromosomes) and cyclins. This figure is modified from Frescas and Pagano (2008).

1.4 *Aspergillus nidulans* as a model system

1.4.1 Aspergilli: ecological importance and impact on humans

The genus *Aspergillus* is comprised of filamentous fungi that are obligate aerobes. They are classified under the phylum Ascomycota and the subdivision Pezizomycotina. Aspergilli are

among some of the best studied filamentous fungi, as members of this genus have significant impacts on human, animal, and crop health and are exploited to produce industrially important commodities [reviewed in (Meyer *et al.*, 2016)]. For example, *Aspergillus niger* is the major source of citric acid, an organic acid that is widely used in foods, beverages, pharmaceuticals, and other applications. Members of this genus also produce secondary metabolites, which include both harmful and medically useful products. An example of a medically useful secondary metabolite is lovastatin, which is a popular anti-cholesterol drug. *Aspergillus terreus* is used to produce lovastatin commercially [reviewed in (Mulder *et al.*, 2015)]. Many species of *Aspergillus* also produce secondary metabolites called aflatoxins, which are extremely toxic and carcinogenic. As some aflatoxin-producing aspergilli, including *Aspergillus flavus, Aspergillus parasiticus,* and *Aspergillus nominus* grow on peanuts and various grains, they cause billions of dollars of losses annually due to contamination of human food and animal feed. The losses are due to direct health impacts on humans and animals and to the fact that the contaminated foods and animal feeds must be destroyed [reviewed in (Schubert *et al.*, 2018)]. Some aspergilli, mainly *Aspergillus fumigatus*, can also infect humans and cause a spectrum of diseases called aspergillosis. Aspergillosis infections typically occur in immunocompromised individuals. Invasive aspergillosis is characterized by *Aspergillus* colonization in the lung which can then spread to the kidneys and brain. Mortality from invasive aspergillosis is high and cases of drug resistant isolates are increasing [reviewed in (Meyer *et al.*, 2016; Osmani and Goldman, 2008)].

1.4.2 Asexual life cycle

Aspergilli begin the asexual life cycle as uninucleate haploid conidia. When conidia encounter a suitable environment, the cells take up water, swell, and undergo the first nuclear

division. The nuclear division cycle is similar to that of other eukaryotes: G_1 (Gap 1), S-phase (when the genomic DNA is replicated), G_2 (Gap 2), and mitosis (when the replicated DNA is separated). Dormant conidia are blocked in G_1 but enter the cell cycle after sufficient incubation on suitable media. After conidia swell, a germtube extends, forming germlings. Polarized growth continues as additional rounds of nuclear division occur to generate a multinucleate germling. After about three rounds of nuclear division, the first septum forms (Harris *et al.*, 1994), dividing the germling into apical and subapical cells. Septation is asymmetrical, dividing the germling into a larger apical cell and a smaller basal cell. Nuclei in apical cells, also called tip cells, are actively and synchronously progressing through the cell cycle. Subapical nuclei are blocked in G_1 but resume the cell cycle when a side branch forms from the cell. Once septa form, the germling is now called a hypha [reviewed in (Osmani and Goldman, 2008)].

As vegetative (hyphal) growth continues, aspergilli produce a highly branched, filamentous, and multinuclear mycelium. Liquid culture permits growth of mycelia, but conidia are not produced in liquid culture (Varanasi *et al.*, 2004). However, on solid medium, vegetative hyphae will undergo asexual development to produce conidia on specific structures called conidiophores. Conidiophores develop in multiple steps. First, specific hyphal segments differentiate into specialized foot cells from which a stalk emerges. A vesicle forms at the end of the stalk, which buds to produce uninucleate metulae. Metulae divide to form phialides, which then undergo repeated nuclear divisions to produce a chain of conidia [reviewed in (Todd *et al.*, 2007)]. A diagram of the asexual life cycle of *Aspergillus nidulans* is shown in **Figure 1.9A**.

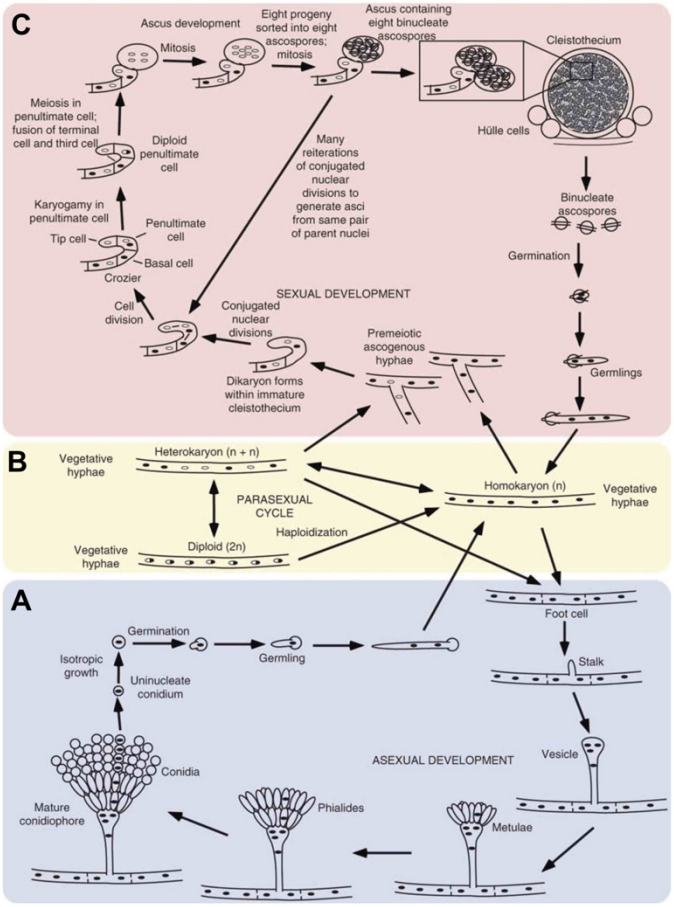

Figure 1.9: Life cycle of *Aspergillus nidulans*

(A) The asexual cycle. *Aspergillus nidulans* starts out its life cycle as haploid, uninucleate conidia that, under the right conditions, will swell, form a germ tube (germination), and undergo polarized growth to form a germling. After approximately 3 rounds of nuclear division, septa form, dividing germlings into subapical cells and apical cells. At this point, the germlings are now called hypha and hyphae continue to undergo polarized growth to form a highly filamentous mycelium. Eventually, specific hyphal segments differentiate into foot cells, which produce a stalk with a vesicle. Vesicles then produce metulae, which further divide into phialides, which then produce chains of conidia. This entire structure is called a mature conidiophore. **(B) The parasexual cycle.** Vegetative hyphae from two separate individuals may fuse to form a heterokaryon (two genetically distinct nuclei in the same cytoplasm). Nuclei from a heterokaryon or homokaryon may fuse to form a diploid. **(C) The sexual cycle.** *A. nidulans* can either self-cross or cross with other individuals. Fruiting bodies called cleistothecia form and contain sac-like structures called asci, with each ascus containing eight binucleate ascospores. One cleistothecium can contain tens of thousands of ascospores which are released upon breakdown of the ascus wall and outer wall of the cleistothecium. Figure modified from Todd *et al.* (2007).

1.4.3 Sexual life cycle

About 64% of aspergilli are only known to reproduce asexually (Dyer and O'Gorman, 2011). However, the remainder of aspergilli, including the model filamentous fungus *Aspergillus nidulans*, can also reproduce sexually. The spores produced from sexual reproduction are called ascospores and can be produced by either a homokaryon (self mating) or a heterokaryon (mating between different strains). The ascospores are produced in closed sexual fruiting bodies called cleistothecia. Cleistothecia in aspergilli can contain up to 100,000 sac-like structures called asci with each ascus containing eight ascospores. In *A.* nidulans, an average cleistothecium may contain ~80,000 viable ascospores. Nuclei in ascospores undergo mitosis to produce mature binucleate ascospores. Ascospores are generally released upon breakdown of the ascus wall and outer wall of the cleistothecium [reviewed in (Dyer and O'Gorman, 2012; Todd *et al.*, 2007)]. A diagram of sexual reproduction is given in **Fig. 1.9C**.

1.4.4 Aspergillus nidulans as a model system for cell cycle research

Aspergillus nidulans is an excellent model for genetic and cell cycle research for many reasons. First, the cell cycle is relatively short, with interphase lasting ~95 minutes and mitosis only lasting ~5 minutes at 32℃ (Bergen and Morris, 1983). Even at a lower temperature of 25℃, the entire cell cycle time is 199 ± 49 minutes with mitosis lasting ~10 minutes (Edgerton-Morgan and Oakley, 2012). In addition, hyphal tip cells are multinuclear with nuclei progressing synchronously through the cell cycle. Hyphae are only ~2.5-3 micrometers in diameter, making it easy to obtain rapid, Z-series microscopic image datasets through the entire hyphal section. The short cell cycle time and thin multinucleate hyphae of *A. nidulans* make it relatively simple to study the *in vivo* localization patterns of cell cycle proteins and to determine how a particular gene

mutation or deletion affects cell cycle progression, nuclear division, microtubule organization, hyphal growth, etc.

A. nidulans is easily transformable with linear molecules of DNA produced by fusion PCR which integrate into the genome via homologous recombination. Transformations with these DNA fragments can result in fusion of a fluorescent protein tag to the N-terminus or C-terminus of a protein, replacement of an endogenous promoter with a regulatable promoter, or the deletion, mutation, or truncation of a gene (discussed further in methods, Chapter 2.5). Integration of such linear DNA at the desired genomic locus occurs with high frequency via homologous recombination in *A. nidulans*. This is because the laboratory strains utilized for our experiments contain the deletion of *nkuA*, the *A. nidulans* homolog of the human KU70 gene. KU70 and KU80 are involved in non-homologous end-joining DNA repair. Deletion of *nkuA* in *A. nidulans* does not affect growth nor does it increase sensitivity to mutagens, but *nkuA*Δ drastically improves gene targeting such that the frequency of single, correct integrations is about 90% (Nayak *et al.*, 2006).

Although *A. nidulans* is normally haploid, asexual diploids and heterokaryons can be generated for genetic analyses to determine dominance and conduct complementation tests. *A. nidulans* is coenocytic and can thus maintain a heterokaryonic state—hyphae containing two genetically different nuclei in a common cytoplasm. Heterokaryons can be generated by the fusion of two strains and are also generated during the transformation procedure. If transformation results in deletion of an essential gene, the null allele can be maintained in heterokaryons, allowing *A. nidulans* to avoid death. This is extremely useful to study the terminal phenotypes of essential genes (discussed further in methods, Chapter 2.8). *A. nidulans* can also form stable diploids if nuclei fuse within a heterokaryon or homokaryon.

Dominance tests are useful to determine whether a particular mutation is dominant or recessive relative to the wild-type allele. This provides clues to the nature of the mutation, as loss-of-function mutations are usually recessive to the wild type, whereas gain-of-function mutations are normally dominant. Complementation tests can be used to identify whether two separately isolated recessive mutations affect the same gene function. If the mutations are in the same gene, the mutations will not usually complement one another. If the mutations are in different genes, the mutations will usually complement one another. Altogether, the ability to generate heterokaryons and diploids provide rapid and easy methods for the genetic analysis of mutant alleles [reviewed in (Todd *et al.*, 2007)].

The genomic sequence for *A. nidulans* has also been published (Galagan *et al.*, 2005), making it much easier to identify homologs of genes of interest or to identify novel genes that might play a role in a particular cellular process. It has a 30.5-megabase genome consisting of eight chromosomes, with over 10,000 predicted genes (http://fungidb.org/fungidb/). *A. nidulans* is also non-pathogenic but is closely related to aspergilli that are pathogenic. *A. nidulans* is easier to work with, but its similarity to pathogenic aspergilli means that findings made with *A. nidulans* will likely carry over to other aspergilli.

1.5 *A. nidulans* γ-tubulin mutants

1.5.1 Creation by alanine-scanning mutagenesis

Conditionally lethal mutants are a useful tool for studying protein function, identifying the region of a protein required for said function(s), and for determining regions of protein-protein interactions. One approach to isolate conditionally lethal mutants is to mutate clustered charged amino acids to alanine. Charged amino acids tend to be found on the outside of proteins and can

be involved in protein-protein interactions. Thus, mutating charged amino acids to alanine, which is neutrally charged and non-polar, can disrupt protein-protein interactions without changing the overall structure of the protein. Typically, two or three charged amino acids in a stretch of five are chosen to be mutated to alanine (Wertman *et al.*, 1992).

Jung *et al.* (2001) created a series of clustered charged-to-alanine mutations (alanine-scanning mutagenesis) of the *A. nidulans* γ-tubulin gene, *mipA*. Of the 41 charged-to alanine mutations of the *mipA* gene, eight of them proved to be conditionally lethal (cold sensitive, heat sensitive, or dependent on antimicrotubule drugs) (Jung *et al.*, 2001) (**Fig. 1.10**). All eight

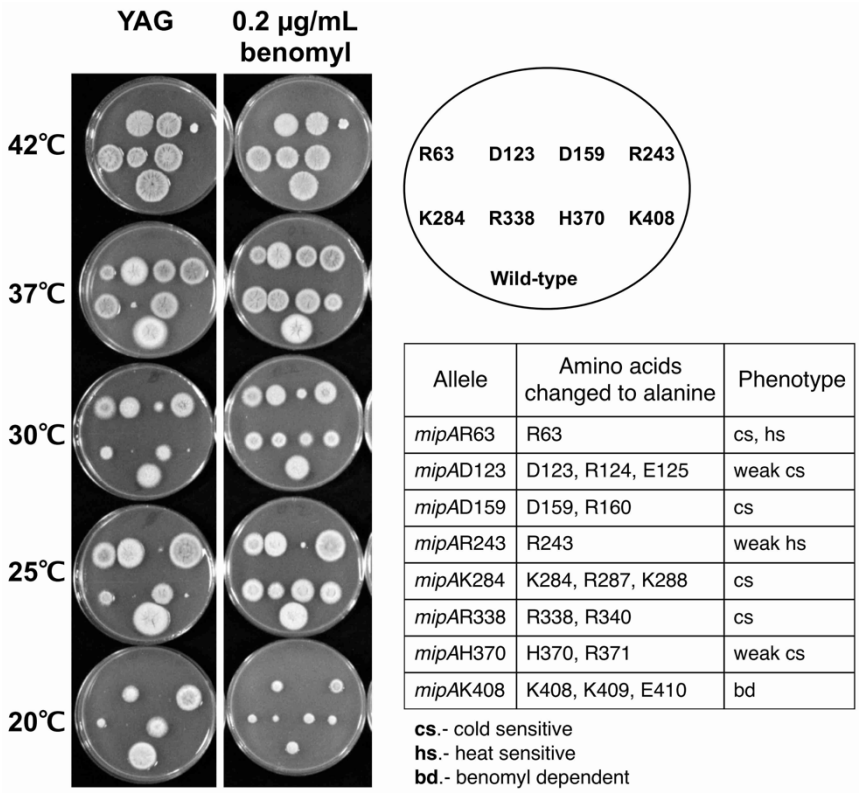

Allele	Amino acids changed to alanine	Phenotype
*mipA*R63	R63	cs, hs
*mipA*D123	D123, R124, E125	weak cs
*mipA*D159	D159, R160	cs
*mipA*R243	R243	weak hs
*mipA*K284	K284, R287, K288	cs
*mipA*R338	R338, R340	cs
*mipA*H370	H370, R371	weak cs
*mipA*K408	K408, K409, E410	bd

cs.- cold sensitive
hs.- heat sensitive
bd.- benomyl dependent

Figure 1.10: Conditionally growth inhibited *mipA* alleles
The eight conditionally lethal *mipA* mutants were stabbed onto complete medium (YAG) and YAG + 0.2 µg/mL of benomyl (microtubule-depolymerizing agent) at various temperatures ranging from 20-42°C to check for temperature sensitivities. Stab plates are from Jung *et al.* (2001). The table displays the full *mipA* mutant name, the amino acids that were changed to alanine, and the growth phenotypes.

conditionally lethal alleles were determined to be recessive, indicating they are likely loss-of-function mutations. The position of *mipA* mutations on a structural model of γ-tubulin is shown in **Fig. 1.11**.

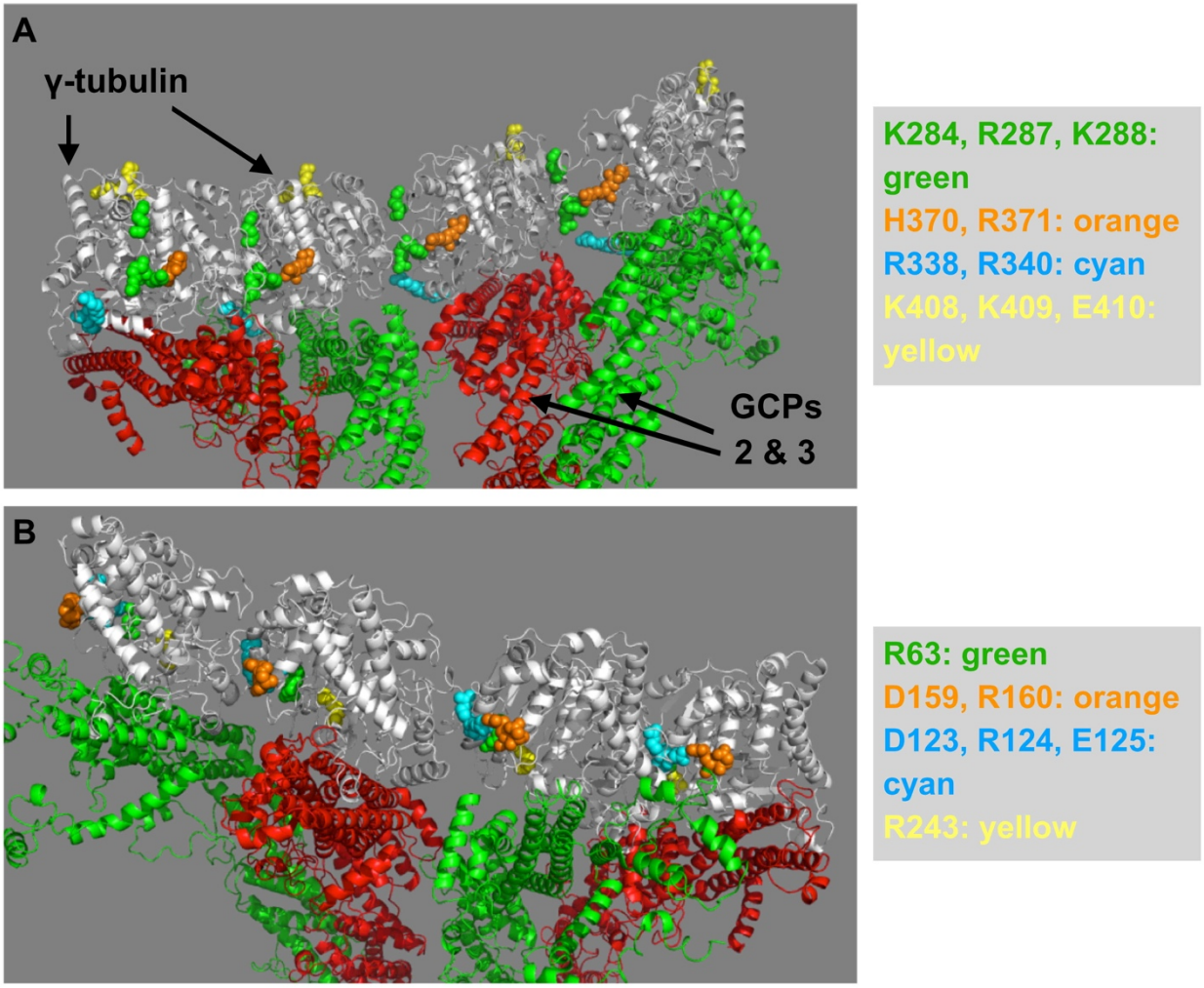

Figure 1.11: Positions of conditionally lethal *mipA* mutations on γ-tubulin structure
Model of four γ-tubulin molecules (grey) plus γ-tubulin complex proteins (GCPs) 2 and 3 (red and green, respectively). This model predicts how four γ-tubulin-bound GCP molecules would interact to form part of the ring structure that nucleates microtubules. Internal view **(A)** an external view **(B).** Models generated by Dr. América Hervás in the Oakley Lab (unpublished work).

1.5.2 Phenotypes of conditionally lethal mipA mutant alleles

After the generation of the conditionally lethal *mipA* mutant alleles, the first task was to determine whether they inhibited microtubule nucleation. As a reminder, the complete deletion of *mipA* essentially eliminated spindle microtubules, and cytoplasmic microtubules were either absent or abnormal (Jung *et al.*, 2001; Martin *et al.*, 1997; Oakley *et al.*, 1990). At restrictive temperatures, two of the *mipA* mutant alleles (*mipA*R243 and *mipA*R63) had reduced γ-tubulin levels at the spindle pole bodies and nucleation of spindle microtubules appeared to be partially inhibited. (Note that *mipA*R63 is both cold-sensitive and heat-sensitive. This phenotype was seen at a high restrictive temperature of 42ºC, but different phenotypes were seen at a low restrictive temperature of 20ºC.) However, the rest of the *mipA* mutants at restrictive temperatures had robust, albeit abnormal, spindles and some had abnormal cytoplasmic microtubule arrays (Jung *et al.*, 2001). The cytoplasmic microtubule abnormalities were different from the microtubule abnormalities seen with the *mipA* deletion, however, in that cytoplasmic microtubules were abundant, sometimes abnormally so. Thus, the next task was to determine why these *mipA* mutants were conditionally lethal if spindle and cytoplasmic microtubule assembly was not inhibited.

A closer examination of the phenotypes of two *mipA* mutants revealed that γ-tubulin or γ-tubulin complexes have a role in controlling mitotic exit. A strain carrying both the *mipA* mutant allele *mipA*D123 and the deletion of a type 14 kinesin (which delays the establishment of spindle bipolarity) caused cells to reenter interphase without successfully completing mitosis (Prigozhina *et al.*, 2001). Another mutant, *mipA*D159, caused premature mitotic exit in the presence of benomyl (a microtubule-depolymerizing agent) which normally activates the spindle-assembly checkpoint (SAC) and results in a lengthy mitotic delay (Prigozhina *et al.*, 2004). Under these

conditions, *mipA*D159 strains exited mitosis sooner than the *mipA*+ control strains even though microtubules were disassembled in both mutant and control strains.

*mipA*D159 strains also displayed errors in the coordination of late mitotic events (anaphase A, anaphase B, and chromosomal disjunction) despite spindle formation (Prigozhina *et al.*, 2004). These data suggested a potential function for γ-tubulin in mitotic checkpoint control, potentially through the SAC. Further work with this allele revealed that homologs of the *A. nidulans* SAC proteins Bub1/R1 and Mps1 were mis-localized at the restrictive temperature, thus abrogating the SAC (Edgerton *et al.*, 2015).

Finally, γ-tubulin has also been shown to play a crucial role in the regulation of the G_1/S transition in *A. nidulans*. These data will be discussed in more detail in the following section.

1.5.3 Failure to inactivate APC/C co-activator CdhA in mipAD159

*mipA*D159 is a cold-sensitive allele that is essentially dead at the restrictive temperature (20℃) and barely grows at the semi-restrictive temperature (25℃) (**Fig. 1.10**). In this allele, residues D159 and R160 were both mutated to alanine (**Fig. 1.10**). These mutations, when mapped on γ-tubulin, do not appear to be involved in the interaction with γ-tubulin complex proteins (GCPs), the lateral interaction with neighboring γ-tubulin molecules in the ring structure, nor the interaction with α-tubulin (**Fig. 1.11B**). Furthermore, *mipA*D159 grown at the restrictive and semi-restrictive temperatures had robust mitotic spindles although some germlings did display bundled or curved cytoplasmic spindles (Jung *et al.*, 2001). Finally, as mentioned in the previous section, *mipA*D159 caused premature mitotic exit in the absence of microtubules or mitotic spindle formation (Prigozhina *et al.*, 2004). Thus, our lab set out to further elucidate the function(s) of *mipA*D159 in mitotic regulation in *A. nidulans.*

Our lab first studied the localization of mitotic regulatory proteins in *mipA*+ and *mipA*D159 strains. Interestingly, when *mipA*D159 strains were incubated at the restrictive temperature of 25℃, a subset of S/G_2 nuclei failed to accumulate the *A. nidulans* cyclin B and cyclin-dependent kinase 1 (cdk1) homologs, NimE and NimX respectively (**Fig. 1.12**).

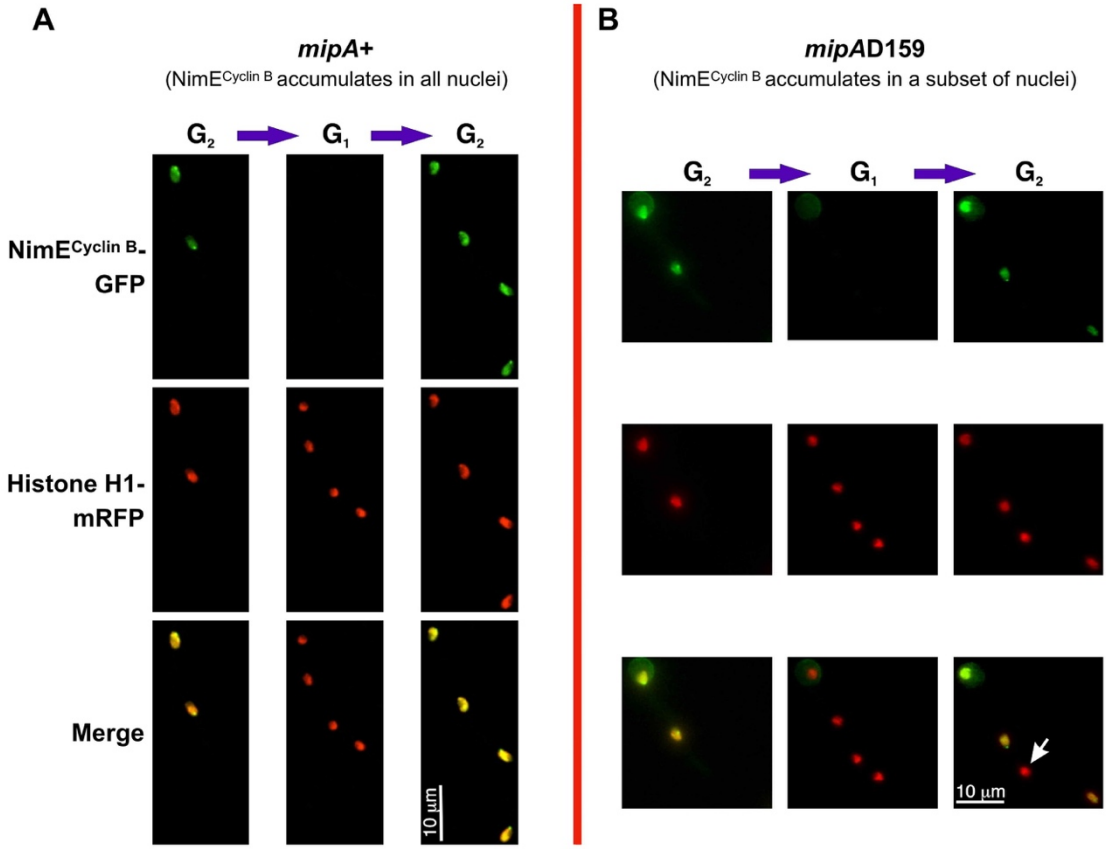

Figure 1.12: NimE$^{Cyclin\ B}$ fails to accumulate in a subset of *mipA*D159 nuclei
(A) In a control, *mipA*+ strain, NimE$^{Cyclin\ B}$ begins to accumulate in nuclei in S phase (not shown) and stays through G_2 and is degraded during mitosis (not shown). In the pictured tip cell, two nuclei undergo nuclear division to generate four daughter nuclei that all accumulate nuclear NimE$^{Cyclin\ B}$ in the subsequent S and G_2 phases. **(B)** In a *mipA*D159 strain, two nuclei in a germling have both accumulated NimE$^{Cyclin\ B}$ and undergone nuclear division to generate four daughter nuclei. As expected, these four daughter nuclei lack NimE$^{Cyclin\ B}$ in the subsequent G_1 phase. However, one of the four daughter nuclei fails to accumulate NimE$^{Cyclin\ B}$ (arrow in merged panel) in the subsequent S and G_2 phases despite being in the same tip cell as the other three daughter nuclei that do accumulate NimE$^{Cyclin\ B}$. The series of images in this figure were taken from a video, and there was no evidence that the *mipA*D159 germling in **(B)** underwent an abnormal nuclear division event leading up to the failure of one of the daughter nuclei to accumulate NimE$^{Cyclin\ B}$. Figure modified from Nayak *et al.* (2010).

A. nidulans is coenocytic and nuclei in tip cells progress synchronously through the cell cycle. Cell cycle regulatory proteins, such as $NimE^{Cyclin\ B}$ and $NimX^{Cdk1}$, accumulate, localize to specific cellular structures (e.g. spindle pole body), and are destroyed or displaced at nearly the same time in all nuclei within the same tip cell. However, in *mipA*D159, the nuclear autonomous failure to accumulate $NimE^{Cyclin\ B}$ and $NimX^{Cdk1}$ resulted in these nuclei being taken out of the cell cycle and they did not undergo nuclear division. Other nuclei in the same S/G_2 tip cell would accumulate these proteins normally, progress through the cell cycle, and undergo nuclear division (Nayak *et al.*, 2010) (**Fig. 1.12**). Our lab determined that the nuclei that failed to accumulate $NimE^{Cyclin\ B}$ and $NimX^{Cdk1}$ was due to a constitutively active APC/C-CdhA, which resulted in the continuous destruction of $NimE^{Cyclin\ B}$. CdhA-GFP, which normally leaves the spindle pole body at the G_1/S transition (**Fig. 1.13**), failed to dissociate from the spindle pole bodies at the G_1/S transition in these affected nuclei (**Fig. 1.14**). Importantly, the deletion of *cdhA,* which is not lethal in *A. nidulans*, restored $NimE^{Cyclin\ B}$ to S/G_2 nuclei in *mipA*D159 strains (**Fig. 1.15A**). Thus, mis-localization of CdhA correlated with constitutively active APC/C-CdhA in these affected S/G_2 nuclei (Edgerton-Morgan and Oakley, 2012).

Although *cdhA*Δ, *mipA*D159 strains no longer contained nuclei with APC/C-CdhA constitutively targeting $NimE^{Cyclin\ B}$ for degradation, these strains were still cold-sensitive, even slightly more so than *cdhA*+, *mipA*D159 strains (**Fig. 1.15B**). These data indicated that constitutively active APC/C-CdhA was not the sole cause of the cold sensitivity. In addition, since *mipA*D159 is a recessive mutation (Jung *et al.*, 2001), it is unlikely that the failure to inactivate CdhA is due to an increased binding affinity of γ-tubulin for CdhA. Thus, at the beginning of my graduate career, the mechanism by which γ-tubulin inactivates APC/C-CdhA at the G_1/S transition

was unknown, but we hypothesized that γ-tubulin interacts directly or indirectly with regulators of CdhA.

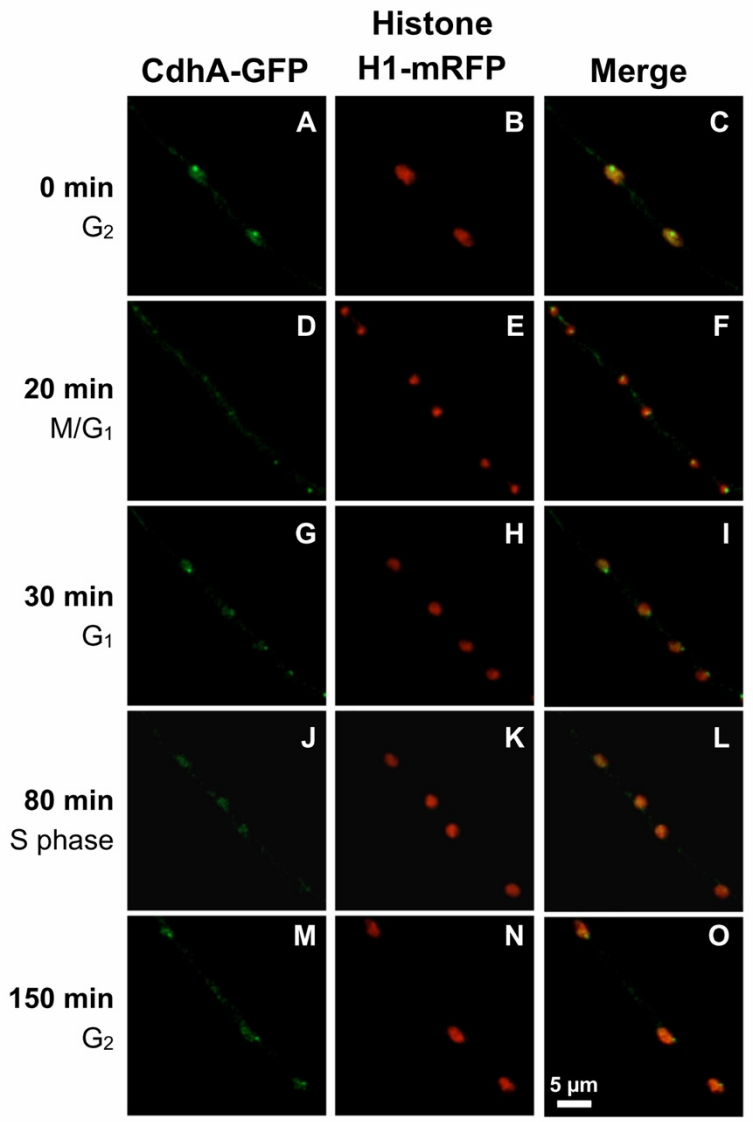

Figure 1.13: Cell cycle localization of CdhA-GFP
Images are maximum intensity projections of Z-series stacks collected at 10-minute intervals of a control, *mipA*+, strain at 25℃. **(A-C)** CdhA-GFP localizes to nuclei and the spindle pole body (SPB) in late G_2. CdhA-GFP is not present during early mitosis and becomes faintly detectable at SPBs in anaphase (not shown). **(D-F)** CdhA-GFP localizes to SPBs at the M to G_1 transition. **(G-I)** In G_1, CdhA-GFP is located in the nucleoplasm and at SPBs. **(J-I)** CdhA-GFP leaves SPBs at the G_1/S transition, although is sometimes faintly observed in the nucleoplasm during S and early G_2. **(M-O)** CdhA-GFP reappears at the SPBs in mid to late G_2. Figure modified from Edgerton-Morgan and Oakley (2012).

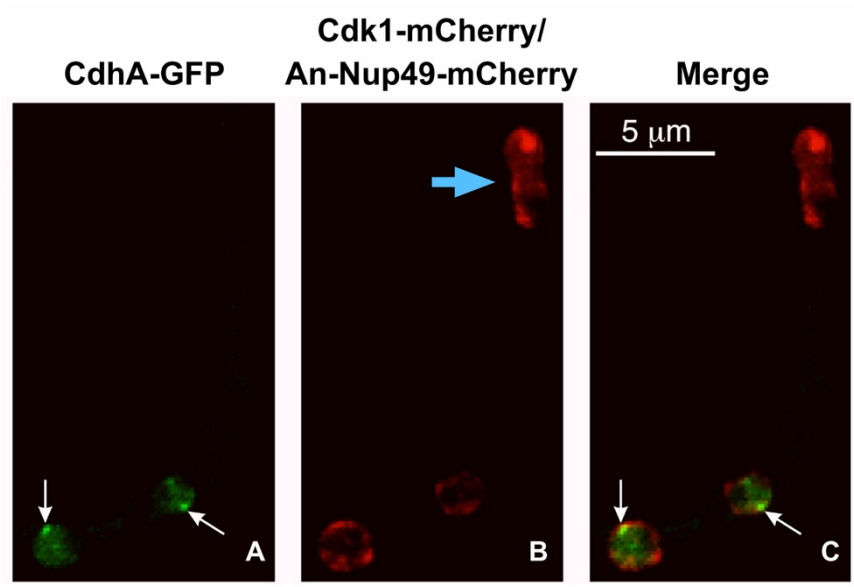

Figure 1.14: CdhA-GFP remains in the nucleoplasm and at the spindle pole bodies in *mipA*D159, cdk1 negative nuclei

Images are a projection of a single time-point Z-series stack of a *mipA*D159 strain incubated at the restrictive temperature 25℃. A tip cell containing three nuclei is shown. In panel **B**, all nuclei show nuclear periphery fluorescence due to An-Nup49-mCherry (An-Nup49 is a nucleoporin). One nucleus (blue arrow) has accumulated Cdk1-mCherry in the nucleoplasm and at the spindle pole body (SPB). The other two nuclei in the same cell have failed to accumulate Cdk1 and the nucleoplasm is clear. In panels **A** and **C**, the two Cdk1 negative nuclei are shown to contain CdhA-GFP in the nucleoplasm and at the SPBs (white arrows). Figure modified from Edgerton-Morgan and Oakley (2012).

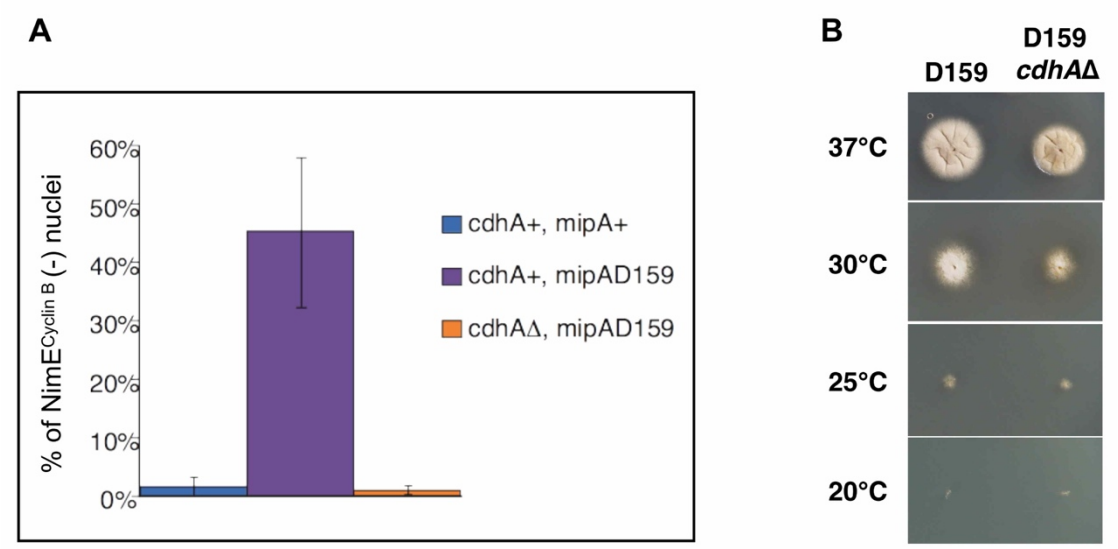

Figure 1.15: Deletion of *cdhA* in *mipA*D159 restores NimE$^{Cyclin\ B}$ accumulation in *mipA*D159 nuclei but *cdhA*Δ, *mipA*D159 strains are still cold-sensitive

(A) The quantification of NimE$^{Cyclin\ B}$ negative (-) nuclei in *cdhA*+, *mipA*+ strains, *cdhA*+, *mipA*D159 strains, and *cdhA*Δ, *mipA*D159 strains. All strains were grown at 25℃, the restrictive temperature for *mipA*D159. NimE$^{Cyclin\ B}$ (-) nuclei are defined as nuclei that fail to accumulate NimE$^{Cyclin\ B}$-GFP in tip cells where at least one nucleus has accumulated NimE$^{Cyclin\ B}$-GFP. Figure modified from Edgerton-Morgan and Oakley (2012). **(B)** A *mipA*D159 strain (LO9804) and a *cdhA*Δ, *mipA*D159 strain (LO9901) were stabbed onto complete media and grown at the temperatures indicated.

1.6 Aims of dissertation research

One goal of my graduate research was to further understand the mechanism by which γ-tubulin regulates CdhA at the G_1/S transition. As mentioned in the previous section, our hypothesis was that γ-tubulin interacts directly or indirectly with regulators of CdhA in order to regulate the G_1/S transition. However, at the start of my graduate career, absolutely nothing was known about the regulation of CdhA in *A. nidulans.*

Fortunately, proteins involved in Cdh1 inactivation and/or inhibition have been identified in other organisms. In many organisms, initial Cdh1 inactivation at G_1/S occurs via cyclin/CDK complexes which then triggers Cdh1 ubiquitination by the skp1-cullin1-F-box-containing (SCF)

complex (Fukushima *et al.*, 2013; Lukas *et al.*, 1999; Sorensen *et al.*, 2001). APC/C-Cdh1 can also be inactivated through binding of inhibitors (e.g. EMI1 in vertebrates, Acm1 in *Saccharomyces cerevisiae*, and Rca1 in *Drosophila melanogaster*), but none of these inhibitors have an obvious homolog in *A. nidulans.* Although a quick BLASTP search revealed that cyclins and components of the SCF complex are present in *A. nidulans*, there was, however, very little functional data on cell cycle-related cyclins (other than $NimE^{Cyclin\ B}$) and SCF components in *A. nidulans* nor other filamentous ascomycetes. This is somewhat surprising as cyclins and the E3 ubiquitin ligases APC/C and SCF are all core components of eukaryotic cell cycle control. Thus, my graduate research has focused primarily on identifying and characterizing cyclins (Chapters 3 and 4) and components of the SCF complex (Chapter 5) in order to improve our understanding of how these essential cell cycle components function in filamentous fungi. I have also determined that CdhA in *A. nidulans* is regulated similarly to that of Cdh1 in other organisms and that these CdhA regulators have interesting, albeit mechanistically unknown, genetic interactions with γ-tubulin (Chapter 6). In chapter 7, I give a summary of my findings and how my work has provided a great deal of new insights into the mechanisms of cell cycle regulation, septation, and development of *A. nidulans*. I also discuss future research, particularly in regard to elucidating the cell cycle function(s) of γ-tubulin.

Chapter 2: Materials and Methods

2.1 Strains and media

A list of strains used in this study along with their genotypes is given in **Table 2.1**. YG (5 g/L yeast extract, 20 g/L D-glucose, supplemented with 400 µL/L of trace element solution (Vishniac and Santer, 1957) was used as a liquid complete medium and YAG (YG plus 15 g/L agar) was used as a solid complete medium. As yeast extract does not provide enough riboflavin to fully supplement the *riboB*2 mutation or enough pyrimidines to supplement the *pyrG*89 mutation, the following were added to YAG if needed: riboflavin (2.5 µg/mL), uridine (2.442 mg/mL), and uracil (1 mg/mL). Liquid minimal medium (MM) for imaging consisted of 6 g/L $NaNO_3$, 0.52 g/L KCl, 0.52 g/L $MgSO_4 \cdot 7H_2O$, 1.52 g/L KH_2PO_4, 10 g/L D-glucose, 400 µL/L of trace element solution (Vishniac and Santer, 1957) and any additional nutrients required to supplement mutations. For solid MM, the same components as liquid MM plus 15 g/L agar was used. Solid medium utilized for plating protoplasts after transformation contained either 342.3 g/L sucrose or 44.7 g/L KCl as osmotic balancers. pH was adjusted to 6.0-6.5.

Strain Number	**Genotype**
LO1385*	*pyrG*89; *pyroA*4; *nkuA*::*argB*
LO1516*	*pyrG*89; *riboB*2; *pyroA*4; *nkuA*::*argB*; *hhoA*-mRFP-*AfriboB*
LO1806*	*pyrG*89; *riboB*2; *pyroA*4; *nkuA*::*argB; hhoA*-mRFP-*AfriboB; cdhA*-GFP-*AfpyrG*
LO2019*	*pyrG*89; *riboB*2; *pyroA*4; *nkuA*::*argB*; *hhoA*-mRFP-*AfriboB; cdhA*::*AfpyrG*
LO2074*	*pyrG*89; *riboB*2; *pyroA*4; *nkuA*::*argB*; *hhoA*-mCherry-*AfpyroA*; *nimE*-GFP-*AfpyrG*
LO3231*	*pyrG*89; *pyroA*4; *nkuA*::*argB*; *sccA*-GFP-*AfpyroA*; *hhoA*-mCherry-*AfpyrG*
LO3938*	*pyrG*89; *pyroA*4?; *riboB*2?; *nkuA*::*argB*?; *nimX*^{cdk1}-mRFP-*Afribo*; *hhoA-T-sapphire-Afpyro*; *mipA*D159
LO6268*	*pyrG*89; *pyroA*4; *riboB*2; *pabaA*1; *chaA*1?; *fwA*1; *cdhA*-GFP-*AfpyrG*; *nimX*^{cdk1}-mCherry-*Afribo*; *An-nup49*-mCherry-*AfpyrG*
LO8388	*pyrG*89; *riboB*2; *pyroA*4; *nkuA*::*argB*; *hhoA*-mRFP-*AfriboB*; *culA*-GFP-*AfpyrG*
LO8743-LO8744	*pyrG*89; *riboB*2; *pyroA*4; *nkuA*::*argB*; *cdhA*::*AfpyrG*; *pucA*::*AfpyroA*; *hhoA*-mRFP-*AfriboB*
LO9225-LO9227	*pyrG*89; *riboB*2; *pyroA*4; *nkuA*::*argB*; *hhoA*-mRFP-*AfriboB*; AfpyrG-GFP-*culA*
LO9481	*pyrG*89; *riboB*2; *pyroA*4?; *chaA1*; *nkuA*::*argB*; *An-nup49*-mCherry-*AfpyrG*; *hhoA*-T-Sapphire-*AfpyroA*
LO9537	*pyrG*89; *riboB*2; *pyroA*4?; *chaA1*; *nkuA*::*argB*; *An-nup49*-mCherry-*AfpyrG*; *hhoA*-T-Sapphire-*AfpyroA*; *wA*::*AfriboB*
LO9560	*riboB*2; *nkuA*::*argB*
LO9732	*riboB*2; *nkuA*::*argB*; *wA*::*AfriboB*
LO9775	*pyrG*89; *riboB*2; *pyroA*4; *nkuA*::*argB*; *An-nup49*-mCherry-*AfpyrG*; *hhoA*-GFP-*AfpyroA*
LO9804	*pyrG*89; *pyroA*4; *nkuA*::*argB*; *wA*::*AtpyrG*; *yA*::*AfpyroA*; *mipA*D159
LO9882	*pyrG*89; *pyroA*4; *nkuA*::*argB*; *cdhA*::*AtpyrG*; *pucA*::*AfpyroA*
LO9891	*pyrG*89; *pyroA*4; *nkuA*::*argB*; *wA*::*AtpyrG*; *yA*::*AfpyroA*
LO9894	*pyrG*89; *pyroA*4; *nkuA*::*argB*; *cdhA*::*AtpyrG*; *pucA*::*AfpyroA*; *mipA*D159
LO9897	*pyrG*89; *pyroA*4; *nkuA*::*argB*; *cdhA*::*AtpyrG*; *yA*::*AfpyroA*
LO9901	*pyrG*89; *pyroA*4; *nkuA*::*argB*; *cdhA*::*AtpyrG*; *yA*::*AfpyroA*; *mipA*D159
LO10066	*pyrG*89; *riboB*2; *pyroA*4; *nkuA*::*argB*; *hhoA*-T-Sapphire-*AfpyrG; SepK*-tdTomato-*AfpyrG; wA::*GFP-*tubA-AfpyroA*
LO10117	*pyrG*89; *pyroA*4; *nkuA*::*argB*; *wA*::*AtpyrG*; *yA*::*AfpyroA*; *mipA*D123

LO10120	*pyrG*89; *pyroA*4; *nkuA*::*argB*; *cdhA*::*AtpyrG*; *yA*::*AfpyroA*; *mipA*D123
LO10123	*pyrG*89; *pyroA*4; *nkuA*::*argB*; *cdhA*::*AtpyrG*; *pucA*::*AfpyroA*; *mipA*D123
LO10126-LO10127	*pyrG*89; *riboB*2; *pyroA*4; *nkuA*::*argB*; *hhoA*-mRFP-*AfriboB*; *clbA*-GFP-*AfpyrG*
LO10129-LO10131	*pyrG*89; *riboB*2; *pyroA*4; *nkuA*::*argB*; *hhoA*-mRFP-*AfriboB*; *clbA*::*AfpyrG*
LO10327	*pyrG*89; *riboB*2; *pyroA*4; *nkuA*::*argB*; *hhoA*-mRFP-*AfriboB*; *wA*::*AfpyrG*
LO10333-LO10335	*pyrG*89; *riboB*2; *pyroA*4; *nkuA*::*argB*; *hhoA*-mCherry-*AfpyroA*; *nimE*-GFP-*AfpyrG*; *wA*::*AtriboB*
LO10431	*pyrG*89; *riboB*2; *pyroA*4; *nkuA*::*argB*; *hhoA*-mRFP-*AfriboB*; *wA*::*alcA*(p)-db1Δ-*clbA*-GFP-*AfpyrG*
LO10434	*pyrG*89; *riboB*2; *pyroA*4; *nkuA*::*argB*; *hhoA*-mRFP-*AfriboB*; *wA*::*alcA*(p)-db2Δ-*clbA*-GFP-*AfpyrG*
LO10476-LO10478*	*pyrG*89; *riboB*2; *pyroA*4; *nkuA*::*argB*; *hhoA*-mRFP-*AfriboB*; *AfpyrG*-GFP-*skpA*
LO10497	*pyrG*89; *riboB*2; *pyroA*4; *nkuA*::*argB*; *hhoA*-mRFP-*AfriboB*; *wA*::*alcA*(p)-FL-*clbA*-GFP-*AfpyrG*
LO10500	*pyrG*89; *riboB*2; *pyroA*4; *nkuA*::*argB*; *hhoA*-mRFP-*AfriboB*; *wA*::*alcA*(p)-FL-*clbA*-*AfpyrG*
LO10503	*pyrG*89; *riboB*2; *pyroA*4; *nkuA*::*argB*; *hhoA*-mRFP-*AfriboB*; *wA*::*alcA*(p)-db1Δ-*clbA*-*AfpyrG*
LO10506	*pyrG*89; *riboB*2; *pyroA*4; *nkuA*::*argB*; *hhoA*-mRFP-*AfriboB*; *wA*::*alcA*(p)-db2Δ-*clbA*-*AfpyrG*
LO10512	*pyrG*89; *pyroA*4; *nkuA*::*argB*; *wA*::*AtpyrG*; *yA*::*AfpyroA*; *mipA*R63
LO10617	*pyrG*89; *pyroA*4; *nkuA*::*argB*; *cdhA*::*AtpyrG*; *pucA*::*AfpyroA*; *mipA*R63
LO10620	*pyrG*89; *pyroA*4; *nkuA*::*argB*; *cdhA*::*AtpyrG*; *yA*::*AfpyroA*; *mipA*R63
LO10623-LO10624	*pyrG*89; *pyroA*4; *riboB*2?; *nkuA*::*argB*; *nimX*^{cdk1}-mCherry-*Afribo*; *An-nup49*-mCherry-*AfpyrG*; *clbA*-GFP-*AfpyroA*; *mipA*D159
LO10750-LO10751	*pyrG*89; *riboB*2; *pyroA*4; *nkuA*::*argB*; *cdhA*::*AfpyrG*; *pucA*::*AfpyroA*; *hhoA*-mRFP-*AfriboB*; *nimE*-GFP-*AfpyrG*
LO10752	*pyrG*89; *pyroA*4; *nkuA*::*argB*; *wA*::*AtpyrG*; *yA*::*AfpyroA*; *mipA*R243
LO10758	*pyrG*89; *pyroA*4; *nkuA*::*argB*; *wA*::*AtpyrG*; *yA*::*AfpyroA*; *mipA*H370
LO10761	*pyrG*89; *riboB*2; *pyroA*4; *nkuA*::*argB*; *An-nup49*-mCherry-*AfpyrG*; *nimE*-GFP-*AfpyrG*
LO10795	*pyrG*89; *riboB*2; *pyroA*4; *nkuA*::*argB*; *An-nup49*-mCherry-*AfpyrG*; *nimE*-GFP-*AfpyrG*; *yA*::*AtriboB*

LO10919	*pyrG*89; *pyroA*4; *nkuA*::*argB*; *cdhA*::*AtpyrG*; *yA*::*AfpyroA*; *mipA*H370
LO10922	*pyrG*89; *pyroA*4; *nkuA*::*argB*; *cdhA*::*AtpyrG*; *pucA*::*AfpyroA*; *mipA*H370
LO10925	*pyrG*89; *pyroA*4; *nkuA*::*argB*; *wA*::*AtpyrG*; *yA*::*AfpyroA*; *mipA*R338
LO10928	*pyrG*89; *pyroA*4; *nkuA*::*argB*; *wA*::*AtpyrG*; *yA*::*AfpyroA*; *mipA*K408
LO10982	*pyrG*89; *pyroA*4; *nkuA*::*argB*; *cdhA*::*AtpyrG*; *yA*::*AfpyroA*; *mipA*R338
LO10987	*pyrG*89; *pyroA*4; *nkuA*::*argB*; *cdhA*::*AtpyrG*; *pucA*::*AfpyroA*; *mipA*R338
LO11067-LO11068	*pyrG*89; *riboB*2; *pyroA*4; *nkuA*::*argB*; *sepk*-tdTomato-*AfpyrG*: *hhoA*-mTagBFP2-*AfriboB*; *ClbA*-GFP-*AfpyroA*
LO11071	*pyrG*89; *pyroA*4; *nkuA*::*argB*; *cdhA*::*AtpyrG*; *yA*::*AfpyroA*; *mipA*R243
LO11073	*pyrG*89; *pyroA*4; *nkuA*::*argB*; *cdhA*::*AtpyrG*; *pucA*::*AfpyroA*; *mipA*R243
LO11076	*pyrG*89; *pyroA*4; *nkuA*::*argB*; *cdhA*::*AtpyrG*; *yA*::*AfpyroA*; *mipA*K408
LO11079	*pyrG*89; *pyroA*4; *nkuA*::*argB*; *cdhA*::*AtpyrG*; *pucA*::*AfpyroA*; *mipA*K408
LO11119-LO11121	*pyrG*89; *riboB*2; *pyroA*4; *nkuA*::*argB*; *hhoA*-mRFP-*AfriboB*; *wA*::*nmtA*(p)-FL-*clbA*-GFP-*AfpyrG*
LO11122-LO11124	*pyrG*89; *riboB*2; *pyroA*4; *nkuA*::*argB*; *hhoA*-mRFP-*AfriboB*; *wA*::*nmtA*(p)-db2Δ-*clbA*-GFP-*AfpyrG*
LO11202	*pyrG*89; *riboB*2; *pyroA*4; *nkuA*::*argB*; *hhoA*-mRFP-*AfriboB*; *sccA*-GFP-*AfpyrG*; *wA*::*AfpyroA*
LO11211	*pyrG*89; *riboB*2; *pyroA*4; *nkuA*::*argB*; *hhoA*-mRFP-*AfriboB*; *sccA*-GFP-A*fpyrG*; *wA*::*nmtA*(p)-db2Δ-*ClbA-AfpyroA*
LO11217	*pyrG*89; *riboB*2; *pyroA*4; *nkuA*::*argB*; *hhoA*-mRFP-*AfriboB*; *sccA*-GFP-*AfpyrG*; *wA*::*nmtA*(p)-dbΔ-*nimE-AfpyroA*
LO11253-LO11254	*pyrG*89*; riboB*2; *pyroA*4; *nkuA*::*argB*; *pabaA*Δ; *biA*Δ; sterigmatocystin cluster (AN7804-AN7825)Δ*; An-ndc80*-mCherry-*AfpyroA; hhoA*-mTagBFP2-*AfriboB*; *clbA*-GFP-*AfpyrG*
LO11357-LO11359	*pyrG*89; *riboB*2; *pyroA*4; *nkuA*::*argB*; *hhoA*-mRFP-*AfriboB*; *wA*::*nmtA*(p)-dbΔ-*nimE-AfpyrG*
LO11517-LO11519	*pyrG*89; *riboB*2; *pyroA*4; *nkuA*::*argB*; *sepK*-tdTomato-*AfpyrG*; *hhoA*-mTagBFP2-*Afribo; skpA*-GFP-*AfpyroA*

Table 2.1: List of strains used in this study

Each strain is given a unique strain number (left column) and the corresponding genotypes are provided (right column). All strains carry *veA*1. Question marks indicate alleles that were present in one of the parents of a genetic cross but were not tested in the progeny. Asterisks designate strains that I did not personally generate via transformations or genetic crosses.

2.2 Induction and repression of regulatable promoters

The *alcA* promoter [*alcA*(p)] is repressed by glucose and some other sugars and induced by several compounds, one of which is threonine. For my experiments, I repressed the *alcA*(p) with complete medium (e.g. YAG) and for induction I used MM in which the D-glucose was replaced with 9 g/L fructose plus 6.25 mM threonine. The *nmtA* promoter [*nmtA*(p)] is strongly repressed by thiamine, which is present in complete medium (e.g. YAG). Repression experiments with the *nmtA* promoter were, thus, carried out in minimal media with the concentrations of thiamine specified in the text.

2.3 Identifying *Aspergillus nidulans* gene homologs

The *Aspergillus nidulans* genome sequence (strain FGSC4) was first made publicly available in 2003 by the Broad Institute [www.broadinstitute.org; (Galagan *et al.*, 2005)]. The FGSC4 DNA sequenced in the genome project was isolated by the Oakley lab and is wild-type except that it carries the *veA*1 mutation. Now, numerous annotations and curations later, the genome is easily searchable through AspGD (www.aspgd.org) and FungiDB (http://fungidb.org/fungidb/).

To identify putative *A. nidulans* cyclins, I performed BLASTP searches using human, *Saccharomyces cerevisiae, Schizosaccharomyces pombe*, and *Candida albicans* cyclin protein sequences as queries against the *A. nidulans* FGSC4 protein database (AspGD). I also identified all *A. nidulans* proteins that contained a predicted N-terminal cyclin domain (IPR006671), a C-terminal cyclin domain (IPR004367), a cyclin Pho80-like domain (IPR013922), and/or a cyclin-like domain (IPR013763). Domain predictions were made using InterProScan software from the European Bioinformatics Institute (EBI) and could be found on AspGD's "Domains/Motifs"

pages. I then conducted a second round of BLASTP searches, using the putative *A. nidulans* cyclins as queries against 31 filamentous ascomycetes (see **Table 3.9** for a list of the fungi analyzed) using NCBI's non-redundant protein database.

SCF components CulA and SkpA were previously identified and named after their human counterparts Cul1 and Skp1 respectively (von Zeska Kress *et al.*, 2012).

2.4 Phylogenetic analyses

Protein sequences were aligned with MAFFT using the L-INS-i method and the Blosum62 matrix (Katoh *et al.*, 2017). Maximum likelihood analysis was done in RAxML v8.2.10 (Stamatakis, 2014) using the rapid bootstrapping (-f a) algorithm with 1000 bootstrap replicates under the PROTCAT + Auto (automatically chooses the best protein substitution matrix with respect to the likelihood). RAxML analyses were performed using the free computational resource CIPRES Science Gateway (Miller *et al.*, 2010). Phylogenetic trees were visualized in iTOL (Letunic and Bork, 2016).

2.5 PCR for gene targeting

Linear DNA constructs for transformation of *A. nidulans* were generated by fusion PCR as previously described (Nayak *et al.*, 2006; Oakley *et al.*, 2012; Szewczyk *et al.*, 2006; Yang *et al.*, 2004; Yu *et al.*, 2004; Zarrin *et al.*, 2005). Q5 Hot Start High Fidelity 2X Master Mix (New England Biolabs) or Phusion (New England Biolabs) DNA polymerases were used for initial amplifications and for fusion PCR. PCR products were purified using the QIAQuick PCR Purification Kit (Qiagen) or the Monarch PCR & DNA Cleanup Kit (NEB) and analyzed by agarose gel electrophoresis.

2.5.1 Selectable markers from Aspergillus fumigatus and Aspergillus terreus

Transformation of *A. nidulans* with linear DNA constructs requires the use of a selectable marker, which complements an auxotrophic mutation, to allow for selection of correct transformants. Plating transformants on media that lacks a required nutrient ensures that only strains carrying the transforming fragment containing the selectable marker will grow. The major auxotrophic mutations used in this work are: *pyrG*89, *pyroA*4, and *riboB*2.

Selectable markers from *A. nidulans* were not used to complement auxotrophic mutations because homologous recombination can occur at the endogenous copy of the selectable marker in addition to the targeted locus. Thus, we utilize *Aspergillus fumigatus* and *Aspergillus terreus* homologs of the *A. nidulans pyrG, pyroA,* and *riboB* selectable markers. These genes are able to complement the *A. nidulans* auxotrophic mutations but do not integrate at the *A. nidulans* mutant loci.

Selectable markers from *A. fumigatus* used in this work were *AfpyrG*, *AfriboB*, and *AfpyroA* (Nayak *et al.*, 2006). The *A. fumigatus riboB* gene used for the mTagBFP2 construct was amplified by PCR from genomic DNA provided by S. Earl Kang, Jr. and Dr. Michelle Momany (The University of Georgia, Athens, GA). *Aspergillus terreus pyrG* and *riboB* genes (*AtpyrG* and *AtriboB*) were amplified by PCR from genomic DNA supplied by Dr. Kenneth Bruno (Pacific Northwest National Laboratory) and further details on those selectable markers were recently published (Dohn *et al.*, 2018) and they are available from the Fungal Genetics Stock Center and from Addgene.

2.5.2 Tagging of genes with fluorescent proteins

To create C-terminal fluorescent fusion proteins (**Fig. 2.1**), the transforming molecules consisted of ~1000-bp of the C-terminal coding sequence of the target protein (using primers to remove the stop codon) fused in frame to a 30-bp glycine-alanine (GA) linker (Yang *et al.*, 2004), which was, in turn, fused in frame with the fluorescent protein coding sequence. The fluorescent protein coding sequence was followed by a 3' untranslated region from *Aspergillus fumigatus* and a selectable marker [the *A. fumigatus pyrG* gene (*AfpyrG*), *riboB* gene (*AfriboB*) or *pyroA* gene (*AfpyroA*)] and a ~1000-bp sequence downstream of the target gene. The GFP variant I used in my experiments was a plant-adapted GFP (Fernandez-Abalos *et al.*, 1998). The mCherry sequence was the original version described by Shaner *et al.* (2004), and the mRFP variant was as previously described (Campbell *et al.*, 2002; Toews *et al.*, 2004). The mCherry and tdTomato clones were a gift from Dr. Roger Tsien. pBAD24-sfGFPx1 was a gift from Sankar Adhya & Francisco Malagon (Addgene plasmid # 51558) and pBAD-mTagBFP2 was a gift from Vladislav Verkhusha (Addgene plasmid # 34632). I found that mTagBFP2 was superior to T-Sapphire because it was brighter, and the emission spectrum did not overlap with GFP. This allowed it to be distinguished easily from GFP in strains expressing proteins tagged with both fluorescent proteins. Initial strains carrying histone H1-mTagBFP2 were generated by Cory Jenkinson (Oakley lab). A strain carrying An-Nup49-mCherry was provided by C. De Souza and S. Osmani (The Ohio State University, Columbus, OH).

N-terminal fluorescent protein tagging was required for SCF components CulA and SkpA. A schematic for generating a five-piece fusion PCR product for the N-terminal tagging of a protein is given in Wong *et al.* (2008) and shown in **Fig. 2.2**. To briefly summarize, I amplified the following three fragments from *A. nidulans* genomic DNA: (1) ~1000-bp of a region of the gene's 5' untranslated region (5'UTR), (2) ~500-bp of the gene's promoter region, and (3) ~1000-bp of

the gene's coding sequence. A selectable marker (*AtpyrG* or *AfpyroA*) was inserted between the 5'UTR flank fragment and the promoter. GFP, which was inserted between the promoter and the gene's coding sequence, was amplified such that it included an ATG at its N-terminus and a GA linker at its C-terminus.

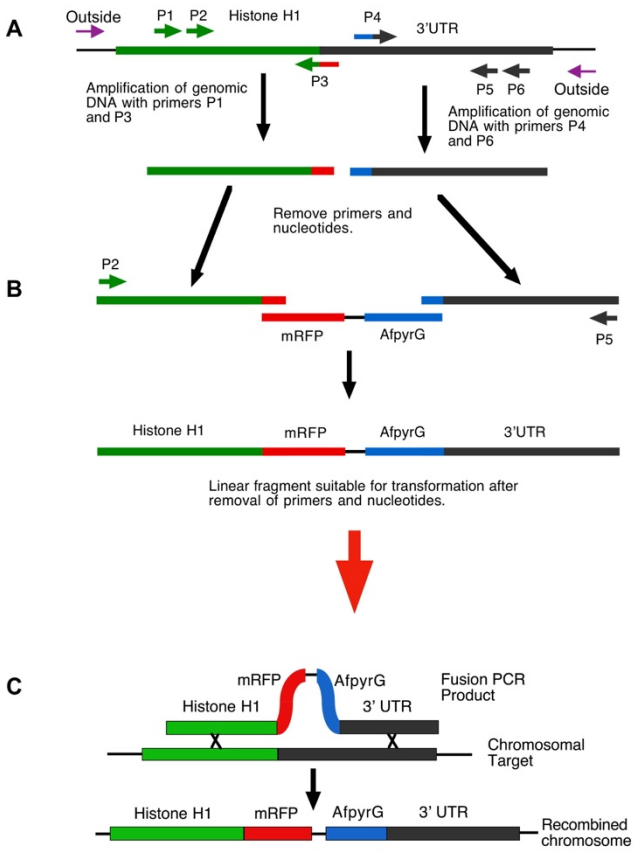

Figure 2.1: Schematic for the C-terminal tagging of a protein with a fluorescent protein sequence

A schematic of the use of PCR to synthesize a fusion fragment of the *hhoA* gene (which encodes histone H1) to the monomeric red fluorescent protein (mRFP) sequence. The C-terminal tagging of other proteins with a fluorescent protein sequence (e.g. mRFP, GFP, mTagBFP2, etc.) follows a similar strategy. **(A)** Two flanking sequences were amplified from *Aspergillus nidulans* genomic DNA: (1) ~1000-bp of the coding sequence upstream of the *hhoA* stop codon was amplified using primers P1 and P3 and (2) ~1000-bp of the *hhoA* 3'UTR downstream of the stop codon was amplified using primers P4 and P6. Primer P3 was designed so as to remove the stop codon from *hhoA*, and it contains a "tail" that overlaps with a cassette that contains the mRFP coding sequence and the *Aspergillus fumigatus pyrG* gene. The cassette contains a five glycine plus alanine linker upstream of the mRFP coding sequence. Primer P4 was designed with a tail consisting of sequences that overlap with the 3' end of the *mRFP-AfpyrG* DNA casssette. (**B**) The three DNA fragments (two flanking fragments and the *mRFP-AfpyrG* cassette) were fused using primers P2 and P5 to generate the linear fragment suitable for transformation. **(C)** Upon transformation, the linear fragment was integrated into the genome via homologous recombination and is under the control of the endogenous *hhoA* promoter. Diagnostic PCR of transformants utilizes outside primers (purple arrows in **A**) that were not used in either the amplification or fusion PCR reactions. Modified from Szewczyk *et al.* (2006).

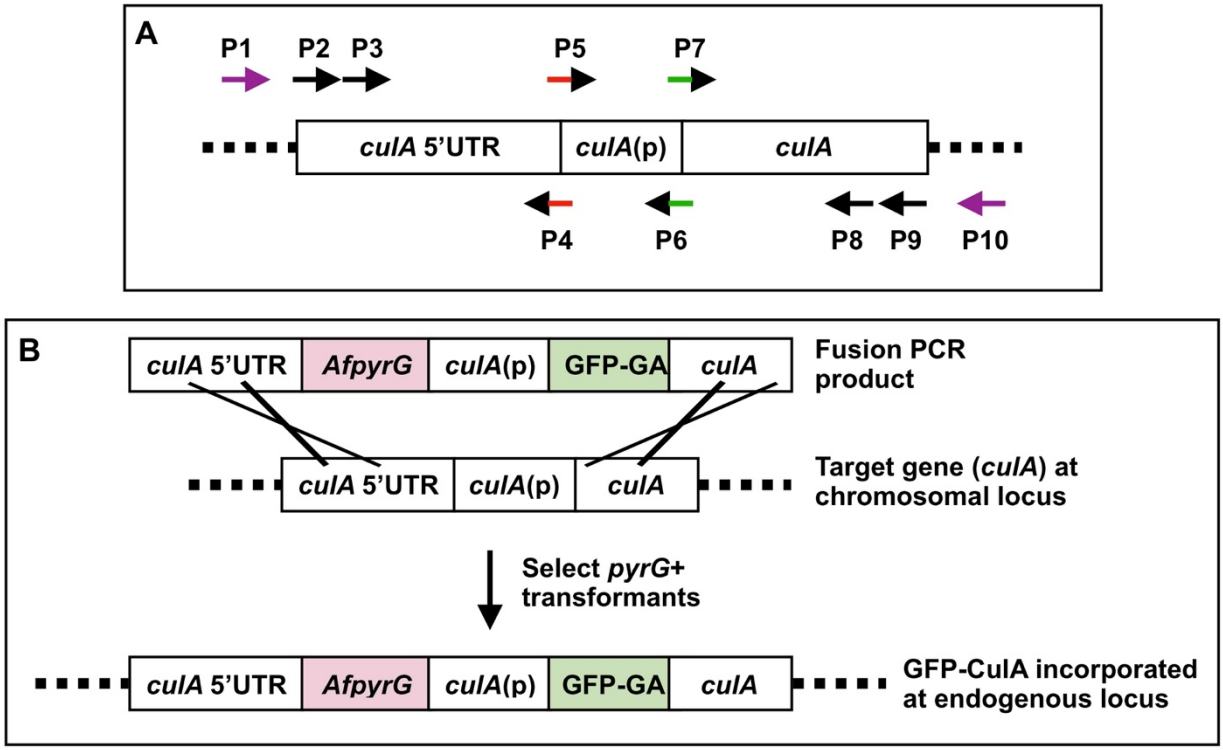

Figure 2.2: Schematic for N-terminally tagging CulA and other proteins

A schematic is shown of the use of PCR to synthesize a transforming molecule used to create a GFP-*culA* fusion under control of the normal *culA* promoter. The N-terminal tagging of other proteins to GFP followed a similar strategy. **(A)** Three fragments were amplified from *Aspergillus nidulans* genomic DNA: (1) ~1000-bp of a region of *culA*'s 5' untranslated region (5'UTR) using primers P2 and P4, (2) ~500-bp of *culA*'s promoter region using primers P5 and P6, and (3) ~1000-bp of *culA*'s coding sequence using primers P7 and P9. Four of the ten primers contained tails: P4 contained a tail that overlapped the 5' end of the selectable marker *AfpyrG*, P5 contained a tail that overlapped the 3' end of *AfpyrG*, P6 contained a tail that overlapped the 5'end of GFP (that included the GFP start codon), and P7 contained a tail that overlapped the 3'end of the GFP-GA DNA fragment. The fusion PCR reaction used nest primers P3 and P8. **(B)** GFP-*culA* linear fusion PCR product was integrated into the genome via homologous recombination with GFP-*culA* under control of the endogenous *culA* promoter. Diagnostic PCR of transformants utilized outside primers P1 and P10, which were sequences not included in amplification or fusion PCR reactions.

2.5.3 Gene deletions

Generation of a fusion PCR product for deleting genes followed the procedure given in Szewczyk *et al.* (2006) as modified by Oakley *et al.* (2012) and is shown in **Fig. 2.3**. To briefly summarize, approximately 1000-bp directly upstream and downstream of the target gene was amplified from *A. nidulans* genomic DNA. A selectable marker was inserted between the 5'UTR and 3'UTR flanks to generate the final fusion product.

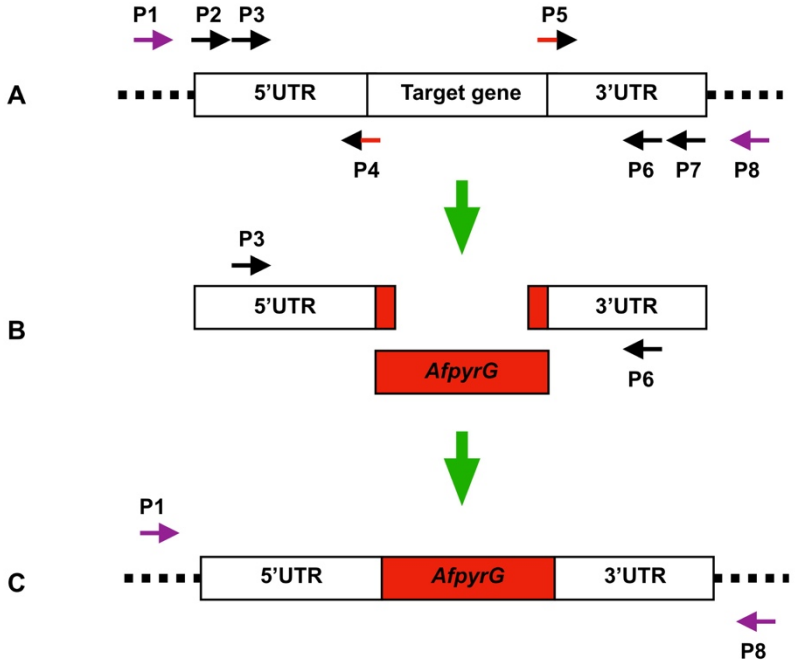

Figure 2.3: Schematic for replacing a gene with a selectable marker
Two flanking regions of the gene of interest that is to be replaced are amplified from *Aspergillus nidulans* genomic DNA: (1) ~1000-bp directly upstream of the target gene using primers P2 and P4 and (2) ~1000-bp directly downstream of the target gene using primers P5 and P7. P4 is designed to contain a tail that will overlap with the 5' end of the selectable marker, which, in this example, is *AfpyrG* (red). P5 is designed to contain a tail that will overlap with the 3' end of *AfpyrG*. The fusion PCR reaction utilizes nested primers P3 and P6. Upon transformation, integration of this fragment via homologous recombination replaces the target gene with the selectable marker *AfpyrG*. Transformants are tested for the correct insert via diagnostic PCR using outside primers P1 and P8.

2.5.4 Expression of d-box deleted cyclins

The dbΔ-NimE$^{Cyclin\ B}$ construct was created as previously described (Nayak *et al.*, 2010). The two truncated forms of ClbA were generated as follows. A fragment of the *clbA* gene extending from nucleotide 342 to the end of the gene (nucleotide 2156) was amplified by PCR to generate db1Δ-ClbA. This fragment excludes the N-terminal 60 amino acids that contain the first putative destruction box (RAAFGDVSN). A second fragment of the *clbA gene* extending from nucleotide 603 to the end of the gene (nucleotide 2156) was amplified by PCR to generate db2Δ-ClbA. This fragment excludes the N-terminal 147 amino acids that contain both the first and second (RKTLNKRAT) putative destruction boxes. The primers used to amplify these fragments were designed with a tail at the 5' end that would anneal to either the *alcA* or the *nmtA* promoter, including a start codon, and a tail at the 3' end that would anneal to either the GA-GFP cassette or to the selectable marker. The complete transforming molecules of d-box-deleted ClbA or NimE$^{Cyclin\ B}$ under the control of either *alcA*(p) or *nmtA*(p) at the *wA* locus consisted of the following: ~1000-bp of 5'UTR from the *wA* gene, 400-bp of *alcA*(p) or 761-bp of *nmtA*(p), d-box-deleted ClbA or NimE$^{Cyclin\ B}$, GA linker + GFP if desired, a 3' untranslated region from *A. fumigatus,* a selectable marker (either *AfpyrG* or *AfpyroA*), and ~1000-bp of 3'UTR from the *wA* gene. A similar strategy was used to generate full length ClbA and NimE$^{Cyclin\ B}$ (with and without a C-terminal fusion to GA-GFP) under control of the *alcA*(p) or *nmtA*(p) at the *wA* locus.

2.6 Transformation of *A. nidulans*

The transformations I completed followed our published transformation protocol manuscripts (Oakley *et al.*, 2012; Szewczyk *et al.*, 2006). In addition, all strains carried a deletion of *nkuA* to improve gene targeting (discussed in 1.4.4).

2.7 Confirmation of accurate gene targeting

2.7.1 Genomic DNA extraction and diagnostic PCR in A. nidulans

Genomic DNA was prepared from transformants using a miniprep procedure (Edgerton-Morgan and Oakley, 2012). Conidia were collected from the surface of a colony using a toothpick or loop and suspended in 50 µL TE buffer (10 mM Tris-HCl, pH 7.5, and 1 mM EDTA) in a microcentrifuge tube. Approximately 50 µL of acid-washed, 425-600 µm glass beads (Sigma) were added and the tube vortexed for 2 min. 2 µL of this solution was immediately removed and added to 18 µL of TE. 2 µL of this 1:10 solution was used for diagnostic PCR using OneTaq Hot Start Quick-Load 2X Master Mix with Standard Buffer (New England Biolabs, Inc.) according to the manufacturer's instructions. Correct gene integration was tested in 6-10 transformants by at least two diagnostic PCR amplifications using different primer pairs: (i) primers outside the target region and (ii) one outside primer and one primer inside the selectable marker.

2.7.2 Temperature growth test on plates

Transformants confirmed to have the correct DNA insertion were then further tested for growth on complete medium at a range of temperatures (20°C, 25°C, 30°C, 37°C, and 42°C). This allows us to verify that (a) all transformants display similar growth patterns and (b) to determine whether the insertion causes a decrease in growth and/or conidiation at a particular temperature(s). If a strain carrying a fluorescently tagged gene grows and conidiates as well as wild-type at all temperatures tested, this strongly indicates that the gene fusion is fully functional. In some of the cases in this work (discussed in later chapters), a GFP fusion to either the C-terminus or N-terminus

of a gene caused a decrease in growth and/or conidiation at a particular temperature(s). This indicates that the GFP tag partially interferes with the protein's function(s).

2.7.3 Fluorescent protein localization patterns

Transformants that were verified to carry a fluorescent gene fusion were analyzed via microscopy to observe their *in vivo* localization patterns. Several transformants were analyzed in each case to ensure they displayed similar fluorescent intensities and similar localization patterns. Checking multiple transformants also increases the confidence that the phenotypes observed are accurate representations of the protein's normal localization pattern.

2.8 Heterokaryon rescue technique

A. nidulans cells are coenocytic and can maintain a heterokaryotic state (two genetically different nuclei in a common cytoplasm). If an essential gene is deleted, *A. nidulans* can avoid death because the null allele is rescued by the spontaneous formation of a heterokaryon as often occurs during transformation. This is useful for studying the phenotypes of deletions of essential genes (Osmani *et al.*, 2006b). A brief summary of the heterokaryon rescue technique is discussed below and shown in **Fig. 2.4**.

Heterokaryons produced after the deletion of an essential gene carry two types of nuclei, parental nuclei and transformed nuclei. Parental nuclei carry a functional copy of the gene of interest but do not carry the selectable marker. Transformed nuclei lack the gene of interest, which was replaced with a selectable marker via homologous recombination. Thus, the heterokaryon can grow on selective media, as parental nuclei provide a copy of the gene of interest while transformed nuclei provide a copy of the selectable marker. Importantly, *A. nidulans* conidia are uninucleate,

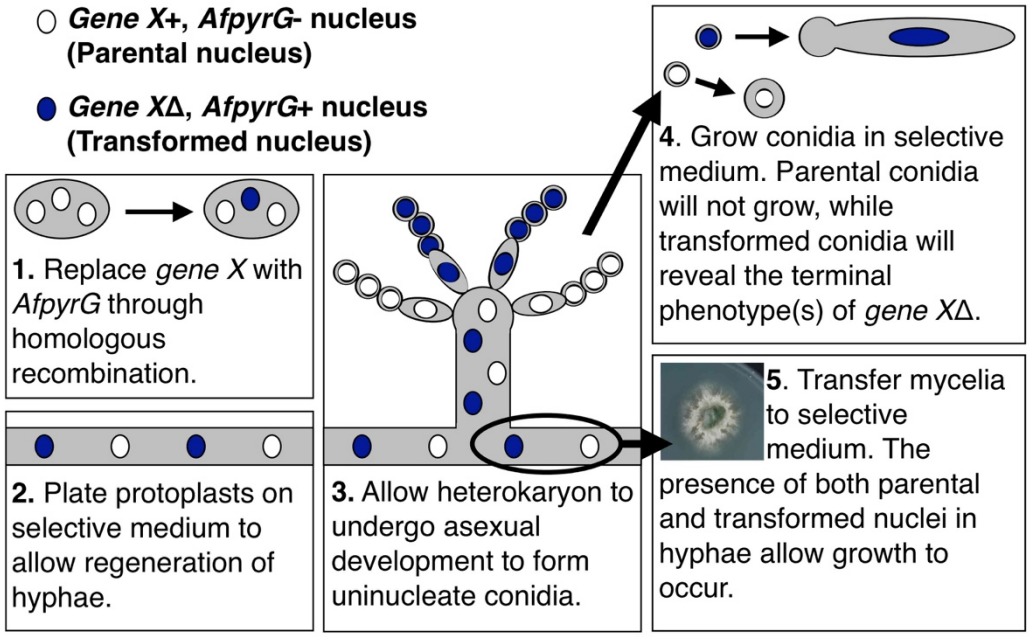

Figure 2.4: Heterokaryon rescue technique

Aspergillus nidulans cells are coenocytic and can maintain a heterokaryotic state (two genetically different nuclei in a common cytoplasm). If an essential gene is deleted, *A. nidulans* can avoid death if the null allele is rescued by the spontaneous formation of a heterokaryon as often occurs during transformation. This is useful for studying the phenotypes of deletions of essential genes. In the figure above, the essential *gene X* is replaced by the selectable marker *AfpyrG* via transformation (**1** and **2**) and a heterokaryon is generated (**3**). In order to characterize the terminal phenotypes(s) of *gene X*Δ, conidia from a heterokaryon are incubated in selective medium (**4**) and imaged via microscopy. Parental conidia (white circles) will not grow, while transformed conidia (blue circles) will reveal the terminal phenotype(s) of *gene X*Δ. Heterokaryons can be maintained by transferring mycelia that contain both parental and transformed nuclei. An example of a heterokaryon growing on a plate is shown in **5**.

so the heterokaryotic state cannot be propagated through conidia. Conidia from a heterokaryon carrying the deletion of an essential gene will not be viable on selective media. By streaking out conidia from the primary transformants on nutritionally selective media, I can determine if the deleted gene is essential by the presence or absence of growth and colony formation (Martin *et al.*, 1997; Osmani *et al.*, 2006b; Osmani *et al.*, 1988). Diagnostic PCR is also used to confirm that heterokaryons were generated. Heterokaryons can be maintained by sub-culturing hyphae onto fresh selective plates every few weeks.

2.9 DAPI and calcofluor white staining and preparation for microscopy

For imaging, conidia were cultured in 400 µL of liquid MM in eight-chambered cover glasses (Lab-Tek; Thermo Fisher Scientific) with necessary supplements to complement nutritional markers. It some experiments, Calcofluor White ST staining solution (American Cyanamid Co., Bound Brook, N.J., USA) was added at a final concentration of 0.00001% 20 minutes prior to imaging. Calcofluor white is used to visualize cell walls and septa. It has been shown to inhibit fungal growth at high concentrations. Therefore, I generated solid media plates containing 100X the working concentration of calcofluor white and did not observe any effect on fungal growth as compared to plates lacking calcofluor white (**Fig. 2.5).**

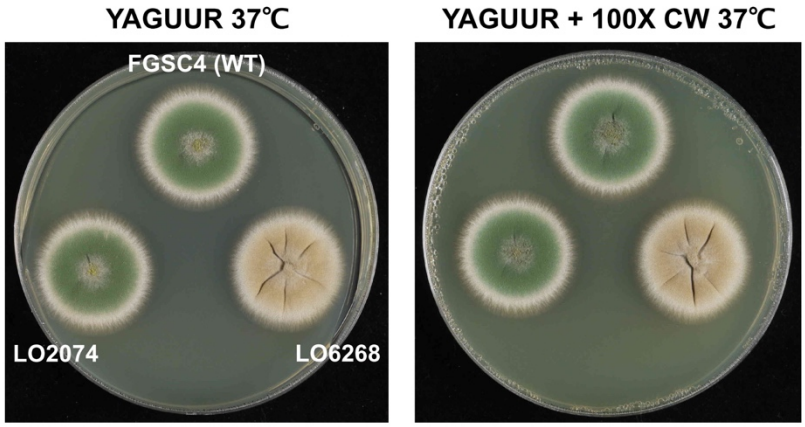

Figure 2.5: Low concentrations of calcofluor white do not affect growth
Three strains (FGSC4, LO2074, and LO6268) were stabbed onto complete medium (YAGUUR) (left plate) and YAGUUR containing 100X the working concentration of Calcofluor White (CW) ST Solution (American Cyanamid Co., Bound Brook, New Jersey) that was used for microscopy (right plate). These plates were incubated at 37℃ at the same time and for the same duration (~2.5 days) and the experiment was replicated three times. LO2074 and LO6268 were included in these growth tests as these were the strains incubated with calcofluor white (Chapters 5 and 6).

In other experiments, germlings were fixed in the wells by removing the liquid medium and adding 400 µL of fixative solution [8% formaldehyde in 50mM piperazine-N,N'-bis(2-ethanesulfonic acid) (PIPES), pH6.7; 25 mM EGTA, pH 7.0; 5 mM $MgSO_4$; and 5% DMSO, pre-warmed to the culture temperature] for 20 min at 37ºC or 30 min at 30ºC. The fixative solution was then removed and replaced with 400 µL 0.00001% Calcofluor White ST staining solution (American Cyanamid Co., Bound Brook, N.J., USA). For DAPI experiments, 5 x 10^7 conidia were grown in 10 mL liquid media plus 0.1% agar (to minimize clumping of germlings) at 30ºC at 140 rpm for 12 h. Samples (900 µL) were added to 100 µL of 10% glutaraldehyde (Electron Microscopy Sciences, Fort Washington, PA), which was previously equilibrated to the culture temperature. They were fixed for 10 min at the culture temperature, spun down for 3 min at 15,500 x g, and then washed 2 x 10 min in double distilled water at room temperature. Samples were resuspended in 0.015 µg/mL DAPI solution.

2.10 Microscopy

Two systems, both with environmental chambers to maintain stable temperatures, were used for imaging. The first system was an inverted Olympus IX71 microscope equipped with a mercury illumination source along with Prior shutters, filter wheels, Z-axis drives, and an ORCA ERAG camera (Hamamatsu Photonics). Images were collected with an Olympus 60X/1.42 numerical aperture Plan Apo objective. Filter sets used were a GFP/DsRed2X2M-B dual-band Sedat filter set (Semrock) with a 459-481nm bandpass excitation filter for GFP, a 546–566 nm excitation filter for mCherry and mRFP, a dual reflection band dichroic (457–480 nm and 542–565 nm reflection bands, 500–529 and 584–679 nm transmission bands), a 499–529 nm emission filter for GFP and a 580–654 nm emission filter for mCherry/mRFP. The second system was an

UltraView VoX spinning disk confocal system (PerkinElmer) mounted on an Olympus IX71 inverted microscope. This system was equipped with a software-controlled piezoelectric stage for rapid Z-axis movement. Images were collected using a 60X/1.42 numerical aperture Plan Apo objective (some images taken using a 1.6x Optovar) and an ORCA ERAG camera (Hamamatsu Photonics). Solid state 405-, 488-, and 561-nm lasers were used for excitation and fluorochrome-specific emission filters were used to prevent emission bleed through between fluorochromes. Both systems were controlled by Volocity software (PerkinElmer) running on Power Mac computers (Apple). Magnifications were calibrated with a stage micrometer. Images were exported directly from Volocity after adjustment of minimum and maximum intensity levels (black and white levels) for each channel. Figures were prepared from exported images using Pages (Apple) with no further adjustments.

2.11 Crossing of strains

Some of the strains used in this work were generated through crosses to obtain progeny with desired alleles, expressing specific tagged proteins, and/or carrying various nutritional markers. I followed the procedure given in Todd *et al.* (2007) to generate genetic crosses with some slight alterations. I will briefly summarize this procedure below.

The two parental strains were stabbed onto complete medium in close proximity and incubated at 37℃ for approximately two days. By this time, the two strains have grown radially toward one another. An agar plug containing hyphae from both strains was cut out and transferred to selective medium. Typically, a cross is more efficient if the parental strains carry complementary nutritional markers. This means that neither parent is capable of growing on selective media, but if their hyphae fused to form a heterokaryon, then the resulting heterokaryon is able to grow on

selective media. The agar plug was incubated on selective media at 37℃ for approximately two days, at which time the plate was sealed with masking tape (to generate slight anaerobic conditions) and incubated for at least two weeks until mature cleistothecia were formed. A method to facilitate identification of hybrid cleistothecia in a cross is for the parental strains to carry different conidial color markers (discussed below) and this approach was used in some cases.

Between 6 and 10 cleistothecia were chosen, harvested with sterile toothpicks and rolled on solid medium to remove any excess conidia sticking to the cleistothecium. Cleistothecia were then separately placed in 1 mL of S/T and stabbed with a sterile toothpick to release the ascospores, which look red in appearance. The ascospores were then placed on media that would allow determination as to whether the ascospores were from a hybrid cleistothecium or a selfed cleistothecium. If the parent strains carried complementary nutritional markers, then a hybrid cleistothecium would contain ascospores that could grow on selective medium whereas a selfed cleistothecium would not contain ascospores that could grow on selective medium. If the parental strain carried different conidial color markers, then the ascospores from a hybrid cleistothecium would grow into colonies containing both colors of the parental strains, whereas if it was a selfed cleistothecium, all of the colonies would be the same conidial color. Once hybrid cleistothecia are identified, then dilutions of the ascospores were plated onto appropriate media and the resulting progeny tested for the desired alleles/traits.

2.12 Storage of strains

Aspergillus nidulans strains were stored by harvesting their conidia in approximately 1.5 mL of sterile 7.5% non-fat milk solution. This conidia/milk suspension was divided into two sterile one-dram vials three quarters full of sterile silica gel desiccant (Certified ACS 6-12 Mesh, Grade

40, Fisher Chemical). The silica vials were chilled prior to adding the conidia/milk suspension, as the absorption of milk into the silica gel releases heat. No more than 750-1000 µL of the conidia-non-fat milk suspension was added to each silica vial, as too much milk prevents proper drying and adsorption of conidia onto the silica gels. Conidia stored in this fashion remain viable for many years and can be easily revived by simply sprinkling a few silica gel granules with adsorbed conidia on proper solid medium and incubating at an appropriate temperature. We have found that conidia can remain viable on silicas for up to 10 years.

Chapter 3: Phylogenetic analyses of cyclins in aspergilli and other filamentous ascomycetes

3.1 Introduction

The eukaryotic cell cycle is driven by the periodic synthesis and destruction of cyclins that bind and activate a class of serine/threonine kinases called cyclin-dependent kinases (CDKs). Distinct cyclin/CDK complexes form and become active at different stages of the cell cycle. Once a cyclin has completed its function, it is targeted for destruction, inactivating its partner CDK. The formation of cyclin/CDK complexes and subsequent cyclin destruction drives the cell through G_1, S, G_2 and mitosis in a sequential and irreversible manner. In addition to cell cycle regulation, cyclin/CDK complexes function in a variety of cellular processes, such as transcriptional regulation, the ubiquitin-proteasome pathway, epigenetic events, metabolism, stem cell self-renewal, neuronal function, spermatogenesis, and the DNA damage response [reviewed in (Lim and Kaldis, 2013)]. Interestingly, there is also evidence that some of these non-canonical functions are carried out by cyclins independent of kinase activity [reviewed in (Hydbring *et al.*, 2016)].

Recent phylogenetic analyses have revealed that cyclins from a variety of different eukaryotes, including yeasts, plants, and humans, can be divided into three major groups (Cao *et al.*, 2014; Ma *et al.*, 2013). Group I is composed of the "classic" cell cycle regulatory cyclins, while group III cyclins tend to function primarily in transcriptional regulation. Group II cyclins have varied functions that include, but are not limited to, roles in cell cycle regulation (Davidson *et al.*, 2009; Jimenez *et al.*, 2013) and development (Liu and Finley, 2010; Mikolcevic *et al.*, 2012; Wu *et al.*, 2004; Zi *et al.*, 2015). However, it is important to note that (1) these phylogenetic analyses incorporated cyclins from a small number of eukaryotes, (2) our understanding of cyclin function is derived from only a handful of model species, and (3) there has been relatively little study of cyclins in filamentous fungi.

Filamentous fungi are, of course, of huge ecological importance and have an enormous impact on human and animal health, agricultural crop production, and industrial production of important commodities (Bok *et al.*, 2006; May and Adams, 1997; Nalley *et al.*, 2016; Pagano *et al.*, 2006). An excellent recent commentary addressed our limited understanding of filamentous fungal biology, the threat filamentous fungi pose to the food supply and to human and animal health, and the critical need to advance fungal biotechnology (Meyer *et al.*, 2016). There is, thus, every reason to investigate cyclin function and cell cycle regulation in filamentous fungi, to help us facilitate their growth when appropriate and inhibit their growth when needed. In addition, it will be of benefit to carry out phylogenetic and functional analyses of cyclins from additional organisms to further our understanding of eukaryotic cell cycle regulation and how these control systems evolved.

The budding yeast *Saccharomyces cerevisiae* and the fission yeast *Schizosaccharomyces pombe* are popular models for studying the cell cycle, and cyclins have been studied extensively in these organisms. While one might imagine that these yeasts can be used as a "reference system" for filamentous fungi, and they are often cited as such in the literature, this is not the case [reviewed in (Meyer *et al.*, 2016)].

In this work I have investigated the cyclin repertoires in the filamentous fungi analyzed in a recent comparative genomics study (de Vries *et al.*, 2017). This group contains 18 species of the genus *Aspergillus* and 14 species from other, phylogenetically diverse, genera. [Please note, the filamentous fungus *Aspergillus zonatus* analyzed in de Vries *et al.* (2017) was reclassified as *Penicilliopsis zonata* (Kocsube *et al.* 2016)]. The list includes 23 species from the order Eurotiales (including *Aspergillus nidulans*), seven species from Onygenales, *Trichoderma reesi* from Hypocreales, and *Neurospora crassa* from Sordariales. The group is well chosen because it allows

one to determine if there are commonalities within the aspergilli and if these commonalities are shared with other, diverse, filamentous ascomycetes. All species in this group fall within the subdivision Pezizomycotina that includes most ascomycetes. This group does not contain members of the Saccharomycotina which includes yeasts such as *S. cerevisiae*, dimorphic fungi such as *Candida albicans* and filamentous fungi such as *Ashbya gossypii* that are closely related to, and probably derived from yeasts, nor does our study group contain any member of the Taphrinomycotina such as *S. pombe* (Wang *et al.*, 2009). Although basidiomycetes and oomycetes are of great interest, they are also outside of this study. Finally, to avoid repeated use of awkwardly long phrases, I will use the term "filamentous ascomycetes" to refer to members of the Pezizomycotina, which are by far the most numerous filamentous ascomycetes, realizing that there are some ascomycetes from outside of this subdivision that have a filamentous growth form.

Our phylogenetic analyses of cyclins in these 32 species of filamentous ascomycetes reveal that, as in other organisms that have been studied (Cao *et al.*, 2014; Ma *et al.*, 2013), cyclins fall into three groups. Strikingly, the complement of cyclins is remarkably conserved. For example, each species surveyed has three group I cyclins. These are particularly important because they typically play critical roles in the regulation of the cell cycle. The group I cyclins fall into three clades with each fungus having a single member of each clade. It follows that the cyclins in these phylogenetically diverse filamentous ascomycetes are likely to be functionally conserved. Lessons learned from studying cyclin function in the model organism *A. nidulans*, are likely to apply across the genus *Aspergillus* and are likely to be informative with respect to many other filamentous ascomycetes, including pathogenic and industrially important species. My analysis also reveals that the complement of cyclins found in these fungi is significantly different from that of yeast models. For example, *S. cerevisiae* has nine group I cyclins while *S. pombe* and *C. albicans* each

have five. The yeasts are, thus, likely to be of limited value in understanding cyclin function in filamentous fungi.

3.2 Results

3.2.1 Identification of the cyclin repertoire of A. nidulans

Phylogenetic analyses of cyclins have recently been carried out on a variety of different organisms including the model yeasts *S. cerevisiae* and *S. pombe* (Cao *et al.*, 2014; Ma *et al.*, 2013). However, these evolutionary studies focused on cyclins with an N-terminal cyclin domain, which omits several fungal cyclins. These fungal cyclins do not have an N-terminal cyclin domain but instead have either a cyclin-like or cyclin pho80-like domain. To ensure that I identified all putative cyclins in *A. nidulans,* I utilized two methods: (1) BLASTP searches of the *Aspergillus* genome database (AspGD) using the published amino acid sequences of *S. cerevisiae* (**Table 3.1**)*, S. pombe* (**Table 3.2**)*, C. albicans* (**Table 3.3**), and human cyclins as queries and (2) using the InterProScan protein motif search tool to identify all *A. nidulans* proteins that contain an N-terminal cyclin domain (IPR006671), a C-terminal cyclin domain (IPR004367), a cyclin Pho80-like domain (IPR013922), and/or a cyclin-like domain (IPR013763). The cyclin-like domain is also present in the transcription factors TFIIB and TFIIB-related Brf1 which are conserved in fungi.

I determined that the *A. nidulans* genome encodes fifteen putative cyclins (**Table 3.4**) of which only six had been previously characterized. Two additional proteins that contain a cyclin-like domain were identified, but they are strong homologs of human TFIIB (AN4928, E-value of 9e-54) and TFIIB-related Brf1 (AN3116, E-value of 4e-68) and are unlikely to be cyclins. Based on both sequence similarity and our phylogenetic analyses, cyclins in fungi fall into three major

groups, consistent with previous cyclin family analyses (Cao *et al.*, 2014; Ma *et al.*, 2013). These results are summarized in **Table 3.4**. The results of the BLASTP searches using *S. cerevisiae, S. pombe, C. albicans,* and human cyclins as queries are shown in **Tables 3.5-3.8**.

Protein Name	SGD ID	Essential ?	Published CDK Partner	Cyclin Group I, II, or III	N-terminal cyclin domain (IPR006671)	C-terminal cyclin domain (IPR004367)	Cyclin Pho80-like domain (IPR013922)	Cyclin-like domain; also found in TFIIB and retinoblastoma-associated protein (IPR013763)
Cln1	S000004812	No	Cdc28	Group I	Yes			Yes
Cln2	S000006177	No	Cdc28	Group I	Yes			Yes
Cln3	S000000038	No	Cdc28	Group I	Yes			Yes
Clb1	S000003340	No	Cdc28	Group I	Yes	Yes		Yes
Clb2	S000006323	No	Cdc28	Group I	Yes	Yes		Yes
Clb3	S000002314	No	Cdc28	Group I	Yes	Yes		Yes
Clb4	S000004200	No	Cdc28	Group I	Yes	Yes		Yes
Clb5	S000006324	No	Cdc28	Group I	Yes	Yes		Yes
Clb6	S000003341	No	Cdc28	Group I	Yes	Yes		Yes
Pcl1	S000005233	No	Pho85	Group II, PCL (PCL1,2-like subfamily)	Yes			Yes
Pcl2	S000002285	No	Pho85	Group II, PCL (PCL1,2-like subfamily)	Yes			Yes
Pcl5	S000001113	No	Pho85	Group II, PCL (PCL1,2-like subfamily)	Yes			
Pcl9	S000002338	No	Pho85	Group II, PCL (PCL1,2-like subfamily)	Yes			Yes
Clg1	S000003183	No	Pho85	Group II, PCL (PCL1,2-like subfamily)				
Pcl6	S000000861	No	Pho85	Group II, PCL (Pho80-like subfamily)			Yes	
Pcl7	S000001312	No	Pho85	Group II, PCL (Pho80-like subfamily)			Yes	
Pcl8	S000006140	No	Pho85	Group II, PCL (Pho80-like subfamily)			Yes	
Pcl10	S000003102	No	Pho85	Group II, PCL (Pho80-like subfamily)			Yes	
Pho80	S000005361	No	Pho85	Group II, PCL (Pho80-like subfamily)			Yes	
Ssn8	S000004970	No	Ssn3/Srb10/Cdk8	Group III, Cyclin C-like	Yes			Yes
Ccl1	S000006229	Yes	Kin28	Group III, Cyclin H-like	Yes			Yes
Ctk2	S000003543	No	Ctk1	Group III, Cyclin T/K-like	Yes			Yes
BUR2	S000004216	No	Bur1/Sgv1	Group III, Cyclin T/K-like				SSF47954 cyclin-like domain
BRF1	S000003478	Yes		None, Transcription factor TFIIIB complex subunit				Yes
SUA7	S000006290	Yes		None, Transcription factor TFIIB				Yes

Table 3.1: Proteins with cyclin and cyclin-like domains in *Saccharomyces cerevisiae*
S. cerevisiae contains 23 cyclins that can be classified into cyclin groups I (green filled-in cells), II (blue filled-in cells), or III (orange filled-in cells). There are two transcription factors that contain the cyclin-like domain (IPR013763). The majority of the information in this table was obtained from the *Saccharomyces* genome database (SGD).

Protein Name	PomBase ID	Essential ?	Published CDK Partner	Cyclin Group I, II, or III	N-terminal cyclin domain (IPR006671)	C-terminal cyclin domain (IPR004367)	Cyclin Pho80-like domain (IPR013922)	Cyclin-like domain; also found in TFIIB and retinoblastoma-associated protein (IPR013763)
Cdc13	SPBC582.03	Yes	Cdc2/Cdk1	Group I	Yes	Yes		Yes
Cig1	SPCC4E9.02	No	Cdc2/Cdk1	Group I	Yes	Yes		Yes
Cig2	SPAPB2B4.03	No	Cdc2/Cdk1	Group I	Yes	Yes		Yes
Rem1	SPBC16E9.17c	No	Cdc2/Cdk1	Group I (meiosis specific cyclin)	Yes	Yes		Yes
Puc1	SPBC19F5.01c	No	Cdc2/Cdk1	Group I	Yes			Yes
Pas1	SPAC19E9.03	No	Pef1/Pho85, Cdc2/Cdk1?	Group II, PCL (PCL 1,2-like subfamily)			Yes	Yes
Clg1	SPBC1D7.03	No	Pef1/Pho85	Group II, PCL (PCL 1,2-like subfamily)			Yes	Yes
Psl1	SPBC20F10.10	No	Pef1/Pho85	Group II, PCL (Pho80-like subfamily)			Yes	
Pch1	SPBC32F12.06	Yes	Cdc2, Cdk9	Group III, Cyclin T-like	Yes	Yes		Yes
Srb11	SPBC12D12.06	No	Srb10	Group III, Cyclin C-like	Yes			Yes
Lcp1	SPAC1296.05c	No	Cdk11	Group III, Cyclin L-like	Yes			Yes
Mcs2	SPBP16F5.02	Yes	Mcs6	Group III, Cyclin H-like	Yes			Yes
Lsc1/ Ctk2	SPBC530.13	No	Lsk1	Group III, Cyclin T/K-like	Yes			Yes
*Sif2	SPCC16C4.01	No		None, Mitochondrial protein (does not fit in with groups)				Yes
**Crs1	SPBC2G2.09c	No		None, Meiosis specific cyclin (does not fit in with groups)	Yes			Yes
Brf1	SPBC13E7.10c	Yes		None, Transcription factor TFIIIB complex subunit				Yes
Sua7	SPAC16E8.16	Yes		None, Transcription Factor TFIIB				Yes

Table 3.2: Proteins with cyclin and cyclin-like domains in *Schizosaccharomyces pombe*

S. pombe contains 13 cyclins that can be classified into cyclin groups I (green filled-in cells), II (blue filled-in cells), or III (orange filled-in cells). There are an additional two proteins that contain cyclin and cyclin-like domains (Sif2 and Crs1) but do not share sequence homology to other *S. pombe* cyclins. There are also two transcription factors that contain the cyclin-like domain (IPR013763). The majority of the information in this table was obtained from Pombase.

Protein Name	CGD ID	Essential?	Published CDK Partner	Cyclin Group I, II, or III	N-terminal cyclin domain (IPR006671)	C-terminal cyclin domain (IPR004367)	Cyclin Pho80-like domain (IPR013922)	Cyclin-like domain; also found in TFIIB and retinoblastoma-associated protein (IPR013763)
Clb2	C2_01410C	Yes	Cdc28/Cdk1	Group I	Yes	Yes		Yes
Clb4	C7_03940C	No	Cdc28/Cdk1	Group I	Yes	Yes		Yes
Ccn1	C5_01680C	No	Cdc28/Cdk1	Group I	Yes	Yes		Yes
Cln3	C5_01100C	Yes (yeast growth)	Cdc28/Cdk1	Group I	Yes			Yes
Hgc1	C1_00780C	No	Cdc28/Cdk1	Group I	Yes			Yes
Pcl1	C5_03310C	No	Pho85	Group II, PCL (PCL 1,2-like subfamily)	Yes			Yes
Pcl2	C1_08570C	No		Group II, PCL (PCL 1,2-like subfamily)	Yes			Yes
Pcl5	C5_05190W	No	Pho85	Group II, PCL (PCL 1,2-like subfamily)	Yes			
Clg1	CR_07240C	No		Group II, PCL (PCL 1,2-like subfamily)			Yes	
Pcl7	C1_06850W			Group II, PCL (Pho80-like subfamily)			Yes	
	C3_02720W			Group II, PCL (Pho80-like subfamily)			Yes	
Pho80	C6_03810W		Pho85	Group II, PCL (Pho80-like subfamily)			Yes	
Ssn8	C3_05740C	No	Ssn3	Group III, Cyclin C-like	Yes			Yes
Ccl1	C1_01820C			Group III, Cyclin H-like	Yes			Yes
	C1_04090C	No		Group III, Cyclin T/K-like	Yes			Yes
Bur2	C5_02670W	No		Group III, Cyclin T/K-like	Yes			Yes
Brf1	CR_05650W			None, Transcription factor TFIIIB complex subunit				Yes
Sua71	C1_03560C			None, Transcription factor TFIIB				Yes
Sua72	CR_05490W			None, Predicted transcription factor				Yes

Table 3.3: Proteins with cyclin and cyclin-like domains in the dimorphic fungus *Candida albicans*

C. albicans contains 16 cyclins that can be classified into cyclin groups I (green filled-in cells), II (blue filled-in cells), or III (orange filled-in cells). There are also three transcription factors that contain the cyclin-like domain (IPR013763). The majority of the information in this table was obtained from the *Candida* genome database (CGD).

Protein Name	AspGD Designation	Essential?	Published CDK Partner	Cyclin Group I, II, or III	N-terminal cyclin domain (IPR006671)	C-terminal cyclin domain (IPR004367)	Cyclin Pho80-like domain (IPR013922)	Cyclin-like domain; also found in TFIIB and retinoblastoma-associated protein (IPR013763)
NimE	AN3648	Yes (Bergen *et al.* 1984; Morris, 1975)	NimX/Cdk1 (Osmani *et al.* 1994)	Group I	Yes	Yes		Yes
PucA	AN3795	Yes (this work)	NimX/Cdk1 (De Souza *et al.* 2014)	Group I	Yes	Yes		Yes
ClbA	AN2137	No (this work)		Group I	Yes	Yes		Yes
PclA	AN0453	No (Schier *et al.* 2001)	NimX/Cdk1 (Schier and Fischer 2002) PtkA (Bathe *et al.* 2010)	Group II (PCL1,2-like subfamily)	Yes			Yes
	AN9500			Group II, PCL (PCL1,2-like subfamily)			Yes	
ClgA	AN1096	No (Yu *et al.* 2014)		Group II, PCL (PCL1,2-like subfamily)			Yes	
	AN4984			Group II, PCL (PCL1,2-like subfamily)			Yes	
	AN3755			Group II, PCL (Pho80-like subfamily)			Yes	
PclB	AN10741	No (Kempf *et al.* 2013)	PtkA (Kempf *et al.* 2013)	Group II, PCL (Pho80-like subfamily)			Yes	Yes
An-Pho80	AN5156	No (Wu *et al.* 2004)	PhoA, PhoB (Wu *et al.* 2004)	Group II, PCL (Pho80-like subfamily)			Yes	
	AN2172			Group III, Putative cyclin C	Yes			Yes
	AN2211			Group III, Putative cyclin H	Yes			Yes
	AN7719			Group III, Putative cyclin L				Yes
	AN10640			Group III, Putative cyclin T/K	Yes			Yes
PchA	AN4981	No, very sick (Bathe *et al.* 2010)	PtkA (Bathe *et al.* 2010)	Group III, Putative cyclin T/K	Yes	Yes		Yes
	AN3116			None, Brf1-like (Transcription factor TFIIIB complex subunit)				Yes
	AN4928			None, Putative TFIIB (similar to yeast SUA7)				Yes

Table 3.4: Proteins with cyclin and cyclin-like domains in *Aspergillus nidulans*

A. nidulans contains 15 putative cyclins. If the cyclin has been previously studied, information on whether it is essential or not essential and/or any identified interacting cyclin-dependent kinase (CDK) partner(s) are provided. My determination of the classification of these cyclins into group I (green filled-in cells), group II (blue filled-in cells), or group III (orange filled-in cells) are shown along with any information about subfamily classification. Two proteins have a cyclin-like domain (IPR013763) in *A. nidulans* but do not share sequence similarity with known cyclins and do not cluster in the three groups of cyclins in our phylogenetic analyses (white filed-in cells). They do, however, share sequence similarity with human and yeast transcription factors TFIIB and TFIIB-related Brf1.

S. cerevisiae Protein Name			Cln1	Cln2	Cln3	Clb1	Clb2	Clb3	Clb4	Clb5	Clb6	Pcl1	Pcl2	Pcl5	Pcl9	Clg1	Pcl6	Pcl7	Pcl8	Pcl10	Pho80	Ssn8	Ccl1	Ctk2	Bur2	Brf1	Sua7
Cyclin Group	Protein	Gene ID (AspGD)	Information in cells: E-value																								
I	NimE	AN3648		3E-07	1E-08	4E-81	4E-85	2E-67	1E-60	5E-58	2E-59																
I	PucA	AN3795	1E-16	3E-15	4E-22	2E-62	6E-20	7E-26	1E-26	1E-17	3E-19																
I	ClbA	AN2137	1E-03	1E-04	1E-05	1E-15	1E-63	1E-86	5E-86	4E-52	1E-53																
II	PclA	AN0453										6E-36	3E-32	3E-02	1E-31						1E-03						
II		AN9500										5E-04	2E-05	9E-11	8E-05	1E-03	1E-07	3E-06									
II	ClgA	AN1096											1E-03	8E-06		1E-11	2E-04	1E-05									
II		AN4984										3E-03	7E-04	2E-03		5E-21	2E-03	4E-06									
II		AN3755															3E-43	2E-26			2E-07						
II	PclB	AN10741															2E-10	5E-17	1E-11	3E-11	2E-05						
II	Pho80	AN5156															2E-06	1E-14		2E-04	7E-32						
III		AN2172																				1E-57	8E-05				
III		AN2211																					7E-36				
III		AN7719																						5E-12			
III		AN10640																				4E-05	2E-06		2E-03		
III	PchA	AN4981																								4E-64	
Putative TFIIB-related Brf1		AN3116																									7E-10
Putative TFIIB		AN4928																									5E-64

Table 3.5: *Saccharomyces cerevisiae* versus *Aspergillus nidulans* cyclins

This table summarizes the results of BLASTP searches using the cyclins from *S. cerevisiae* (Table 3.1) as queries against the *Aspergillus nidulans* FGSCA4 (AspGD) protein database (default search parameters). The cell colors indicate the following: green (group I cyclins), blue (group II cyclins), orange (group III cyclins), and no color (transcription factors TFIIB and TFIIB-related Brf1). For *A. nidulans*, the cyclin group, protein name, and ID are indicated in the leftmost columns. The *S. cerevisiae* cyclin names are shown along the top row. The data in the cells are E-values and only E-values < 1 x 10-2 are shown.

S. Pombe Protein Name			Cdc13	Cig1	Cig2	Rem1	Puc1	Pas1	Clg1	Psl1	Pch1	Srb11	Lcp1	Mcs2	Lsc1/ Ctk2	Brf1	Sua7	*Sif2	**Crs1
Cyclin Group	Protein	Gene ID (AspGD)	Information in cells: E-value																
I	NimE	AN3648	1E-118	3E-62	3E-86	3E-42	2E-17												
I	PucA	AN3795	2E-31	4E-23	8E-29	2E-20	1E-32												
I	ClbA	AN2137	4E-80	7E-79	2E-69	7E-51	7E-19												
II	PclA	AN0453						7E-03											
II		AN9500						1E-24	1E-05	1E-04									
II	ClgA	AN1096						2E-09	2E-11	3E-06									
II		AN4984						2E-07	5E-25	8E-03									
II		AN3755						1E-04		3E-28									
II	PclB	AN10741								3E-19									
II	Pho80	AN5156								3E-14									
III		AN2172									3E-09	5E-29		7E-05	6E-05				
III		AN2211									5E-05			2E-26					
III		AN7719									2E-12	8E-03	6E-15						
III		AN10640									2E-13				2E-29				
III	PchA	AN4981									3E-54		1E-07						
Putative TFIIB-related Brf1		AN3116														6E-80	5E-09		
Putative TFIIB		AN4928														3E-07	2E-92		

Table 3.6: *Schizosaccharomyces pombe* versus *Aspergillus nidulans* cyclins

This table summarizes the results of BLASTP searches using the cyclins from *S. pombe* (Table 3.2) as queries against the *Aspergillus nidulans* FGSCA4 (AspGD) protein database (default search parameters). The cell colors indicate the following: green (group I cyclins), blue (group II cyclins), orange (group III cyclins), no color (transcription factors TFIIB and TFIIB-related Brf1), and gray (*S. pombe* proteins with cyclin-like domains that do not cluster into any of the three groups). For *A. nidulans*, the cyclin group, protein name, and ID are indicated in the leftmost columns. The *S. pombe* cyclin names are shown along the top row. The data in the cells are E-values and only E-values < 1 x 10-2 are shown. **S. pombe* Sif2 shares homology with *A. nidulans* AN10806 (6e-105). AN10806 does not have any predicted cyclin domains nor comes up in an BLASTP searches with-known cyclins. Sif2 was included as it has a predicted cyclin-like domain (IPR013763) via InterProScan. ** *S. pombe* Crs1 has no obvious homolog in *A. nidulans*. Crs1 was included as it has a predicted cyclin-like domain (IPR013763) via InterProScan.

C. Albicans Protein Name			Clb2	Clb4	Ccn1	Cln3	Hgc1	Pcl1	Pcl2	Pcl5	Clg1	Pcl7	*C3_02720W	Pho80	Ssn8	Ccl1	C1_04090C	Bur2	Brf1	Sua71	Sua72
Cyclin Group	Protein	Gene ID (AspGD)	Information in cells: E-value																		
I	NimE	AN3648	5E-89	5E-72	5E-30	4E-18	6E-13														
I	PucA	AN3795	5E-22	9E-30	7E-56	6E-35	3E-16														
I	ClbA	AN2137	4E-67	1E-101	9E-28	2E-13	7E-07														
II	PclA	AN0453						5E-38	2E-35					5E-04							
II		AN9500						5E-06	2E-05	3E-11		5E-06		8E-04							
II	ClgA	AN1096						3E-04			4E-07	1E-05		4E-04							
II		AN4984						2E-04			2E-15	3E-04		4E-06							
II		AN3755										5E-47		8E-12							
II	PclB	AN10741										4E-13		5E-09							
II	Pho80	AN5156							4E-04			2E-08		1E-30							
III		AN2172													3E-53	1E-04	3E-05				
III		AN2211														4E-34					
III		AN7719																			
III		AN10640															4E-05				
III	PchA	AN4981													1E-05	2E-05	1E-04	1E-19			
Putative TFIIB-related Brf1		AN3116																	2E-66	1E-06	1E-04
Putative TFIIB		AN4928																	2E-09	2E-82	6E-65

Table 3.7: *Candida albicans* versus *Aspergillus nidulans* cyclins

This table summarizes the results of BLASTP searches using the cyclins from *C. albicans* (Table 3.3) as queries against the *Aspergillus nidulans* FGSCA4 (AspGD) protein database (default search parameters). The cell colors indicate the following: green (group I cyclins), blue (group II cyclins), orange (group III cyclins), and no color (transcription factors TFIIB and TFIIB-related Brf1). For *A. nidulans*, the cyclin group, protein name, and ID are indicated in the leftmost columns. The *C. albicans* cyclin names are shown along the top row. The data in the cells are E-values and only E-values < 1 x 10-2 are shown. **C. albicans* C3_02720W has no obvious homolog in *A. nidulans*.

Human Protein Name			Cyclin A1	Cyclin A2	Cyclin B1	Cyclin B2	Cyclin B3	Cyclin D1	Cyclin D2	Cyclin D3	Cyclin E1	Cyclin E2	Cyclin F	Cyclin G1	Cyclin G2	Cyclin I	Cyclin I2	Cyclin J	Cyclin J-like	Cyclin O	Cyclin Y	Cyclin Y-like protein 1	Cyclin C	Cyclin H	Cyclin K	Cyclin L1	Cyclin L2	Cyclin M (Fam58A)	Fam58B	Cyclin T1	Cyclin T2	TFIIB	Brf1
Cyclin Group	Protein	Gene ID (AspGD)																															
I	NimE	AN3648	6E-49	1E-38	2E-57	5E-61	1E-40	2E-14	3E-13	1E-11	5E-20	3E-17	3E-18	8E-04	5E-04	2E-07	6E-05	1E-07	9E-07	3E-20														4E-68
I	PucA	AN3795	3E-19	2E-19	8E-19	6E-17	3E-15	1E-06	3E-05	8E-02	6E-08	3E-06	7E-15	4E-05	8E-02	1E-04	4E-02	2E-09		7E-16												6E-11	3E-05
I	ClbA	AN2137	6E-48	1E-38	1E-48	1E-53	6E-46	9E-17	3E-12	6E-13	9E-19	1E-19	2E-14	3E-05	2E-05	2E-08	6E-03	2E-06	2E-01	7E-20												9E-54	
II	PclA	AN0453																															
II		AN9500																															
II	ClgA	AN1096																			1E-02												
II		AN4984																				4E-02											
II		AN3755																			2E-02												
II	PclB	AN10741																															
II	Pho80	AN5156																															
III		AN2172																					6E-29	4E-12	5E-12	1E-03	2E-05	4E-05	4E-03	4E-07	7E-07			
III		AN2211																					3E-04	1E-24	3E-04					3E-04	2E-02			
III		AN7719																							2E-08	7E-21	8E-25	2E-08		2E-13	3E-12			
III		AN10640																					2E-02		8E-19	2E-07	6E-07	2E-04	4E-01	5E-16	2E-14			
III	PchA	AN4981																					8E-13	3E-03	1E-27	8E-18	1E-19	2E-14	3E-10	7E-20	4E-23			
Putative TFIIB-related Brf1		AN3116																														6E-11	4E-68
Putative TFIIB		AN4928																														9E-54	3E-05

Table 3.8: Human versus *Aspergillus nidulans* cyclins

This table summarizes the results of BLASTP searches using human cyclins as queries against the *Aspergillus nidulans* FGSCA4 (AspGD) protein database (default search parameters). The cell colors indicate the following: green (group I cyclins), blue (group II cyclins), orange (group III cyclins), and no color (transcription factors TFIIB and TFIIB-related Brf1). For *A. nidulans*, the cyclin group, protein name, and ID are indicated in the leftmost columns. The human protein names are shown along the top row. The data in the cells are E-values.

3.2.2 The complement of cyclins is highly conserved in filamentous ascomycetes

I conducted BLASTP searches of the NCBI protein database for cyclins in the 31 filamentous ascomycetes analyzed in de Vries *et al.* (2017) using the amino acid sequences of *A. nidulans* cyclins as a query. The most striking (and perhaps surprising) result of these analyses was the degree of conservation among cyclins, not just in the *Aspergillus* species, but also in the other species which are phylogenetically diverse. In most of the fungi analyzed, I identified a single, strong homolog of each of the fifteen cyclins present in *A. nidulans.* A few absences were observed, which may, in part, be due to annotation errors. A few incidents of gene duplication were also observed (discussed below). The results of the BLASTP searches is summarized in **Table 3.9**.

Consistent with previous work, my phylogenetic analyses of all putative cyclins from the 32 species, including *A. nidulans*, indicate that the cyclins fall into three major groups. The cyclins in group I are the most highly conserved of the three groups based on E-value, query coverage, and the lack of any gene duplications or absences (**Table 3.10**). All species I analyzed have three identifiable group I cyclins. They fall into two groups that I designate Cln-like and B-type. The B-type cyclins further fall into two well-separated clades. The group I cyclins from filamentous ascomycetes, thus, fall into three clades with each fungus having a single member of each clade (**Fig. 3.1**). The *A. nidulans* members of the three clades are PucA, NimE$^{\text{Cyclin B}}$, and ClbA.

The *A. nidulans* group II cyclins do not share strong sequence homology with either group I or group III cyclins, and they only appeared as "hits" when I conducted BLASTP searches using the model yeasts group II cyclins as queries. The majority of the species in my study have seven group II cyclins that are strong homologs of the seven *A. nidulans* group II cyclins. I also observed two subfamilies (Pcl1,2 and Pho80 subfamilies) similar to those observed in *S. cerevisiae.*

However, some evidence of gene duplications was observed with group II cyclins. For example, I found that both *Penicillium chrysogenus* and *Penicillium rubens* have three PclA-like proteins and three Pho80-like proteins while *Penicillium digitatum* has only one copy of each. There are three species with only six group II cyclins, all of which were lacking one member of the Pho80 subfamily. However, the missing cyclins could be due to missing or inaccurate annotations. These results are summarized in **Table 3.9**.

The group III cyclins in *A. nidulans* also do not share strong sequence similarities with either group I or group II cyclins. They are easily detected in BLASTP searches, however, using group III cyclins from yeasts as queries. Group III cyclins are well-conserved in the species in our study. The majority of the species analyzed have only five group III cyclins and they are strong homologs of the *A. nidulans* group III cyclins. Only four species have four instead of five cyclins, but in at least three of the four cases, another sequenced strain of the same species has all five cyclins, so the apparent absence may simply be due to sequencing or annotation error. I did not observe any gene duplications in this group. These results are summarized in **Table 3.9**.

	Species	Group I		Group II						Group III				Total
		Cln-like	B-type	PCL 1,2,9-	PCL 5-like	Clg1-like	Pho80-like	PCL 6,7-like	PCL 8,10-like	C-like	H-like	L-like	T/K-like	
Yeasts	*Saccharomyces cerevisiae*	3	6	3	1	1	1	2	2	1	1	-	2	23
	Schizosaccharomyces pombe	1	4	-	1	1	-	1	-	1	1	1	2	13*
	Candida albicans	3	2	2	1	1	1	1	1	1	1	-	2	16
Filamentous Fungi	***Aspergillus nidulans***	**1**	**2**	**1**	**1**	**2**	**1**	**1**	**1**	**1**	**1**	**1**	**2**	**15**
	Aspergillus niger	1	2	1	1	2	1	1	1	1	1	1	2	15
	Aspergillus luchuensis	1	2	1	1	2	1	1	1	1	1	NH	2	14
	Aspergillus tubingensis	1	2	1	1	2	1	1	1	1	1	1	2	15
	Aspergillus brasiliensis	1	2	1	1	2	1	1	1	1	1	1	2	15
	Aspergillus carbonarius	1	2	1	1	1	1	1	2	1	1	1	1	14
	Aspergillus aculeatus	1	2	1	1	2	1	1	1	1	1	1	2	15
	Aspergillus versicolor	1	2	1	1	2	1	1	1	1	1	1	2	15
	Aspergillus sydowii	1	2	1	1	2	1	1	1	1	1	1	2	15
	Aspergillus flavus	1	2	1	1	2	1	1	1	1	1	1	2	15
	Aspergillus oryzae	1	2	1	1	2	1	1	1	1	1	1	2	15
	Aspergillus terreus	1	2	1	1	2	1	1	1	1	1	1	2	15
	Aspergillus fumigatus	1	2	1	1	2	1	1	1	1	1	1	2	15
	Aspergillus fischeri	1	2	1	1	2	1	1	1	1	1	1	2	15
	Aspergillus clavatus	1	2	1	1	2	1	1	1	1	1	1	2	15
	Aspergillus glaucus	1	2	1	1	2	NH	1	1	1	1	1	2	14
	Aspergillus wentii	1	2	1	1	2	1	1	1	1	1	1	2	15
	Penicillium chrysogenum	1	2	3	1	2	3	1	1	1	1	1	2	19
	Penicillium rubens	1	2	3	1	2	3	1	1	1	1	1	2	19
	Penicillium digitatum	1	2	1	1	2	1	1	1	1	1	1	2	15
	Aspergillus zonatus	1	2	1	1	2	1	1	1	1	1	1	2	15
	Talaromyces marneffei	1	2	1	1	2	1	1	1	1	1	1	2	15
	Talaromyces stipitatus	1	2	1	1	2	1	1	1	1	1	1	2	15
	Coccidioides immitis	1	2	1	1	2	1	1	1	NH	1	1	2	14
	Coccidioides posadasii	1	2	1	1	2	1	1	1	1	1	1	2	15
	Uncinocarpus reesii	1	2	1	1	2	1	1	1	1	1	1	2	15
	Microsporum canis	1	2	1	1	2	1	1	NH	1	1	1	2	14
	Trichophyton rubrum	1	2	1	1	2	1	1	NH	1	1	1	2	14
	Histoplasma capsulatum	1	2	1	1	2	1	1	1	NH	1	1	2	14
	Paracoccidioides brasiliensis	1	2	1	1	2	1	1	1	1	1	1	2	15
	Trichoderma reesei	1	2	1	1	2	1	1	1	1	1	1	2	15
	Neurospora crassa	1	2	1	1	2	1	1	1	1	1	1	2	15

Table 3.9: Cyclins in ascomycetes

Table summarizing the number of cyclins in group I, group II, and group III in three model yeasts (*Saccharomyces cerevisiae, Schizosaccharomyces pombe,* and *Candida albicans*) and in 32 filamentous ascomycetes, including *Aspergillus nidulans* (red bold font). Cyclin subfamilies are indicated at the top, and the total number of cyclins identified in each organism is at the far right. NH = no hits. Asterisk indicates that *S. pombe* contains 13 obvious cyclins, but there are an additional 2 proteins present in *S. pombe* with cyclin-like domains that have no significant sequence similarity to cyclins in humans or other fungi.

Table 3.10 *(continued on next page)*

Species	Strain	Class	Order	Section	Genome size (Mb)	Total # of Group I Cyclins	Cyclins homologous to *A. nidulans* NimE NCBI/GenBank Accession: query cover; E-value; % Ident	Cyclins homologous to *A. nidulans* ClbA NCBI/GenBank Accession: query cover; E-value; % Ident	Cyclins homologous to *A. nidulans* PucA NCBI/GenBank Accession: query cover; E-value; % Ident	Notes
Aspergillus niger	ATCC1015	Eurotiomycetes	Eurotiales	*Nigri*	35	3	EHA26624.1: 97%; 0.0; 78%	EHA24861: 98%; 0.0; 68%	EHA24246.1: 99%; 0.0; 85%	
Aspergillus luchuensis	CBS106.47	Eurotiomycetes	Eurotiales	*Nigri*	37	3	OJZ92350.1: 97%; 0.0; 78%	OJZ85680.1: 98%; 0.0; 68%	OJZ83391.1: 99%, 0.0; 85%	
Aspergillus tubingensis	CBS134.48	Eurotiomycetes	Eurotiales	*Nigri*	35	3	OJI86778.1: 99%; 0.0; 78%	OJI79470: 98%; 0.0; 68%	OJI82277.1: 99%; 0.0; 85%	
Aspergillus brasiliensis	CBS101740	Eurotiomycetes	Eurotiales	*Nigri*	36	3	OJJ74767.1: 97%; 0.0; 78%	OJJ66903.1: 99%; 0.0; 67%	OJJ72880.1: 99%; 0.0; 85%	
Aspergillus carbonarius	ITEM 5010	Eurotiomycetes	Eurotiales	*Nigri*	36	3	OOF95759.1: 97%; 0.0; 79%	OOF91673.1: 92%; 0.0; 71%	OOF96073.1: 99%; 0.0; 84%	
Aspergillus aculeatus	ATCC 16872	Eurotiomycetes	Eurotiales	*Nigri*	35	3	XP_020054161.1: 99%; 0.0; 72%	XP_020053462.1: 99%, 0.0; 67%	XP_020059391.1: 99%, 0.0; 86%	
Aspergillus versicolor	CBS583.65	Eurotiomycetes	Eurotiales	*Nidulantes*	33	3	OJJ05686.1: 97%; 0.0; 93%	OJI99157.1: 99%; 0.0; 81%	OJJ02440.1: 99%; 0.0; 93%	
Aspergillus sydowii	CBS593.65	Eurotiomycetes	Eurotiales	*Nidulantes*	34	3	OJJ57494.1: 97%; 0.0; 93%	OJJ65038 : 99%; 0.0; 80%	OJJ59848.1: 99%; 0.0; 94%	
Aspergillus flavus	NRRL3357	Eurotiomycetes	Eurotiales	*Flavi*	37	3	XP_002374333.1: 95%; 0.0; 72%	XP_002375485.1: 91%; 0.0; 69%	XP_002373665.1: 99%; 0.0; 88%	
Aspergillus oryzae	RIB40	Eurotiomycetes	Eurotiales	*Flavi*	38	3	XP_001820104.2: 99%, 0.0; 76%	XP_001727241.2: 97%; 0.0; 69%	XP_001818433.1: 99%; 0.0; 88%	
Aspergillus terreus	NIH2624	Eurotiomycetes	Eurotiales	*Terrei*	29	3	XP_001213030.1: 99%; 0.0; 79%	XP_001211507.1: 99%; 0.0; 68%	**XP_001212824.1: 32%; 3e-88; 93%** *See note	XP_001212824.1 is not annotated correctly. Upstream of the predicted start is a string of Ns (gap in sequencing).
Aspergillus fumigatus	Af293	Eurotiomycetes	Eurotiales	*Fumigati*	29	3	XP_751615.2: 99%; 0.0; 82%	XP_755950.1: 97%; 0.0; 67%	XP_749524.1: 99%; 0.0; 82%	
Aspergillus fischeri	NRRL181	Eurotiomycetes	Eurotiales	*Fumigati*	33	3	XP_001266819.1: 93%; 0.0; 81%	XP_001261079.1: 97%; 0.0; 67%	XP_001260026.1: 99%; 0.0; 84%	
Aspergillus clavatus	NRRL1	Eurotiomycetes	Eurotiales	*Clavati*	28	3	XP_001272070.1: 99%; 0.0; 83%	XP_001275899.1: 97%; 0.0; 68%	XP_001272792.1: 99%; 0.0; 83%	
Aspergillus glaucus	CBS516.65	Eurotiomycetes	Eurotiales	*Aspergillus*	30	3	OJJ82151.1: 98%; 0.0; 76%	OJJ88540.1: 98%; 0.0; 59%	OJJ83795.1: 99%; 0.0; 81%	
Aspergillus wentii	DTO 134E9	Eurotiomycetes	Eurotiales	*Cremei*	31	3	OJJ40519.1: 97%; 0.0; 79%	OJJ37536.1: 99%; 0.0; 67%	OJJ35557.1: 95%; 0.0; 85%	
Penicillium chrysogenum	unknown (taxid:5076)	Eurotiomycetes	Eurotiales	*Chrysogena*	31	3	KZN85804.1: 97%; 0.0; 73%	KZN88022.1: 97%; 0.0; 50%	KZN92176.1: 97%; 0.0; 70%	
Penicillium rubens	Wisconsin 54-1255	Eurotiomycetes	Eurotiales	*Chrysogena*	32	3	XP_002564565.1: 94%; 0.0; 73%	XP_002567256.1: 97%; 0.0; 50%	XP_002562322.1: 97%; 0.0; 70%	
Penicillium digitatum	PHI26	Eurotiomycetes	Eurotiales	*Penicillium*	26	3	EKV12836.1: 94%; 0.0; 73%	EKV07686.1: 97%; 0.0; 50%	EKV09446.1: 97%; 0.0; 70%	
Aspergillus zonatus	CBS506.65	Eurotiomycetes	Eurotiales	*Unclassified*	29	3	OJJ49378.1: 99%; 0.0; 78%	OJJ51202.1: 99%; 0.0; 65%	OJJ46953.1: 94%; 0.0; 79%	
Talaromyces marneffei	ATCC18224	Eurotiomycetes	Eurotiales	*Talaromyces*	29	3	XP_002151367.1: 96%; 0.0; 72%	XP_002145534.1: 98%; 0.0; 55%	XP_002149039.1: 93%; 0.0; 72%	
Talaromyces stipitatus	ATCC10500	Eurotiomycetes	Eurotiales	*Talaromyces*	36	3	XP_002341657.1: 97%; 0.0; 73%	XP_002486999.1: 75%; 0.0; 82%	XP_002485137.1: 97%; 0.0; 68%	
Coccidioides immitis	RS	Eurotiomycetes	Onygenales		29	3	XP_001247875.1: 96%; 0.0; 67%	XP_001239907.2: 97%; 0.0; 51%	XP_001240904.1: 99%; 0.0; 71%	
Coccidioides posadasii	C735 delta SOWgp	Eurotiomycetes	Onygenales		27	3	XP_003065605.1: 96%; 0.0; 66%	XP_003067420.1: 97%; 0.0; 52%	XP_003065211.1: 99%; 0.0; 71%	
Uncinocarpus reesii	1704	Eurotiomycetes	Onygenales		22	3	XP_002584683.1: 93%; 0.0; 67%	XP_002584103.1: 96%; 0.0; 51%	XP_002542833.1: 95%; 0.0; 71%	
Microsporum canis	CBS113480	Eurotiomycetes	Onygenales		23	3	XP_002844305.1: 92%; 0.0; 63%	XP_002848334.1: 97%; 0.0; 56%	XP_002849563.1: 93%; 0.0; 70%	
Trichophyton rubrum	CBS118892	Eurotiomycetes	Onygenales		23	3	XP_003232490.1: 96%; 0.0; 63%	XP_003234697.1: 97%; 0.0; 54%	**XP_003233977.1: 63%; 5e-161; 76%** *See note	*XP_003233977.1 is not annotated correctly (sequencing gap). Another strain (Trichophyton_rubrum_CBS_202.88_EZG20130.1) has a strong homolog of PucA (EZG20130.1: 93%; 0.0; 62%)
Histoplasma capsulatum	NAm1	Eurotiomycetes	Onygenales		33	3	**XP_001544431.1: 44%; 1e-56; 54%** *See note	XP_001538844.1: 97%; 0.0; 57%	XP_001536868.1: 96%; 0.0; 73%	*XP_001544431.1 is not annotated correctly (sequencing gap). Another strain (Histoplasma_capsulatum_G186AR_EEH08047.1) has a strong homolog of NimE (EEH08047.1: 98%; 0.0; 68%)
Paracoccidioides brasiliensis	Pb03	Eurotiomycetes	Onygenales		29	3	EEH21027.1: 97%; 0.0; 69%	EEH20407.2: 77%; 0.0; 82%	EEH20492.1: 96%; 0.0; 70%	
Trichoderma reesei	QM6a	Sordariomycetes	Hypocreales		33	3	XP_006963161.1: 93%; 0.0; 60%	XP_006969069.1: 96%; 2e-168; 47% PARTIAL	XP_006965634.1: 93%; 9e-134; 55%	
Neurospora crassa	OR74A	Sordariomycetes	Sordariales		41	3	XP_963851.1 Clb1: 99%; 2e-175; 56%	XP_961608.2 Clb3: 53%; 8e-167; 69%	XP_964108.1 Cln1: 91%; 5e-138; 54%	

*This portion of the table was adapted from de Vries *et al.* (2017)

(continued from previous page)

Table 3.10: BLASTP analysis: Group I cyclins in 31 filamentous ascomycetes
Aspergillus nidulans group I cyclin protein sequences (NimE, ClbA, PucA) were used as queries in BLASTP searches of the NCBI nonredundant protein database (default search parameters) to identify cyclins in 31 filamentous ascomycetes. This table summarizes the results of those searches. All filamentous ascomycetes analyzed had a single strong homolog of each of the *A. nidulans* group I cyclins. I have included, for each putative group I cyclin, the NCBI/GenBank accession and the query cover, E-value, and % identity to its respective *A. nidulans* group I cyclin homolog. Other than what is listed in the table, I did not identify any additional proteins in these filamentous fungi with homology to *A. nidulans* group I cyclins (E-value < 10-2). Bold purple font = slightly lower homology than expected (see notes in rightmost column).

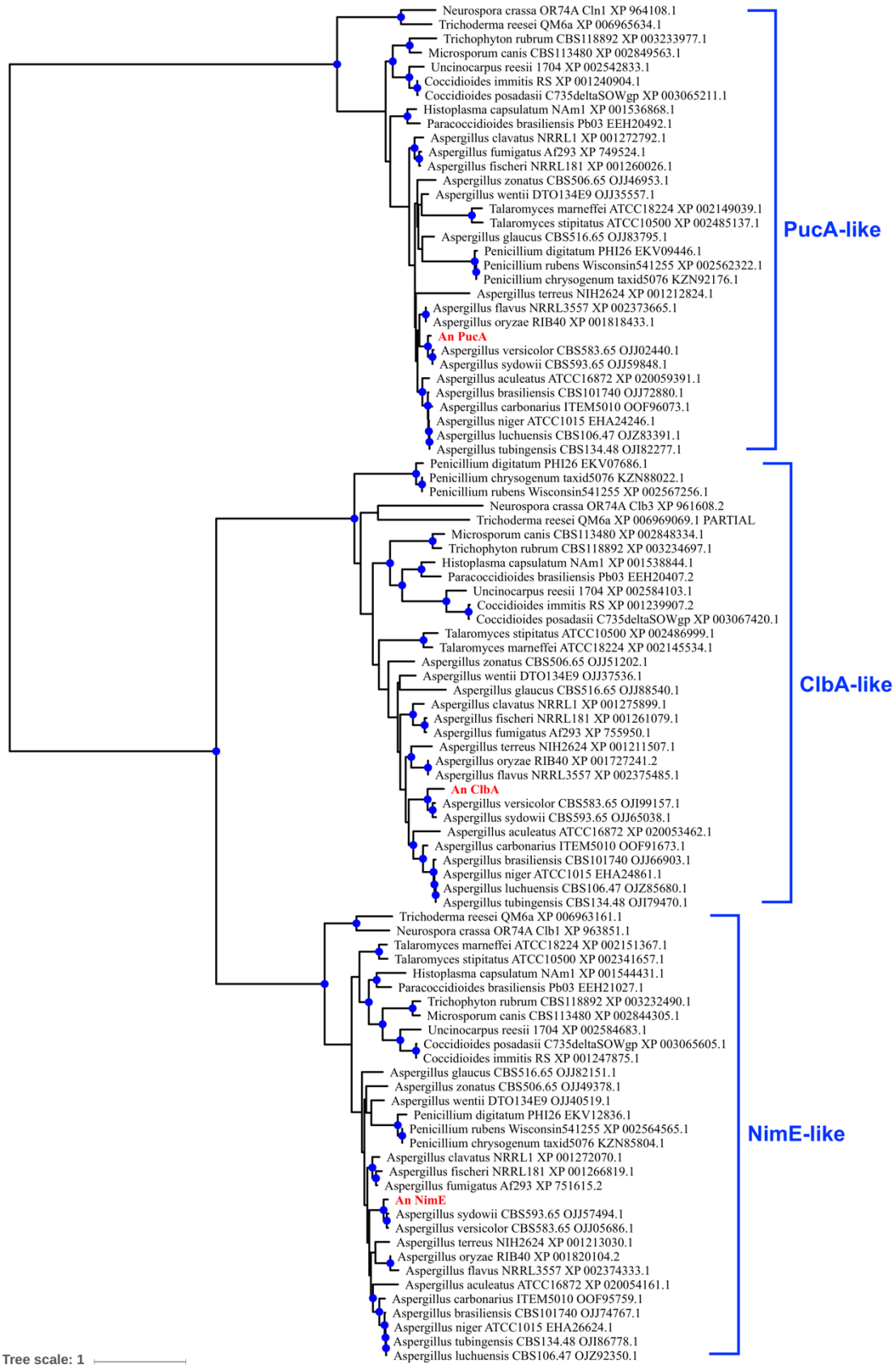

Figure 3.1 *(continued on next page)*

(continued from previous page)

Figure 3.1: Group I cyclins in 32 filamentous ascomycetes
Midpoint-rooted maximum-likelihood phylogenetic tree of group I cyclins in 18 species of *Aspergillus* and 14 members of other genera of filamentous ascomycetes. The group I cyclins in the model filamentous fungus *Aspergillus nidulans* (An) are shown in bold, red font. All filamentous ascomycetes analyzed in this work have three group I cyclins and, as they are strongly homologous to the *A. nidulans* group I cyclins, we designate the three clades of group I cyclins as PucA-like, ClbA-like, or NimE-like (bold, blue font). The species name, strain name, and NCBI/GenBank accession for each group I cyclin is shown. Blue circles indicate well-supported nodes (bootstrap values 70% or greater).

3.2.3 Model yeasts and filamentous ascomycetes contain different complements of cyclins

The yeasts *S. cerevisiae* and, in particular, *S. pombe*, have been instrumental in revealing the general principles of cell cycle regulation. The pathogenic fungus *C. albicans* has also been studied extensively because of its significance as a pathogen. I will refer to *C. albicans* as a yeast, although it is dimorphic and has both yeast and filamentous phases. Since these are well-studied ascomycetes, one might expect that they would be good models for understanding cyclin function in aspergilli and other filamentous ascomycetes. These model yeasts are quite phylogenetically distant, however, from the aspergilli and other members of the Pezizomycotina which make up the great majority of filamentous ascomycetes. The sole filamentous ascomycete in which the functions of group I cyclins have been studied at some depth is *Ashbya gossypii*. *A. gossypii* is a member of the Saccharomycotina, however, and is thus closely related to *S. cerevisiae* and related yeasts and quite distant, phylogenetically, from the great majority of filamentous ascomycetes (Wang *et al.*, 2009).

My analyses reveal that the complement of cyclins in the fungi in my study is significantly different from those of *S. cerevisiae, S. pombe* and *C. albicans*. For simplicity, I will present my

comparison of the cyclins of *A. nidulans* to those of these model yeasts, but, as mentioned, *A. nidulans* fairly reflects the complement of cyclins in the other fungi in my study. The sequence homology and phylogenetic relationships between *A. nidulans* and the three model yeasts is shown in **Tables 3.5-3.7** and **Fig. 3.2-3.3**.

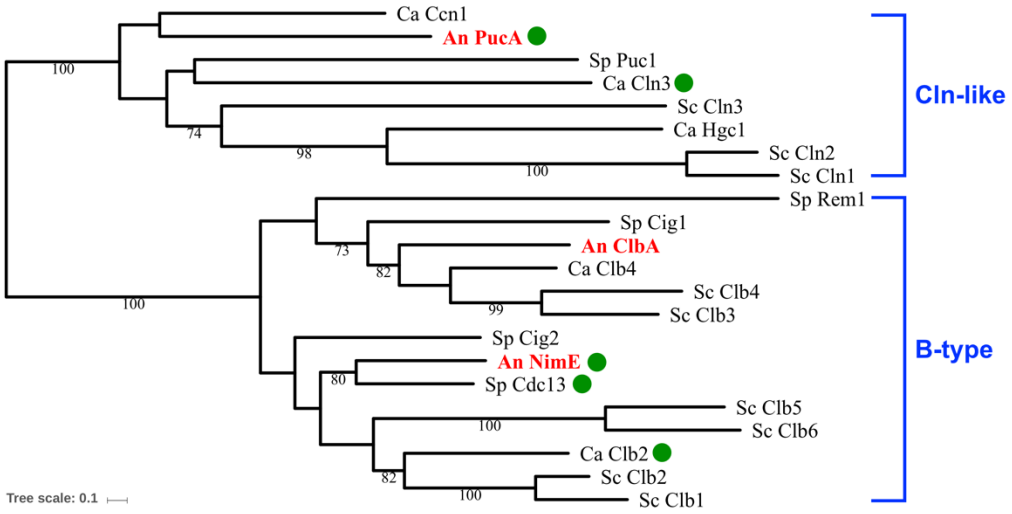

Figure 3.2: Group I cyclin complements of model yeasts and *A. nidulans*
Midpoint-rooted maximum-likelihood phylogenetic tree of group I cyclins in *Aspergillus nidulans* (An), *Saccharomyces cerevisiae* (Sc), *Schizosaccharomyces pombe* (Sp), and *Candida albicans* (Ca). Fungal group I cyclins cluster into two subfamilies, which are indicated in blue font. The abbreviated name of the fungal organism (e.g. An) is followed by the protein name. Cyclins that have been published as essential, or that we have determined are essential in this work, have green dots to the right of their name. Branch support values (70-100% bootstrap support) are displayed on the branches.

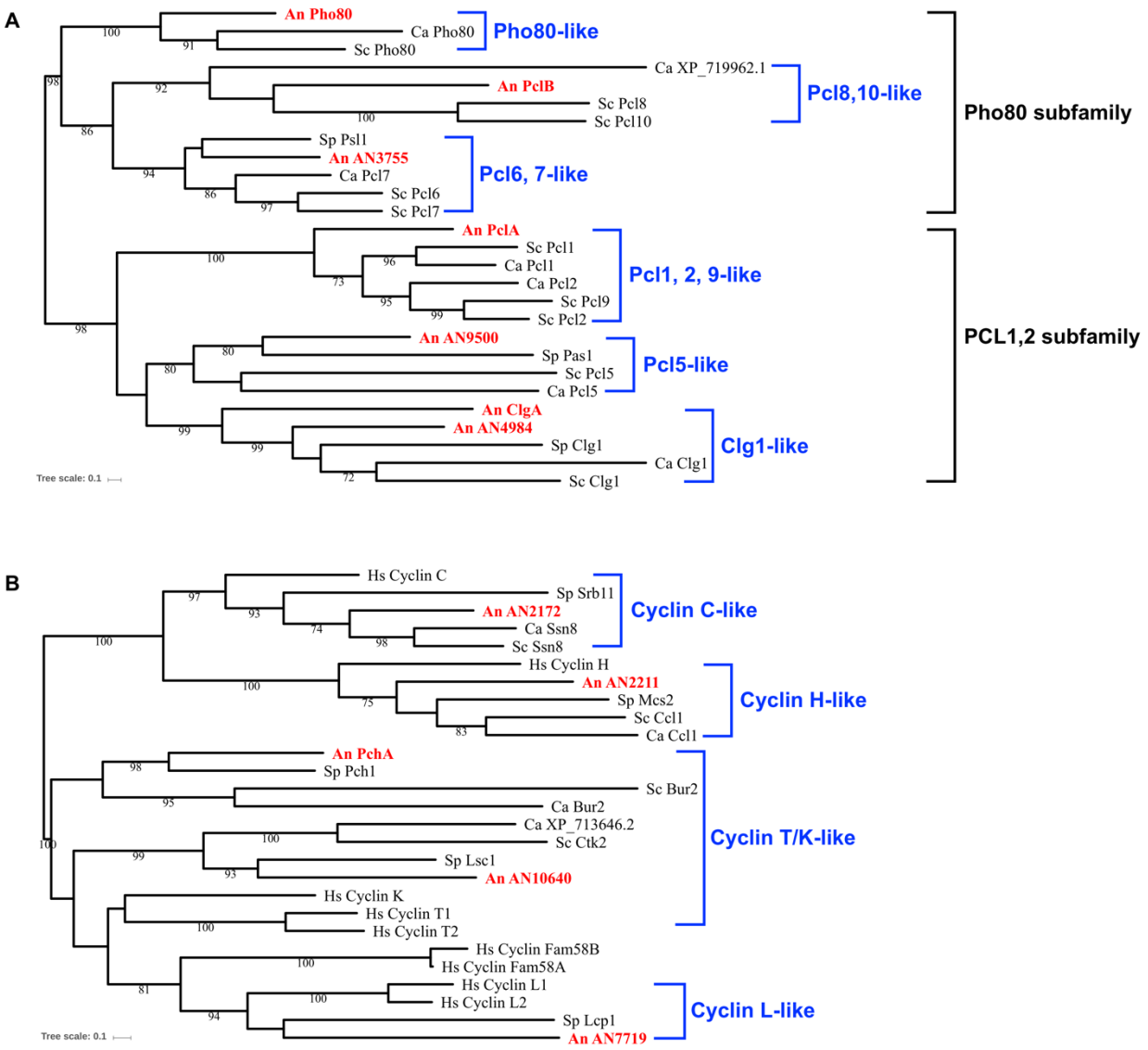

Figure 3.3: Group II and III cyclin complements of model yeasts and *A. nidulans*
Midpoint-rooted maximum-likelihood phylogenetic trees of group II **(A)** and group III **(B)** cyclins in *Aspergillus nidulans* (An), *Saccharomyces cerevisiae* (Sc), *Schizosaccharomyces pombe* (Sp), and *Candida albicans* (Ca). The name of the fungal organism (e.g. An) is followed by the protein name, and *A. nidulans* group I cyclin homologs are shown in bold, red font. **(A)** Fungal group II cyclins cluster into two subfamilies (Pho80 and PCL1,2) which are indicated in bold, black font. They also cluster reliably into 6 clades, which I designate as the following after the *S. cerevisiae* group II cyclin members: Pho80-like, PCL8,10-like, PCL6,7-like, PCL1,2,9-like, PCL5-like, and Clg1-like (bold, blue font). **(B)** As group III cyclins from both humans and fungi separate into several distinct clades, I included the human group III cyclins in this analysis and named the clades

after the human group III cyclin member(s) (bold, blue font). Cyclin C-like and cyclin H-like subfamilies are particularly well-conserved. A cyclin-L like homolog is only found in humans, A. nidulans, and S. pombe. The cyclin T/K-like fungal cyclins do not cluster strongly with huamn cyclins T and K in our phylogenetic analysis despite the fact that they share the most sequence similarity to cyclins T and K in humans. However, previous work determined that the common ancestor for cyclins T and K originated early in evolutionary history and that homologous proteins of the cyclin T and K subfamily in fungi could only be identified as a common ancestor of the two subfamilies (Cao et al., 2014). Thus, I tentatively designate these groups of cyclins as cyclin T/K-like.

With respect to group I cyclins, the most obvious difference between *A. nidulans* and the model yeasts is that whereas *A. nidulans* has only three group I cyclins, *S. cerevisiae, S. pombe and C. albicans* have nine, five and five group I cyclins respectively (**Table 3.9**, **Fig. 3.2**). *S. cerevisiae* and *S. pombe* have six and four B-type cyclins respectively whereas *A. nidulans* and *C. albicans* have only two. *S. cerevisiae* and *C. albicans* each have three cln-like cyclins, while *S. pombe* and *A. nidulans* have only a single cln-like cyclin. The multiplicity of cyclins in *S. cerevisiae* may reflect an ancient whole genome duplication (Wolfe and Shields, 1997). This may have resulted in functional redundancy accounting for the fact that none of the cyclins are individually essential in this organism. *S. pombe* and *C. albicans* are not thought to have undergone whole genome duplications, and the extra cyclins likely have arisen through individual gene duplications. *A. gossypii* has five group I cyclins, including two cln-like cyclins and three B-type cyclins. One of the two cln-type cyclins is essential and two of the B-type cyclins are essential (Hungerbuehler *et al.*, 2007).

The number of group II cyclins varies significantly among model yeasts and differs between the model yeasts and *A. nidulans.* Group II cyclins in the three model yeasts are called Pho85 cyclins (PCLs) after their interacting CDK partner, Pho85. PCLs were first identified and

characterized in *S. cerevisiae. S. cerevisiae* has ten PCLs and they separate into two sub-families: the Pcl1,2 subfamily (Pcl1, Pcl2, Pcl5, Pcl9, and Clg1) and the Pho80 subfamily (Pho80, Pcl6, Pcl7, Pcl8, and Pcl10) (Measday *et al.*, 1997). *S. pombe* in contrast has only three group II cyclins. *A. nidulans* has seven group II cyclins, PclA, AN9500, ClgA, AN4984, AN3755, PclB, and Pho80, that cluster with group II cyclins (**Table 3.9**, **Fig. 3.3A**) as does *C. albicans.* Although the number is the same, the complement of cyclins in *C. albicans* and *A. nidulans* is significantly different. For example, *C. albicans* has an uncharacterized cyclin (C3_02720W) that has no obvious homolog in *A. nidulans.* In addition, *A. nidulans* has two *clg1*-like genes (*clgA* and an uncharacterized gene AN4984), while *C. albicans* has only one *clg1* gene. Based on the sequence homology and phylogenetic analyses of these four fungi, I observe six major clades of PCL cyclins which I designate as the following, based on the *S. cerevisiae* PCL naming scheme: Pcl1,2,9-like, Pcl5-like, Clg1-like, Pho80-like, Pcl6,7-like, and Pcl8,10-like. The sequence homology and phylogenetic relationship between *A. nidulans* and model yeasts group II cyclins is shown in **Tables 3.5-3.7** and **Fig. 3.3A**.

A. nidulans has five group III cyclins that I named after the human group III cyclin counterpart: AN2172 (cyclin C-like), AN2211 (cyclin H-like), AN7719 (cyclin L-like), and PchA and AN10640 (cyclin T/K-like) (**Table 3.9, Fig. 3.3B**). The cyclin C-like and cyclin H-like families are well-conserved with the three model yeasts and with humans. However, a cyclin L-like homolog is not found in *S. cerevisiae* and *C. albicans*, but is found in *S. pombe*, *A. nidulans*, and all of the filamentous ascomycetes analyzed in this study.

3.3 Discussion

Given the significance of cyclins in cell cycle regulation and cell growth, there has been surprisingly little study of cyclins in filamentous ascomycetes. I report the identification and phylogenetic analysis of all cyclin domain-containing proteins in the model filamentous fungus *A. nidulans* as well as 31 diverse filamentous ascomycetes. My analyses reveal that cyclins in these species fall into three distinct groups as is the case for other eukaryotes that have been studied (Cao *et al.*, 2014; Ma *et al.*, 2013). My analyses also revealed that the cyclin repertoires of *Aspergilli* and the other species in my study are remarkably similar. These species include phylogenetically diverse members of the subdivision Pezizomycotina, which includes most filamentous ascomycetes. It follows that the complement of cyclins is highly conserved throughout filamentous ascomycetes. It is worth noting, however, that there may be functional specializations of cyclins, particularly non-essential cyclins, that do not change the number or phylogenetic relationships of the cyclins.

3.3.1 Group I cyclins

All of the filamentous ascomycetes analyzed in this study have three group I cyclins that fall into three distinct clades. Two clades cluster more strongly together, and the cyclins in these two clades are B-type cyclins. The cyclins in the third clade are more similar to yeast "Cln-like" cyclins than to B-type cyclins. Importantly, each species has only a single member of each of these three clades. Group I cyclins in filamentous ascomycetes are less numerous than in the model yeasts, *S. cerevisiae, S. pombe* and *C. albicans*. In particular, *S. cerevisiae* has nine group I cyclins, none of which are essential for cell cycle progression. The multiplicity of cyclins in *S. cerevisiae*

is likely the consequence of a whole genome duplication (Wolfe and Shields, 1997), resulting in functional redundancy.

3.3.2 Group II cyclins

Most of the species I have analyzed have seven group II cyclins. Four of the seven *A. nidulans* group II cyclins have been functionally characterized to some extent. As their functions may be instructive with respect to group II cyclins in other filamentous ascomycetes, I will briefly summarize the known functions of the *A. nidulans* group II cyclins.

None of the four group II cyclins in *A. nidulans* (An-Pho80, PclA, PclB, and ClgA) are essential, and all appear to play roles in development. An-Pho80 is involved in the negative regulation of phosphate acquisition enzymes and in promoting the switch from asexual to sexual development (Wu *et al.*, 2004). PclA expression is cell cycle regulated and peaks during S-phase (Schier *et al.*, 2001). PclA is upregulated during the late stages of conidiation (Bathe *et al.*, 2010; Schier *et al.*, 2001), while PclB is upregulated at both early and late stages of conidiation (Kempf *et al.*, 2013). Deletion of *pclA* reduces the number of conidia (Schier *et al.*, 2001), and the effects of *pclA*Δ on conidiation are additive with the effects of *pclB*Δ (Kempf *et al.*, 2013). PclA has also been shown to bind and activate $NimX^{Cdk1}$ (Schier and Fischer, 2002), and it is predicted to play a role in the rapid cell divisions that occur during sporulation (Schier *et al.*, 2001). Finally, deletion of *clgA* reduces vegetative growth and sporulation at higher temperatures, while also delaying and repressing the development of cleistothecia (Yu *et al.*, 2014).

Interestingly, three filamentous ascomycetes have gone through gene duplication events of one or two group II cyclin members. *Aspergillus carbonarius* has two PclB-like proteins. Both *Penicillium chrysogenus* and *Penicillium rubens* have three PclA-like proteins and three Pho80-

like proteins, while *Penicillium digitatum* has only one copy of each. I did not find evidence for duplications of group I or group III cyclins in the species analyzed.

3.3.3 Group III cyclins

The majority of the species I have analyzed have five group III cyclins. Only one group III cyclin, PchA, has been functionally characterized in *A. nidulans.* Deletion of *pchA* is not lethal, although *pchA*Δ reduces vegetative growth and production of conidia. Deletion of *pchA* is synthetically lethal with *pclA*Δ (Bathe *et al.*, 2010; Kempf *et al.*, 2013).

Chapter 4: *Aspergillus nidulans* has three cell cycle-related cyclins with distinct, non-redundant functions

4.1 Introduction

My phylogenetic analyses in Chapter 3 highlight how under-studied the cyclins of aspergilli and other Pezizomycotina are. Only a single group I cyclin has been analyzed thoroughly, $NimE^{Cyclin\ B}$ of *A. nidulans.* $NimE^{Cyclin\ B}$ (O'Connell *et al.*, 1992) is a binding partner of the Cdk1 homolog NimX (Osmani *et al.*, 1994). $NimE^{Cyclin\ B}$ is required for both S-phase and G_2/M, and its destruction during mitosis is required for mitotic exit (De Souza *et al.*, 2009; Nayak *et al.*, 2010). Up to now, $NimE^{Cyclin\ B}$ is the only cyclin that has been shown to be essential in *A. nidulans* and the only cyclin shown to have clear, cell cycle-related functions. The other two *A. nidulans* group I cyclins are a named but uncharacterized cyclin, PucA, and a previously unstudied cyclin encoded by gene AN2137 [using the AspGD (http://aspgd.org/) and FungiDB (http://fungidb.org/fungidb/) gene designation].

Given the importance of group I cyclins and the dearth of data on the functions of these proteins in filamentous ascomycetes in general and aspergilli in particular, I have carried out a functional analysis of PucA and AN2137. My genetic and live imaging data reveal that PucA is an essential G_1/S cyclin that is required for the inactivation of the anaphase promoting complex/cyclosome (APC/C) complexed with its binding partner CdhA. Deletion of the *pucA* gene is lethal, but viability is restored if the *cdhA* gene is also deleted. I designate AN2137, the previously unnamed B-type cyclin gene, *clbA.* ClbA localizes to kinetochores from mid-G_2 until just before chromosomal condensation. Deletion of *clbA* does not affect viability. Timely destruction of cyclins is critical for their function, and cyclins are normally targeted for destruction by APC/C binding to one or both of two conserved sequences called destruction boxes (d-boxes)

or KEN boxes. Using a regulatable promoter system new to *A. nidulans*, I have found that expression of a version of ClbA in which the d-boxes have been removed results in a mitotic block, a high frequency of chromosomal nondisjunction, and consequent lethality. Using the same promoter system, I have found that expression of d-box-deleted $NimE^{Cyclin\ B}$ results in nondisjunction in addition to its previously reported phenotypes. My functional characterization of *A. nidulans* group I cyclins provide new insights into cell cycle control mechanisms that are likely to be generally applicable to filamentous ascomycetes.

4.2 Results: Functional analysis of PucA

While it will ultimately be important to characterize all the groups of cyclins in filamentous ascomycetes, the group I cyclins are particularly important because they are key cell cycle regulators. As mentioned above, in the aspergilli and the other fungi in my study they fall into three clades with each fungus having one member of each clade (**Table 3.9**, **Table 3.10**, and **Fig. 3.1**). This suggests that the group I cyclins are functionally conserved and that functional information gleaned from one fungus is likely to carry over to many filamentous ascomycetes. Perhaps surprisingly, given the importance of filamentous ascomycetes and the importance of group I cyclins, they have been studied relatively little. The functions of only a single group I cyclin from a member of the aspergilli, $NimE^{Cyclin\ B}$ from *A. nidulans*, has been analyzed extensively. A few other group I cyclins from the organisms in my study have been named, but functional analyses have not been carried out in depth.

$NimE^{Cyclin\ B}$ is an essential B-type cyclin required for both S-phase and mitosis (Bergen *et al.*, 1984; Nayak *et al.*, 2010; O'Connell *et al.*, 1992). Members of the other two clades of group I cyclins have hardly been studied at all in filamentous ascomycetes. I have, consequently, chosen

to study the functions of the other two group I cyclins of *A. nidulans,* PucA and the unnamed cyclin encoded by AN2137. PucA was named by De Souza *et al.* (2014) on the basis of similarity to *S. pombe* Puc1 (Pombe unidentified cyclin 1) (E-value of 5e-37), a cyclin that associates with $Cdc2^{Cdk1}$ to regulate the length of G_1 (Martin-Castellanos *et al.*, 2000). PucA was found to co-purify with a dual localization-affinity purification (DLAP) tagged version of $NimX^{Cdk1}$. AN2137 has not been characterized at all, nor has it been given a standard *A. nidulans* gene designation. I now designate it *clbA*.

4.2.1 PucA is essential for viability

In order to determine if PucA is essential, I attempted to delete the *pucA* gene (1312-bp) by transforming the strain LO1516 (genotype listed in **Table 2.1**) with a fragment carrying a selectable marker, (*AfpyrG*), flanked by ~1000-bp *pucA* flanking sequences. When essential genes are deleted in *A. nidulans,* nuclei carrying the null allele are often maintained in heterokaryons spontaneously formed during transformation. Such heterokaryons carry two types of nuclei, parental nuclei and transformed nuclei. Parental nuclei carry a functional copy of the gene under study but do not carry the selectable marker. In transformed nuclei the gene under study has been deleted by replacement with a selectable marker that supports growth on selective media. Such heterokaryons are able to grow on selective media. Importantly, *A. nidulans* conidia are uninucleate, so each conidium carries a parental nucleus or deletant nucleus but not both. The conidia from a heterokaryon carrying a deletion of an essential gene will, thus, not be viable on selective media. By streaking out conidia from the primary transformants on nutritionally selective media, we can determine if the deleted gene is essential by the presence or absence of growth and colony formation (Martin *et al.*, 1997; Osmani *et al.*, 2006b; Osmani *et al.*, 1988). In the case of

PucA, multinucleate mycelia transferred to selective media from the primary transformants grew, but conidia from transformants did not grow to form colonies (**Fig. 4.1**). This indicates that *pucA* is essential. Diagnostic PCR on DNA prepared from conidia revealed bands diagnostic for both *pucA*Δ and *pucA*+ (data not shown), confirming that the colonies are, indeed, heterokaryons. The fact that the deletion of *pucA* does not block growth in heterokaryons reveals that it is recessive.

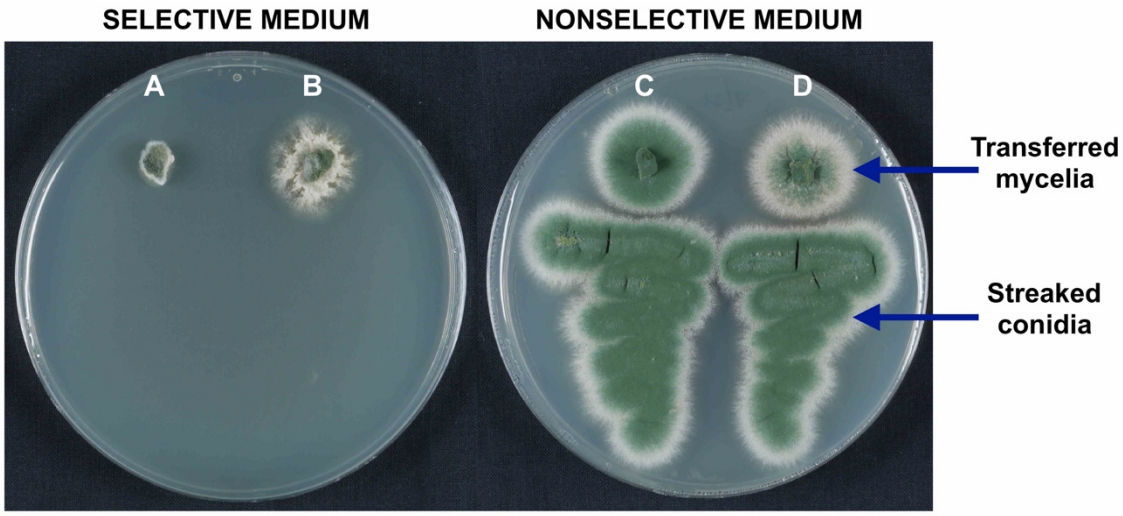

Figure 4.1: PucA is an essential cyclin in *A. nidulans*
I used the heterokaryon rescue technique to determine if PucA is essential. A parental, *pyrG*89 auxotrophic strain (LO1516) was transformed with a fragment designed to delete *pucA* (*pucA*Δ) by replacing it with *AfpyrG*. If PucA is essential, conidia carrying *pucA*Δ will not support growth. However, if a heterokaryon is generated during transformation that carries both *pucA*Δ and parental nuclei, hyphae will grow on selective medium (medium lacking uridine and uracil) because parental nuclei provide PucA and transformed nuclei complement *pyrG*89. The conidia produced by the heterokaryon are uninucleate, so they will have either parental nuclei or *pucA*Δ nuclei, and neither will grow on the selective medium. Squares of agar from the parental strain **(A, C)** and a *pucA*Δ transformant heterokaryon **(B, D)** have been placed on the selective medium (left plate) and the nonselective medium (right plate). On the selective medium, hyphae do not grow from the parental square **(A)** but do grow from the transformant, creating a colony with rough edges as is typical for a heterokaryon **(B)**. Conidia have been streaked below each colony. As expected, parental conidia do not grow **(A)**. Crucially, conidia from the transformant colony also do not grow **(B)**, revealing that the transformant is a heterokaryon carrying the lethal deletion *pucA*Δ. The fact that the heterokaryon hyphae grow reveals that *pucA*Δ is recessive. As expected, both hyphae and conidia from the parental strain and the heterokaryon grow on the nonselective medium **(C, D)**.

4.2.2 PucA is a G_1/S cyclin

PucA has homology to G_1/S cyclins in other organisms, and I hypothesized that the essential function of PucA is to regulate the G_1/S transition. In G_1, the APC/C bound to its activator Cdh1 functions to ubiquitinate S-phase cyclins and other substrates and, thus, targets them for destruction. In order for nuclei to enter S-phase the APC/C-Cdh1 complex must be inactivated by cyclin/CDK complexes (Fukushima *et al.*, 2013; Lukas *et al.*, 1999; Sorensen *et al.*, 2001). CdhA, the *A. nidulans* Cdh1 homolog, has been shown to function similarly to Cdh1 in other organisms by preventing $NimE^{Cyclin\ B}$ accumulation in G_1 (Edgerton-Morgan and Oakley, 2012). Previously, we found that the deletion of *cdhA* was not lethal and had little effect on growth, but the length of G_1 was shortened and $NimE^{Cyclin\ B}$-GFP fluorescence started to become visible shortly after mitosis (Edgerton-Morgan and Oakley, 2012) . If PucA is a G_1/S cyclin involved in the inactivation of CdhA in *A. nidulans*, then the lethality of *pucA*Δ is predicted to be due to failure of inactivation of the APC/C-CdhA complex and consequent blockage of the cell cycle in G_1. If this were the case, deletion of *cdhA* should allow progression through the cell cycle and enable growth of strains carrying *pucA*Δ. I tested this possibility by attempting to delete *pucA* in a *cdhA*Δ strain (LO2019). I obtained numerous transformants that were viable and could be streaked to single colony (**Fig. 4.2A**). Diagnostic PCR revealed that *pucA* was deleted in the transformants (data not shown). Deletion of *pucA* is, thus, not lethal in a *cdhA*Δ background, and this strongly supports the hypothesis that the essential function of *pucA* is to inactivate CdhA at the end of G_1 allowing the accumulation of $NimE^{Cyclin\ B}$ and progression into S phase.

I used heterokaryon rescue to determine the phenotype of *pucA*Δ in a $cdhA^+$ strain. As mentioned, although *pucA*Δ is lethal in a $cdhA^+$ background, nuclei carrying *pucA*Δ can be maintained in heterokaryons along with nuclei carrying $pucA^+$ and a selectable nutritional marker.

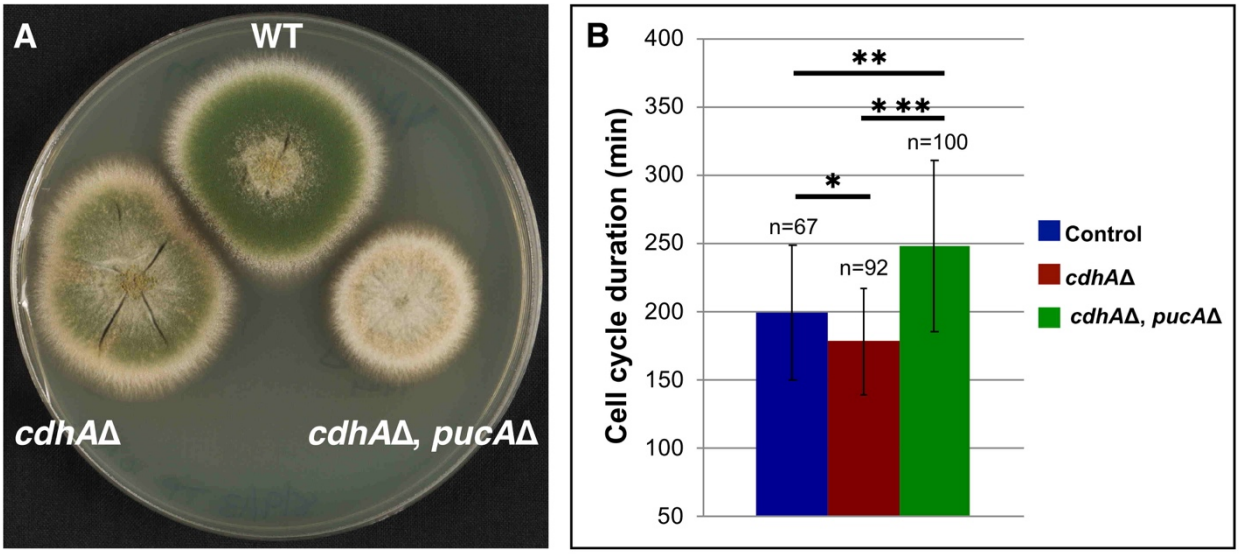

Figure 4.2: Deletion of *pucA* in *cdhA*Δ strains is not lethal

(**A**) Strains FGSC4/WT, LO2019, and LO8743 were stabbed on complete medium and incubated at 37°C for two days. The *pucA*Δ, *cdhA*Δ strain [LO8743 (*cdhA::AfpyrG, pucA::AfpyroA*)] displays reduced growth and conidiation compared to *cdhA*Δ [LO2019 (*cdhA::AfpyrG*)] and WT (FGSC 4) strains at all temperatures tested (other temperatures not shown). (**B**) Cell cycle duration was calculated using time-lapse images collected at 10-min intervals of a control (LO1806), *cdhA*Δ (LO2019), and *pucA*Δ, *cdhA*Δ (LO8743) strains, all of which contained histone H1-mRFP. Cell cycle duration was calculated as the time from the end of one mitosis to the end of the next mitosis. Differences in cell cycle duration were statistically significant (* = p value of 0.005, ** = p value of 8e-08, *** = p value of 6e-17). Values are means and error bars indicate standard deviation. n = number of nuclei.

The phenotype of *pucA*Δ can then be examined in germinating conidia from the heterokaryon. In the past, we have often used *pyrG*89 as a selectable mutation for heterokaryon rescue. Untransformed spores carrying *pyrG*89 barely germinate on selective media, allowing easy identification of germlings carrying the deletion of interest. I have found, however, that *riboB*2 is an even better selectable marker for heterokaryon rescue. Conidia carrying *riboB*2 swell, but do not extend a germ tube and there is no nuclear division, whereas nuclear division occasionally occurs in *pyrG*89 conidia. It is, thus, easy to distinguish untransformed *riboB*2 conidia among the conidia produced by a heterokaryon. I deleted *pucA* by replacing it with *AtriboB* in strain

LO10761, which carries NimE$^{Cyclin\ B}$-GFP as well as An-Nup49-mCherry. An-Nup49 is a nucleoporin and An-Nup49-mCherry allows visualization of the nuclear envelope. NimE$^{Cyclin\ B}$ accumulates in S phase and if *pucA*Δ prevents inactivation of CdhA, nuclei should be blocked at G_1/S and NimE$^{Cyclin\ B}$ should not accumulate.

I found that An-Nup49-mCherry and NimE$^{Cyclin\ B}$ fluorescence was preserved by a fixation procedure we routinely use and was, in fact, stable for days after fixation. This allowed me to score large numbers of germlings from particular time points easily. Although the fluorescence was stable, I scored germlings within 24 h of fixation. I separately incubated conidia at 37ºC from two heterokaryons as well as a control strain (LO10795), which was constructed by inserting *AtriboB* at the *yA* locus. I fixed the germlings at 4, 6, and 8 h after inoculation. I collected through-focus Z-series image stacks of random fields and scored germinated conidia for number of nuclei and presence of NimE$^{Cyclin\ B}$. At the 4-h time point, 35.5 ± 0.8% (2 experiments) of spores had germinated in the control strain. I scored *pucA*Δ germlings at the same time point, realizing that some *pucA*Δ conidia would not have germinated at that time. As **Fig. 4.3** shows, nuclear division was almost completely blocked in the *pucA*Δ germlings. NimE$^{Cyclin\ B}$ accumulation was also almost completely blocked. No NimE$^{Cyclin\ B}$ nuclei were seen at the 4-h time point and less than 1% of *pucA*Δ nuclei contained NimE$^{Cyclin\ B}$ at the 6-h and 8-h time points. In the control strain 40.6 ± 3.3% of nuclei were NimE$^{Cyclin\ B}$ positive at the 4-h time point, 64.4 ± 0.4% were NimE$^{Cyclin\ B}$ positive at the 6-h time point, and 64.7 ± 4.5% were NimE$^{Cyclin\ B}$ positive at the 8-h time point (**Fig. 4.3**).

Interestingly, the NimE$^{Cyclin\ B}$ positive nuclei in the control strain at the 4-h time point tended to be in germlings with a single nucleus whereas nuclei in binucleate germlings tended to be NimE$^{Cyclin\ B}$ negative. Our interpretation is that the single nuclei were in the first S or G_2 phase

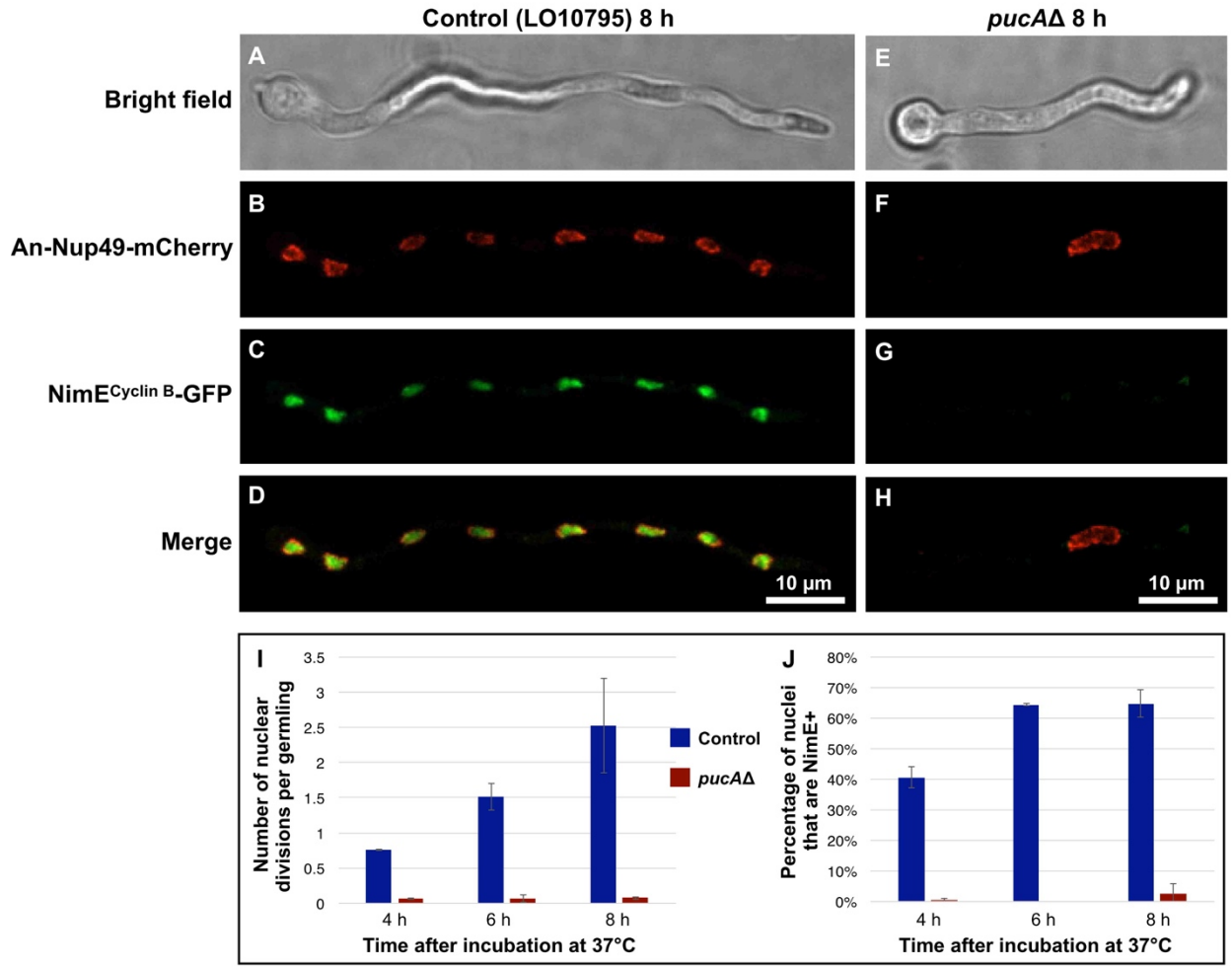

Figure 4.3: Deletion of *pucA* blocks cell cycle progression

Bright field images are of single focal planes (**A, E**) and images **B-D** and **F-H** are maximum intensity projections from Z-series stacks. Images are of a representative control (**A-D**) and *pucA*Δ (**E-H**) germling fixed after 8 h of growth at 37°C. Three rounds of nuclear division have occurred in the control strain resulting in 8 nuclei. A single nucleus is present in the *pucA*Δ germling, and NimE$^{Cyclin\ B}$-GFP fluorescence is not apparent. (**I**) Very few *pucA*Δ germlings have undergone nuclear division at the 4-, 6-, and 8-h time points, while the control strain has undergone 2-3 rounds of nuclear division by the 8-h time point. (**J**) *pucA*Δ germlings do not accumulate NimE$^{Cyclin\ B}$. Over 100 fixed germlings were imaged and scored at each time point for each of two experiments for both control (strain LO10795) and *pucA*Δ (2 transformants). Error bars indicate mean ± standard deviation of two experiments.

after germination and that the binucleate nuclei tended to be in G_1 following mitosis. The percentages of NimE$^{Cyclin\ B}$ positive nuclei at the 6-h and 8-h time points are consistent with our

previous observations (Edgerton-Morgan and Oakley, 2012; Nayak *et al.*, 2010).

These data, in aggregate, reveal that PucA is an essential cyclin that is required for the G_1/S transition and that it functions by inactivating CdhA, and thus the APC/C, and by doing so allows the accumulation of $NimE^{Cyclin\ B}$. Furthermore, this indicates that there are no additional cyclins in *A. nidulans* that are sufficient to inactivate CdhA at the G_1/S boundary and that there are no redundant pathways for CdhA inactivation as has been observed in humans and in *S. cerevisiae* [reviewed in (Sivakumar and Gorbsky, 2015)].

4.2.3 Deletion of pucA allows nuclear growth but inhibits the DNA replication cycle resulting in nuclei with very diffuse chromatin

To observe nuclear behavior in a *pucA*Δ strain, I deleted *pucA* in several *cdhA*$^+$ strains carrying different fluorescent proteins, in each case replacing it with *AfriboB*. Since *pucA* is essential in *cdhA*$^+$ strains, I used the heterokaryon rescue technique in all cases and observed the phenotype of *pucA*Δ in germlings that grew from conidia produced by the heterokaryon. I first deleted *pucA* in LO9481, a strain expressing histone H1-T-Sapphire and An-Nup49-mCherry. A control *pucA*+, *riboB*+ strain (LO9537) was constructed by inserting *AfriboB* at the *wA* locus in the parent strain LO9481. Conidia from the control strain and from the *pucA*Δ heterokaryon were incubated separately at 30℃ for 12 h at which time both control conidia and *pucA*Δ conidia had germinated. Z-series stacks of random fields were then captured over the next hour. Separate, identically grown samples were also imaged at the 14-15 h and 16-17 h periods. Representative control and *pucA*Δ images at 16-17 h are shown in **Fig. 4.4**. Surprisingly, *pucA*Δ germlings at these time points contained either faint or no obvious histone H1-T-Sapphire fluorescence (**Fig. 4.4F**). I consistently observed this phenotype in *pucA*Δ germlings from several additional strains with

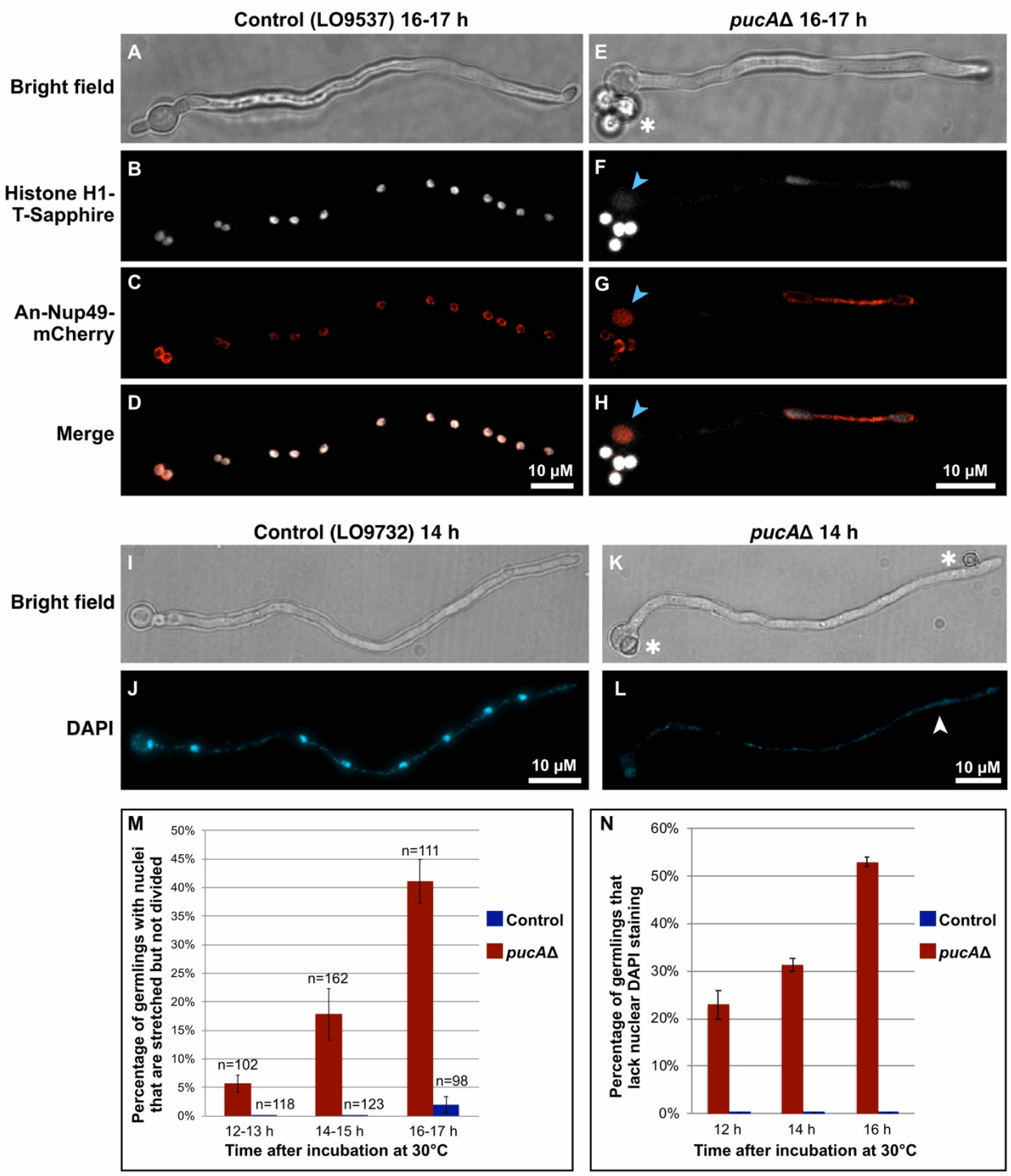

Figure 4.4 *(continued on next page)*

(continued from previous page)

Figure 4.4: *pucA*Δ results in stretched nuclei with diffuse DNA and histones
(A-H) Control *pucA*$^{+}$ (LO9537) (**A-D**) and *pucA*Δ (**E-H**) conidia were incubated at 30ºC for 16 h and imaged. Bright field images (**A** and **E**) are single focal plane images, and other images are maximum intensity projections from Z-series stacks. An-Nup49-mCherry allows visualization of the nuclear envelope. The control strain has gone through several cell cycles resulting in many nuclei. The nuclei are normal sized. In the *pucA*Δ germling, however, there is only one large nucleus, and it is extremely stretched as shown by An-Nup49-mCherry fluorescence. There is also faint mCherry and T-Sapphire fluorescence in the vacuole in the conidial swelling of the germling (blue arrowhead in **F-H**). The histone H1 fluorescence in the *pucA*Δ strain is very faint. Note there are four ungerminated parental conidia below the conidial swelling that show bright histone H1-T-Sapphire fluorescence. (**I-L**) DAPI staining of control and *pucA*Δ germlings incubated for 14 h at 30ºC and fixed. **I** and **K** are single focal plane images, and **J** and **L** are maximum intensity projections of Z-series stacks. Nuclear fluorescence is barely visible in **L** even though software was used to increase the brightness level 3.5X in **L** relative to **J**. The arrowhead in **L** points to a possible nucleus. The punctate DAPI staining is mitochondrial DNA. (**M-N**) Control (LO9537) and *pucA*Δ (*pucA*Δ heterokaryon made in parent strain LO9481) conidia containing histone H1-T-Sapphire and An-Nup49-mCherry were grown for 12, 14, and 16 h at 30ºC and then live imaged for one hour at 30ºC. The percentage of germlings with stretched nuclei was scored (**M**); error bars indicate mean ± standard deviation of three separate experiments. n = the number of germlings. Similarly, germlings were scored for the presence of obvious nuclear DAPI staining (**N**); error bars indicate mean ± standard deviation of two experiments (n=100 germlings per time point). All germlings scored displayed mitochondrial DAPI staining, indicating DAPI staining was successful.

different fluorescent proteins (mRFP and GFP) fused to histone H1 (data not shown). The loss of histone fluorescence is not due to the T-Sapphire fluorescent protein. DAPI staining of *pucA*Δ germlings (deletion made in parent strain LO9560) showed a similar loss of nuclear DNA staining over time, with over 50% of *pucA*Δ germlings lacking obvious nuclear DAPI staining at the 16-h time point (incubation at 30°C, 2 experiments, n=50 germlings per experiment) (**Fig. 4.4 I-L, N**). Mitochondrial DNA staining was still apparent in all the *pucA*Δ germlings (**Fig. 4.4L**), assuring us that the lack of nuclear DNA staining was not due to failed DAPI staining. Additionally, I DAPI

stained a *pucA*$^{+}$ control strain (LO9732) and *pucA*Δ germlings side-by-side with identical conditions and timing and imaged them on the same day, and all control germlings had visible nuclear and mitochondrial fluorescence. Thus, loss of nuclear DNA fluorescence over time parallels the loss of histone H1 fluorescence.

To help understand this phenomenon I deleted *pucA* in strain LO10761 (which carries An-Nup49-mCherry). Live imaging revealed that *pucA*Δ resulted in nuclei growing to be much larger than control nuclei (**Fig. 4.4B vs F**). Upon longer incubation periods, the nuclear envelope of *pucA*Δ nuclei exhibited varying degrees of invagination and many became stretched **(Fig. 4.5A-F**). Two or more spindle-pole bodies (SPBs) attaching to cytoplasmic microtubules might result in forces being applied to nuclei from different directions. This would, in turn, result in nuclear stretching. I was, consequently, curious as to whether deletion of *pucA* blocked nuclei in G_1 but allowed for SPB duplication. I deleted *pucA* in strain LO10066 which carries GFP-alpha-tubulin, HH1-T-Sapphire, and SepK-tdTomato (a SPB marker). *pucA*Δ germlings were incubated at 37℃ for 8 h and then z-series stacks of random fields were captured over the next hour (two separate experiments). At this time point and temperature, control strains have undergone 2-3 rounds of nuclear division. Most *pucA*Δ germlings (35/49) had either a single nucleus or no obvious histone H1 fluorescence germlings) and, of these germlings, most (33/35) had a single SPB despite the fact that many of the nuclei were severely stretched (14/33). Scoring germlings with two nuclei was challenging as the faint histone H1 signal made it difficult to determine whether the nuclei were completely separate or still connected. However, of the germlings that we scored as having two nuclei (14/49 germlings), most (11/14) had a single SPB (**Fig. 4.5J**). These data indicate that abnormal SPB duplication is not the cause of the stretching we observe. These results also indicate that the SPB is not the only site where forces are applied to the nucleus.

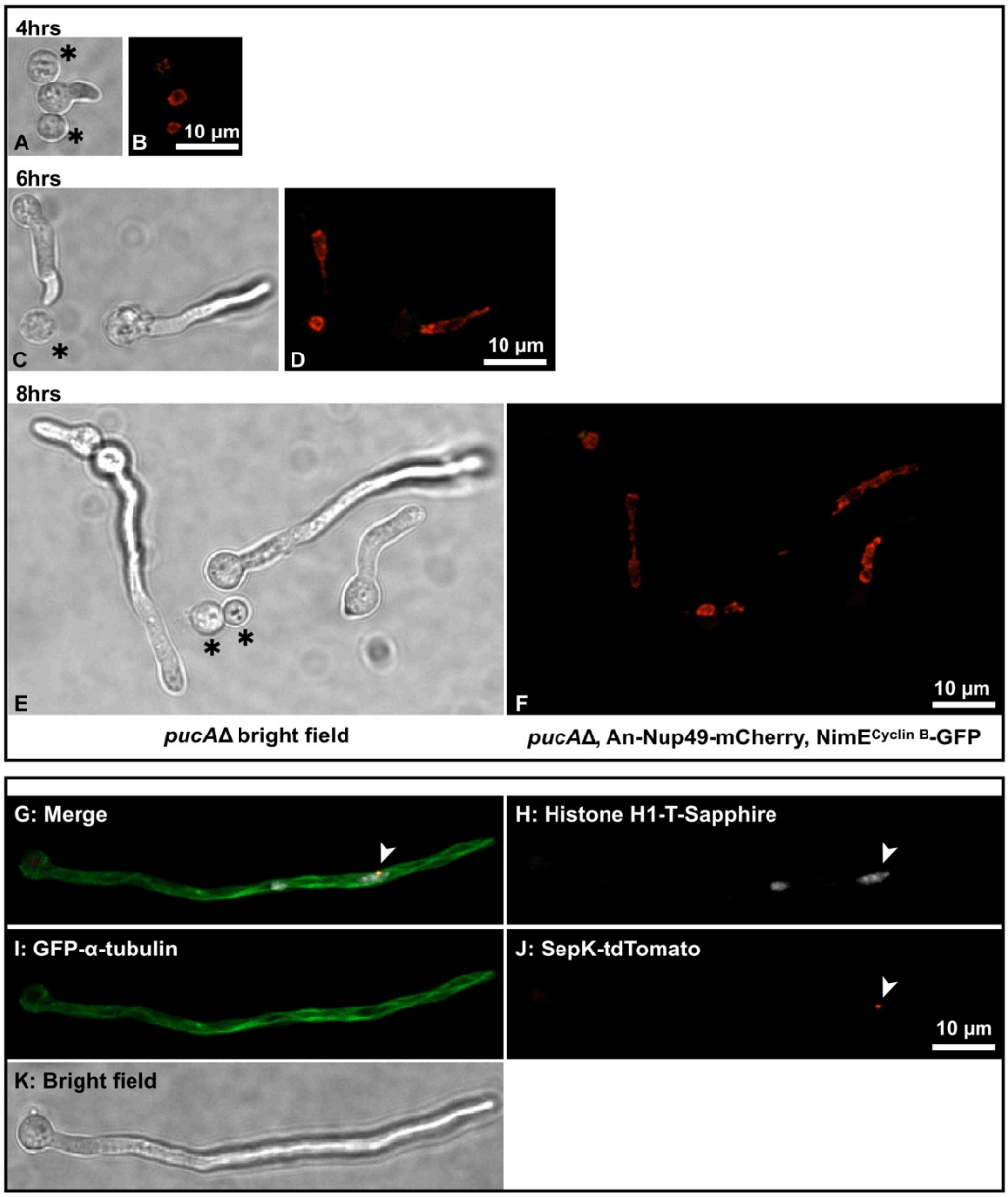

Fig. 4.5: Deletion of *pucA* causes nuclear morphological abnormalities that worsen over time and are not caused by multiple spindle pole bodies

Bright field images are of a single focal plane, and all other images are maximum intensity projections from Z-series stacks. **(A-F)** Representative images from *pucA*Δ germlings (parent strain LO10761) incubated at 37ºC and fixed after 4 h (**A-B**), 6 h (**C-D**), and 8 h (**E-F**) are shown. Asterisks indicate swollen, ungerminated conidia that are likely parental, untransformed conidia. For representative images of control germlings fixed at 8 h, see Fig. 4.3. **G-K**: Representative images of a *pucA*Δ germling (parent strain LO10066) in a strain that carries GFP-α-tubulin, SepK-tdTomato, and histone H1-T-Sapphire. Only one of the two nuclear masses is associated with SepK-tdTomato, a SPB marker (arrow in **G, H, J**).

Long-term time-lapse imaging of *pucA*Δ germlings carrying An-Nup49-mCherry and histone H1-GFP (*pucA*Δ heterokaryon made in parent strain LO9775) revealed that, given sufficiently long incubation, some *pucA*Δ germlings would eventually undergo what appeared to be nuclear division (14/23 germlings imaged for 16-18 h at 37ºC). However, this was difficult to evaluate because determining whether nuclei underwent nuclear division or were simply pulled apart was sometimes challenging. Interestingly, in those *pucA*Δ germlings that did undergo obvious nuclear division, the histone H1 fluorescence would change rapidly from not apparent to brightly visible as the chromatin condensed (**Fig. 4.6**). These data demonstrate that chromosomes are present in the large *pucA*Δ nuclei even though they are not visible in interphase. Our interpretation is that DNA replication is strongly inhibited by *pucA*Δ but nuclear growth proceeds, and this results in very large nuclei with very diffuse chromatin. Eventually, the *pucA*Δ-induced G_1 block is overcome in some germlings resulting in a form of mitosis, but, even in those germlings it is not clear that the cell cycle proceeded normally from G_1 to M or that mitosis was normal.

Notably, this diffuse nuclear histone H1 fluorescence phenotype has been described previously for the deletion of the *nimX*^{cdk1} gene (De Souza *et al.*, 2013). NimX^{Cdk1} has been shown to physically interact with both PucA and NimE$^{Cyclin\ B}$ in *A. nidulans* (De Souza *et al.*, 2014). It is, thus, possible that the phenotype I observed in *pucA*Δ germlings is caused by a lack of NimX kinase activity due to the absence of its binding partner PucA.

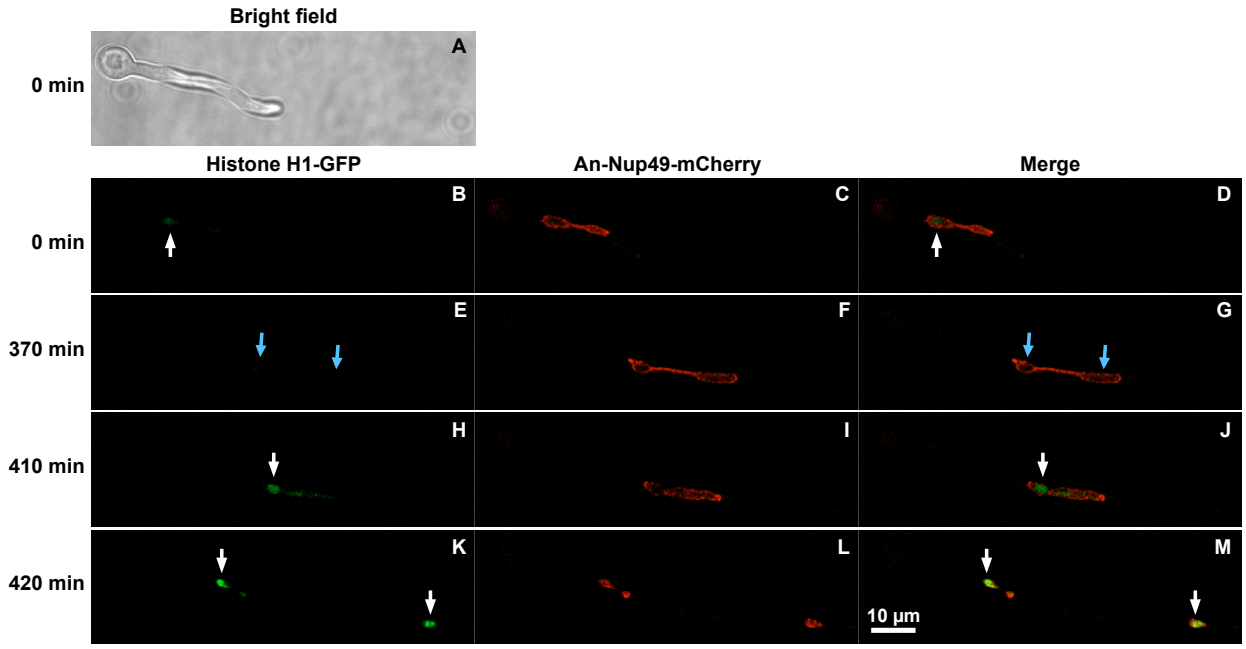

Figure 4.6: Histone H1 fluorescence becomes visible during and immediately after mitosis in *pucA*Δ germlings.
Images are projections of Z-series stacks captured at 10-min intervals and follow a *pucA*Δ germling (parent strain LO9775) carrying histone H1-GFP (left panel) and An-Nup49-mCherry (middle panel). GFP and mCherry channels are merged in the right panel. A bright field image of the *pucA*Δ germling (**A**) is of a single focal plane taken just prior to time-lapse imaging (**B-M**). *pucA*Δ conidia were incubated at 37℃ for ~7 hours prior to imaging. At the first time point (0 min), the *pucA*Δ germling has a single, large nucleus with faint histone H1-GFP fluorescence (white arrow in **A**, **D**). Over the next ~6 hours, the histone H1-GFP fluorescence disappears (blue arrows in **E**, **G**) and the nucleus remains stretched. At the 410-minute timepoint, the histone H1-GFP becomes apparent (white arrow in **H**, **J**) and a likely nuclear division occurs at 420 minutes, which is ~14 hours after the initial incubation at 37℃.

4.2.4 Deletion of pucA in cdhAΔ strains results in an interphase cell cycle delay

The deletion of *pucA* in a *cdhA*Δ strain results in a decrease in growth and conidiation compared to that of the *cdhA*Δ parent (**Fig. 4.2A**). This indicates that PucA has non-essential functions in addition to its essential function of inactivating APC/C-CdhA. To determine if the cell cycle time was altered in the double mutant, I generated a strain carrying *pucA*Δ and *cdhA*Δ and

expressing histone H1-mRFP (LO8743, LO8744) to allow me to observe nuclear division. The cell cycle duration was calculated using time-lapse images collected at 10-min intervals at 25°C. The cell cycle durations for control strains (199 ± 49 min) and *cdhA*Δ strains (178 ± 39 min) at 25°C have been determined previously (Edgerton-Morgan and Oakley, 2012). I scored a different control strain (LO10327) and found it has an essentially identical cell cycle time (198 ± 38 min, n=72 nuclei). Compared to control and *cdhA*Δ strains, the length of the cell cycle was increased in *pucA*Δ, *cdhA*Δ strains (248 ± 63 min, n=100 nuclei) (**Fig. 4.2B**). The increase was statistically significant. The p-value for *pucA*Δ, *cdhA*Δ vs the control strain was 7.76e-8 and for *pucA*Δ, *cdhA*Δ vs *cdhA*Δ the p-value was 5.74e-17 (unpaired Student's *t*-test). The duration of mitosis in the *pucA*Δ, *cdhA*Δ strain at 25ºC (10 ± 2 min, n = 36) was not significantly different from the control strain (9 ± 1 min, n = 40). It follows that the increased cell cycle time in the *pucA*, *cdhA* double deletant was due to a delay in interphase.

Hyphal growth outpaced nuclear replication in *pucA*Δ, *cdhA*Δ germlings, and this resulted in nuclei being spaced far apart. To quantify this, I fixed control (LO10327), *cdhA*Δ (LO2019), and *pucA*Δ, *cdhA*Δ (LO8743) germlings after 20 h of incubation at 25°C and used calcofluor white to visualize the hyphal walls. I scored the distances between interphase nuclei in tip cells that could be seen on the same XY plane using Volocity 6.3 software (Perkin-Elmer). I found that nuclei were 14.5 ± 4.4 µm apart in the control strain (n=100), nuclei were 12.3 ± 4.3 µm apart in the *cdhA*Δ strain (n=97), whereas nuclei were 22.5 ± 7.1 µm apart in the *pucA*Δ, *cdhA*Δ strain (n=89).

NimE$^{\text{Cyclin B}}$ is required for both S-phase and entry into mitosis (Bergen *et al.*, 1984; Morris, 1975). I was curious if PucA had a role in regulating NimE$^{\text{Cyclin B}}$ accumulation in S and/or G_2 and, if so, whether that was the cause of the interphase delay we observe in *pucA*Δ, *cdhA*Δ mutants. I generated strains containing *pucA*Δ and *cdhA*Δ and expressing NimE$^{\text{Cyclin B}}$-GFP and histone H1-

mRFP (LO10750, LO10751). NimE$^{Cyclin\ B}$-GFP is absent in G_1, becomes visible in early S phase, and remains apparent in G_2. The length of G_1 is proportional to the percentage of interphase nuclei with no visible NimE$^{Cyclin\ B}$-GFP. Previous work from our lab revealed that the mean percentage of tip cells in *cdhA*$^+$ strains that contained visible NimE$^{Cyclin\ B}$-GFP was 60.0 ± 5.4% compared to 87.2 ± 3.5% in *cdhA*Δ strains (Edgerton-Morgan and Oakley, 2012). In the *pucA*Δ, *cdhA*Δ double mutant strains (LO10750 and LO10751), I found that 89.2 ± 4.8% of tip cells contained visible NimE$^{Cyclin\ B}$-GFP (4 experiments, n=120 tip cells), and this is essentially identical to *pucA*$^+$, *cdhA*Δ strains. Therefore, the lengthened cell cycle in the double mutant does not appear to be due to a delay in NimE$^{Cyclin\ B}$ accumulation. NimE$^{Cyclin\ B}$ localization appeared normal with a clear enrichment of NimE$^{Cyclin\ B}$ at SPBs.

4.2.5 Deletion of pucA in cdhAΔ strains does not increase mitotic defects but causes interphase nuclear abnormalities

To determine if *pucA* has functions in mitosis, I incubated spores from control (LO1806), *cdhA*Δ (LO2019), and *pucA*Δ, *cdhA*Δ (LO8743) at 25ºC, captured Z-series image stacks at 3-min intervals and scored the following mitotic errors: 1) failure of nuclei to divide, 2) mitotic delay (abnormally long periods with condensed chromosomes), 3) apparent nuclear division followed by separated chromatin masses coming back together to reform a single nucleus, and 4) abnormal chromosome segregation (**Fig. 4.7**). *cdhA*Δ mutants showed an increase in the rate of total mitotic errors (8.5% of nuclei, n=177) compared to control (0.94% of nuclei, n=106). The percentage, however, of mitotic errors observed in the *pucA*Δ, *cdhA*Δ strain (10% of nuclei, n=160) was not significantly different from that observed in *cdhA*Δ. As presented above, I found no significant difference in the length of mitosis in the *pucA*Δ, *cdhA*Δ strain vs control strains. Taken together,

my data indicate that *pucA*Δ does not add significantly to the mitotic abnormalities seen with *cdhA*Δ strains.

In the course of looking for mitotic abnormalities, I observed a number of abnormalities in nuclear appearance and behavior that were rarely or never seen in control strains. Most of these were also seen in *cdhA*Δ strains, but their frequency was enhanced in the *cdhA*Δ, *pucA*Δ strain. These abnormalities included abnormally large nuclei, nuclei that were pulled or stretched visibly (**Fig. 4.7 D, E**), and, most strangely, nuclei in which the chromatin partially condensed and decondensed without mitosis occurring. This phenotype of chromatin partially condensing and decondensing happened to individual nuclei within a cell while the chromatin in other nuclei remained decondensed (**Fig. 4.7 F**). Altogether, these abnormalities were significant in number with 33.6% of *cdhA*Δ, *pucA*Δ nuclei exhibiting at least one of these abnormalities in the 30 min prior to mitosis and 22.4% exhibiting them in the 30 min after mitosis. These abnormalities are quantified in **Fig. 4.7**. The abnormally large and stretched nuclear phenotypes are notable in that they are also seen in *pucA*Δ, *cdhA*$^{+}$ germlings from heterokaryons. We looked for microtubule abnormalities that might account for the nuclear stretching, but none were evident (results not shown). The untimely chromosomal condensation and decondensation phenotype was never seen in control cells. These data suggest that PucA, possibly in combination with CdhA, has a role in regulating chromosomal condensation, and, more specifically, in preventing untimely chromosomal condensation.

A. 0-30 min Prior to Mitosis					
	Abnormally large nuclei	Nuclei pulled/ stretched	Nuclei partially condense and decondense	Multiple problems	% total abnormalities
Control n=106 nuclei	0.00%	0.94%	0.00%	0.00%	0.94%
cdhAΔ n=164 nuclei	0.00%	5.49%	5.49%	0.61%	11.59%
pucAΔ, cdhAΔ n=152 nuclei	5.92%	16.45%	7.24%	3.95%	33.56%

B. During Mitosis							
	Nucleus Fails to Divide	Mitotic delay	Nuclei separate but come back together	Abnormal # of daughter nuclei	Non-disjunction	Multiple problems	% total abnormalities
Control n=106 nuclei	0.00%	0.94%	0.00%	0.00%	0.00%	0.00%	0.94%
cdhAΔ n=177 nuclei	1.13%	2.26%	1.13%	0.56%	1.69%	1.69%	8.46%
pucAΔ, cdhAΔ n=160 nuclei	2.50%	2.50%	0.63%	1.25%	0.63%	2.50%	10.01%

C. 0-30 min After Mitosis					
	"Jumping" nuclei	Nuclei pulled/ stretched	Nuclei partially condense and decondense	Multiple problems	% total abnormalities
Control n=106 nuclei	0.49%	0.98%	0.00%	0.00%	1.47%
cdhAΔ n=164 nuclei	0.32%	4.53%	3.24%	1.62%	9.71%
pucAΔ, cdhAΔ n=152 nuclei	0.00%	12.10%	6.41%	3.91%	22.42%

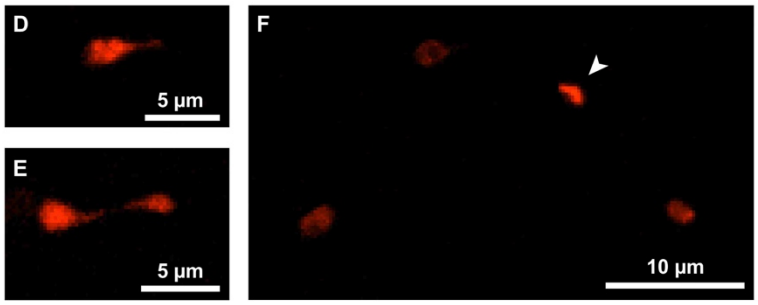

Figure 4.7: Nuclear abnormalities during interphase in *pucA*Δ, *cdhA*Δ mutants
Control strain LO1806, *cdhA*Δ strain LO2019, and *pucA*Δ, *cdhA*Δ strain LO8743 all carried histone H1-mRFP. Z-series stacks were captured at 3-min intervals at 25°C. **A-C**: Tables summarizing nuclear abnormalities that occurred within the 30 min period prior to mitotic entry (**A**), during mitosis (**B**), and within 30 min after mitotic exit (**C**). Germlings were scored for mitotic errors that included 1) failure of nuclei to divide, 2) mitotic delay (abnormally long periods with condensed chromosomes), 3) nuclei division followed by the chromosomes coming back together to reform a single nucleus, and 4) abnormal chromosome segregation (e.g. non-disjunction). They were also scored for interphase nuclear abnormalities. These abnormalities included 1) abnormally large nuclei, 2) nuclei that were pulled/stretched, 3) chromosomes that condensed and decondensed repeatedly, and 4) nuclei that "jumped" around the cell aberrantly. **D, E**: Representative *pucA*Δ, *cdhA*Δ nuclei that display nuclear stretching during interphase. **F**: The four nuclei are in the same interphase cell. One nucleus (arrow) is aberrantly condensed, while the three other nuclei are not condensed. Images are maximum intensity projections from Z-series stacks.

4.2.6 Attempts to localize PucA

For clarifying the functions of PucA it would obviously be advantageous to observe its localization. I have not been successful in doing so, but I will summarize our efforts here because I believe they are informative. I generated an N-terminal GFP fusion to PucA but did not obtain transformants with the correct DNA insertion even after two separate transformation attempts. This could indicate that the N-terminal fusion is lethal. Transformants carrying a C-terminal GFP fusion to PucA were viable but no fluorescence signal was observed. It is likely that PucA is present at levels too low to detect and/or that its half-life is too short to allow GFP to fold and become fluorescent before the protein is destroyed (a particular problem with short lived proteins such as cyclins). I tested a fast-folding fluorescent protein, Superfolder GFP (sfGFP) (Malagon, 2013), fusing it to PucA and to $NimE^{Cyclin\ B}$. I did not see a fluorescent signal for the C-terminal tagged version of PucA with sfGFP. Interestingly, the fluorescent signal for C-terminal tagged $NimE^{Cyclin\ B}$ with sfGFP was weaker than the signal from the GFP variant we currently utilize in the lab (Fernandez-Abalos *et al.*, 1998), suggesting that the variant we use is superior to sfGFP.

4.3 Results: Functional analysis of ClbA (AN2137)

4.3.1 Localization of ClbA

I generated strains that carried ClbA-GFP and histone H1-mRFP (LO10126 and LO10127), and these strains grew as well as wild-type strains at all temperatures tested (data not shown). Long-term live time-lapse imaging at 37°C revealed that ClbA-GFP was first detectable as a single dot in the nucleus 23 ± 10 min before mitosis (n=73). This correlated to 23% of the cell cycle. G_2 of *A. nidulans* lasts approximately 40% of the cell cycle at 37°C (Bergen and Morris, 1983), and, thus, ClbA becomes detectable in mid-G_2. Imaging at 1-min intervals revealed that ClbA-GFP

began to disappear from most nuclei just prior to chromatin condensation (51/58 nuclei), whereas in some nuclei it disappeared at the first sign of chromatin condensation (**Fig. 4.8 A-O'**). ClbA-GFP was rarely observed in nuclei during anaphase or telophase, but occasionally I observed faint ClbA-GFP between the separating chromatin masses in anaphase.

The "dot" localization pattern is consistent with localization to the SPB and/or kinetochores (KTs). In *A. nidulans*, the KTs are immediately adjacent to the SPB during interphase, and they do not separate from the SPB except in prometaphase through early anaphase (De Souza *et al.*, 2009; Yang *et al.*, 2004). To confirm that ClbA-GFP localizes to the SPB and/or KTs, I generated two additional strains that carried ClbA-GFP. Both carried histone H1-mTagBFP2 (Subach *et al.*, 2011), but one carried the outer SPB marker SepK-tdTomato (Xiong and Oakley, 2009), while the other carried the KT marker An-Ndc80-mCherry. Interestingly, I noticed that ClbA-GFP and SepK-tdTomato did not fully overlap and instead localized immediately adjacent to each other (**Fig. 4.8 P-R'**) while ClbA-GFP and An-Ndc80-mCherry did overlap precisely (**Fig. 4.8 S-U'**).

This result suggests that ClbA co-localizes with KTs. I performed colocalization analysis with Volocity 6.3 software (Perkin-Elmer) using the Costes Pearson's Correlation algorithm (Barlow *et al.*, 2010; Costes *et al.*, 2004; Manders *et al.*, 1993). With this algorithm, higher correlation values indicate more precise 3D co-localization (1.0 = 100% overlap of signal). In some cases, optical systems can cause an apparent lateral displacement of objects imaged at different wavelengths. To control for this, I imaged microspheres that fluoresce at both GFP and tdTomato/mCherry wavelengths (Molecular Probes' PS-Speck Microscope Point Source Kit) and found a correlation value of 0.905 ± 0.044 (n = 22 microspheres) when using the 488 nm and 561 nm lasers. The high correlation value indicates that the two wavelengths are not shifted significantly in the XY dimension in our system. We found a correlation value of 0.253 ± 0.234 of

ClbA-GFP to SepK-tdTomato (n = 86 nuclei, 2 strains LO11067 and LO11068) and a correlation value of 0.761 ± 0.100 of ClbA-GFP to An-Ndc80-mCherry (n = 89 nuclei, 2 strains LO11253 and LO11254). (Note that the same filter set was used to image SepK-tdTomato and An-Ndc80-mCherry.) These data indicate strongly that ClbA is co-localizing with KTs.

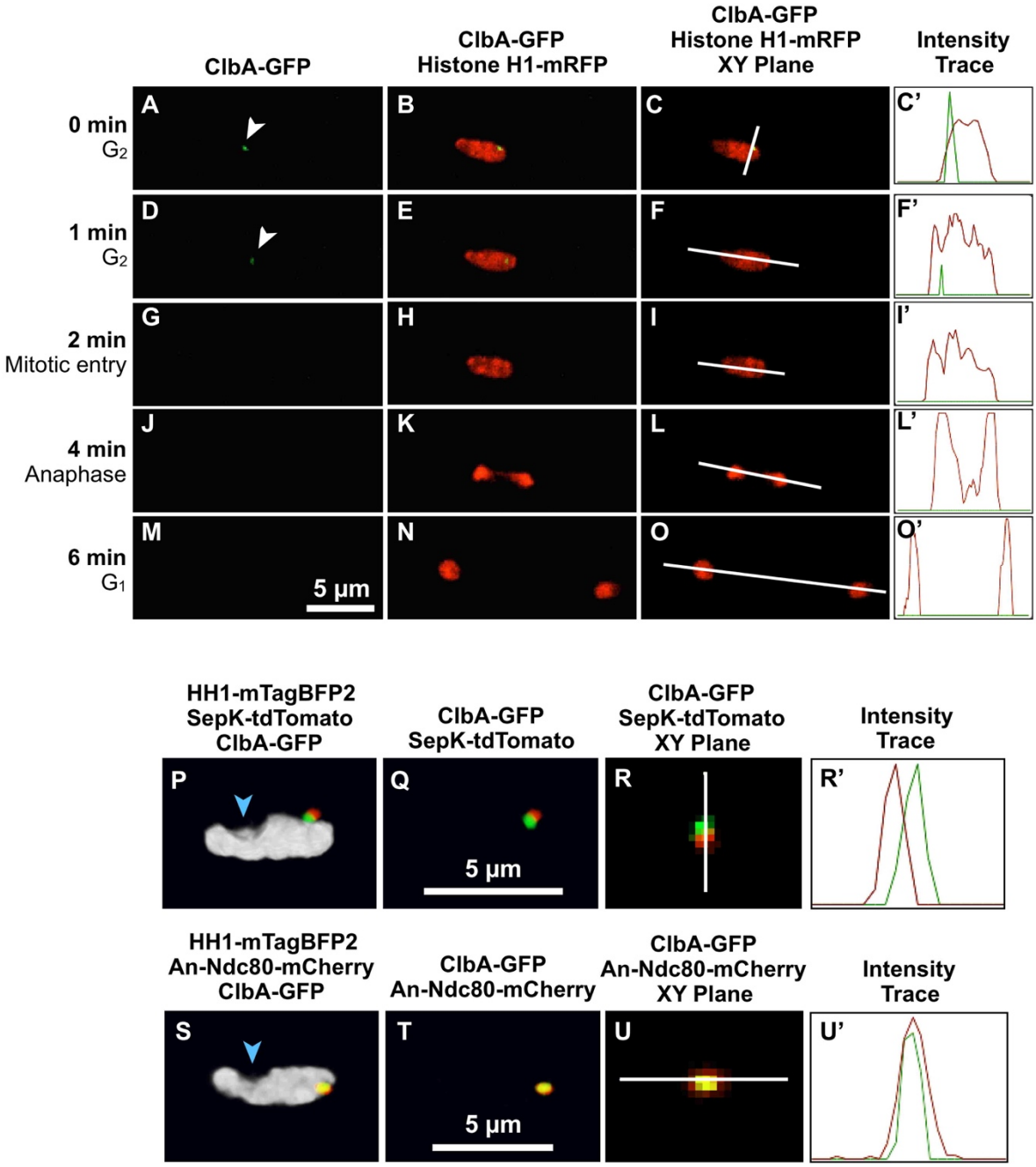

Figure 4.8 *(continued on next page)*

(continued from previous page)

Figure 4.8: ClbA localizes with kinetochores in G_2 and disappears at mitotic entry
All images were obtained with a spinning disk confocal microscope. T = 0 min is in late G_2 and the nucleus transits into mitosis in the following 2 min. Anaphase is underway by 4 min and nuclear division is largely completed by 6 min. The **A-M** and **B-N** columns show maximum intensity projections of Z-series stacks. The **C-O** column shows single focal plane images taken from the same data set, and the **C'-O'** column shows intensity traces over the lines shown in the **C-O** column with ClbA-GFP fluorescence shown in green and histone H1-mRFP shown in red. ClbA-GFP localizes to a dot in the nucleus in G_2 (arrows in **A**, **D)** and disappears during mitotic entry (**G**). ClbA-GFP is not observed as a dot in the nucleus again until the next G_2. **(P-R')** ClbA-GFP localizes adjacent to the SPB marker SepK**.** Histone H1-mTagBFP2 is shown in gray, SepK-tdTomato in red, and Clb-GFP in green. **P** and **Q** are three dimensional projections, while **R** is a single focal plane image from the the Z-series stack. The minimal overlap is verified by intensity traces in R', which are along the line shown in **R**. The tdTomato trace is shown in red and the GFP trace in green. **(S-U')** ClbA-GFP co-localizes with a kinetochore marker An-Ndc80. **S** and **T** are three dimensional projections from a Z-series stack with HH1-mTagBFP2 shown in gray, An-Ndc80-mCherry in red and ClbA-GFP in green. **U** is a single focal plane image from the same series. The overlap is verified by intensity traces in the mCherry (red) and GFP (green) channels in **U'** along the line shown in **U**. In **P** and **S** the position of the nucleolus is shown by the absence of histone fluorescence (blue arrows).

4.3.2 ClbA is not essential but destruction of ClbA is required for viability

To determine if *clbA* is essential I deleted it by replacing it with *AfpyrG*. I found that *clbA*Δ strains (LO10129-LO10131) grew like WT strains at all temperatures tested (data not shown).

An important characteristic of group I cyclins is that their destruction is important for their roles in the cell cycle. In this regard, group I cyclins, particularly the B-type cyclins, have motifs called destruction boxes (d-boxes, RXXLXXXXN) that are recognized by the APC/C. They are then ubiquitinated by the APC/C, and this leads to their destruction by the proteasome. The d-boxes are typically near the N-terminus of these cyclins, and truncation of the N-terminus to delete the d-box or boxes results in a cyclin that drives the cell cycle but arrests the cell cycle at a point

at which destruction of the cyclin is required (Murray *et al.*, 1989). Removal of the d-box of NimE$^{\text{Cyclin B}}$, for example, causes a mitotic exit arrest and consequent growth inhibition (De Souza *et al.*, 2009; Nayak *et al.*, 2010).

ClbA contains two putative d-boxes in its N-terminal region (**Fig. 4.9A**). The first putative d-box in ClbA (RAAFGDVSN) is not canonical, but it is almost identical to the NimE$^{\text{Cyclin B}}$ d-box (RAALGDVSN). The second putative d-box in ClbA (RKTLNKRAT) contains the conserved "RXXL" but not the conserved asparagine at the 9$^{\text{th}}$ position. No other identifiable d-box motifs are present in the N-terminus of ClbA. I wished to determine if ClbA d-box motifs play a role in ClbA destruction and, if so, whether destruction of ClbA is important for cell cycle progression.

I created a version of ClbA in which I removed the first d-box (db1Δ-ClbA, eliminating amino acids 2-60) and another version in which I deleted the N-terminal region that contained both putative d-boxes (db2Δ-ClbA, eliminating amino acids 2-147) (**Fig. 4.9A**). I also created versions of the d-box-deleted ClbA and two d-box-deleted ClbA in which GFP was fused to the C-terminus (db1Δ-ClbA-GFP and db2Δ-ClbA-GFP). I initially placed db1Δ-ClbA, db1Δ-ClbA-GFP, db2Δ-ClbA, db2Δ-ClbA-GFP, full length (FL) ClbA, and FL-ClbA-GFP (separately) under the control of the regulatable *alcA* promoter [*alcA*(p)] at the white (wA) locus in a strain expressing histone H1-mRFP (parental strain LO1516). In these strains, the endogenous *clbA* gene was not altered. On repressing media, all six strains grew like wild-type and control strains (**Fig. 4.9B**). On inducing media, the expression of db1Δ-ClbA or db1Δ-ClbA-GFP significantly decreased growth while the expression of db2Δ-ClbA or db2Δ-ClbA-GFP almost completely inhibited growth and conidiation. Induction of expression of FL-ClbA or FL-ClbA-GFP did not alter growth compared to wild-type strains. Since the endogenous copy of *clbA* was not altered in these strains, these data

indicate that destruction of ClbA is essential for viability and that d-box-deleted versions of ClbA act in a dominant negative fashion.

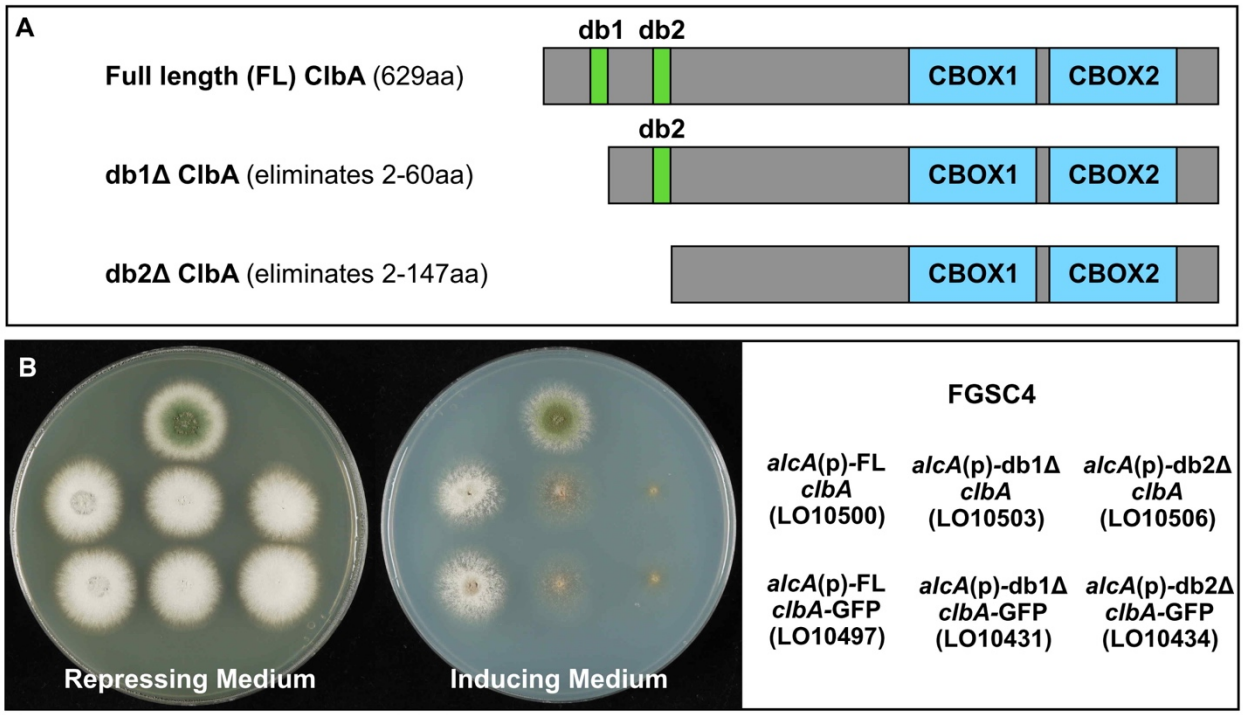

Fig. 4.9: Truncated ClbA is lethal

(A) Diagram of full-length (FL) ClbA with two putative destruction box motifs, db1 (RAAFGDVSN) and db2 (RKTLNKRAT), and two truncated versions of ClbA. CBOX1 designates the first cyclin box fold, also called the N-terminal cyclin domain, and CBOX2 designates the C-terminal cyclin box domain. Constructs shown in A were fused to the *nmtA* regulatable promoter and placed at the *wA* locus. **(B)** Strains are grown on both repressing medium (YAG) and inducing medium (MM with 9g/L fructose and 6.25 mM threonine). Each strain carries endogenous c*lbA* driven by its normal promoter. The *alcA*(p)-FL-*clbA* strain (LO10500) and *alcA*(p)-FL-*clbA*-GFP strain (LO10497) grow like the WT (FGSC4) under both repressing and inducing conditions. The *alcA*(p)-db1Δ-*clbA* strain (LO10503) and *alcA*(p)-db1Δ-*clbA*-GFP strain (LO10431) grow like the WT under repressing conditions, but they are sick and conidiate poorly under inducing conditions. The *alcA*(p)-db2Δ-*clbA* strain (LO10506) and *alcA*(p)-db2Δ-*clbA*-GFP strain (LO10434) grow as well as the WT under repressing conditions but barely grow and do not conidiate under inducing conditions.

I also wished to determine the phenotype caused by failure of destruction of ClbA. Since the growth phenotypes caused by db2Δ-ClbA expression and db2Δ-ClbA-GFP expression appear to be the same, I have used GFP fusions for the bulk of our experiments, because the GFP allows us to monitor the location of the molecules. I encountered difficulty with the *alcA*(p) due to its "leakiness". While colony growth was normal on *alcA* repressing media (**Fig. 4.9B**), spore viability was very low in strains carrying the *alcA*(p) driving expression of db2Δ-ClbA or db2Δ-ClbA-GFP even on *alcA*(p) repressing media, making it difficult to determine the phenotype of db2Δ-ClbA-GFP via microscopy. We reasoned that this was due to leakiness of *alcA*(p) therefore, we searched for a more strongly repressible promoter.

4.3.3 The nmtA promoter can be regulated more effectively than the alcA promoter

In *S. pombe, nmt1* has been shown to be highly transcribed in minimal medium and strongly repressed by the addition of thiamine (Maundrell, 1990; Tamm, 2012). Cory Jenkinson in our lab had previously analyzed the promoter activity of a 761-bp sequence immediately upstream of the *A. nidulans nmt1* homolog (AN8009) *nmtA*. This 761bp *nmtA* promoter [*nmtA*(p)] fused to GFP was placed at the *yA* locus and found to repress GFP fluorescence in the presence of thiamine and allow constitutive GFP expression in the absence of thiamine.

I placed FL-ClbA-GFP and db2Δ-ClbA-GFP under control of the *A. nidulans nmtA*(p) at the *wA* locus in a strain that carries histone H1-mRFP (parental strain LO1516). The endogenous copy of *clbA* was not altered. I found that a thiamine concentration of 0.1 μM repressed *nmtA*(p)-driven expression of db2Δ-ClbA-GFP sufficiently to allow nearly normal growth, and 1.0 μM or more was sufficient to allow growth like the wild-type on solid (**Fig. 4.10**) and in liquid medium.

These results suggested that the *nmtA*(p) can be more strongly repressed than the *alcA*(p) and this, in fact, proved to be the case (see results below).

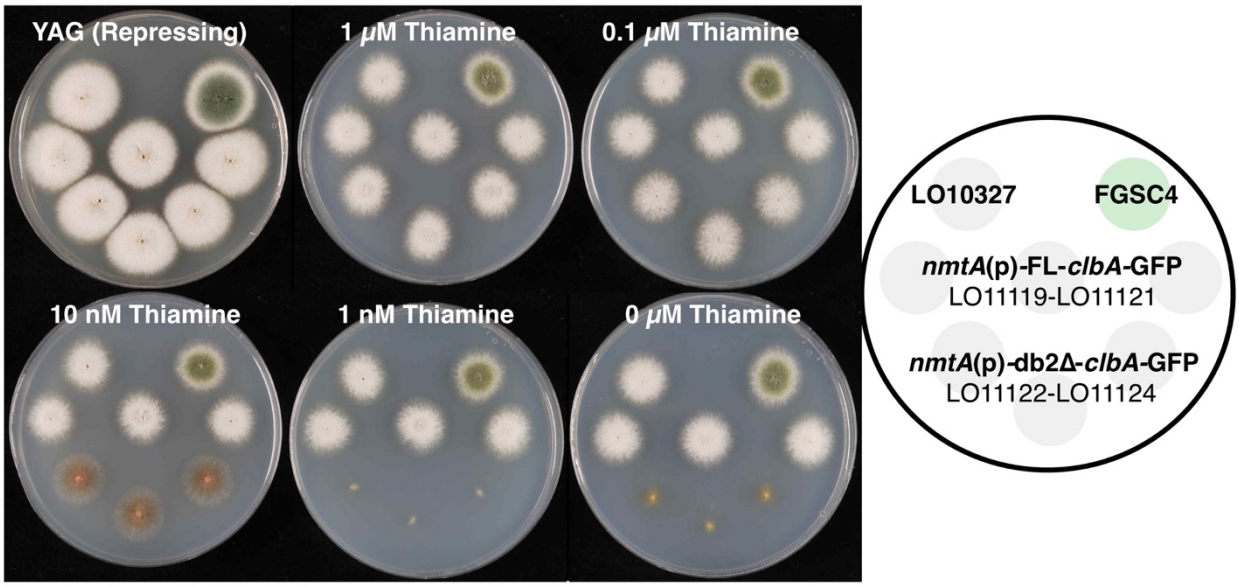

Figure 4.10: Inducing expression of full-length and truncated ClbA via the regulatable *nmtA* promoter

The *nmtA* promoter [*nmtA*(p)] was fused to the N-terminus of both FL-ClbA fused to GFP and truncated (db2Δ) ClbA fused to GFP. These fusion fragments were then placed at the *wA* locus. The endogenous *clbA* gene was not altered in any of the above strains. Three *nmtA*(p)-FL-*clbA*-GFP strains (LO11119-LO11121) grow as well as the control and wild-type strains (LO10327 and FGSC4) under both repressing (high thiamine) and non-repressing (low or no thiamine) conditions. Three *nmtA*(p)-db2Δ-*clbA*-GFP strains (LO11122-LO11124) grow as well as the wild-type under repressing conditions (YAG and 1.0 μM thiamine) and grow nearly normally at a thiamine concentration of 0.1 μM. They are extremely sick under partially-repressing conditions (10 nM thiamine) and dead under non-repressing conditions (1.0 nM thiamine or less). Although GFP-tagged strains are shown, identical results were obtained with strains expressing non-GFP-tagged FL ClbA and db2Δ-ClbA.

4.3.4 Failure to degrade ClbA results in a mitotic arrest as well as nondisjunction

To determine the phenotype of db2Δ-ClbA-GFP, I collected conidia from strains carrying double d-box-deleted, GFP-tagged ClbA, [LO11122 (*nmtA*(p)-db2Δ-*clbA*-GFP)], a strain carrying

clbA$^+$ fused to GFP and under control of *nmtA*(p) [LO11119 (*nmtA*(p)-FL-*clbA*-GFP)], and a control *clbA*$^+$ strain (LO10327). The conidia were collected from material grown on solid medium containing a concentration of 0.1 μM thiamine, a concentration that partially represses expression (**Fig. 4.10**). To allow expression from *nmtA*(p), I inoculated these conidia into liquid media without thiamine. I incubated them at 30°C for ~ 6 h, and then captured Z-axis image stacks at 10-min intervals for 12 h. I found that LO11122 conidia [*nmtA*(p)-db2Δ-*clbA*-GFP] generated short germ tubes, and, once the cells entered mitosis, they became blocked in mitosis. The mitotically arrested nuclei displayed one or more of the following defects: failure of anaphase A, failure of anaphase B, nondisjunction, or chromatin collapsing back into a single mass after initially separating.

To better quantify these observations, I fixed LO11122, LO11119, and LO10327 germlings after 12 h of growth at 30°C. At this time and temperature, control germlings (LO10327) had undergone 2.0 ± 0.1 nuclear divisions and contained ~ 4 nuclei (206 germlings scored from 2 separate experiments). Expression of FL-ClbA-GFP from *nmtA*(p) (strain LO11119) in the absence of thiamine slightly decreased the number of nuclear divisions to 1.8 ± 0.1 (207 germlings scored from 2 separate experiments). FL-ClbA-GFP is predicted to be over expressed in these strains, and this was confirmed by microscopy. This overexpression, however, had a modest effect on the cell cycle, if any. Expression of db2Δ-ClbA-GFP (LO11122), however, drastically reduced the number of nuclear divisions to 0.3 ± 0.1 (180 germlings scored from 2 separate experiments). This indicates that destruction of ClbA is required for nuclear replication. Additionally, we found that chromatin was condensed in 53.8% ± 3.1% of germlings in the db2Δ-ClbA-GFP expressing strain (LO11122) nuclei compared to 5.9% ± 2.1% in the FL-ClbA-GFP expressing strain (LO11119) and 4.5 ± 1.6% in the *clbA*$^+$ strain (LO10327). These data reveal that expression of db2Δ-ClbA-GFP results in a strong mitotic block.

To determine the nature of the mitotic arrest, I needed to be able to collect Z-series image stacks at short intervals. I found that if I collected LO11122 conidia from solid medium with a concentration of 1.0 μM thiamine and then grew those conidia at 30°C in liquid media without thiamine, germination and initial growth were normal. Germlings underwent 2-3 rounds of normal nuclear divisions and then began to show mitotic abnormalities and mitotic blockage. This approach allowed me to find and image cells entering mitosis and displaying the phenotypes caused by expression of db2Δ-ClbA-GFP.

Imaging revealed that, as anticipated, little or no of db2Δ-ClbA-GFP was present initially. The absence of db2Δ-ClbA-GFP is almost certainly due to the conidia carrying over enough thiamine to inhibit expression from *nmtA*(p). Upon continued incubation without thiamine, db2Δ-ClbA-GFP began to be visible at KTs. The exact timing of its appearance varied to some extent among germlings, but it generally became detectable between the second and third nuclear divisions. Nuclei often went through one round of mitosis after db2Δ-ClbA-GFP became visible. In these cases, I found that db2Δ-ClbA-GFP was removed from the KTs, and this strongly correlated with mitotic entry. In most cases mitosis appeared normal. Immediately after mitosis, however, db2Δ-ClbA-GFP became visible at KTs (in marked contrast to controls), and db2Δ-ClbA-GFP fluorescence increased markedly through interphase. At the end of this interphase db2Δ-ClbA-GFP left the KTs, nuclei entered mitosis, and a catastrophic mitosis followed (**Fig. 4.11**). Full condensation of chromatin was never observed until db2Δ-ClbA-GFP left the KTs (n = 46/46 nuclei, strains LO11122 and LO11123). These data indicate that ClbA is removed from KTs by a mechanism other than simple destruction and they are consistent with the hypothesis that ClbA must be removed from KTs in order for mitotic entry to occur.

During these catastrophic mitoses, although db2Δ-ClbA-GFP left the KTs at mitotic onset, it was present at higher levels in the nucleoplasm than in the cytoplasm in the majority of nuclei (45/46 nuclei; **Fig. 4.11 F, J**). Overexpressed ClbA-GFP or ClbA-GFP driven by its endogenous promoter rapidly disappeared from the nucleoplasm of mitotic nuclei. The vast majority of nuclei in db2Δ-ClbA-GFP germlings entered anaphase (43/46 nuclei; **Fig. 4.11 M-P**) relatively quickly after chromosomal condensation but displayed obvious nondisjunction (42/43 nuclei; **Fig. 4.11 M-T**). The chromatin in many nuclei eventually collapsed back into one mass (34/43 nuclei) after initially separating in anaphase. This phenotype is consistent with force being exerted on the chromosomes by the mitotic apparatus, causing chromosomal separation but daughter chromatids failing to disjoin from each other and the elasticity of chromatin pulling the chromatids back into a single mass. During these failed anaphase attempts, db2Δ-ClbA-GFP could be seen faintly on the spindle, in the nuclei, and/or at dot(s) in the separating chromatin (46/46 nuclei) (**Fig. 4.11 N-P, R-T**). These data, in aggregate indicate that destruction of ClbA is required for chromosomal disjunction.

Interestingly, I observed that *nmtA*(p)-driven expression of either ClbA-GFP or db2Δ-ClbA-GFP resulted in a GFP signal at septa. This was not observed in strains in which expression of ClbA-GFP was driven by its endogenous promoter, even when the laser and exposure settings were increased to allow imaging of very faint signals (data not shown).

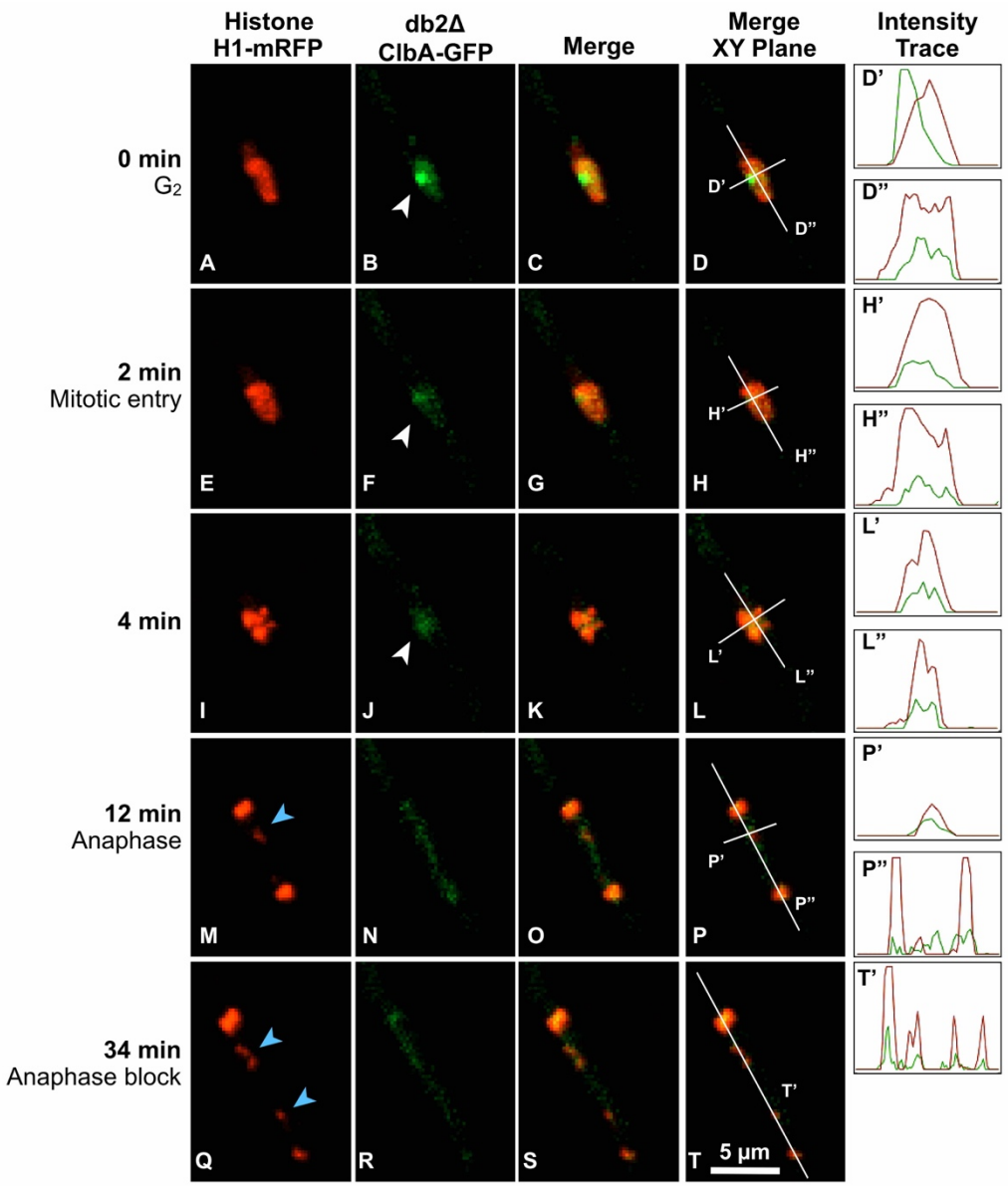

Figure 4.11: Expression of db2Δ-ClbA-GFP results in nondisjunction and mitotic arrest in anaphase

Conidia carrying *nmtA*(p)-db2Δ-*clbA*-GFP and histone H1-mRFP (strains LO11122-LO11124) were collected from hyphae growing on media containing 1.0 µM thiamine, incubated at 30°C for 10-12 h in non-repressing liquid media (i.e. lacking thiamine), and then imaged in 2-min intervals. Images are maximum intensity projections from Z-series stacks. In G_2, db2Δ-ClbA-GFP localizes strongly to the kinetochores (KTs) and faintly to the nucleoplasm (**A-D**). At mitotic entry, db2Δ-ClbA-GFP leaves the KTs but can be seen faintly in the nucleoplasm (**E-H**). Mitosis is stalled or blocked in anaphase, and db2Δ-ClbA-GFP can be seen faintly along the spindle and at a dot in the separating chromatin (**M-T**). White arrows designate db2Δ-ClbA-GFP at the KTs and/or nucleoplasm (**B, F, J**). Blue arrows point to chromosomes that failed to disjoin properly (**M, Q**).

4.3.5 Destruction of NimE$^{Cyclin\ B}$ is important for chromosomal disjunction

Expression of destruction box-deleted NimE$^{Cyclin\ B}$ (dbΔ-NimE$^{Cyclin\ B}$) also results in a strong mitotic block. dbΔ-NimE$^{Cyclin\ B}$-GFP expressing cells enter mitosis and progress through anaphase before becoming blocked in telophase with dbΔ-NimE$^{Cyclin\ B}$-GFP remaining at the spindle poles (De Souza *et al.*, 2009; Nayak *et al.*, 2010). I utilized the same destruction box-deleted cyclin B construct used in previous work (De Souza *et al.*, 2009; Nayak *et al.*, 2010) fused to GFP (dbΔ-NimE$^{Cyclin\ B}$-GFP) but placed it under the control of the *A. nidulans nmtA* promoter at the *wA* locus (LO11357-LO11359). My results were consistent with previous studies (data not shown). However, when I followed nuclei through mitosis by capturing time-lapse Z-series stacks at one-minute intervals, I also observed a high frequency of nondisjunction in dbΔ-NimE$^{Cyclin\ B}$-GFP expressing cells (19/32 nuclei), which was not previously reported. Thus, destruction of both ClbA and NimE$^{Cyclin\ B}$ during mitosis is required for proper chromosomal disjunction.

4.3.6 Cohesin is removed from chromosomes in db2Δ-ClbA and dbΔ-NimE$^{Cyclin\ B}$ expressing strains

The cohesin complex holds sister chromatids together, and its removal is required for chromosomal disjunction. Cohesin complex removal is regulated by mitotic cyclins and the APC/C [reviewed in (Wong, 2010)]. Failure of cohesin complex removal is, thus, a plausible cause for the high frequencies of nondisjunction caused by db2Δ-ClbA and dbΔ-NimE$^{Cyclin\ B}$. Although the cohesin complex has been studied extensively in other organisms, there is very little information on it in filamentous fungi. To determine if db2Δ-ClbA and dbΔ-NimE$^{Cyclin\ B}$ altered the removal

of the cohesin complex, we first had to investigate the localization and removal of the complex in control cells (this work was done by Dr. Tetsuya Horio while in the Oakley lab).

The core cohesin complex is composed of Scc1 (also known as Rad21 in humans and Mcd1 in *S. cerevisiae*), Scc3, and two SMC (Structural Maintenance of Chromosomes) proteins called SMC1 and SMC3. The *A. nidulans* homolog of human Rad21 and *S. cerevisiae* Mcd1 is AN7465 (E-value of 2E-29 and 3E-17, respectively), which we now designate *sccA*. Strains carrying SccA-GFP and HH1-mRFP (LO3231) had previously been constructed in our lab. We found that SccA-GFP localizes to nuclei but not nucleoli throughout interphase (arrows in **Fig. 4.12A-C**), and, as expected, it leaves the chromatin during mitosis. To narrow down the timing of disappearance of

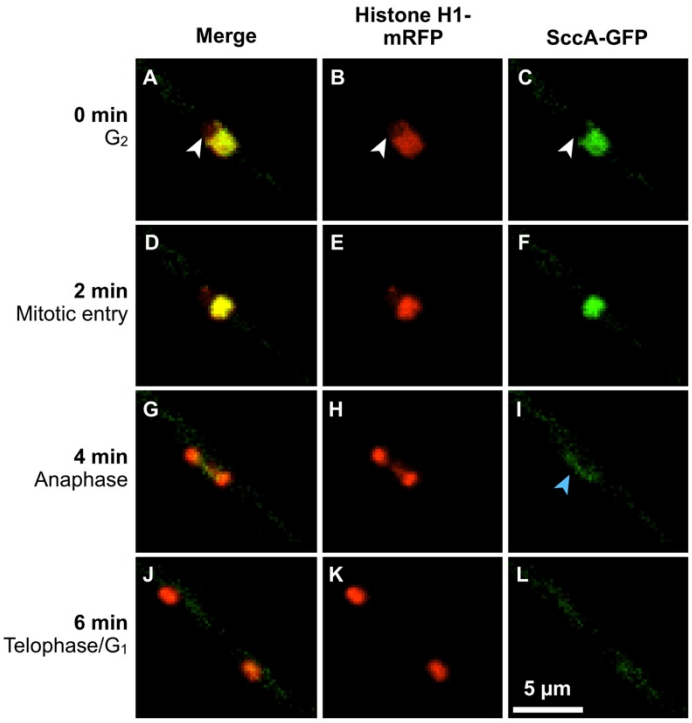

Figure 4.12: SccA-GFP localization during mitosis
(**A-C**) SccA localizes to the nucleoplasm during interphase but is excluded from the nucleolus (white arrow). SccA is present in the nucleus during early mitosis (**D-F**) but disappears from chromatin at the beginning of anaphase (**G-I**). In some cases, SccA localizes between the separating chromosomes in early anaphase (blue arrow in **I**), but it is completely absent in telophase/G_1 (**J-L**). Images are maximum intensity projections from a time-lapse data set collected at 1-min intervals at 25°C by Dr. Tetsuya Horio. Figure was generated by Vitoria Paolillo.

SccA-GFP from chromosomes during mitosis, we captured Z-series image stacks at 1-min intervals (n= 42 nuclei). SccA-GFP localized to condensed chromatin (42/42 nuclei, **Fig. 4.12D-F**) early in mitosis but, as expected, disappeared at the beginning of anaphase. In some cases (10/42 nuclei), SccA-GFP was observed between the separating chromatin in early anaphase (**Fig. 4.12G-I**, see blue arrow), but this signal always disappeared in late anaphase. After mitosis, SccA-GFP slowly accumulated in nuclei in early G_1, and this signal intensified as the cell cycle progressed.

I next wanted to determine if SccA was removed from chromosomes during mitosis in db2Δ-ClbA and dbΔ-NimE$^{Cyclin\ B}$ expressing cells. I generated strains that carried SccA-GFP, histone H1-mRFP, and either *nmtA*(p)-db2Δ-*clbA* (LO11211) or *nmtA*(p)-dbΔ-*nimE*$^{cyclin\ B}$ (LO11217) inserted at the *wA* locus. A control strain (LO11202) that carried SccA-GFP and histone H1-mRFP, was constructed by inserting *AfpyroA* at the *wA* locus. The endogenous *clbA* and *nimE* genes were not altered in any strain. I harvested conidia from each of these strains grown on media with 1.0 μM thiamine. I inoculated conidia into liquid media lacking thiamine (allowing expression of the d-box-deleted cyclins), incubated the cultures at 30°C for ~6 h, and then captured images of Z-axis stacks at 10-min intervals for 12 h.

Expression of db2Δ-ClbA (**Fig. 4.13**) or dbΔ-NimE$^{Cyclin\ B}$ (**Fig. 4.14**) led to a mitotic arrest in the second or third nuclear division cycle, as seen in previous experiments. Perhaps surprisingly, I found that SccA-GFP disappeared in all nuclei at anaphase onset in both LO11211 (db2Δ-clbA, n=31/31 nuclei) and LO11217 (dbΔ-NimE$^{Cyclin\ B}$, n=38/38 nuclei). I followed these nuclei over long periods of time and found that they stayed in mitosis for a long (although variable) time after cohesin removal/anaphase (the range was 30-300+ min but most were in mitosis more than 1 h). However, eventually SccA-GFP would begin to re-accumulate faintly in condensed nuclei, and the chromosomes of some nuclei would decondense and accumulate SccA-GFP more brightly.

Interestingly, I found that mitotic exit did not occur for all nuclei at the same time in the same cell, and some nuclei would remain condensed even if SccA-GFP accumulated (**Figs 4.13 P-U, 4.14 P-U**). These cells continued to cycle and attempt additional mitoses, and the number of nuclear fragments, likely due to repeated nondisjunction, increased (**Figs 4.13, 4.14**). I also imaged these strains in short, 2-min, intervals and obtained similar results. These data indicate that SccA-GFP is removed from chromosomes during mitosis in cells expressing either db2Δ-ClbA or dbΔ-NimE$^{\text{Cyclin B}}$, and, thus, failure of cohesin complex removal is not the cause of the failure of chromosomal disjunction I observe.

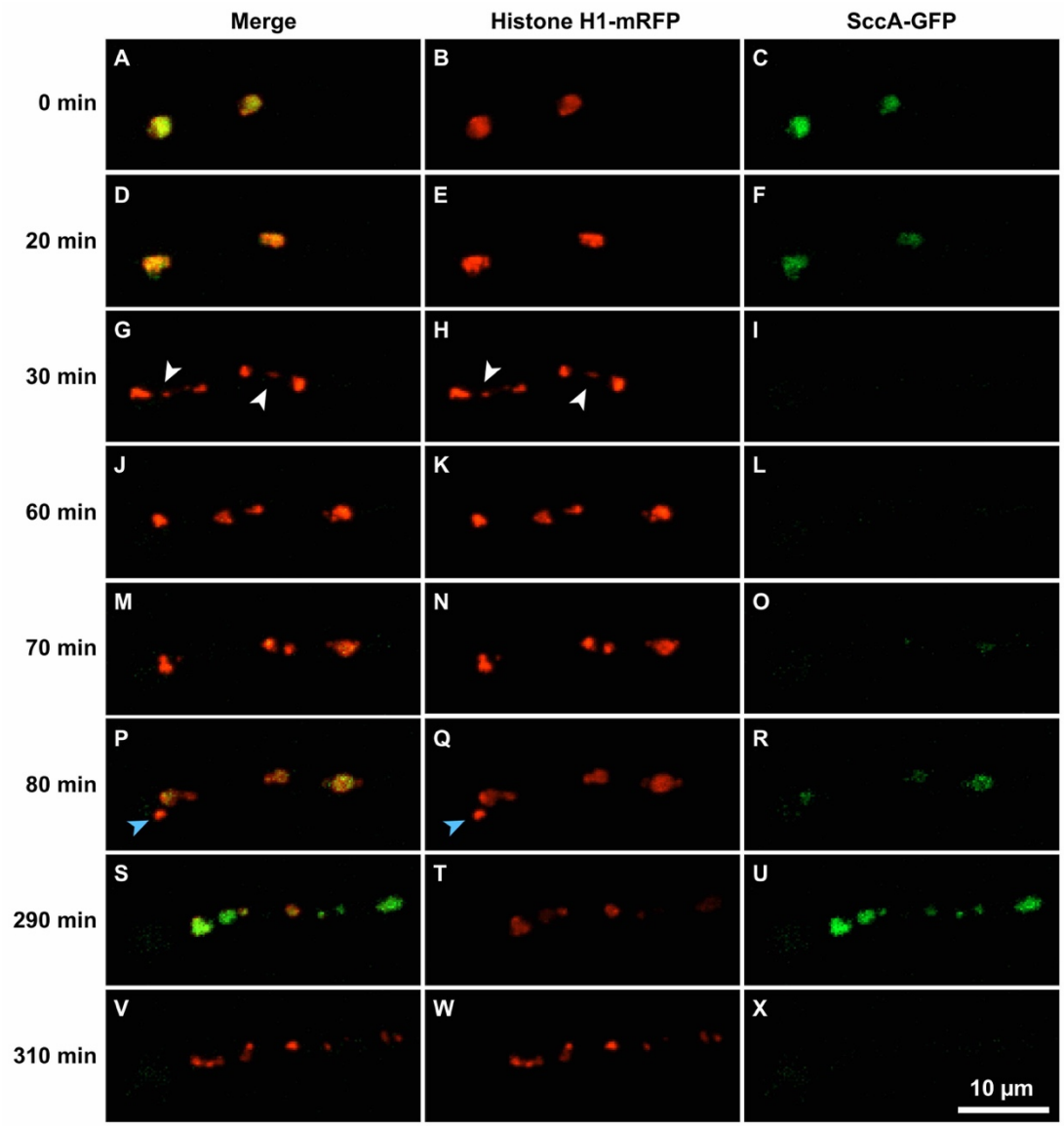

Figure 4.13: SccA-GFP is removed from chromatin in db2Δ-ClbA expressing strains
Conidia from strain LO11211 [which carries *nmtA*(p)-db2Δ-*clbA*, SccA-GFP, histone H1-mRFP] were collected from 1.0 µM thiamine plates and incubated in liquid medium without thiamine at 30°C. Images are projections from a time-lapse data set collected at 10-min intervals at 30°C. At T=0 min, two nuclei are in G_2 with SccA-GFP present in the nucleoplasm, but not in the nucleoli (**A-C**). Nuclei enter mitosis with SccA-GFP still present in the nucleoplasm (**D-F**). SccA-GFP leaves chromatin during mitosis (**G-I**) despite obvious nondisjunction (arrows in **G-H**). SccA-GFP remains absent from nuclei during a lengthy mitotic block (**D-R**) (60+ min) until nuclei begin to exit mitosis (**M-R**). Not all nuclei exit mitosis at the same time (blue arrow in **P-Q** indicates a nucleus that is slow in exiting). Nuclear fragments and nuclei of different sizes are apparent during interphase (**S-U**). Fragmented chromatin enters another aberrant mitosis (**V-X**), and SccA leaves chromatin once more (**X**).

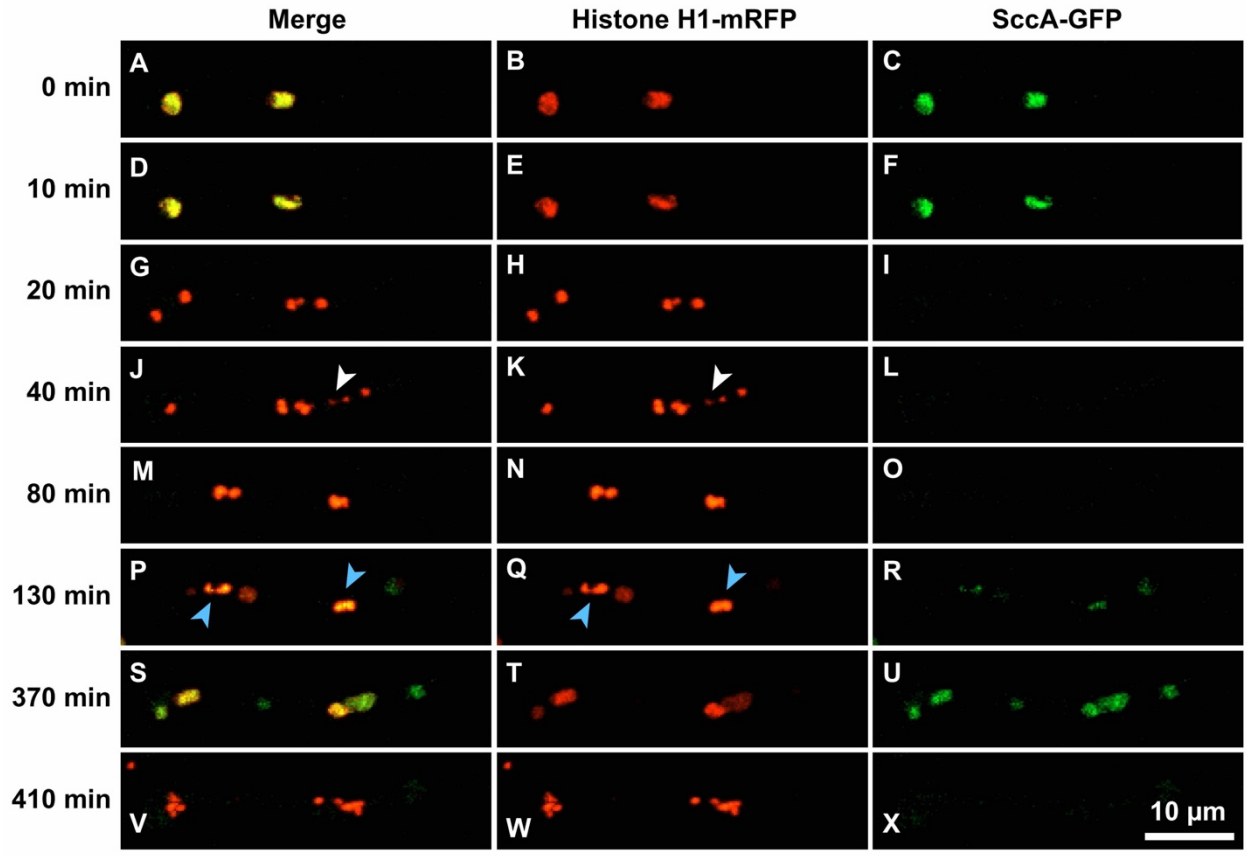

Fig. 4.14: SccA is removed from chromatin in dbΔ-NimE$^{\text{Cyclin B}}$ expressing strains

Conidia from strain LO11217 [which carries *nmtA*(p)-dbΔ-*nimE*$^{cyclin\ B}$, SccA-GFP, and histone H1-mRFP] were collected from 1.0 µM thiamine plates and incubated in liquid media without thiamine at 30°C. Images are maximum intensity projections from a time-lapse data set collected at 10-min intervals at 30°C. At T=0, two nuclei are in G_2, and SccA-GFP is present in the nucleoplasm (**A-C**). Nuclei enter mitosis with SccA-GFP still present (**D-F**). SccA-GFP disappears from chromatin as nuclei enter anaphase **(G-I)**. SccA-GFP is completely absent from chromatin during an extended failed mitosis **(J-O)** despite obvious nondisjunction (arrow in **J-K**). SccA starts to return when nuclei begin to exit mitosis (**P-R**). Not all nuclei exit mitosis at the same time. Blue arrows in **P-Q** indicate nuclei that remain partially condensed, while others in the same cell have decondensed. Nuclear fragments and nuclei of different sizes are apparent during interphase (**S-U**). Nuclei enter another mitosis (**V-X**), and SccA leaves chromatin once more (**X**).

4.3.7 Expression of db2Δ-ClbA, but not dbΔ-NimE$^{Cyclin\ B}$, extends interphase

Although the mitotic phenotypes caused by expression of db2Δ-ClbA and dbΔ-NimE$^{Cyclin\ B}$ are similar, I found the effects of their expression on cell cycle timing were very different. To examine the effects of db2Δ-ClbA and dbΔ-NimE$^{Cyclin\ B}$ on the cell cycle, I grew strains LO11211 [*nmtA*(p)-db2Δ-*clbA*] and LO11217 [*nmtA*(p)-dbΔ-*nimE$^{cyclin\ B}$*] on 1.0 μM thiamine, harvested spores, and inoculated them into media with no thiamine. As mentioned above, the thiamine is gradually depleted, and the d-box-deleted cyclins become expressed, resulting in a mitotic block. The presence of a mitotic block indicates that the d-box-deleted cyclin was expressed in the previous cell cycle. By timing the cell cycle prior to a mitotic block, I can determine if the d-box-deleted cyclin alters the length of the cell cycle. In LO11202 (control), I found the average cell cycle duration (time in min from the beginning of one mitosis to the beginning of the next mitosis) at 30ºC for the first 3 nuclear divisions was 150 ± 34 min (n = 63 nuclei). In LO11217 [*nmtA*(p)-dbΔ-*nimE$^{cyclin\ B}$*], I found the cell cycle duration was 150 ± 36 (n = 21 nuclei) when followed by a normal mitosis and 155 ± 39 min (n = 35) when followed by an abnormal mitosis. These values were not significantly different from the control. Expression of dbΔ-NimE$^{Cyclin\ B}$, thus, does not significantly alter the length of the cell cycle. LO11211 which expresses db2Δ-ClbA, however, had an average cell cycle time of 183 ± 28 min (n = 49 nuclei) when followed by a normal mitosis and an average cell cycle time of 209 ± 49 min (n = 31 nuclei) when followed by an abnormal mitosis. These were both significantly different from the control ($p < 0.001$). Expression of db2Δ-ClbA, thus, does increase the length of interphase. We attribute the lengthened cell cycle before normal mitosis to the accumulation of a small amount of db2Δ-ClbA at levels insufficient to arrest mitosis as noted above. These data strongly indicate that ClbA has an inhibitory role in cell cycle progression in interphase.

4.4 Discussion

4.4.1 Cln-like cyclin PucA

I have now found that PucA is an essential G_1/S cyclin in *A. nidulans* that is required for cells to accumulate $NimE^{Cyclin\ B}$ and enter S-phase. I have determined that PucA promotes entry into S phase by inactivating CdhA, the activator of the APC/C, during late mitosis and G_1. Although *pucA*Δ is lethal, deletion of *pucA* in a *cdhA*Δ background is viable. This result indicates that PucA is necessary and sufficient to inactivate APC/C-CdhA at the G_1/S transition. It also reveals that no other proteins, including other cyclins, can sufficiently inactivate CdhA at the G_1/S boundary to allow cell cycle progression. If there were other sufficient mechanisms for CdhA inactivation in *A. nidulans,* deletion of *pucA* would not have been lethal. This result is different from results in other organisms that have been studied, as CdhA is typically regulated by several redundant mechanisms. In both humans and *S. cerevisiae*, multiple cyclin/CDK complexes (e.g. Cln1, Cln2, Clb5, and Clb6 in *S. cerevisiae*) phosphorylate and inactivate Cdh1 at G_1/S. APC/C-Cdh1 can also be inactivated through binding of inhibitors (e.g. EMI1 in vertebrates, Acm1 in *S. cerevisiae*, and Rca1 in *Drosophila melanogaster*), but none of these inhibitors have an obvious homolog in *A. nidulans.* Thus, although Cdh1 inactivation is regulated by multiple proteins in other organisms [reviewed in (Sivakumar and Gorbsky, 2015)], APC/C-CdhA is inactivated at G_1/S in *A. nidulans* solely by a mechanism requiring PucA.

Although my evidence indicates that deletion of *pucA* causes a G_1 arrest, it allows continuous nuclear growth. As *pucA*Δ nuclei increased in size, I observed a concurrent loss of both nuclear DAPI fluorescence and histone H1 fluorescence. Some *pucA*Δ nuclei would eventually overcome the G_1 block and undergo mitosis, and, in those cases, the histone H1 signal would

suddenly become visible as the chromosomes condensed. This indicates that the chromatin is present in interphase nuclei, but it is very diffuse. Interestingly, this diffuse chromatin phenotype has also been observed with a deletion of *nimX*^{cdk1} (De Souza *et al.*, 2013), and NimX^{Cdk1} has been shown to interact with PucA (De Souza *et al.*, 2014). It is also important to note that we have worked with other mutants that result in very large, stretched nuclei (e.g. the ɣ-tubulin mutant *mipA*D159), but these nuclei have very bright histone H1 fluorescence and are obviously polyploid. It is likely that deletion of *pucA* inhibits DNA replication but not nuclear growth, resulting in large nuclei with diffuse chromatin. It is also possible that this phenotype is caused by a lack of NimX activity, as PucA is a binding partner of NimX and both *pucA*Δ and *nimX*^{cdk1}Δ result in similar phenotypes.

PucA also has non-essential functions in interphase in addition to inactivating APC/C-CdhA at the G_1/S transition. In *pucA*Δ, *cdhA*Δ double mutant strains I observed nuclear abnormalities such as severe stretching and partial condensation and decondensation of chromatin in a nuclear autonomous fashion. These interesting interphase phenotypes are not due to obvious microtubule abnormalities, inhibition of polarized growth, or failure to accumulate NimE$^{Cyclin\ B}$ in the nucleus or at the SPB.

4.4.2 B-type cyclins ClbA and NimE$^{Cyclin\ B}$

Prior to this study, the B-type cyclin NimE was the only cyclin shown to be essential in *A. nidulans* and the only cyclin with clear cell cycle regulatory functions. The *nimE* gene was identified more than 40 years ago (Morris 1975) and found to be required for both S-phase and entry into mitosis(Bergen *et al.*, 1984; Morris, 1975). We have now analyzed the functions of a second B-type cyclin, which we have named ClbA.

I have found that ClbA localizes with KTs from mid-G_2 until mitotic onset. *clbA* is not essential, but expression of a version of ClbA with two d-boxes deleted (db2Δ-ClbA) completely blocked growth. To carry out this work, I needed to develop a more tractable repressible promoter system than the *alcA* system that has been used extensively in *A. nidulans.* I found that the *nmtA* promoter in *A. nidulans* could be repressed more effectively than the *alcA* promoter, and this provided me with the ability to determine the phenotypes of db2Δ-ClbA expression via microscopy. I found that expressing db2Δ-ClbA resulted in mitotic catastrophe at anaphase with a high frequency of chromosomal non-disjunction as well as a mitotic arrest. Expression of db2Δ-ClbA-GFP resulted in abundant GFP signals at KTs and nuclei throughout interphase, but, interestingly, I observed that db2Δ-ClbA-GFP was still removed from KTs at mitotic entry. This indicates that ClbA is removed from kinetochores by a mechanism other than destruction. However, db2Δ-ClbA-GFP remained present in the nucleoplasm, and when anaphase occurred, db2Δ-ClbA-GFP could be seen along the spindle and at the poles of nuclei in aberrant anaphases. This was in contrast to full-length ClbA-GFP which was never seen in nuclei or at the poles during anaphase/telophase, whether overexpressed or expressed only from its native promoter. In addition, I found that expression of db2Δ-ClbA-GFP caused a lengthening of interphase. The facts that ClbA-GFP is removed from kinetochores at mitotic entry and that expression of db2Δ-ClbA-GFP causes a lengthening of interphase suggest ClbA might have a role in the G_2/M checkpoint in addition to its role mitotic progression.

Expression of dbΔ-NimE$^{\text{Cyclin B}}$-GFP has been shown previously to cause a mitotic block in telophase with dbΔ-NimE$^{\text{Cyclin B}}$-GFP remaining at the poles (De Souza *et al.*, 2009; Nayak *et al.*, 2010). My use of the *nmtA* promoter to regulate expression of dbΔ-NimE$^{\text{Cyclin B}}$-GFP has allowed me to determine that its expression also causes a high frequency of nondisjunction.

Destruction of both ClbA and NimE$^{Cyclin\ B}$ are, thus, required for chromosomal disjunction in mitosis.

I also determined that the high frequency of chromosomal nondisjunction observed in both db2Δ-ClbA-GFP and dbΔ-NimE$^{Cyclin\ B}$-GFP cells was not caused by a failure of removal of the cohesin complex. For disjunction to occur successfully, two processes must occur. The cohesin complex must be removed and catenanes (DNA intertwinings) of the daughter chromatids must be resolved by topoisomerase II. Since the cohesin complex is removed in strains expressing db2Δ-ClbA or dbΔ-NimE$^{Cyclin\ B}$, it follows that destruction of both ClbA and NimE$^{Cyclin\ B}$ are required for DNA decatenation, presumably through regulation of topoisomerase II. Indeed, the phenotypes I observe are consistent with a failure of decatenation. Unlike the cohesin complex, catenanes cannot resist the pulling forces of microtubules [reviewed in (Haarhuis *et al.*, 2014)]. A failure to resolve catenanes would not block anaphase but is predicted to lead to chromosome stretching and failure of disjunction, as we have observed.

4.4.3 Summary of cell cycle regulation by group I cyclins in filamentous ascomycetes

Now that the three group I cyclins have been substantially characterized in *A. nidulans*, it is clear that they have distinct, non-redundant functions in cell cycle regulation. My current findings, and previous findings from other labs, greatly clarify the functions of group I cyclins in cell cycle regulation in *A. nidulans*, and I will now summarize what we know about those functions. I anticipate, given the conservation of group I cyclins, that many of these findings will apply to other filamentous ascomycetes.

Starting my summary at the G_1/S transition, PucA activity is required to inactivate APC/C-CdhA and allow accumulation of NimE$^{Cyclin\ B}$ and consequent entry into S-phase. NimE$^{Cyclin\ B}$ is

required for S-phase and for entry into mitosis. Non-degradable ClbA, but not non-degradable $NimE^{Cyclin\ B}$, causes a delay in interphase, so destruction of ClbA is important for normal progression through interphase. This fact, along with the fact that ClbA is removed from kinetochores at mitotic onset, leads us to speculate that ClbA may play an inhibitory role in the G_2-to-M checkpoint. Destruction of both ClbA and $NimE^{Cyclin\ B}$ during mitosis is required for chromosomal disjunction (likely through topoisomerase II resolution of catenanes) and removal of $NimE^{Cyclin\ B}$ from the SPB (which is normally brought about by destruction of $NimE^{Cyclin\ B}$ earlier in mitosis) is required for the M-to-G_1 transition (**Fig. 4.14**).

Chapter 5: SCF components CulA and SkpA are essential for controlling cell cycle progression and for maintaining multinuclear tip cells in *A. nidulans*

5.1 Introduction

The coordinated synthesis and destruction of cell cycle regulatory proteins ensures that the cell cycle progresses in a sequential and irreversible manner. The targeted destruction of proteins (proteolysis) occurs via the ubiquitin-proteasome system (UPS). Ubiquitin-mediated proteolysis is carried out when E3 ubiquitin ligases mediate the transfer of ubiquitin molecules to a particular protein, thus targeting that protein for degradation via the 26S proteasome. In addition to regulating the stability of proteins, protein ubiquitination can also regulate the localization and function of target substrates. Two major E3 ubiquitin ligases involved in regulating cell cycle progression in eukaryotes include the Skp/Cullin/F-box-containing (SCF) and the anaphase-promoting complex/cyclosome (APC/C) complexes [reviewed in (Teixeira and Reed, 2013)]. Perturbation of the UPS system can lead to uncontrolled cell proliferation and cancer.

SCF complexes are composed of a core of three invariable components: Skp1 (S-phase kinase-associated protein 1), Cul1 (Cullin 1), and Rbx1 (RING-box protein 1). Cul1 acts as a scaffold protein that binds both Rbx1 and Skp1. Rbx1 recruits the E2 enzyme and Skp1 recruits F-box proteins. F-box proteins are the variable component of the SCF complex, and they are responsible for recruiting substrates in a highly specific manner [reviewed in (Teixeira and Reed, 2013)].

I was interested in studying the function of the SCF complex in the filamentous fungus *Aspergillus nidulans* for two major reasons. The first is that filamentous fungi are hugely important medically, agriculturally and commercially [reviewed in (Meyer *et al.*, 2016)], and it is important to understand the cell biology of filamentous fungi to be able to combat fungal pathogens and to

maximize the growth of commercially valuable fungi and their production of desirable products. The SCF complex plays a central role in the regulation of the cell cycle, and there is very limited information on its function in filamentous fungi. *Aspergillus nidulans* is an excellent model organism for studying fungal cell biology. The *A. nidulans* homologs of Skp1 and Cul1 (*skpA* and *culA*) have been deleted in *A. nidulans* and found to be essential (von Zeska Kress *et al.*, 2012). No localization data has been published in *A. nidulans*, however, and there is little information on the functions of the SCF complex in the cell cycle or other important cellular processes in *A. nidulans* or other filamentous fungi. Although *skpA* and *culA* are essential genes, in *A. nidulans* the heterokaryon rescue technique (described in detail in Chapter 2.8) allows us to examine the phenotypes of deletions of essential genes.

The second reason is that, as described in Chapter 1, we have previously found that γ-tubulin has an unexpected and microtubule independent role in inactivating the APC/C at the G_1/S boundary that results in cell cycle blockage in G_1 (Edgerton-Morgan and Oakley, 2012; Nayak *et al.*, 2010). A temperature-sensitive γ-tubulin mutation causes a nuclear autonomous failure of the destruction or removal of the activator protein Cdh1 (the *A. nidulans* homolog is CdhA), which results in constitutive APC/C^{CdhA} activity and failure of affected nuclei to enter S phase. Since, in organisms that have been studied, Cdh1 is targeted for destruction by the SCF complex (Choudhury *et al.*, 2016; Fukushima *et al.*, 2013), I wanted to characterize components of the SCF complex and determine whether the SCF has a role in CdhA regulation in *A. nidulans.*

Here I report the successful GFP-tagging and imaging of SkpA and CulA through mitosis and the cell cycle, and I have found that, as expected, the SCF complex plays an important role in regulating the abundance of CdhA. Most surprisingly, we have found that the SCF complex plays a critical role in suppressing septation near the growing hyphal tip. Inhibition of septation near

the hyphal tip is important because it results in the formation of multinucleate tip cells that facilitate rapid hyphal growth.

5.2 Results

5.2.1 Localization of SkpA

I initially fused GFP to the C-terminus of SkpA (SkpA-GFP). Transformation with this construct resulted in the generation of either heterokaryons or transformants that showed an incorrect DNA insertion when I tested them via diagnostic PCR. This likely indicates that the C-terminal fusion is lethal. I was, however, able to obtain viable transformants with an N-terminal GFP fusion to SkpA (GFP-SkpA). Expression of the fusion gene was under control of the endogenous *skpA* promoter. Strains expressing GFP-SkpA (strains LO10476-LO10478) displayed a slight reduction in growth compared to wild-type (FGSC4) at all temperatures tested (**Fig. 5.1**). Strains are listed in **Table 2.1**.

To determine the localization pattern of SkpA, I imaged strains LO10476-LO10478 which carried GFP-SkpA and histone H1-mRFP. I first collected Z-series stacks at 10-minute intervals at 37℃. I found that GFP-SkpA localized to all interphase nuclei but was faint or completely absent in nucleoli (n = 62 nuclei). GFP-SkpA was also present faintly in the cytoplasm throughout the cell cycle. Interestingly, I observed rapidly moving GFP-SkpA "dots" and larger, more static "spots" in the cytoplasm, particularly between the tip most nucleus and the hyphal tip. In many hyphae, GFP-SkpA was also concentrated at the Spitzenkörper (SPK) (**Fig. 5.2A-G**), particularly

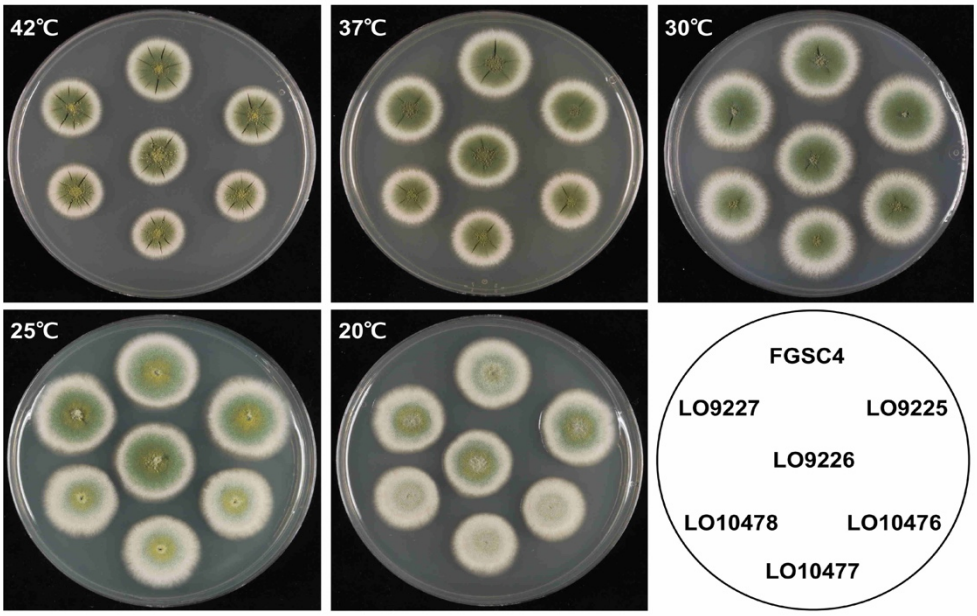

Figure 5.1: Temperature growth tests of strains carrying GFP-CulA and GFP-SkpA
Three different strains carrying GFP-CulA (LO9225-LO9227) and GFP-SkpA (LO10476-LO10478) were stabbed onto complete media and incubated at various temperatures. Strains carrying GFP-SkpA display a slight reduction in growth compared to the wild-type strain (FGSC4) at all temperatures tested.

in germlings that had undergone three or more nuclear divisions. The SPK ("apical body" or "tip body") is a structure found at the tips of growing hyphae in many fungi that is thought to be necessary for tip growth [reviewed in (Harris *et al.*, 2005; Steinberg *et al.*, 2017)]. In order to quantify GFP-SkpA localization to the SPK, I incubated conidia at 37ºC for 14 hours and then collected Z-series stacks of random fields over the next hour. I determined that GFP-SkpA showed an obvious concentration at the SPK in 76 ± 7% of tip cells with three or more nuclei (n = 197 tip cells, 3 separate experiments using strains LO10476-LO10478). In addition, 52 ± 11% of tip cells with three or more nuclei had GFP-SkpA dots or larger spots in the cytoplasm near the hyphal tip. Short tip cells with 1 or 2 nuclei did not display these localization patterns, as only 4 ± 6% had GFP-SkpA at the SPK (n = 25 tip cells, 3 separate experiments). I also imaged GFP-SkpA strains

in short, 1-sec intervals and found that the larger, GFP-SkpA spots tended to be more static (**Fig. 5.2 B-G**, blue arrows). The smaller dots moved much more rapidly, as mentioned earlier, but they are hard to observe in single time-points and more easily observed in movies (data not shown).

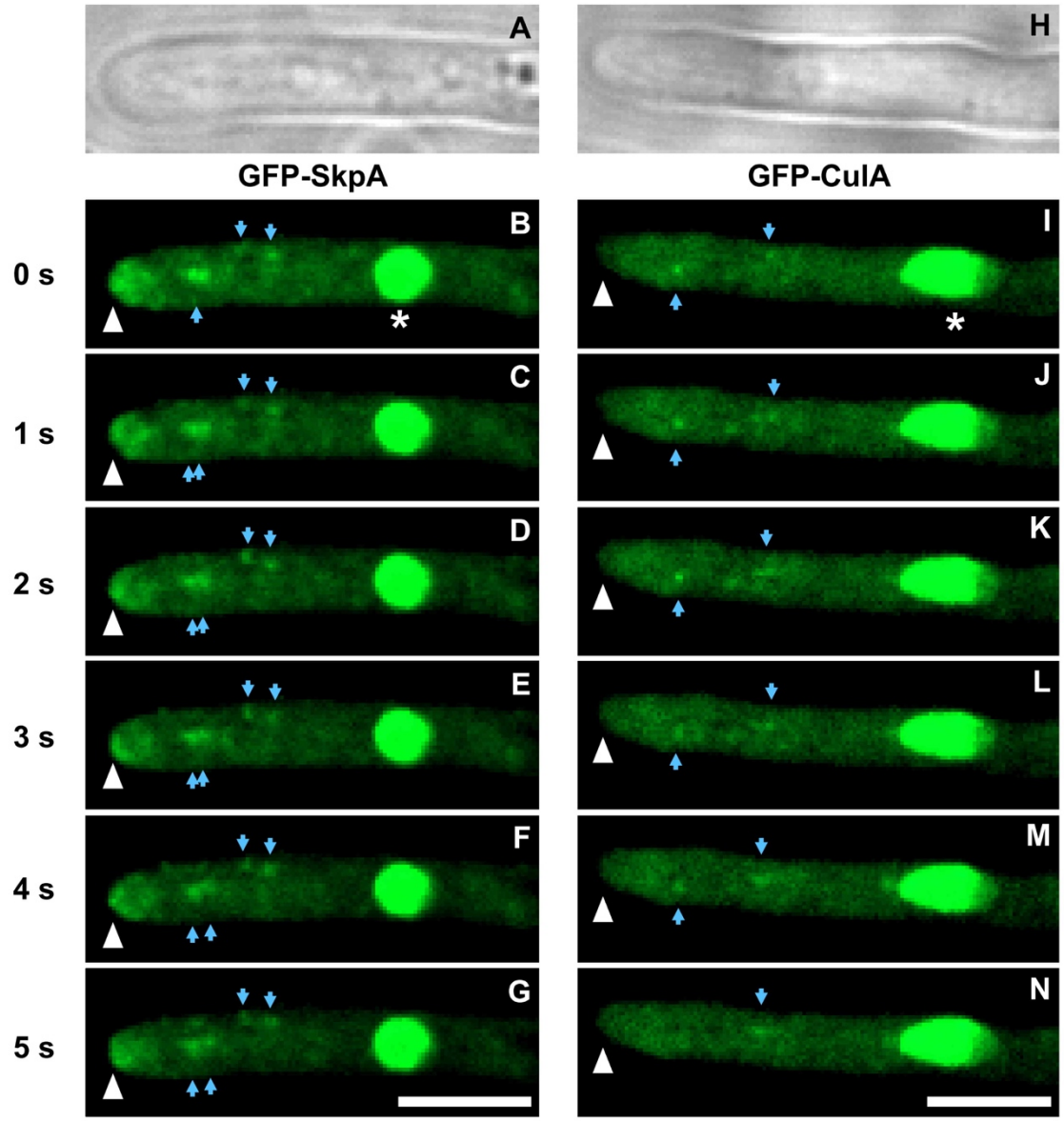

Figure 5.2: GFP-SkpA localizes to hyphal tips and both GFP-SkpA and GFP-CulA localize to bodies in the cytoplasm between the tip and the tip nucleus

All images are from a single-focal plane and were obtained with a spinning disk confocal microscope. Strains carrying either GFP-SkpA or GFP-CulA were imaged at 25°C in 1-second intervals. Representative images from a time-lapse dataset of GFP-SkpA (**B-G**) and GFP-CulA (**I-N**) are shown. Bright field images of the corresponding hyphal tips are shown in panels **A** and **H**. GFP-SkpA localizes to the hyphal tip (white arrowheads in **B-G**) while GFP-CulA does not localize to the hyphal tip (white arrowheads in **I-N**). Both GFP-SkpA and GFP-CulA localize to dots and larger spots in the cytoplasm between the hyphal tip and the tip nucleus. The movement of larger spots is relatively static (blue arrows in **B-G** and **I-N**). Asterisks indicate nuclei in **B** and **I**.

At mitotic entry, nuclear GFP-SkpA levels dropped to cytoplasmic levels before reappearing briefly at "dots" in mitotic nuclei. Mitosis lasts only about 5 min at 37ºC and, to follow the localization of GFP-SkpA through mitosis, I imaged at 45-second intervals at 25ºC (mitosis is about 10 minutes at 25ºC) (n = 18 nuclei). In some nuclei, GFP-SkpA would first appear as a single dot and in others as two dots. These dots are likely SPBs and GFP-SkpA probably begins to localize to the SPBs around the time of SPB separation (**Fig. 5.3E**). GFP-SkpA disappeared from the two separating "dots" in anaphase (**Fig. 5.3 I, J**), and often a faint localization to the region between the dots (putatively the mitotic spindle) was observed between the separating chromosomes. To confirm that GFP-SkpA was indeed localizing to separating SPBs during mitosis, I generated strains carrying GFP-SkpA, histone H1-mTagBFP2, and SepK-tdTomato (a SPB marker) (strains LO11517-LO11519). I found that GFP-SkpA was concentrated at the SPB (**Fig. 5.3K-Q**) (n=30 nuclei). Although the GFP-SkpA and SepK-tdtomato signals overlapped, the peak of the GFP-SkpA signal was lightly inside (i.e. toward the nucleoplasm rather than the cytoplasm) of the peak of the SepK-tdtomato fluorescence (**Fig. 5.3 P, Q**). The homolog of SepK in *S. cerevisiae*, Nud1, is a component of the outer plaque of the SPB, but it does not localize to the inner plaque of the SPB (Wigge *et al.*, 1998). Thus, our co-localization data suggest that GFP-SkpA localizes to the inner surface of SPBs during mitosis and that SepK localizes farther outside, perhaps to the outer surface of the SPB.

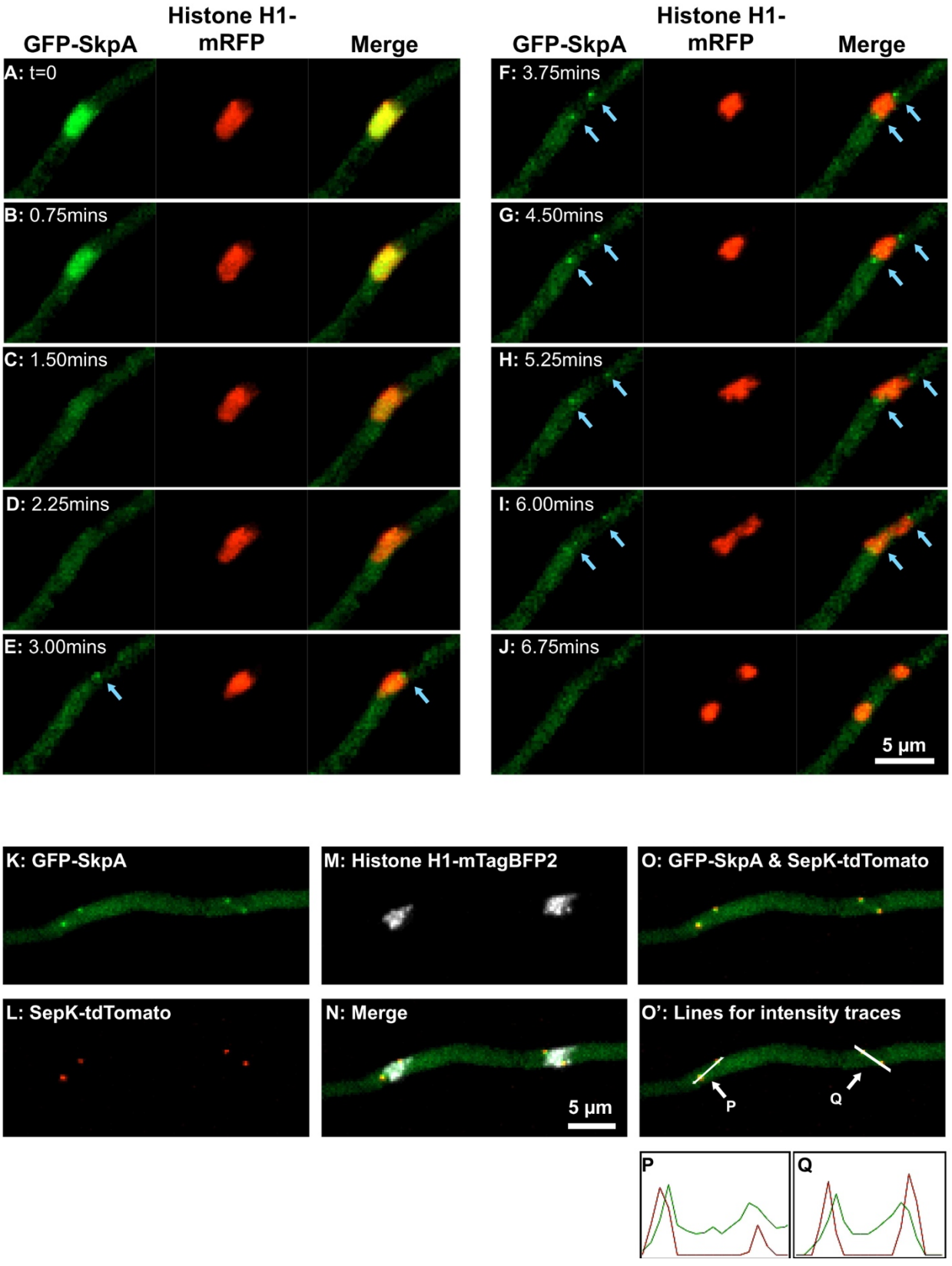

Figure 5.3 *(continued on next page)*

continued from previous page

Figure 5.3: Localization of GFP-SkpA during mitosis
All images are maximum intensity projections from Z-series stacks. (**A-J**) A strain carrying histone H1-mRFP and GFP-SkpA was imaged at 25℃ in 45-second intervals (strain LO10476). (**A**) The nucleus in t = 0 is in late G_2 with GFP-SkpA present in the nucleoplasm but not the nucleolus. GFP-SkpA levels are reduced in the nucleoplasm in **B** as the nucleus transits into mitosis. As the chromosomes condense, GFP-SkpA accumulates faintly at a single "dot" in the nucleus (**E**, blue arrow). GFP-SkpA localizes to two "dots" at the poles of the mitotic nucleus and is most intense in **G**. In early anaphase, GFP-SkpA is reduced at the poles (**I**) and is gone from the poles in late mitosis/G_1 (**J**). (**K-Q**) A strain carrying histone H1-mTagBFP2, SepK-tdTomato (outer spindle pole body marker), and GFP-SkpA was imaged at 25℃ (strain LO11517). SepK-tdTomato and GFP-SkpA mostly overlap (**O**) and the overlap is verified by intensity traces in **P** and **Q** (intensity traces are along the lines shown in **O'**).

5.2.2 Localization of Cullin A (CulA)

In order to observe the localization pattern of CulA throughout the cell cycle in *A. nidulans*, I attempted to make fusions of CulA to GFP. I first fused GFP to the 3' end of the *culA* gene, at the *culA* locus, maintaining expression of the fusion gene under control of the endogenous *culA* promoter. I obtained viable transformants that I verified by diagnostic PCR and that exhibited GFP fluorescence. However, I found *the culA*-GFP fusion caused a slight reduction of growth at 42℃ and a significant reduction of conidia production at 25℃ and 20℃, indicating that the C-terminal GFP fusion had reduced function, particularly at low temperatures. I next fused GFP to the N-terminus of CulA (GFP-CulA), once again maintaining expression of the fusion gene under control of the endogenous *culA* promoter (see **Fig. 2.2**). Verified transformants carrying GFP-*culA* grew like wild-type at all temperatures tested (**Fig. 5.1**) and also produced detectable GFP signals. The GFP-CulA signal was quite weak, however, and this placed limitations on my imaging.

I collected Z-series stacks, at 10-minute intervals, of strains carrying GFP-CulA and histone H1-mRFP (LO9225-LO9227) at 37℃. Consistent with the localization pattern of GFP-

SkpA, I found that GFP-CulA localized predominately to nuclei but was faint or absent in nucleoli. Very weak GFP-CulA fluorescence in the cytoplasm was also detected throughout the cell cycle. Nuclear GFP-CulA dropped to cytoplasmic levels during mitosis, but it quickly became concentrated in nuclei again in G_1 (n=78 nuclei). Collecting Z-series stacks at 2-minute intervals at 37°C, I found that GFP-CulA levels were reduced to cytoplasmic levels either just prior to or at the first sign of obvious chromatin condensation in all nuclei (32 nuclei) (**Fig. 5.4 D-F**). This is the time at which the nuclear pore complexes of *A. nidulans* partially disassemble (De Souza *et al.*, 2004; Osmani *et al.*, 2006a). I did not observe GFP-CulA above cytoplasmic levels in mitotic nuclei (**Fig. 5.4 G-I**). In addition, I did not observe accumulation of GFP-CulA at the SPK, as seen with GFP-SkpA. However, I noticed that nuclear GFP-SkpA fluorescence was much brighter than nuclear GFP-CulA fluorescence when using the same illumination and exposure conditions. Thus, I increased the 488-laser power used to excite GFP to 100% (30% laser power was used for imaging GFP-SkpA) so that the nuclear GFP-CulA intensity was higher than that of nuclear GFP-SkpA. I incubated conidia from strains LO9225-LO9227 (in three separate experiments) at 37ºC for 14 hours and then collected Z-series stacks of random fields over the next hour using maximum laser power. Despite these conditions, I determined that only 4 ± 2% of hyphal tip cells contained GFP-CulA concentrated at the SPK (n = 163 tip cells with three or more nuclei). Despite the fact that GFP-CulA did not localize at the SPK, 31 ± 2% of hyphal tip cells contained faint GFP-CulA dots or larger spots *near* the hyphal tip. These cytoplasmic dots and larger spots were not as numerous nor as bright as observed in strains carrying GFP-SkpA. I also imaged GFP-CulA strains in 1-second intervals and found that the larger spots were more static (**Fig. 5.2 I-N**).

As GFP-SkpA localizes to the SPBs in mitotic nuclei, I decided to image GFP-CulA at 45-second intervals at 25°C to ensure I was not missing GFP-CulA localization to SPBs during

mitosis. I found that some mitotic nuclei had very faint "dot" localization of GFP-CulA that disappeared very quickly. However, this localization pattern was not consistent from nucleus to nucleus and the GFP signal was faint and bleached rapidly (**Fig. 5.4 P-R**).

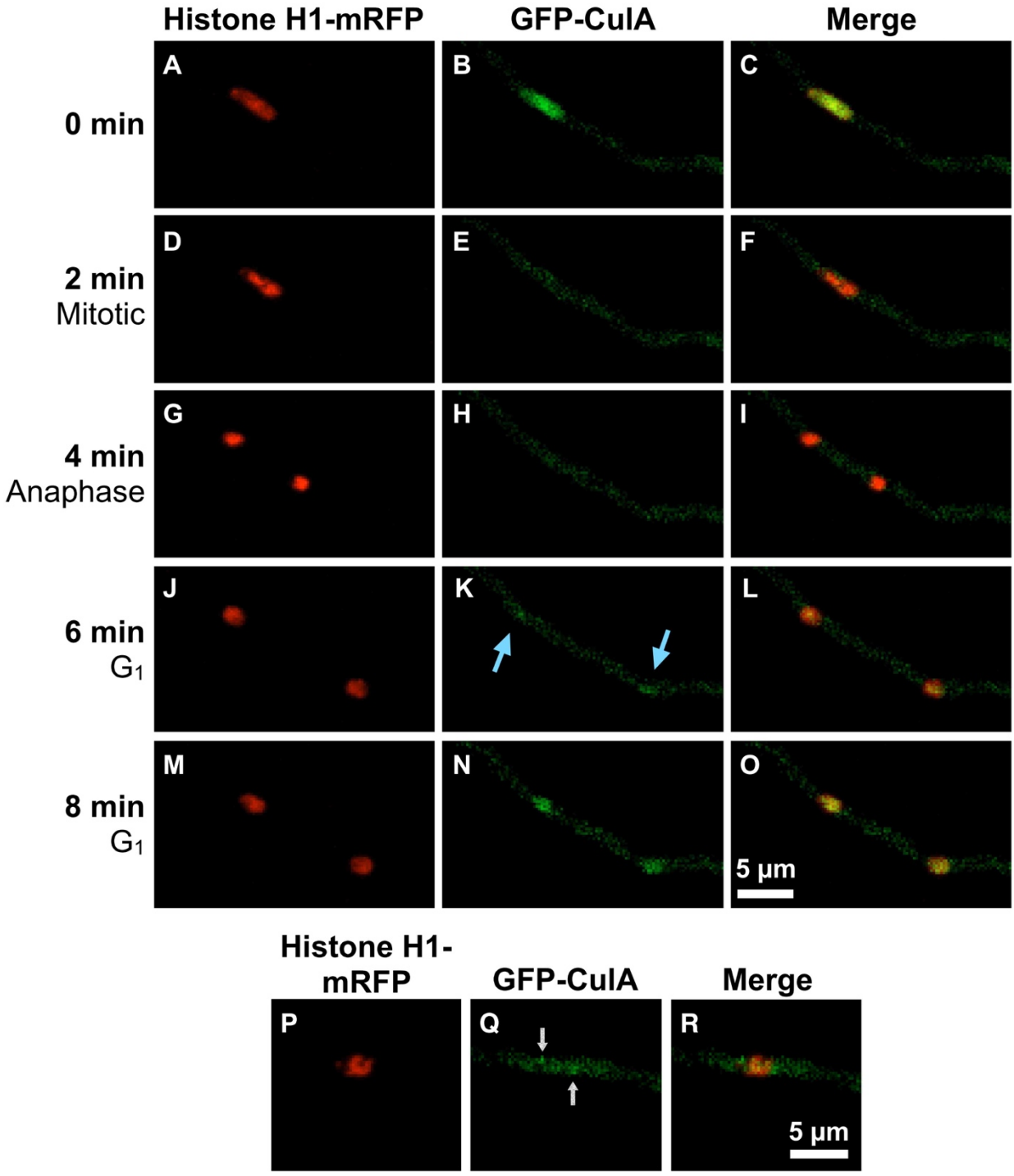

Figure 5.4 *(continued on next page)*

(continued from previous page)

Figure 5.4: Localization of GFP-CulA during mitosis
A-C: GFP-CulA localizes to interphase nuclei, but faintly to nucleoli, and is present faintly in the cytoplasm. **D-F**: GFP-CulA is reduced to cytoplasmic levels at the first indication of chromatin condensation. **G-I**: GFP-CulA is not excluded from nuclei during mitosis. **J-L**: CulA begins to reappear in the nucleus in early G_1. In some cases, CulA localizes to a dot in the nucleus before spreading to the rest of the nucleus (blue arrows in **K**). **P-R:** GFP-CulA is occasionally observed as 2 "dots" in mitotic nuclei (arrows in **Q**). All images are projections of Z-series stacks captured at 37℃ of a strain carrying histone H1-mRFP and GFP-CulA (LO9226). Images **A-O** were captured in 2-minute intervals while images **P-R** are from a single time point.

5.2.3 SkpA and CulA are essential for growth and important for nuclear replication

It is possible to study the phenotypes of deletions of essential genes in *A. nidulans* using heterokaryon rescue (Martin *et al.*, 1997; Osmani *et al.*, 2006b; Osmani *et al.*, 1988). I deleted *skpA* and *culA*, separately, by replacing them with the *Aspergillus terreus riboB* gene (*AtriboB*) (Dohn *et al.*, 2018) in strain LO2074, which carries $NimE^{Cyclin\ B}$-GFP and histone H1-mRFP. Control strains were generated by inserting *AtriboB* at the *wA* locus in strain LO2074 (LO10333-LO10335).

When essential genes are deleted, *A. nidulans* is capable of forming heterokaryons that carry two genetically different types of nuclei, parental nuclei and transformed nuclei. Parental nuclei carry a functional copy of the gene of interest but lack the selectable marker. In transformed nuclei, the gene of interest is replaced with a selectable marker that supports growth on selective media. The primary transformants created by deletion of most essential genes can maintain a heterokaryotic state and grow on selective media. However, *A. nidulans* conidia are uninucleate, so the conidia produced from the heterokaryon carry a parental nucleus or a transformed nucleus (carrying a deletion of the target gene) but not both. By streaking out conidia from primary

transformants on selective media, we can determine whether the deleted gene is essential by the presence or absence of growth and colony formation (Martin *et al.*, 1997; Osmani *et al.*, 2006b; Osmani *et al.*, 1988). If the target gene is not essential, conidia carrying transformed nuclei will germinate and grow into colonies on selective media. If the target gene is essential neither parental conidia nor transformed conidia carrying the deletion of the target gene will grow to form colonies on selective media. Heterokaryons, transferred as clumps of hyphae containing both types of nuclei will grow on selective media, however. I found that the transformants resulting from deletion of either *skpA* or *culA* were heterokaryons, and that the spores produced did not support growth on selective media. These results confirmed the finding of von Zeska Kress *et al.* (2012) that *skpA* and *culA* are essential. The heterokaryon rescue approach also allows the microscopic phenotypes of deletions of essential genes to be determined by simply incubating conidia in selective media. Parental conidia do not germinate and *skpA* or *culA* deletion conidia exhibit the phenotype caused by the deletion. Additional details regarding the heterokaryon rescue technique can be found in Chapter 2.8.

To study the terminal phenotype(s) of *culA*Δ and *skpA*Δ, I separately incubated conidia from *culA*Δ and *skpA*Δ heterokaryons as well as control strains LO10333 and LO10335. Conidia were incubated at 30ºC for 12 hours and Z-series stacks of random fields were then captured over the next hour. Separate, but identically grown, samples were also imaged at the 14-15-hour and 16-17-hour periods. I added a low concentration of calcofluor white, which binds chitin, to all samples 20 minutes prior to imaging in order to visualize septa. At high concentrations, calcofluor white inhibits fungal growth, but, even at 100X the concentration I used, no inhibition of growth was observed (**Fig. 2.5**)

Initial polarized growth and nuclear division occurred in both *culA* and *skpA* deletants (**Fig. 5.5 B, C**). However, nuclear replication was significantly slowed relative to control strains. For example, at the 16-17-hour time period, control strains had an average of 26 ± 7 nuclei (n = 30 germlings; 3 separate experiments), *culA*Δ germlings had an average of 8 ± 4 nuclei (n = 85 germlings; 3 separate experiments), and *skpA*Δ germlings had an average of 5 ± 2 nuclei (n = 141 germlings; 3 separate experiments). The number of nuclei in control, *culA*Δ, and *skpA*Δ germlings at the various time periods are shown in **Fig. 5.5D**. The fact that cell cycle progression and nuclear division was not completely inhibited in these germlings was unexpected as the SCF complex plays crucial roles at multiple stages of the cell cycle. However, it is likely that some CulA and SkpA are carried over from the parental heterokaryon in *culA*Δ and *skpA*Δ conidia and they allow cell cycle progression until their protein levels are sufficiently depleted.

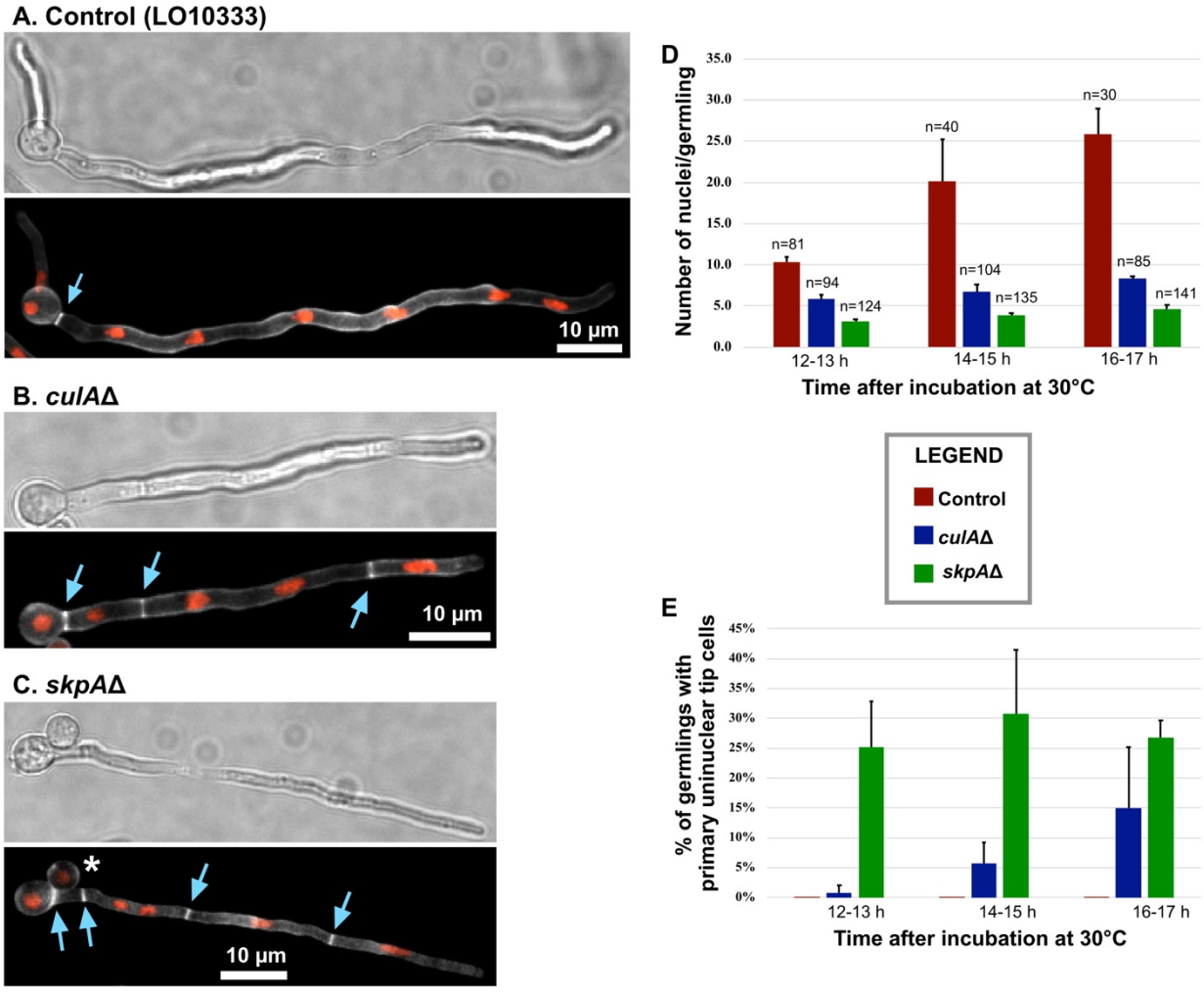

Figure 5.5: Terminal phenotypes of *culA*Δ and *skpA*Δ

(**A-C**) Images are maximum intensity projections from Z-series stacks taken with a spinning disk microscope. A representative control strain (LO10333) imaged ~12 hours after incubation at 30°C is shown (**A**). Representative *culA*Δ (**B**) and *skpA*Δ (**C**) germlings (heterokaryons made in parental strain LO2074) imaged ~16 hours after incubation at 30°C are shown. Asterisk in **C** indicates a parental, untransformed conidium. All germlings carried histone H1-mRFP and were stained with calcofluor white prior to imaging to visualize septa (blue arrows). Control (LO10333, LO10335) conidia and conidia from *culA*Δ and *skpA*Δ heterokaryons were grown for 12, 14, and 16 h at 30°C in minimal media and then live imaged for one hour at 30°C. Calcofluor white was added 20 minutes prior to imaging. The number of nuclei per germling was scored (**D**) in addition to the percentage of germlings with a primary uninucleate tip cell (primary tip cell = first hyphal protrusion generated) (**E**). Error bars indicate mean ± standard deviation of three separate experiments. n = the number of germlings.

5.2.4 CulA is important for destruction of CdhA

The SCF complex targets Cdh1 for destruction in other organisms (Choudhury *et al.*, 2016; Fukushima *et al.*, 2013), and I was consequently interested in determining if the SCF complex in *A. nidulans* played an important role in destroying CdhA. I deleted *culA* by replacing it with *AfpyroA* in the parental strain LO6268 which carried CdhA-GFP, An-Nup49-mCherry (to visualize the nuclear periphery), and $NimX^{Cdk1}$-mCherry. $NimE^{Cyclin\ B}$ and $NimX^{Cdk1}$ form a complex and both proteins accumulate in the nucleoplasm during S and G_2 phases when the APC/C-CdhA is inactive. $NimX^{Cdk1}$ negative nuclei (G_1 nuclei) are easily distinguished from $NimX^{Cdk1}$ positive nuclei as An-Nup49-mCherry only labels the nuclear periphery while $NimX^{Cdk1}$ localizes to the nucleoplasm.

I incubated spores from a *culA*Δ heterokaryon and from the parent strain LO6268 at 30℃ for 18 hours. I added calcofluor white 20 minutes prior to imaging. Z-series stacks of random fields were then captured over a one-hour period using the same laser and exposure settings for *culA*Δ and control germlings. In *culA*+ cells, CdhA is visible and concentrated at SPBs in G_1, disappears from the SPB at the G1/S transition and reappears at the SPB in late G_2 (Edgerton-Morgan and Oakley, 2012). I found that deletion of *culA* resulted in a nearly all tip cell nuclei containing visible CdhA-GFP regardless of cell cycle stage (98.7 ± 2%, 3 experiments, n = 341 nuclei) as opposed to 54.5 ± 6% in the parental control (3 experiments, n = 334 nuclei).

The nuclear abundance of CdhA-GFP was also much greater in *culA*Δ germlings than in the control regardless of cell cycle stage. In control germlings, CdhA-GFP was visible as dots corresponding to the spindle pole bodies (**Fig. 5.6 A-I**), whereas in *culA*Δ germlings CdhA-GFP fluorescence filled the nuclei (**Fig. 5.6 J-U**), note that the same illumination and exposure

conditions were used for the control and *culA*Δ strains). These data strongly suggest that in *A. nidulans* as in humans, the SCF complex targets the Cdh1 homolog for destruction.

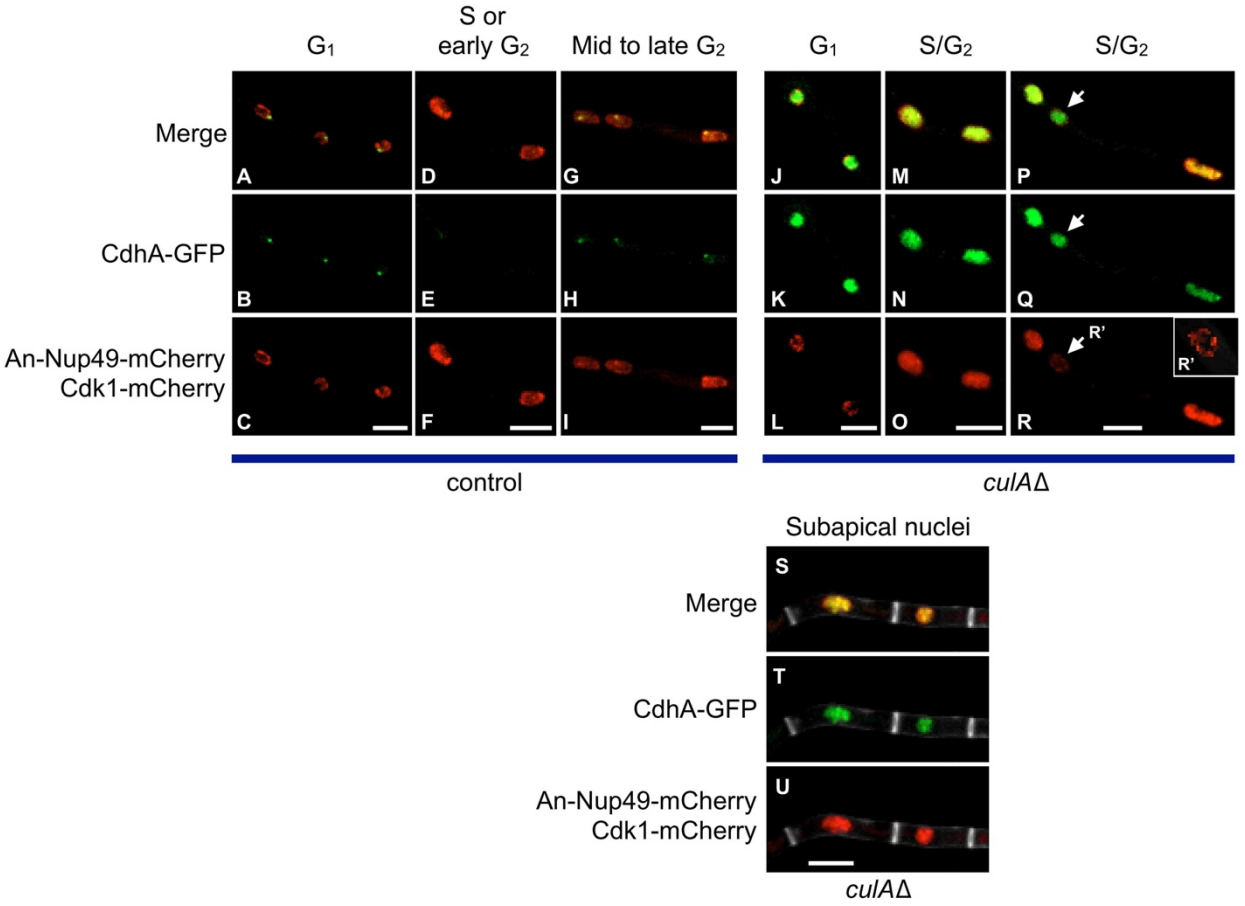

Figure 5.6: Deletion of *culA* increases the nuclear abundance of CdhA
culA was deleted in strain LO6268, which carries *cdhA*-GFP, *An-nup49*-mCherry, and *nimX*^{cdk1}-mCherry. Conidia from the parental strain (LO6268) and a *culA*Δ heterokaryon were grown at 30°C in minimal media for 18 hours and then live imaged for one hour at 30°C. Calcofluor white was added 20 minutes prior to imaging (staining not shown in **A-R'**). Representative images from parental germlings that are in G_1 (**A-C**), S phase or early G_2 (**D-F**), and mid to late G_2 (**G-I**) are shown. Representative images from *culA*Δ germlings that are in G_1 (**J-L**) and S/G_2 (**M-R**) are shown. A *culA*Δ tip cell containing two Cdk1+ nuclei and one Cdk1- nucleus (arrows in **P-R, R'**) is also depicted. (**A-R'**) The same illumination and exposure conditions were used for CdhA-GFP imaging for the control and *culA*Δ germlings. (**S-U**) Two subapical cells (as visualized by calcofluor white staining) are shown containing nuclei that have accumulated both CdhA-GFP and Cdk1-mCherry. All images are maximum intensity projections from Z-series stacks and scale bars = 5 μm.

5.2.5 The SCF regulates NimE$^{Cyclin\ B}$ and NimX^{Cdk1} in subapical nuclei

In *A. nidulans*, only tip cells actively progress through the cell cycle whereas subapical cells are blocked in G_1 and do not accumulate NimE$^{Cyclin\ B}$ (Nayak *et al.*, 2010) (**Fig. 5.7 A-D, M**). Subapical nuclei resume the cell cycle and accumulate NimE$^{Cyclin\ B}$ once a side branch emerges from the cell, thus making it a new tip cell (Nayak *et al.*, 2010). Since the SCF complex targets CdhA for destruction, as demonstrated in Chapter 5.2.4, one might expect that deletion of *skpA* or *culA* might result in constitutive APC/C activity and NimE$^{Cyclin\ B}$ negative nuclei in subapical cells, as is seen in wild-type controls. Surprisingly, I found that both *culA*Δ and *skpA*Δ germlings (parental strain LO2074) had significant numbers of NimE$^{Cyclin\ B}$ positive subapical nuclei (representative images shown in **Fig. 5.7 E-H** and **I-L**). In particular, more than 60% of subapical nuclei were NimE$^{Cyclin\ B}$ positive in *culA*Δ germlings, (**Fig. 5.7 M**). To determine if these nuclei were actively passing through the cell cycle, I imaged subapical *culA*Δ nuclei at 30ºC, collecting Z-series image stacks at 10-minute intervals for 120-360 min. Only a small fraction of *culA*Δ subapical nuclei that accumulated NimE$^{Cyclin\ B}$ underwent nuclear division (4/39 nuclei). Thus, although NimE$^{Cyclin\ B}$ accumulates in a large proportion of *culA*Δ subapical nuclei, most of these nuclei are either not going through the cell cycle or are cycling abnormally slowly. This is still markedly different from the wild-type in which no subapical nuclei cycle until a growing tip forms.

It is important to note that deletion of *culA* in the parental strain LO6268 (which carries *cdhA*-GFP, *An-nup49*-mCherry, and *nimX^{cdk1}*-mCherry) resulted in 70 ± 29% of subapical nuclei containing visible NimX^{Cdk1} when imaged at 18 hours (3 experiments, n = 125 subapical nuclei) (**Fig. 5.6 S-U**). This is consistent with the percentage of NimE$^{Cyclin\ B}$ subapical nuclei found in *culA*Δ (parental strain LO2074) as described above. In addition, all *culA*Δ subapical nuclei

contained visible CdhA-GFP (3 experiments, n = 125 nuclei) (**Fig. 5.6 S-U**). Thus, both NimE$^{Cyclin\ B}$ and NimX^{Cdk1} accumulate in the majority of *culA*Δ subapical nuclei despite the presence of CdhA.

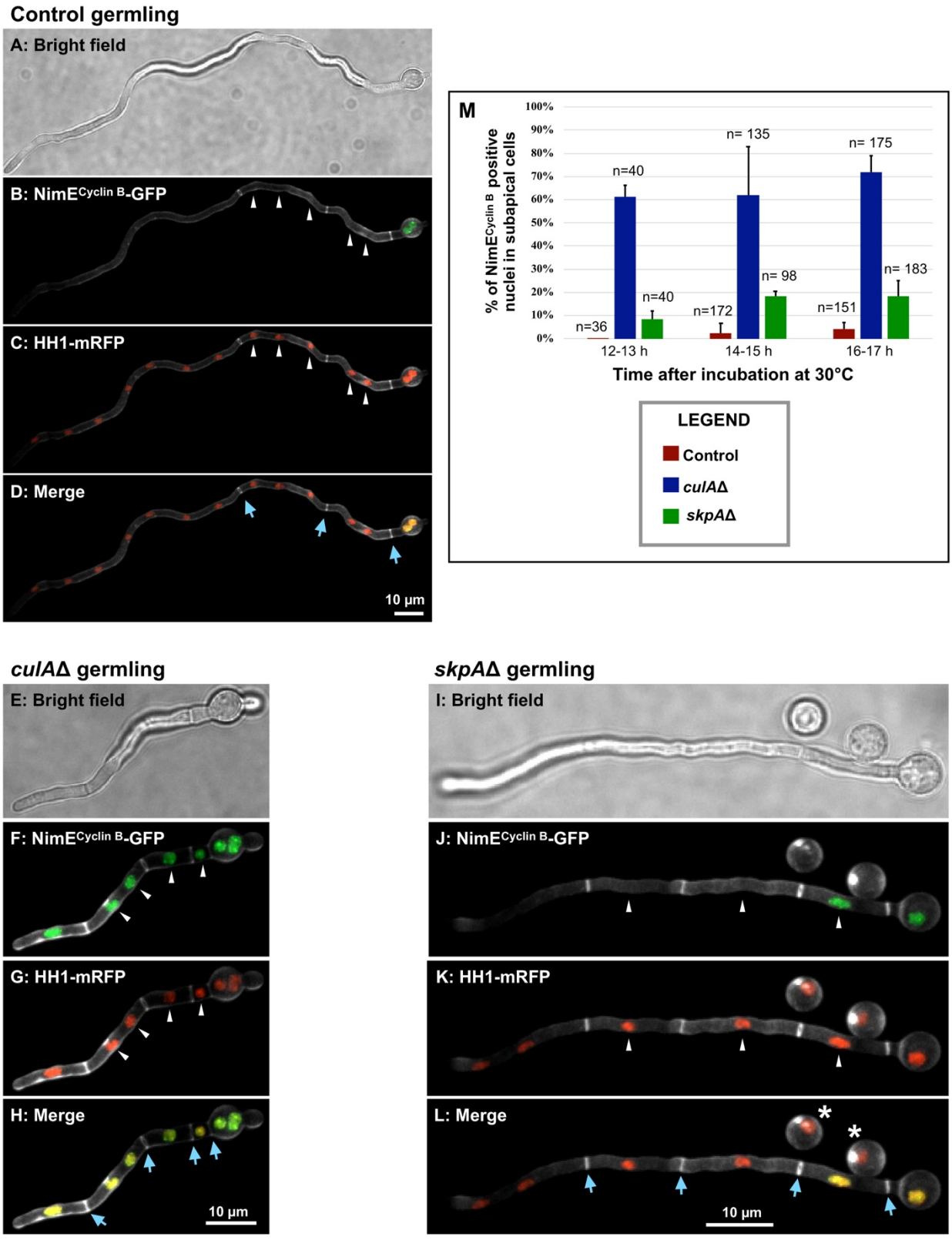

Figure 5.7 *(continued on next page)*

(continued from previous page)

Figure 5.7: The SCF complex plays a role in regulating NimE$^{\text{Cyclin B}}$ and NimX$^{\text{Cdk1}}$ in subapical nuclei

Both *culA* and *skpA* were deleted (separately) in strain LO2074 that carries histone H1-mRFP and NimE$^{\text{Cyclin B}}$-GFP. Similar to **Fig. 5.5**, control conidia and conidia from *culA*Δ and *skpA*Δ heterokaryons were grown for 12, 14, and 16 hours at 30℃ in minimal media and then live imaged for one hour at 30℃. Calcofluor white was added 20 minutes prior to imaging. The percentage of nuclei in subapical cells that accumulated NimE$^{\text{Cyclin B}}$ was scored (**M**); error bars indicate mean ± standard deviation of three separate experiments. n = the number of subapical nuclei. A representative image of a wild-type germling (A-D), a *culA*Δ germling (**E-F**), and a *skpA*Δ germling (**I-K**) imaged ~14 hours after incubation at 30℃ are shown. Blue arrows indicate septa and asterisks indicate swollen, ungerminated conidia that are likely parental, untransformed conidia. White arrowheads indicate subapical nuclei. Images are maximum intensity projections from Z-series stacks.

5.2.6 CulA and SkpA are important for suppressing septation near the growing hyphal tip

When *A. nidulans* conidia germinate, septation is suppressed until a size threshold is achieved, which is generally after the completion of three rounds of nuclear division (Harris *et al.*, 1994). The first septation is asymmetric, with the septum forming near the conidium resulting in a multinucleate tip cell. Subsequent rounds of nuclear division in the tip cell are followed by septation, but septation near the hyphal tip is suppressed, resulting in asymmetric cell division, forming large, multinucleate tip cells. The formation of multinucleate tip cells is likely an adaptation that facilitates rapid hyphal growth (Taheri-Talesh *et al.*, 2008).

I found that deletion of either *culA* or *skpA* led to increased septum formation (**Figs 5.5, 5.7**). In addition, some *culA*Δ and *skpA*Δ germlings had multiple septa directly adjacent to one another, generating cells with no nuclei, while in many others a septum formed behind the nucleus closest to the hyphal tip, generating a tip cell with only a single nucleus (**Fig. 5.5 B, C**). Control germlings were never observed with a uninucleate primary tip cell after the first nuclear division

(primary tip cell = first hyphal protrusion generated) (**Fig. 5.5 A**). The percentage of *culA*Δ germlings with a uninucleate primary hyphal tip cell increased over time, with the highest percentage at the 16-17-hour time period (15.0 ± 10.3%, n = 85 germlings, 3 experiments) (**Fig. 5.5 E**). The percentage of *skpA*Δ germlings with a uninucleate primary hyphal tip cell was even higher; 25.1 ± 7.8% at the 12-13-hour time period, 30.7 ± 10.8% at the 14-15-hour time period, and 26.8 ± 2.8% at the 16-17-hour time period (**Fig. 5.5 E**). These data, in aggregate, suggest that the SCF complex has a role in suppressing septation near growing hyphal tips.

In *A. nidulans*, mitosis is restricted to tip cell nuclei and septation occurs shortly after nuclear division (Clutterbuck, 1970; Fiddy and Trinci, 1976; Harris, 2001). In principle, the relative abundance of septa and the presence of septa near the hyphal tip might be due *culA*Δ and *skpA*Δ inhibiting nuclear division but not inhibiting septation. To test this possibility, I imaged *culA*Δ germlings at 30 ºC in 10-minute intervals. These time-lapse images revealed that septum formation occurred 19 ± 8 minutes after mitosis in *culA*Δ germlings and did not occur randomly throughout the cell cycle (n = 68 septa). Thus, it appears that the SCF complex does not play an important role in the regulation of timing of septation with respect to nuclear division. Rather it plays an important role in the inhibition of septation near hyphal tips, which is, in turn, critical for the formation of multinucleate tip cells.

5.3 Discussion

My initial interest in *culA* and *skpA* was driven by a previous finding in our lab that a γ-tubulin mutation *mipA*D159 causes a nuclear autonomous failure of destruction of CdhA, the *A. nidulans* Cdh1 homolog, at the G_1/S boundary that results in constitutive destruction of $NimE^{Cyclin\ B}$ (Edgerton-Morgan and Oakley, 2012). CulA and SkpA are members of the SCF complex that

has been shown, in other organisms, to target homologs of Cdh1 for ubiquitination, which leads to their destruction (Fukushima *et al.*, 2013; Lukas *et al.*, 1999; Sorensen *et al.*, 2001). My deletion of *culA* resulted in bright CdhA-GFP fluorescence in all nuclei, confirming that the SCF plays a critical role in targeting CdhA for destruction as expected. Our analyses of the phenotypes of these deletions, however, revealed additional, and in some cases unexpected functions of *culA* and *skpA*.

5.3.1 The SCF complex plays an important role in suppressing septation near growing hyphal tips

An unexpected phenotype observed in *culA*Δ and *skpA*Δ germlings was the presence of abundant septa near the growing hyphal tip. In *A. nidulans*, septum formation is normally inhibited until a size threshold is attained, usually after the completion of the third round of nuclear division (Harris *et al.*, 1994). The first septation is asymmetrical with the septum forming distal to the hyphal tip. Thereafter, each round of nuclear division is followed closely by a round of septation, but septum formation is again asymmetrical and distal to the hyphal tip. The initial inhibition of septation and the subsequent asymmetry of septation are almost certainly two aspects of the same phenomenon, the suppression of septum formation by the growing hyphal tip, be it in germlings or mature tip cells. The result of repeated rounds of asymmetric septation is a hyphal tip cell with many nuclei. Asymmetric septation and resulting multinuclear tip cells are an adaptation that enables rapid tip growth [discussed in (Horio and Oakley, 2005)].

The mechanism of septation suppression by the hyphal tip is unknown. I have found that deletion of *culA* or *skpA* results in septa forming near the hyphal tip. It follows that these proteins, and by inference the SCF complex, play a critical role in suppression of septation near the hyphal

tip. Deletion of *culA* did not, however, affect the timing of septation relative to mitosis. Septation still occurred shortly after mitosis, but the positions of septal formation were dramatically altered.

5.3.2 CulA and SkpA play a role in blockage of subapical nuclei in G_1

Nuclei in subapical cells of wild-type *A. nidulans* are blocked in G_1 and do not accumulate $NimE^{Cyclin\ B}$ or $NimX^{Cdk1}$ (Edgerton-Morgan and Oakley, 2012; Nayak *et al.*, 2010). They contain the APC/C complexed with the activator CdhA, and the APC/C-CdhA complex targets $NimE^{Cyclin\ B}$ for destruction. Deletion of CdhA, which is not essential in *A. nidulans*, resulted in subapical nuclei accumulating $NimE^{Cyclin\ B}$ (Edgerton-Morgan and Oakley, 2012). The accumulation of $NimE^{Cyclin\ B}$, of itself, was not sufficient to drive the cell cycle, however, because nuclear division did not occur (Edgerton-Morgan and Oakley, 2012). As mentioned, the SCF complex plays a key role in targeting Cdh1 for ubiquitination and subsequent destruction in other organisms (Fukushima *et al.*, 2013; Lukas *et al.*, 1999; Sorensen *et al.*, 2001), and our data on $NimE^{Cyclin\ B}$ accumulation in tip cells strongly indicates that the same is true in *A. nidulans.* It follows that deletion of *culA* or *skpA* should inactivate the SCF complex and allow accumulation of active APC/C-CdhA in subapical nuclei. This would result in the absence of $NimE^{Cyclin\ B}$. Phenotypically, this should be inconsequential since the APC/C-CdhA complex is active in these nuclei in wild-type strains and $NimE^{Cyclin\ B}$ does not accumulate. Surprisingly, I found that deletion of *culA* or *skpA* resulted in a substantial fraction of nuclei in subapical cells being $NimE^{Cyclin\ B}$-GFP positive even though, as anticipated, there was bright GFP-CdhA fluorescence in these nuclei. Equally surprisingly, the percentage of $NimE^{Cyclin\ B}$ positive subapical nuclei was much higher in *culA*Δ germlings (reaching 70% at 16-17 h of incubation) than in *skpA*Δ germlings (less than 20% at the same time point). Several conclusions can be drawn from these findings. First, the CdhA in the

NimE$^{Cyclin\ B}$ positive nuclei must be inactive. Relatedly, Edgerton-Morgan and Oakley (Edgerton-Morgan and Oakley, 2012) have shown that CdhA is present in G_2 nuclei of *A. nidulans,* but it is inactivated such that it does not drive destruction of NimE$^{Cyclin\ B}$ at this stage. A plausible mechanism of inactivation, based on data from *S. cerevisiae*, is phosphorylation by the NimE$^{Cyclin\ B}$-NimE^{Cdk1} complex (Edgerton-Morgan and Oakley, 2012; Zachariae *et al.*, 1998). Second, CulA and SkpA have important, but unanticipated, roles in preventing the accumulation of NimE$^{Cyclin\ B}$ in subapical nuclei. The roles could be direct (e.g. a role in targeting NimE$^{Cyclin\ B}$ for destruction) or indirect. Third, the fact that the percentage of NimE$^{Cyclin\ B}$-GFP positive nuclei was so much higher in the *culA*Δ strain than in the *skpA*Δ strain suggests that the roles of the two proteins in this process may be different from each other and separable from the function of the SCF complex. Deletion of either *culA* or *skpA* results in strong effects on septation and accumulation of CdhA, indicating that SCF function is strongly reduced. If the effects on NimE$^{Cyclin\ B}$-GFP and NimX^{Cdk1}-mCherry accumulation were solely a function of reduced SCF activity, one would expect that *culA* and *skpA* deletions would have quantitatively similar effects. Instead they are quite different. Finally, in the *culA*Δ strain, a few subapical nuclei that contained NimE$^{Cyclin\ B}$ underwent division, suggesting that the accumulation of NimE$^{Cyclin\ B}$ activated the cell cycle. These nuclei constituted a very low percentage of the total, however, and most nuclei were still blocked or cycled very slowly, perhaps due to other effects of *culA*Δ.

5.3.3 Localization patterns of SkpA and CulA

In mammalian cells, Skp1 and Cul1 have been shown to localize to nuclei, centrosomes, and faintly to the cytoplasm (Freed *et al.*, 1999; Furukawa *et al.*, 2000; Huang *et al.*, 2011). In *A. nidulans*, I observed that both CulA and SkpA localized to interphase nuclei and were excluded

from nucleoli. However, I did not observe obvious localization to the spindle-pole body (SPB), the functional equivalent of the centrosome, during interphase. GFP-SkpA and GFP-CulA fluorescence levels in nuclei dropped to cytoplasmic levels when the nuclear pore complexes partially disassembled at mitotic entry. GFP-SkpA then concentrated transiently at the nuclear face of SPBs of mitotic nuclei before disappearing during anaphase. I occasionally observed faint GFP-CulA accumulation in mitotic nuclei at what appear to be the poles, but the weakness of the GFP-CulA signal made it difficult to determine, unambiguously, if this was also SPB localization. Interestingly, the nuclear staining pattern of Cul1 was also less prominent than Skp1 in mammalian cells (Freed *et al.*, 1999), suggesting that this is a conserved phenomenon.

Although both GFP-SkpA and GFP-CulA localized to the cytoplasm, the patterns were not identical. GFP-SkpA accumulated at the very tip of apical cells at a structure called the Spitzenkörper. This localization pattern was rarely observed in GFP-CulA strains even when using maximum laser power which allowed other CulA localizations to be imaged easily. Both GFP-SkpA and GFP-CulA appeared as both small dots and larger, often irregularly shaped, spots in the cytoplasm, particularly between the tip most nucleus and the hyphal tip. GFP-SkpA dots/spots, however, were seen more often than GFP-CulA dots/spots. The smaller GFP-SkpA and GFP-CulA dots were highly dynamic, consistent with them being early endosomes or secretory vesicles. The larger spots were much more static, consistent with the possibility that they are late endosomes and/or Golgi equivalents, both of which have been shown previously to be relatively static (Abenza *et al.*, 2009; Pantazopoulou and Penalva, 2009).

As SkpA concentrates at hyphal tips and CulA does not, SkpA might function separately from CulA and the SCF complex in some cases. The punctate fluorescence of GFP-SkpA is characteristic of secretory vesicles that are involved in tip growth, and we deduce that GFP-SkpA

is delivered to the tip via secretory vesicles. In *Saccharomyces cerevisiae*, Skp1 was shown to interact with the F-box protein Rcy1, which localized to areas of polarized growth and was required for recycling of the v-SNARE Snc1. Skp1 directly interacted with Rcy1 and loss of Skp1 impaired recycling of Snc1. Furthermore, the function of Skp1 in this process was thought to occur in a SCF-independent manner. (Galan *et al.*, 2001). More recent work determined that deletion of *rcy1* caused un-ubiquitinated Snc1 to accumulate in early endosomes and prevented its transport from the endosomes to the Golgi so it could be recycled (Chen *et al.*, 2011). The failure of Snc1 to be ubiquitinated suggested that Rcy1/Skp1 was part of a functional SCF complex. The authors proposed that, since Rcy1 localized to the Golgi and to endosomes (Chen *et al.*, 2005), that proteins are marked with ubiquitin in endosomes and that this ubiquitination is required for recycling to the Golgi (Chen *et al.*, 2011).

The homologs of Rcy1 and Snc1 in *A. nidulans*, RcyA and SynA respectively, have been identified (Herrero *et al.*, 2014; Taheri-Talesh *et al.*, 2008) and GFP-RcyA shows remarkably similar cytoplasmic and Spitzenkörper localization patterns (Herrero *et al.*, 2014) to that of GFP-SkpA. However, deletion of *rcyA* did not affect the accumulation of SynA at the hyphal tip and Spitzenkörper (Herrero *et al.*, 2014), which suggests that RcyA does not play a major role in SynA recycling. It is very possible that SkpA and RcyA are not involved in SynA recycling, as found in *S. cerevisiae*, and play different role(s) at regions of polarized growth in filamentous fungi. It will be of interest in the future to determine whether SkpA and RcyA directly interact, identify the structure(s) both proteins localize with in the cytoplasm, and elucidate their function(s) at the Spitzenkörper and, since CulA does not localize to the Spitzenkörper, whether these function(s) are SCF-independent.

Chapter 6: Functions of γ-tubulin in cell cycle regulation: Adding pieces to the puzzle

6.1 Introduction

As detailed in Chapter 1, we discovered several years ago that γ-tubulin has an unexpected, and microtubule-independent, role in inactivating the APC/C at the G_1/S boundary that results in cell cycle blockage in G_1 (Edgerton-Morgan and Oakley, 2012; Nayak *et al.*, 2010). *mipA*D159, a temperature-sensitive γ-tubulin mutation, caused a nuclear autonomous failure of the destruction or removal of the activator protein Cdh1 (the *A. nidulans* homolog is CdhA), which resulted in constitutive APC/C-CdhA activity and failure of affected nuclei to enter S phase. Based on our data (see Chapter 1), we predicted that γ-tubulin was functioning directly or indirectly through regulators of CdhA instead of directly interacting with CdhA. However, CdhA regulation had not been studied in our model organism, *Aspergillus nidulans*, nor in any other filamentous fungus at the start of my graduate career. Thus, my first priority was to identify and characterize regulators of CdhA (Chapters 3-5), an important task in itself. Studying the cell biology of filamentous fungi is crucial if we are to successfully treat humans and animals for fungal infections, prevent fungi from contaminating crops, and optimize their growth for the production of desirable products.

I have determined that the G_1/S cyclin, PucA, is an essential regulator of CdhA in *A. nidulans*, and that there are no redundant mechanisms that can inactivate CdhA sufficiently to support growth in the absence of PucA (Chapter 4). Deletants of *pucA* in a *cdhA*Δ strain were viable, indicating that the essential function of PucA is to inactivate CdhA. Unfortunately, I was unable to determine the localization pattern of PucA, which would have permitted me to compare PucA localization in *mipA*+ and *mipA*D159 strains. Instead, I generated strains carrying *pucA*Δ, *cdhA*Δ and *mipA* mutant alleles to determine whether there were any revealing genetic interactions. Through these studies, I identified specific genetic interactions between *pucA* and two *mipA*

mutant alleles, but not with four other *mipA* mutant alleles, indicating that this interaction is allele specific. In addition, I determined that the B-type cyclin ClbA fails to localize to nuclei with constitutively active APC/C^{CdhA} in *mipA*D159 strains.

I have also determined that CulA, the scaffold protein for the SkpA-CulA-F-box containing (SCF) complex in *A. nidulans*, also plays a role in CdhA regulation by controlling nuclear CdhA abundance (Chapter 5). My next question, thus, was whether CulA was a candidate through which γ-tubulin acts to control APC/C-CdhA activity. In this chapter, I demonstrate that deletion of *culA* recapitulates a *mipA*D159 phenotype, and I reveal an interesting genetic interaction between CulA and γ-tubulin.

6.2 Results

6.2.1 PucA function is required for some of the growth limiting effects observed in two mipA mutants

Previously in the lab, Dr. América Hervás utilized a two-step gene replacement procedure (**Fig. 6.1**) to incorporate eight conditionally lethal *mipA* mutant alleles (separately) at the wild-type chromosomal *mipA* locus in the parental strain LO1385. The resulting *mipA* mutant strains carried auxotrophic mutations *pyrG*89 and *pyroA*4 and were, thus, pyrG(-) and pyro(-) (unpublished results). The generation of *mipA* mutant strains via two-step gene replacement was done following the strategy previously published by our lab (Dunne and Oakley, 1988; Jung *et al.*, 2001).

In order to study the effects of deleting *pucA* in the various γ-tubulin mutants, I first replaced *cdhA* with *Aspergillus terreus pyrG* (*AtpyrG*) in seven of the eight *mipA* mutant strains. Transformations with *mipA*K284 were unsuccessful, and it is, thus, not included in this work. After successful deletion of *cdhA* into the seven *mipA* mutants, I then deleted *pucA* in these stains by

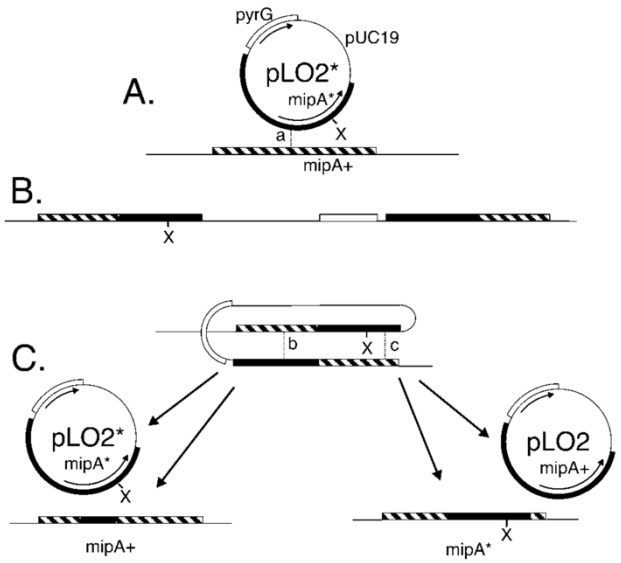

Figure 6.1: Two-step gene replacement at the *mipA* locus
The replacement of the wild-type chromosomal *mipA* allele (*mipA*+) with a mutant allele (*mipA**) carried on plasmid pLO2 (pLO2* designates that it carries a mutated copy of *mipA*). pLO2* also carries the *A. nidulans pyrG* gene. The "X" designates the *mipA* mutation. (**A**) Integration of pLO2* occurs via crossing over at point "a", which (**B**) creates both a mutant copy and wild-type copy of *mipA* with flanking pUC19 and *pyrG* sequences. The mutant copy can either be at the right or at the left (shown in **B**) depending on the crossover point. (**C**) Once a strain carrying the duplication is generated, mitotic crossing over between the two copies of *mipA* occurs at a low frequency, leading to the eviction of one of the two copies of *mipA*. The plasmid pLO2* carrying *mipA** will be evicted if crossing over occurs at point "b", which leaves the wild-type *mipA* allele in the chromosome. If crossing over occurs at point "c", then the plasmid pLO2 carrying the wild-type *mipA* allele will be evicted, leaving the *mipA** allele in the chromosome. 5-Fluoro-orotic acid is used to select for evictants that are *pyrG*(-) and evictants carrying the *mipA** allele are distinguished from those carrying the wild-type *mipA* allele depending on the phenotype of *mipA**.

replacing it with the *Aspergillus fumigatus* selectable marker *pyroA* (*AfpyroA*). Various *mipA*+ and *mipA* mutant control strains were generated by replacing the *wA* gene with *AtpyrG* and/or the *yA* locus with *AfpyroA* to complement the auxotrophic mutations *pyrG*89 and *pyroA*4, respectively. The deletion of the *wA* and/or *yA* genes have no effect on growth but do cause a change in spore color (*wA*Δ = white, *yA*Δ = yellow, *wA*Δ, *yA*Δ = white).

The deletion of *cdhA* in six of the seven *mipA* mutants resulted in a slight reduction in growth compared to the *mipA* mutant control. For example, *cdhA*Δ*, mipA*D159 strains exhibited reduced growth at 37℃ and 30℃ relative to *mipA*D159 control strains (**Fig. 6.2**). Interestingly, deletion of *pucA* in both *cdhA*Δ*, mipA*D159 and *cdhA*Δ*, mipA*R63 strains resulted in partial growth restoration compared to the *mipA*D159 and *mipA*R63 control strains (**Figs 6.2 and 6.3**). This genetic interaction between *pucA* and *mipA*D159 and *mipA*R63 is allele specific, as deletion of *pucA* in other *cdhA*Δ*, mipA* mutants (*mipA*D123, *mipA*H370, *mipA*R338, and *mipA*R243) resulted in either no change in growth or a slight reduction in growth compared to the *cdhA+, mipA* mutant control strains (**Figs 6.5-6.8**).

Interestingly, the deletion of *cdhA* in combination with the *mipA*K408 allele resulted in growth on media lacking benomyl, a microtubule-depolymerizing agent. *mipA*K408 causes cells to be dependent on benomyl for growth (Jung *et al.*, 2001). We were surprised to find that *cdhA*Δ*, mipA*K408 strains were able to grow at 20-30ºC on media lacking benomyl, although growth was very slow (**Fig. 6.4**). Strains carrying *pucA*Δ, *cdhA*Δ*,* and *mipA*K408 grew similarly to *cdhA*Δ*, mipA*K408 strains, indicating that, in this specific case, the genetic interaction is between *cdhA* and the *mipA*K408 allele.

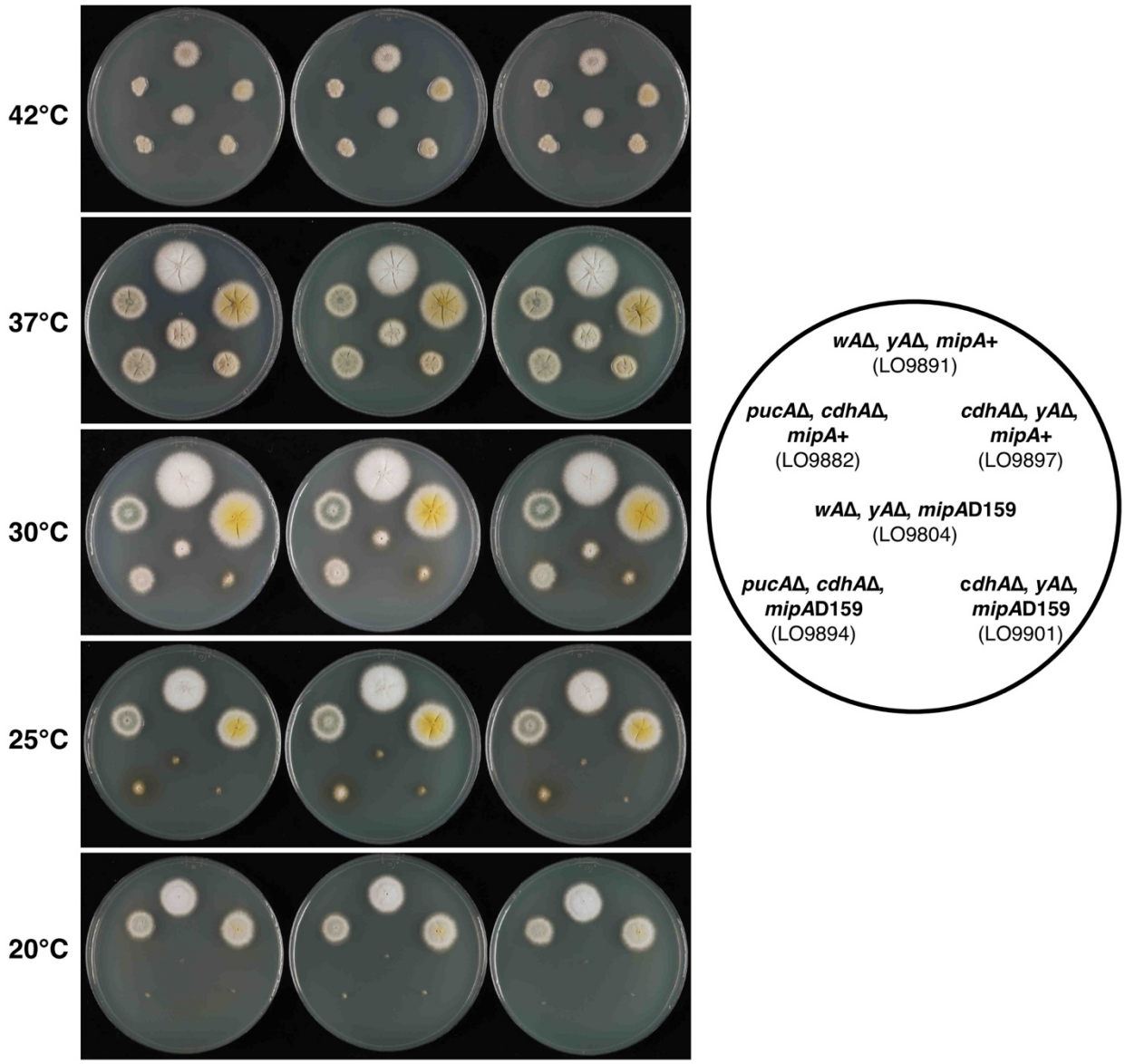

Figure 6.2: Genetic interaction between *pucA* and *mipA*D159

mipA+ and *mipA*D159 strains were stabbed onto complete media (in 3 replicates) and incubated at the various temperatures indicated on the far left. The genotypes and strain names are shown in the circle on the right. The deletion of *cdhA* in *mipA*D159 (strain LO9901) slightly exacerbates growth at 37℃ and 30℃ compared to the *mipA*D159 control strain (LO9804). Deletion of *pucA* in *cdhA*Δ*, mipA*D159 (strain LO9894) partially restores growth at 37℃, 30℃, and 25℃ compared to both the *mipA*D159 control strain (LO9804) and the *cdhA*Δ*, mipA*D159 strain (LO9901).

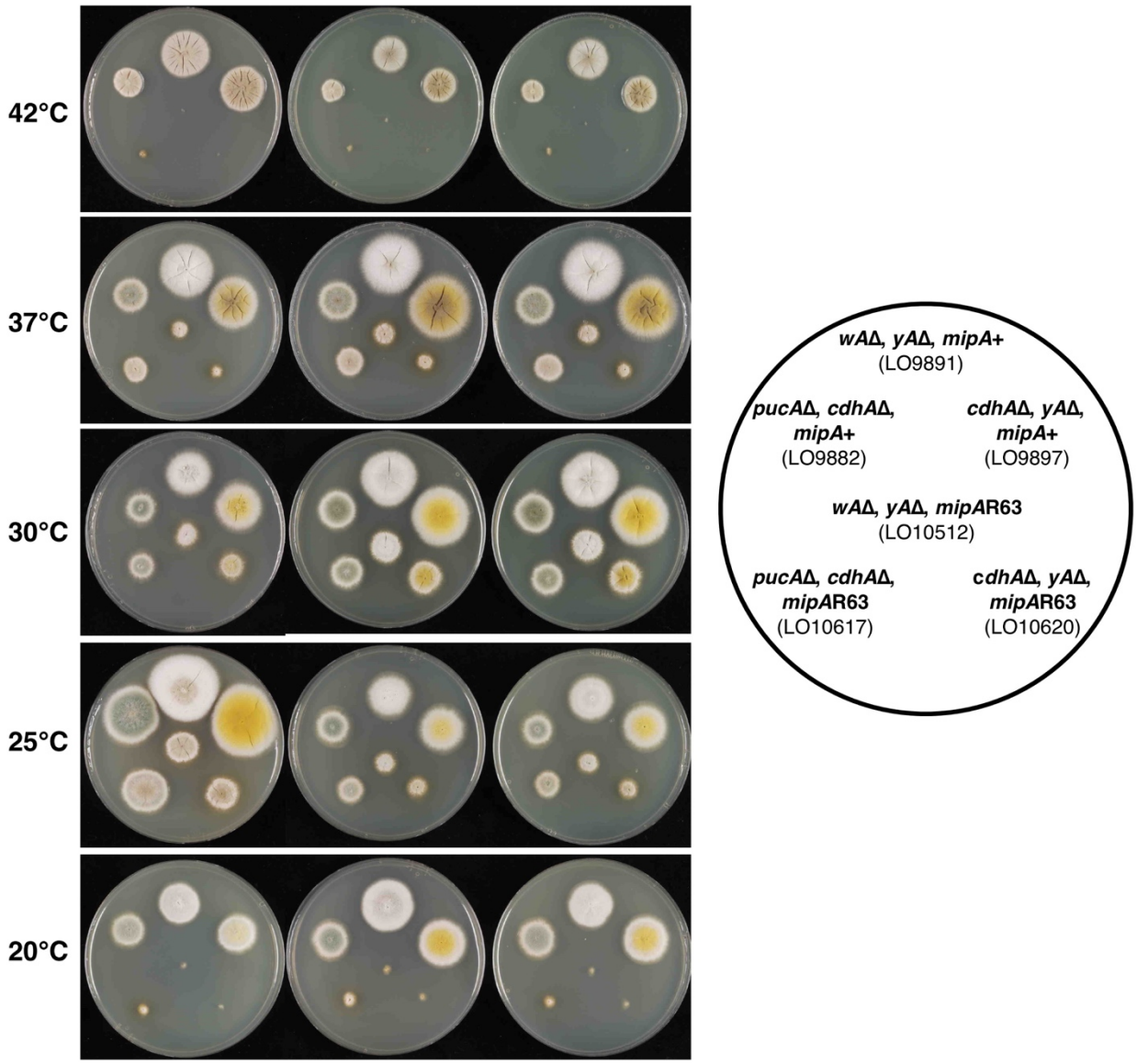

Figure 6.3: Genetic interaction between *pucA* and *mipA*R63

mipA+ and *mipA*R63 strains were stabbed onto complete media (in 3 replicates) and incubated at the various temperatures indicated on the far left. The genotypes and strain names are shown in the circle on the right. The deletion of *cdhA* in *mipA*R63 (strain LO10620) slightly exacerbates growth at 37℃ compared to the *mipA*R63 control strain (LO10512). Deletion of *pucA* in *cdhA*Δ, *mipA*R63 (strain LO10617) partially restores growth at 37℃, 25℃, and 20℃ compared to both the *mipA*R63 control strain (LO10512) and the *cdhA*Δ, *mipA*D159 strain (LO10620).

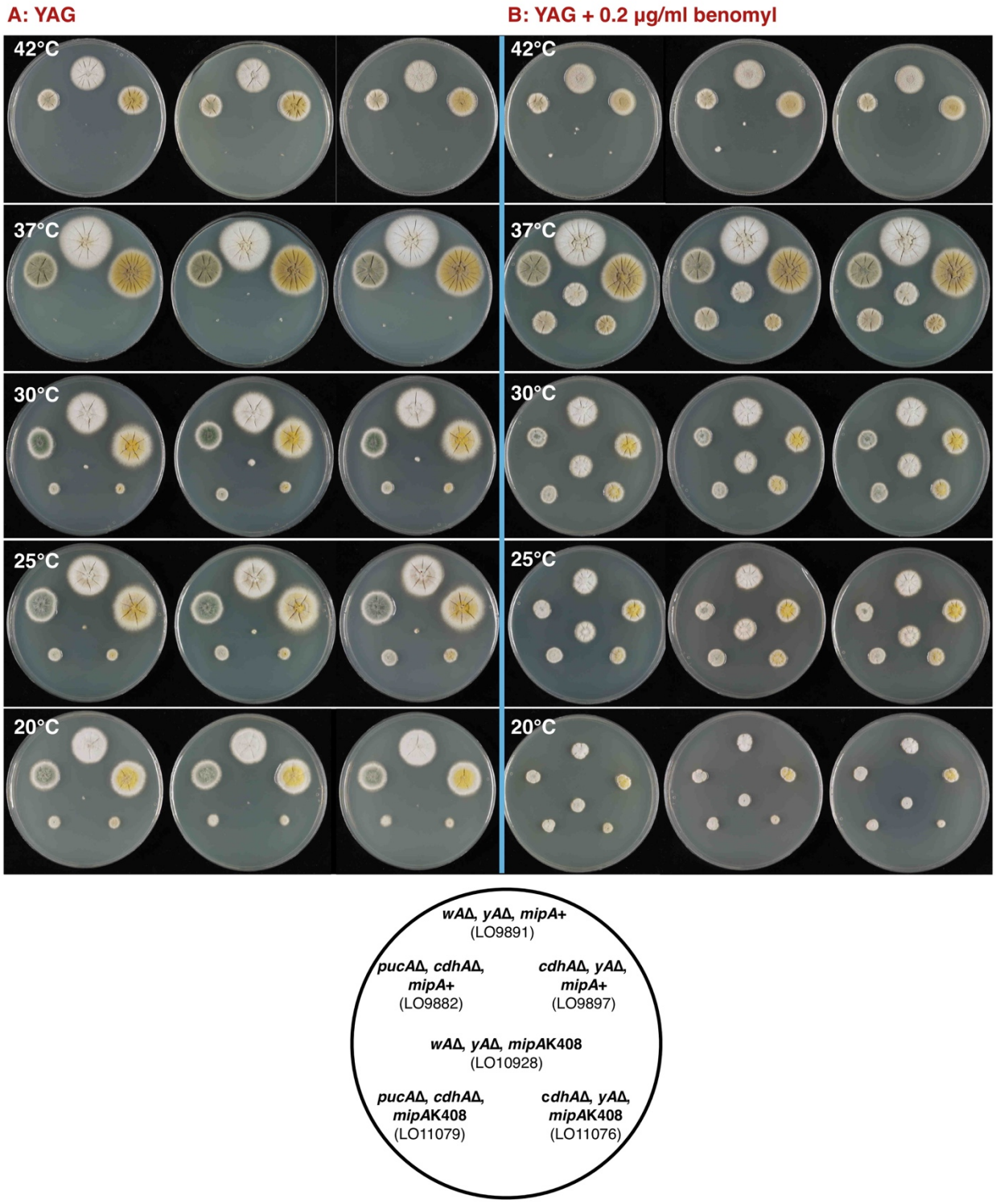

Figure 6.4 *(continued on next page)*

(continued from previous page)

Figure 6.4: Genetic interaction between *cdhA* and *mipA*K408
mipA+ and *mipA*K408 strains were stabbed onto complete media and complete media containing 0.2 μg/ml of benomyl (a microtubule-depolymerizing agent) (3 replicates of each). The plates were incubated at the various temperatures and the genotypes and strain names are shown in the circle at the bottom. The control *mipA*K408 strain (LO10928) requires low concentrations of benomyl to grow. (**A**) A *cdhA*Δ, *mipA*K408 strain (LO11076) and a *pucA*Δ, *cdhA*Δ, *mipA*K408 strain (LO11079) both display partial growth restoration at 30℃, 25℃, and 20℃ compared to the *mipA*K408 control strain (LO10928) on media lacking benomyl. (**B**) A *cdhA*Δ, *mipA*K408 strain (LO11076) displays reduced growth at 20-37℃ compared to the *mipA*K408 control strain (LO10928) on media containing benomyl. A *pucA*Δ, *cdhA*Δ, *mipA*K408 strain (LO11079) slightly exacerbates growth at 30℃, 25℃, and 20℃ compared to the *mipA*K408 control strain (LO10928) on media with benomyl.

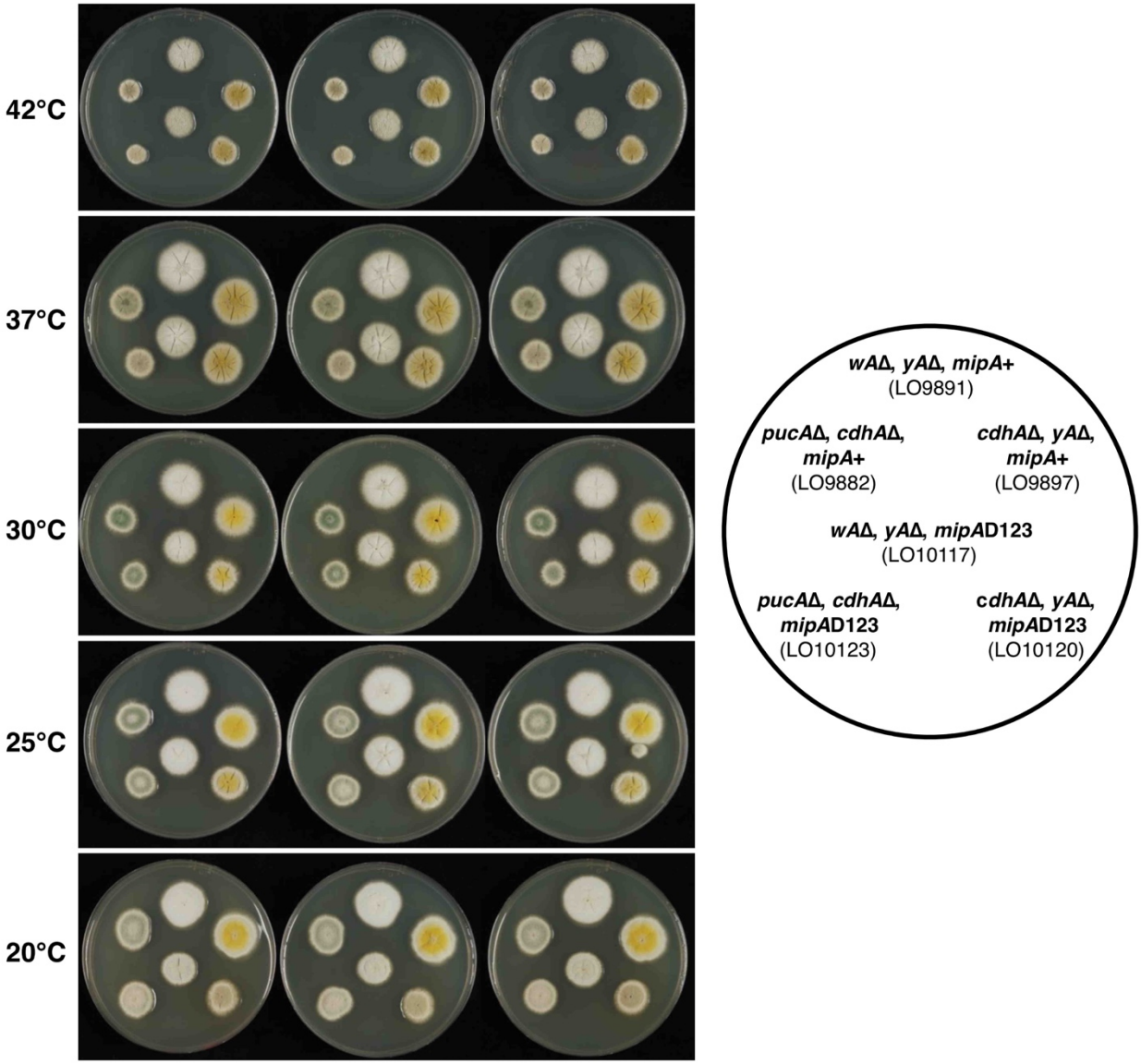

Figure 6.5: No genetic interaction between *pucA* and *mipA*D123

mipA+ and *mipA*D123 strains were stabbed onto complete media (in 3 replicates) and incubated at the various temperatures indicated on the far left. The genotypes and strain names are shown in the circle on the right. The deletion of *cdhA* in *mipA*D123 (strain LO10120) slightly exacerbates growth at 42℃ and 25℃ compared to the *mipA*D123 control strain (LO10117). Deletion of *pucA* in *cdhA*Δ, *mipA*D123 (strain LO10123) partially exacerbates growth at 25-42℃ compared to both the *mipA*D123 control strain (LO10117) and the *cdhA*Δ, *mipA*D159 strain (LO10120).

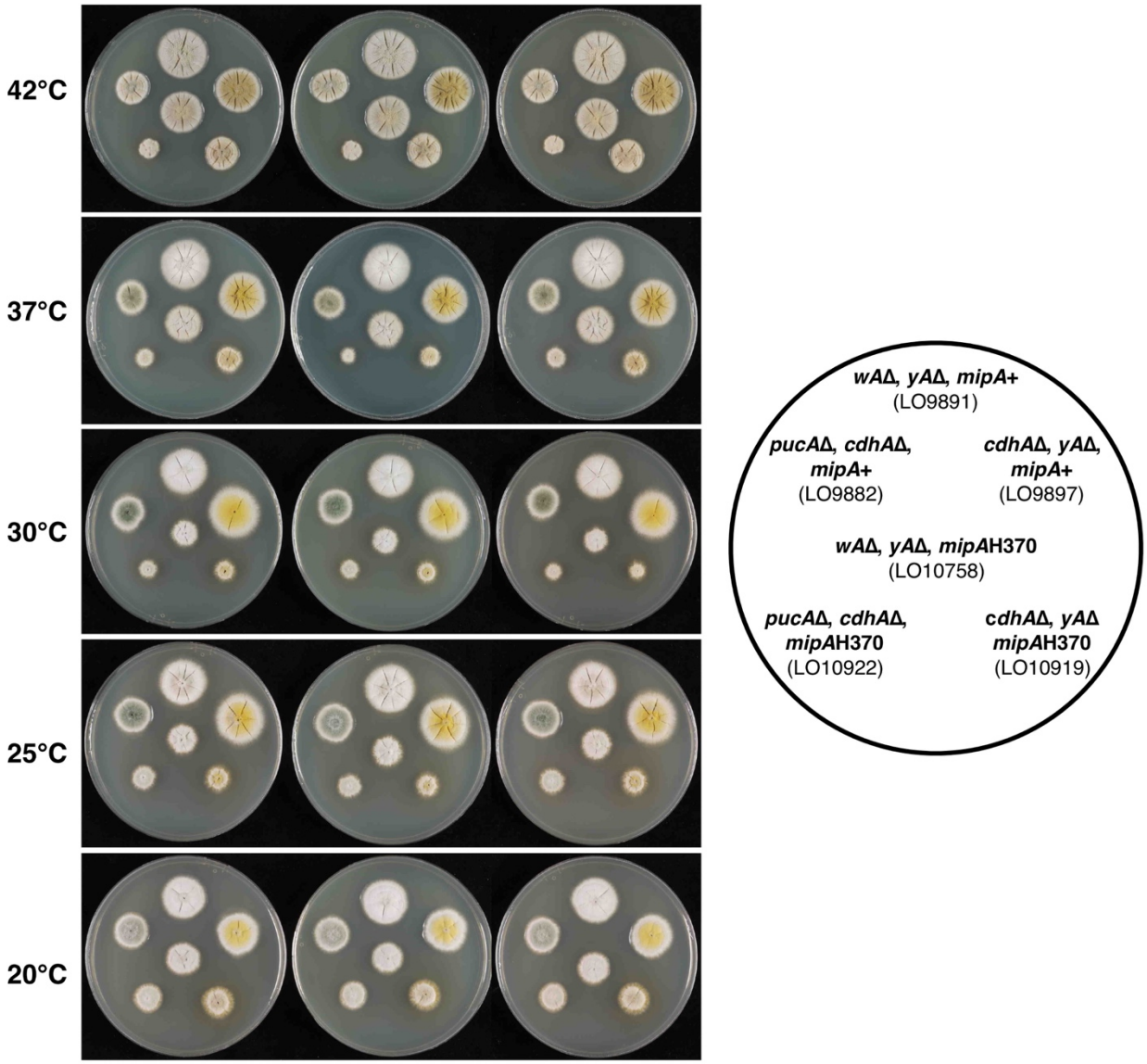

Figure 6.6: No genetic interaction between *pucA* and *mipA*H370

mipA+ and *mipA*H370 strains were stabbed onto complete media (in 3 replicates) and incubated at the various temperatures indicated on the far left. The genotypes and strain names are shown in the circle on the right. A *cdhA*Δ, *mipA*H370 strain (LO10919) and a *pucA*Δ, *cdhA*Δ, *mipA*H370 strain (LO10922) both display a reduction in growth compared to the control *mipA*H370 (LO10758) at all temperatures. The *pucA*Δ, *cdhA*Δ, *mipA*H370 strain displays a more significant growth reduction at higher temperatures compared to that of the *cdhA*Δ, *mipA*H370 strain.

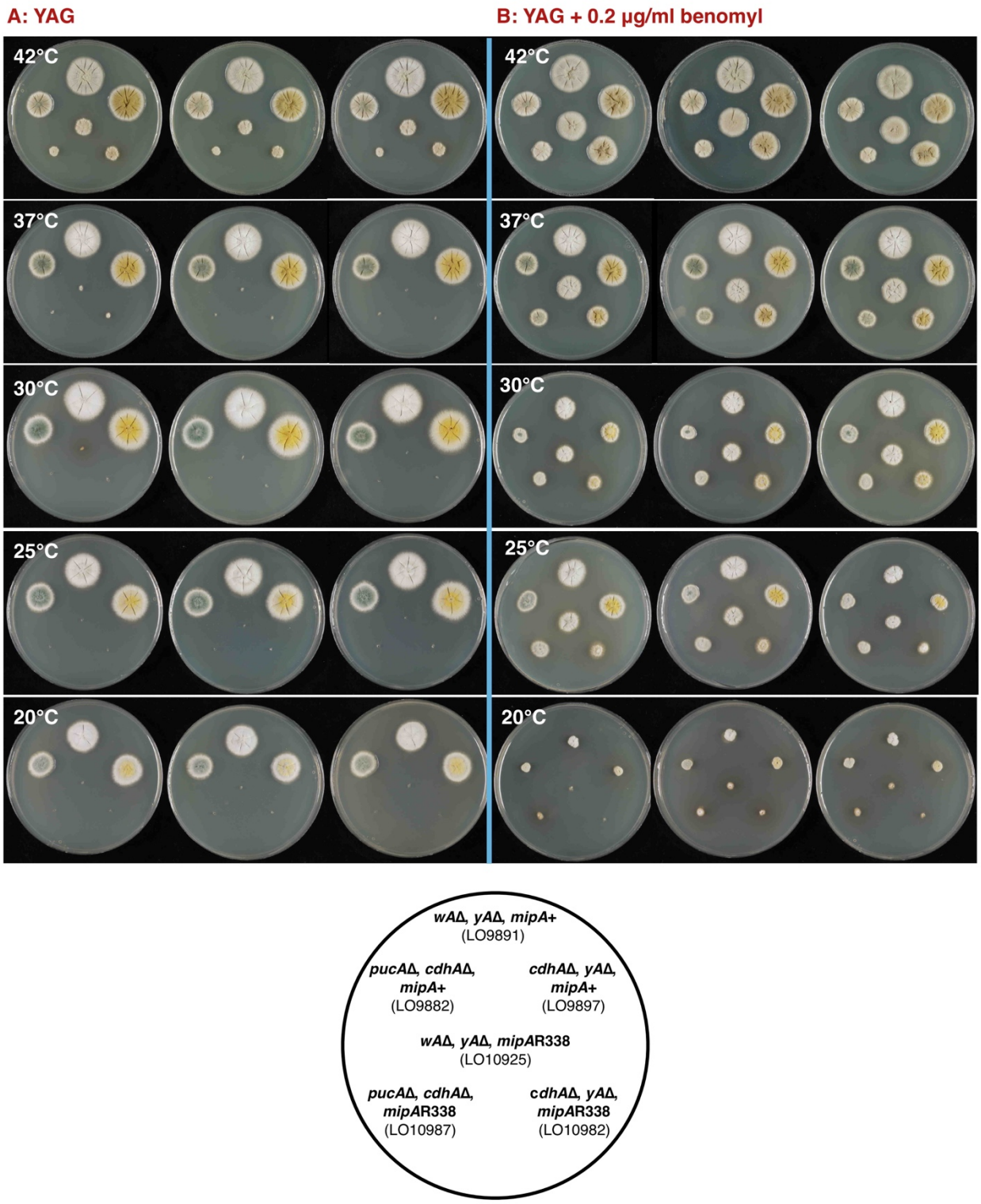

Figure 6.7 *(continued on next page)*

(continued from previous page)

Figure 6.7: No genetic interaction between *pucA* and *mipA*R338
mipA+ and *mipA*R338 strains were stabbed onto complete media and complete media containing 0.2 μg/ml of benomyl (a microtubule-depolymerizing agent) (3 replicates of each). The plates were incubated at the various temperatures and the genotypes and strain names are shown in the circle at the bottom. The control *mipA*R338 strain (LO10925) can only grow on media lacking benomyl at 42℃; *mipA*R338 strains can only grow at other temperatures if the media contains low concentrations of benomyl. (**A**) A *cdhA*Δ, *mipA*R338 strain (LO10982) and a *pucA*Δ, *cdhA*Δ, *mipA*R338 strain (LO10987) both grow slightly worse than the *mipA*R338 control strain at 42℃ and do not grow at the other temperatures. (**B**) A *cdhA*Δ, *mipA*R338 strain (LO10982) grows slightly worse than the *mipA*R338 control strain at 37℃, 25℃, and 20℃. A *pucA*Δ, *cdhA*Δ, *mipA*R338 strain (LO10987) grows slightly worse at 25-42℃ compared to the *mipA*R338 control strain.

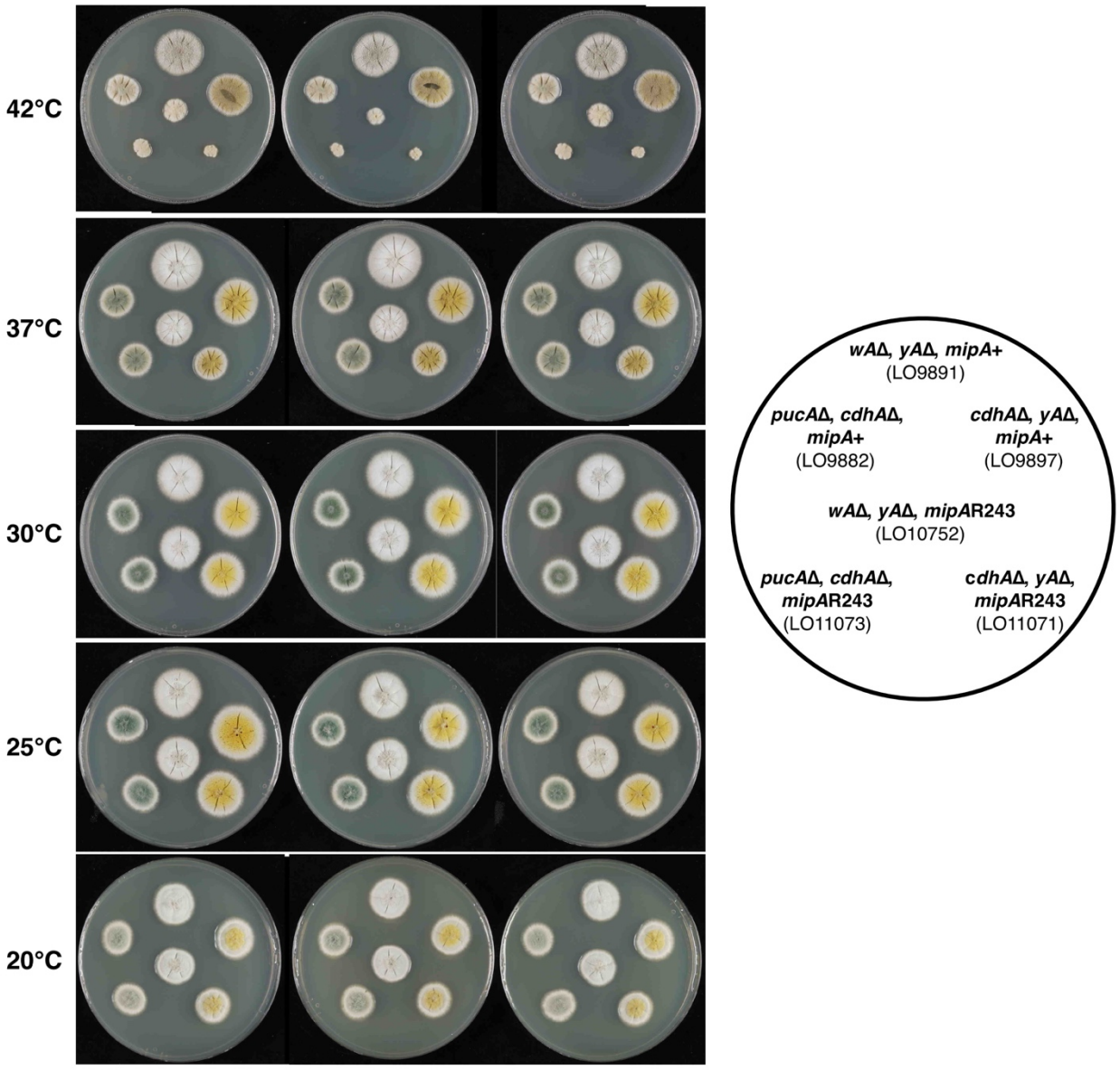

Figure 6.8: No genetic interaction between *pucA* and *mipA*R243

mipA+ and *mipA*R243 strains were stabbed onto complete media (in 3 replicates) and incubated at the various temperatures indicated on the far left. The genotypes and strain names are shown in the circle on the right. The deletion of *cdhA* in *mipA*R243 (strain LO11071) slightly exacerbated growth at 42℃, 37℃, and 20℃ compared to the *mipA*243 control strain (LO10752). Deletion of *pucA* in a *cdhA*Δ, *mipA*R243 (strain LO11073) slightly exacerbated growth at 42℃ compared to the mipAR63 control strain (LO10512). The *pucA*Δ, *cdhA*Δ, *mipA*R243 strain (LO11073) grew identically to the *pucA*Δ, *cdhA*Δ strain (LO9882) at 20-37℃.

6.2.2 mipAD159 causes a failure of accumulation of both B-type cyclins NimE$^{Cyclin\ B}$ and ClbA

As previously mentioned in Chapter 1.5.3, a subset of nuclei in *mipA*D159 strains failed to accumulate the B-type cyclin NimE$^{Cyclin\ B}$ and the cyclin-dependent kinase NimX^{Cdk1} due to a constitutively active APC/C-CdhA, which continuously targeted NimE$^{Cyclin\ B}$ for degradation (Edgerton-Morgan and Oakley, 2012; Nayak *et al.*, 2010). NimE$^{Cyclin\ B}$ is recognized by the APC/C-CdhA due to the presence of a destruction box motif, called the d-box (consensus sequence RXXLXXXXN), in its N-terminus. Furthermore, spindle assembly checkpoint proteins MpsA (the *A. nidulans* Mps1 homolog) and SldA (the *A. nidulans* Bub1/R1 homolog) both contain putative destruction box motifs, and both failed to accumulate in a subset of *mipA*D159 nuclei (Edgerton *et al.*, 2015). In Chapter 4.3.2, I have reported results that reveal that the B-type cyclin ClbA contains two putative destruction box motifs and that its destruction is required for viability. Thus, I was curious as to whether ClbA-GFP would accumulate in the NimE$^{Cyclin\ B}$/NimX^{Cdk1} negative nuclei in *mipA*D159.

I generated strains carrying *clbA*-GFP, *nimX^{cdk1}*-mCherry, *An-nup49*-mCherry (to visualize the nuclear periphery), and the *mipA*D159 allele (strains LO10623-624). Conidia from these strains were incubated in minimal media at 25℃. After ~17 hours, germlings were imaged at 25℃ with Z-series stacks captured at 4-minute intervals from S/G_2 until mitotic entry. I found that the subset of nuclei that failed to accumulate NimX^{Cdk1} also failed to accumulate ClbA-GFP (51/51 nuclei) and that the majority of nuclei that accumulated NimX^{Cdk1} also accumulated ClbA-GFP (102/104 nuclei) (**Fig. 6.9**). Thus, my data likely indicate that ClbA-GFP is a target of APC/C-CdhA.

A

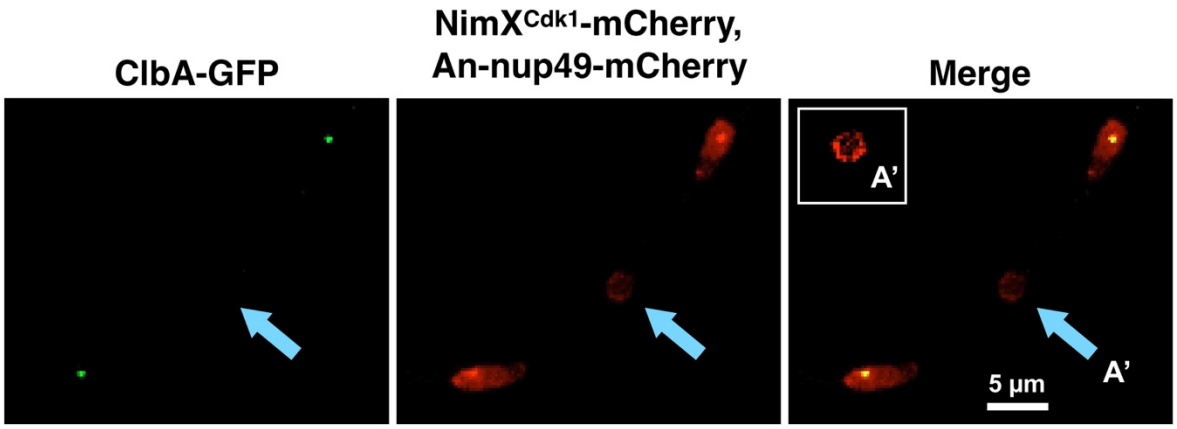

B

	Cdk1+/ClbA+	Cdk1-/ClbA-	Cdk1-/ClbA+	Cdk1+/ClbA-
Number of nuclei (n=155)	102	51	0	2
Percentage of S/G_2 nuclei	65.81%	32.90%	0.00%	1.29%

Figure 6.9: Failure of accumulation of ClbA in NimX^{Cdk1} negative in *mipA*D159
Conidia from strains carrying *clbA*-GFP, *nimX^{cdk1}*-mCherry, *An-nup49*-mCherry (to visualize the nuclear periphery), and *mipA*D159 (strains LO10623-624) were incubated in minimal media at 25°C. After ~17 hours, germlings were imaged in 4-minute intervals at 25°C. S/G_2 tip cells (1+ nuclei containing NimX^{Cdk1}) were scored for the absence or presence of ClbA-GFP prior to mitotic entry (**B**). Almost all NimX^{Cdk1} positive nuclei contained ClbA-GFP (102/104 nuclei) and all NimX^{Cdk1} negative nuclei failed to accumulate ClbA-GFP at any point prior to mitotic entry (51/51 nuclei). (**A**) A representative tip cell of three nuclei, two of which have accumulated NimX^{Cdk1}-mCherry and ClbA-GFP. The middle nucleus has failed to accumulate both NimX^{Cdk1}-mCherry and ClbA-GFP. The brightness of the middle nucleus was increased to more easily display the empty, Cdk1 negative nucleoplasm (inset **A'**). Images are maximum intensity projections from Z-series stacks.

6.2.3 Deletion of culA recapitulates a mipAD159 phenotype

A. nidulans is coenocytic and nuclei in tip cells progress synchronously through the cell cycle. Cell cycle regulatory proteins, such as NimE$^{Cyclin\ B}$ and NimX^{Cdk1}, accumulate, localize to specific cellular structures (e.g. the SPB), and are destroyed or displaced at nearly the same time

in all nuclei within the same tip cell. As mentioned earlier, we previously determined that the cold-sensitive γ-tubulin mutation *mipA*D159, incubated at the restrictive temperature of 25℃, caused a subset of S/G_2 nuclei to fail to accumulate $NimE^{Cyclin\ B}$ and $NimX^{Cdk1}$. These nuclei exited the cell cycle and did not undergo nuclear division. Other nuclei in the same S/G_2 tip cells accumulated these proteins normally, progressed through the cell cycle, and underwent nuclear division (Nayak *et al.*, 2010). Our lab determined that the failure to accumulate $NimE^{Cyclin\ B}$ and $NimX^{Cdk1}$ was due to a constitutively active APC/C-CdhA complex that resulted in the continuous destruction of $NimE^{Cyclin\ B}$. The constitutively active APC/C-CdhA correlated with the failure of CdhA to dissociate from the SPB at G_1/S (Edgerton-Morgan and Oakley, 2012).

Since the SCF complex is involved in the targeting of Cdh1 for destruction in other organisms, we expected that deletion of *culA* or *skpA* would result in failure of CdhA destruction, as confirmed above, and, consequently, constitutive APC/C activity. This should result in failure of $NimE^{Cyclin\ B}$ to accumulate. Our results were more complex than anticipated, however. We did find that a subset of nuclei in *culA*Δ tip cells (parental strain LO2074) failed to accumulate $NimE^{Cyclin\ B}$ when other nuclei in the same cell accumulated $NimE^{Cyclin\ B}$ normally (i.e. were in S or G_2) (**Fig. 6.10 A-D, E**). The percentage of nuclei exhibiting this phenotype was rather modest, however, increasing from about 5% in a sample imaged at an incubation time of 12-13 h to almost 14% at 16-17 h. Surprisingly, this phenotype was not observed in *skpA*Δ tip cells (**Fig. 6.10 E**).

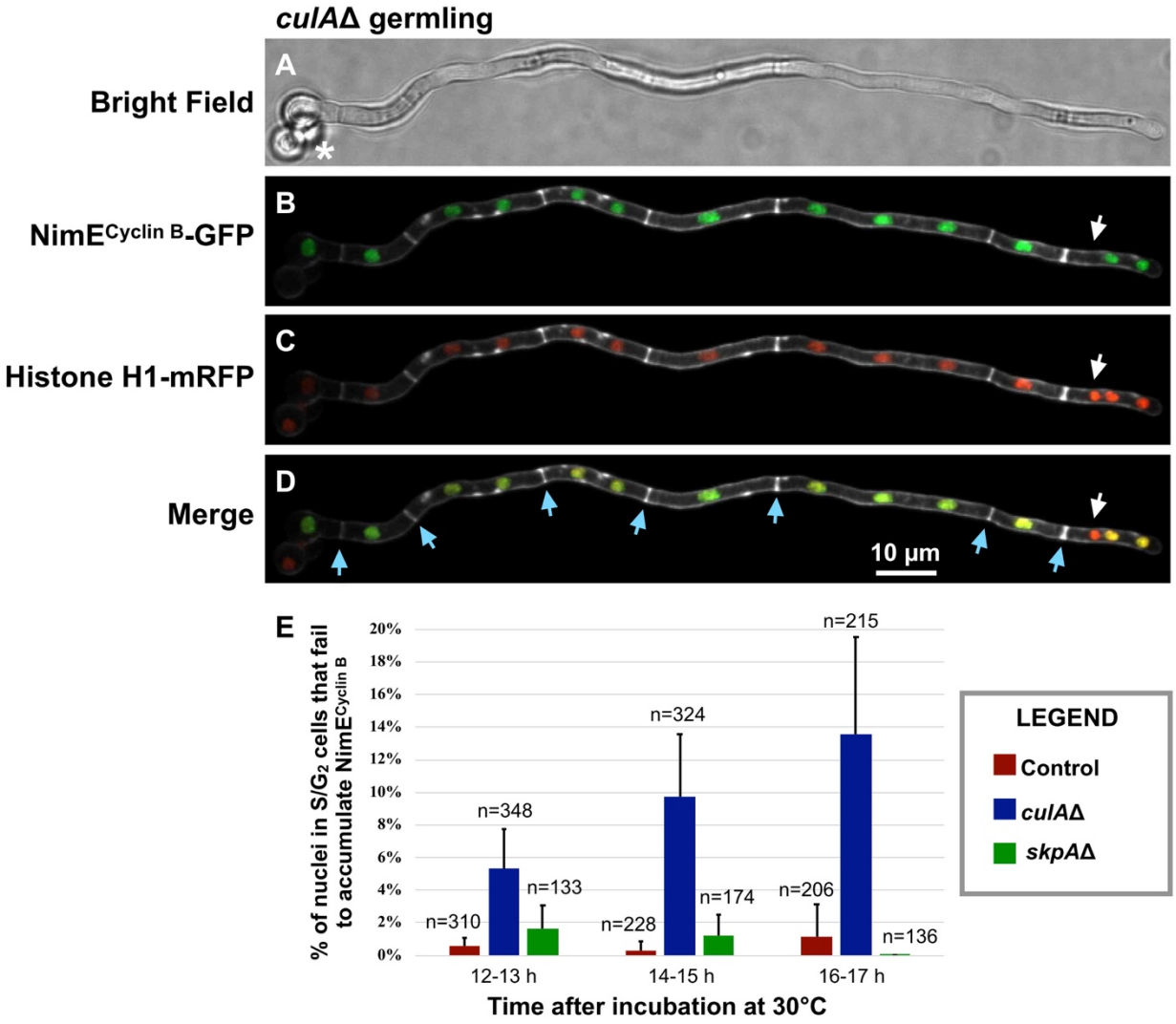

Figure 6.10: The deletion of *culA* recapitulates a *mipA*D159 phenotype.
Both *culA* and *skpA* were deleted (separately) in strain LO2074 that carries histone H1-mRFP and NimE$^{Cyclin\ B}$-GFP. Similar to **Fig. 4**, control conidia and conidia from *culA*Δ and *skpA*Δ heterokaryons were grown for 12, 14, and 16 hours at 30°C in minimal media and then live imaged for one hour at 30°C. Calcofluor white was added 20 minutes prior to imaging. The percentage of nuclei in S/G_2 tip cells that failed to accumulate NimE$^{Cyclin\ B}$ was scored (**E**); error bars indicate mean ± standard deviation of three separate experiments. n = the number of S/G_2 nuclei. (**A-D**) A representative image of a *culA*Δ germling imaged ~14 hours after incubation at 30°C is shown. Blue arrows in **D** indicate septa and asterisks indicate swollen, ungerminated conidia that are likely parental, untransformed conidia. White arrows in **B-D** indicate a NimE$^{Cyclin\ B}$ negative nucleus in a tip cell with two NimE$^{Cyclin\ B}$ positive nuclei. Images are maximum intensity projections from Z-series stacks.

6.2.4 γ-tubulin and CulA are involved in a common function required for growth or viability

As mentioned previously, strains carrying a C-terminal fusion of GFP to CulA (CulA-GFP) were slightly heat sensitive and conidiation was impaired at low temperatures (**Fig. 6.11**, strain LO8388), indicating that the GFP tag reduces CulA function, particularly at lower temperatures.

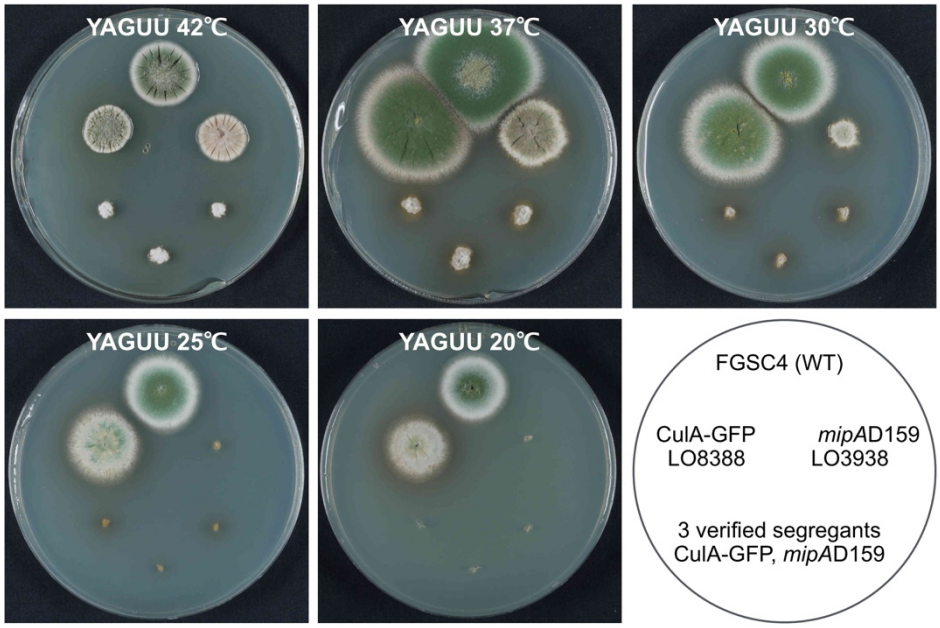

Figure 6.11: Synthetic interaction between *mipA*D159 and *culA*-GFP
The C-terminal fusion of GFP to CulA was viable but had a slight effect on growth at 42℃ and a significant effect on conidiation at 25℃ and 20℃. A strain carrying *culA*-GFP (LO8388) was crossed to a *mipA*D159 strain (LO3938) to generate *culA*-GFP, *mipA*D159 segregants. A wild-type strain (FGSC4), the two parental strains (LO8388 and LO3938), and three *culA*-GFP, *mipA*D159 segregants were stabbed onto complete media and incubated at various temperatures. The *culA*-GFP, *mipA*D159 segregants are synthetically sick compared to the two parental strains.

Because *mipA*D159 and CulA both play roles in the regulation of CdhA, I was curious as to whether *mipA*D159 and CulA-GFP would display synthetic genetic interactions. I crossed a strain carrying CulA-GFP (LO8388) to a *mipA*D159 strain (LO3938). I able to isolate and verify segregants carrying *mipA*D159 and GFP-*culA*, but they were strongly inhibited for growth at all temperatures (**Fig. 5.11**). The synthetic growth inhibition was particularly evident at 42ºC and

37ºC where the parental *mipA*D15 and GFP-*culA* strains grow reasonably well, but the double mutants barely grow.

6.3 Discussion

My initial interest in cell-cycle related cyclins and the SCF complex was based on the fact that γ-tubulin has a microtubule-independent role in inactivating CdhA, and thus the APC/C, at the G_1/S transition. The failure to inactivate APC/C-CdhA in a γ-tubulin mutant, *mipA*D159, resulted in the nuclear autonomous failure of accumulation of $NimE^{Cyclin\ B}$/$NimX^{Cdk1}$ (Edgerton-Morgan and Oakley, 2012; Nayak *et al.*, 2010). The mechanism by which γ-tubulin inactivates CdhA is not known, although our data do not support a direct interaction between γ-tubulin and CdhA. In many organisms, initial Cdh1 inactivation at G_1/S occurs via phosphorylation by cyclin/CDK complexes which then triggers Cdh1 ubiquitination by the Skp1-Cullin1-F-box (SCF) complex (Fukushima *et al.*, 2013; Lukas *et al.*, 1999; Sorensen *et al.*, 2001). Thus, plausibly, γ-tubulin and cyclins and/or components of the SCF complex might be functionally related. My results provide several items of evidence that this is the case.

First, deletion of the G_1/S cyclin *pucA* in both *cdhA*Δ*, mipA*D159 and *cdhA*Δ*, mipA*R63 strains partially suppresses the growth restriction conferred by the *mipA*D159 and *mipA*R63 alleles, respectively. These data indicate that PucA function is required for some of the growth limiting effects observed in *mipA*D159 and *mipA*R63 strains. Crucially, this partial growth restoration phenotype was not observed with four other *mipA* mutants. These data reveal that the genetic interaction between *pucA* and γ-tubulin is allele-specific. Allele specificity is often an indication that the interaction is functionally meaningful. In addition, the *mipA*D159 and *mipA*R63 mutations are close to one another in the γ-tubulin molecule (**Fig. 1.11**), further supporting the specificity of

the interaction between *pucA* and γ-tubulin. The mechanism of this interaction is not yet understood, but my data indicate that these genetic interactions occur independently of CdhA function.

I have also determined that the B-type cyclin ClbA fails to accumulate in a subset of *mipA*D159 nuclei which lack NimX^{Cdk1}. This is likely due to the presence of two destruction box motifs in the N-terminus of ClbA. In the *mipA*D159 nuclei that fail to accumulate NimX^{Cdk1}, which we have previously shown is due to constitutively active APC/C-CdhA, the destruction boxes of ClbA likely target it for continuous destruction by APC/C-CdhA. Although this was not an unexpected result, it is consistent with previous work in which other cell cycle regulators containing destruction box motifs failed to accumulate in *mipA*D159 nuclei containing constitutively active APC/C^{CdhA} (e.g. NimE$^{Cyclin\ B}$, SldA$^{Bub1/R1}$, MpsA) (Edgerton *et al.*, 2015; Nayak *et al.*, 2010).

The deletion of *culA*, a component of the SCF complex, resulted in a nuclear autonomous failure of NimE$^{Cyclin\ B}$ accumulation in tip cells in which other nuclei accumulated NimE$^{Cyclin\ B}$ normally. Deletion of *culA*, thus, mimics an unusual phenotype of *mipA*D159. Furthermore, I identified an interesting genetic interaction between CulA and γ-tubulin. The C-terminal GFP fusion to CulA causes a reduction in conidiation at lower temperatures, indicating that the C-terminal GFP tag may cause a slight loss of function. *culA*-GFP and *mipA*D159 displayed a strong, synthetic growth inhibition. This genetic interaction indicates that the SCF complex and γ-tubulin play separate roles in a common function that is required for growth. One obvious candidate function is inactivation of CdhA.

In conclusion, I have uncovered interesting genetic interactions between γ-tubulin and two regulators of CdhA, PucA and CulA. The genetic interaction between *pucA* and γ-tubulin is

independent of CdhA function, while it is unknown whether the genetic interaction between *culA* and γ-tubulin is dependent on CdhA activity. My data support that PucA and CulA are strong candidates through which γ-tubulin acts to control APC/C-CdhA activity (and possibly other cell cycle functions of γ-tubulin that are independent of CdhA) and are worthy of follow-up studies.

Chapter 7: Concluding remarks

My dissertation work provides new insights into the cell cycle functions of γ-tubulin, cyclins, and E3 ubiquitin ligases in the model filamentous fungus *Aspergillus nidulans.* Filamentous fungi have significant impacts on humans, ranging from human, animal, and crop plant pathogenesis to production of desirable products (e.g. citric acid, statins, antibiotics, etc.). It is, thus, important that we overcome our limited understanding of the basic principles of cell cycle control in filamentous fungi in order to elucidate how cell cycle regulators affect fungal growth and development. Furthermore, this knowledge will aid in the quest for new anti-fungal drugs, as targeting fungal cell cycle regulators will arrest the cell cycle and, thus, growth. For example, a new compound called 089 has anti-fungal activity against *S. cerevisiae* cells by causing a G_2 cell cycle block, which Stefanini *et al.* (2018) shows is likely caused by an inhibition of cyclin-dependent kinase activity in G_2. With the numerous genetic tools at our disposal, *A. nidulans* is an ideal model system for the identification and study of cell cycle regulators in aspergilli as well as related filamentous fungi and may provide new targets for anti-fungal drugs.

The initial question that drove my dissertation work was based on the fact that our lab previously determined that γ-tubulin has a microtubule-independent role in inactivating CdhA, and, thus, the anaphase promoting complex/cyclosome (APC/C), at the G_1/S transition in *A. nidulans* (Edgerton-Morgan and Oakley, 2012; Nayak *et al.*, 2010). The mechanism by which γ-tubulin inactivates CdhA is not yet understood, but our data do not support a direct interaction between γ-tubulin and CdhA. Instead, we hypothesize that γ-tubulin interacts directly or indirectly with regulators of CdhA. Although the APC/C is an essential and ubiquitous component of the eukaryotic cell cycle regulatory system, the regulation of its activator CdhA had not yet been studied in *A. nidulans* nor any other filamentous fungus at the start of my graduate career. Thus, it

was important to first identify and characterize regulators of CdhA in *A. nidulans* because of (1) the lack of data on APC/C-CdhA regulation in filamentous fungi and because (2) this knowledge is likely to be valuable in determining the role of γ-tubulin in APC/C-CdhA inactivation. To this end, I successfully identified and characterized two regulators of CdhA and additionally determined that both CdhA regulators have interesting genetic interactions with γ-tubulin, making them candidates for molecules through which γ-tubulin acts to control APC/C-CdhA inactivation at the G/S transition.

At the G_1/S transition in many eukaryotic organisms, including humans, initial Cdh1 inactivation occurs via phosphorylation by cyclin/CDK complexes which then triggers Cdh1 ubiquitination by the E3 ubiquitin ligase Skp1-Cullin1-F-box (SCF) (Fukushima *et al.*, 2013; Lukas *et al.*, 1999; Sorensen *et al.*, 2001). Prior to my work, very little was known about the functions of cell cycle-related cyclins in filamentous ascomycetes, other than the essential B-type cyclin $NimE^{Cyclin\ B}$ in *A. nidulans*. Little was also known about the SCF complex in filamentous ascomycetes except that CulA and SkpA are essential.

7.1 Summary of cyclins in aspergilli, the functional characterization of group I cyclins in *A. nidulans*, and new insights into the functions of gamma-tubulin

In Chapter 3, I reported my identification of the cyclin complement in *A. nidulans*. There are fifteen cyclin genes in the genome. The cyclin complement I identified in *A. nidulans* is different from those of the model yeasts *Saccharomyces cerevisiae, Schizosaccharomyces pombe,* and *Candida albicans*. Model yeasts (in particular *S. cerevisiae*) have traditionally been used as a reference system for filamentous fungal biology. In fact, in the comparative genomic study of cyclins in Ma *et al.* (2013) and Cao *et al.* (2014), the representative fungi were the yeasts *S.*

cerevisiae and *S. pombe.* However, it is becoming clear that model yeasts are not good reference systems for filamentous fungi [reviewed in (Meyer *et al.*, 2016)], and my phylogenetic data comparing the cyclin complements in *A. nidulans* and the three model yeasts further strengthens this argument. Instead, I propose that *A. nidulans* is a more suitable model system for studying filamentous fungal biology.

In order to determine if *A. nidulans* is an appropriate model for studying cell cycle regulators in filamentous fungi, I investigated the cyclin repertoires of 31 additional filamentous ascomycetes (17 species from the genus *Aspergillus* and 14 species from other, phylogenetically diverse, genera) all within the subdivision Pezizomycotina (de Vries *et al.*, 2017). This subdivision includes most of the 1,000,000+ species of filamentous ascomycetes. In Chapter 3, I demonstrated that the complement of cyclins is remarkably conserved among the filamentous ascomycetes in my study. In addition, my work is the first to show that cyclins from numerous diverse filamentous ascomycetes cluster into three major cyclin groups. This finding is consistent with previous work that determined that the cyclin family in other eukaryotes can be divided into three groups (Groups I, II, and III) (Cao *et al.*, 2014; Ma *et al.*, 2013). It is important to mention that these two studies together analyzed only a small number of eukaryotes (27 different species). Thus, my analysis of the cyclin complements in a total of 32 different species of filamentous ascomycetes, including *A. nidulans*, strengthens their model that eukaryotes contain three major cyclin groups.

Ma *et al.* (2013) and Cao *et al.* (2014) demonstrated that cyclins in a particular group tend to have similar functions. Group I cyclins typically have cell cycle-related functions, while group III cyclins tend to function primarily in transcriptional regulation. Group II cyclins have varied functions that are species-specific but tend to function in various developmental processes. As I was particularly interested in cyclins that were likely to play critical roles in the regulation of the

cell cycle, I took a closer look at the group I cyclins in *A. nidulans* and other filamentous ascomycetes.

I determined that all 32 filamentous ascomycetes, including *A. nidulans*, have only three group I cyclins. Furthermore, the group I cyclins fall into three clades with each fungus having a single member of each clade. In *A. nidulans*, the group I cyclins are $NimE^{Cyclin\ B}$, PucA, and ClbA. As mentioned earlier, $NimE^{Cyclin\ B}$ has previously been studied. The other two *A. nidulans* group I cyclins are a named but uncharacterized cyclin, PucA, and a previously unstudied cyclin, which we designated ClbA. Based on my phylogenetic analyses, both PucA and ClbA were strong candidates for cyclins with cell cycle-related functions, so my next step was to functionally characterize both cyclins. Because of the strong sequence similarities of these cyclins to the group I cyclins in other filamentous ascomycetes, my functional analyses the group I cyclins in *A. nidulans* are likely to carry over to group I cyclins in many other filamentous ascomycetes, including pathogenic and industrially important species.

In Chapter 4, I demonstrated that PucA is an essential G_1/S cyclin in *A. nidulans* that promotes entry into S-phase, and, consequently, the nuclear accumulation of $NimE^{Cyclin\ B}$, by inactivating CdhA. Although *pucA*Δ is lethal in a $cdhA^+$ background it is viable in a *cdhA*Δ background. This result reveals that PucA is required for APC/C-CdhA inactivation but also that no other proteins, including cyclins, can sufficiently inactivate CdhA at the G_1/S transition to allow progression into S phase. This is an important finding, as Cdh1 inactivation in other organisms that have been studied typically occurs by several redundant mechanisms. For example, in both humans and *S. cerevisiae*, multiple cyclin/CDK complexes are capable of phosphorylating and inactivating Cdh1 at G_1/S. Various inhibitors can also bind and inactivate APC/C-Cdh1 (e.g. EMI1 in vertebrates, Acm1 in *S. cerevisiae*, and Rca1 in *Drosophila melanogaster*), but none of these

inhibitors has an obvious homolog in *A. nidulans.* Thus, although Cdh1 inactivation is regulated by multiple proteins in other organisms [reviewed in (Sivakumar and Gorbsky, 2015)], APC/C-CdhA inactivation at G_1/S in *A. nidulans* relies solely on a mechanism requiring PucA.

In addition to inactivating APC/C-CdhA at the G_1/S transition, PucA also has non-essential functions in interphase that are independent of CdhA. For example, in *pucA*Δ, *cdhA*Δ double mutant strains, I observed severe nuclear stretching and nuclei in which the chromatin condensed and decondensed in a nuclear autonomous fashion. In an attempt to determine the cause of these interphase phenotypes, I looked for microtubule abnormalities, inhibition of polarized growth, and mis-localization of $NimE^{Cyclin\ B}$, but I found no evidence for these abnormalities in *pucA*Δ, *cdhA*Δ double mutant strains. One highly speculative idea is that the kinase, NimA, might be involved in these phenotypes. Previous work found that overexpression of NimA resulted in premature chromatin condensation in *A. nidulans* and *S. pombe* (O'Connell *et al.*, 1994) and also in *Xenopus* and human cells (Lu and Hunter, 1995). NimA stability has been shown to be regulated by the APC/C (Ye *et al.*, 1998), which might account for the small percentage of nuclei in which the chromatin condenses and decondenses abnormally in the *cdhA*Δ single mutant. As NimA-GFP is excluded from nuclei during interphase in *A. nidulans*, a future project could study the localization of NimA in *pucA*Δ, *cdhA*Δ strains and determine whether NimA localizes to those nuclei that partially condense and decondense abnormally during interphase.

Finally, I also determined that *pucA* interacts genetically with two out of seven *mipA* mutants, revealing that the interaction is allele specific. The deletion of *pucA* in both *cdhA*Δ*, mipA*D159 and *cdhA*Δ*, mipA*R63 strains resulted in a partial suppression of the growth inhibition caused by the *mipA*D159 and *mipA*R63 alleles, respectively. This result was unexpected, as it indicates that PucA function is required for some of the growth limiting phenotypes in *mipA*D159

and *mipA*R63 strains and that this occurs in a CdhA-independent manner. Although it is too early to speculate on the mechanism behind this genetic interaction, it would be illuminating to determine in future studies whether PucA and γ-tubulin directly interact and whether this interaction is lost in *mipA*D159 and *mipA*R63 strains.

Moving on to the functional characterization of ClbA (Chapter 4), I determined that ClbA is a non-essential, B-type cyclin. I also fluorescently tagged ClbA and determined that ClbA localizes with kinetochores from mid-G_2 until mitotic onset, at which time ClbA-GFP is no longer visible. Furthermore, I identified that ClbA contains two destruction box motifs, which are sequences recognized by the APC/C, and determined that expression of a version of ClbA lacking both destruction box motifs (db2Δ-ClbA) is lethal. It is important to note that in order to carry out this work, I had to utilize a repressible promoter to prevent db2Δ-ClbA expression, as its expression is lethal, until desired. My experiments led me to determine that the *alcA* system, which is used extensively in *A. nidulans*, is leaky and could not be sufficiently repressed to prevent db2Δ-ClbA expression. Instead, I found that the *nmtA* promoter in *A. nidulans* (which had not been previously used as a repressible promoter system in *A. nidulans*) could be repressed very effectively and easily, and I optimized its use for my experiments. My work with the *nmtA* promoter offers a new and valuable tool that the *Aspergillus* community can utilize to more effectively repress the expression of target genes.

Using time-lapse fluorescence microscopy, I found that expression of db2Δ-ClbA-GFP led to mitotic catastrophe during anaphase with a very high frequency of chromosomal nondisjunction and mitotic arrest. Interestingly, db2Δ-ClbA-GFP still left the kinetochore region during mitotic entry, but it remained present in the nucleoplasm and could be seen at the spindle and poles during the aberrant anaphases. Importantly, full length ClbA-GFP was never visible in nuclei or at the

poles during anaphase/telophase. I also used the *nmtA* promoter to regulate expression of a non-degradable version of NimE$^{\text{Cyclin B}}$ (dbΔ-NimE$^{\text{Cyclin B}}$), which has been previously shown to cause a mitotic block in telophase with dbΔ-NimE$^{\text{Cyclin B}}$-GFP persisting at the poles (De Souza *et al.*, 2009; Nayak *et al.*, 2010). I determined that expression of dbΔ-NimE$^{\text{Cyclin B}}$-GFP also caused a very high frequency of nondisjunction, a phenotype that had not been previously published. Thus, inappropriate cyclin activity during mitosis causes chromosomal nondisjunction. Finally, I determined that non-degradable ClbA, but not non-degradable NimE$^{\text{Cyclin B}}$, caused a delay in interphase. Taken together, I hypothesize that ClbA localizes with kinetochores in G_2 and its presence there inhibits mitotic entry until it is removed from the kinetochore region.

The failure of chromosomal disjunction in db2Δ-ClbA-GFP and dbΔ-NimE$^{\text{Cyclin B}}$-GFP cells was very intriguing to me as nondisjunction is often observed in both *mipA*D159 (Prigozhina *et al.*, 2004) and *mipA*R63 (Li *et al.*, 2005) mutants. There are many explanations that might account for the similarity in the nondisjunction phenotypes, but one possibility is that the failure of chromosomal disjunction is a consequence of mis-regulation of the cohesion complex and/or a failure to resolve DNA catenanes.

There are two major processes that must occur for successful disjunction of chromosomes. First, the cohesin complex must be removed and, second, catenanes (DNA intertwinings) of the daughter chromatids must be resolved by topoisomerase II. I determined that the cohesion complex is removed in strains expressing db2Δ-ClbA and dbΔ-NimE$^{\text{Cyclin B}}$. Similarly, previous work in the lab by Dr. Tetsuya Horio revealed that the cohesion complex is removed in *mipA*D159 nuclei, even those nuclei with chromosomes that fail to disjoin properly (unpublished data). It follows that both γ-tubulin activity and the timely destruction of ClbA and NimE$^{\text{Cyclin B}}$ during mitosis are required for DNA decatenation, presumably through regulation of topoisomerase II. The phenotypes

observed are consistent with a failure of decatenation and, unlike the cohesin complex, catenanes are unable to resist the pulling forces of microtubules [reviewed in (Haarhuis *et al.*, 2014)]. Thus, a failure to resolve catenanes would not block anaphase and is likely to lead to chromosome stretching and nondisjunction, which we observed in the strains expressing the non-degradable cyclins as well as in strains carrying *mipA*D159 or *mipA*R63. Future studies should focus on determining whether topoisomerase II is the source of the nondisjunction observed in strains expressing db2Δ-ClbA, dbΔ-NimE$^{\text{Cyclin B}}$, *mipA*D159, and *mipA*R63. These studies should provide clarity as to the mitotic functions of cyclins and γ-tubulin and whether they function in a similar pathway.

Finally, I also determined that ClbA does not localize to a subset of nuclei (NimX$^{\text{Cdk1}}$ negative nuclei) in *mipA*D159 strains. This phenotype was not unexpected, as ClbA contains destruction motifs that can be recognized by APC/C-CdhA. It is, however, significant as it is consistent with our previous findings that NimE$^{\text{Cyclin B}}$/NimX$^{\text{Cdk1}}$ negative nuclei in *mipA*D159 strains contain active APC/C-CdhA complexes that constitutively target proteins with destruction box motifs for destruction. We previously showed that MpsA (the *A. nidulans* Mps1 homolog) and SldA (the *A. nidulans* Bub1/R1 homolog) fail to accumulate in a subset of *mipA*D159 nuclei (Edgerton *et al.*, 2015) and now I have added ClbA to the list of cell cycle regulatory proteins that do not accumulate in these nuclei.

7.2 Summary of the functions of the SCF complex in *A. nidulans* and new insights into the functions of gamma-tubulin

In Chapter 5, I reported my characterization of two SCF complex components, SkpA and CulA. Both proteins were previously shown to be essential (von Zeska Kress *et al.*, 2012) but no

further characterization of SkpA and CulA had been completed prior to my work. I first fluorescently tagged both proteins with GFP at their N-termini to study their *in vivo* localization during the cell cycle. I found they displayed similar localization patterns during interphase (cytoplasmic, nuclear, absent from nucleoli) and that their levels were reduced in the nucleoplasm during mitosis. GFP-SkpA also briefly localized to the inner surface of SPBs during mitosis and disappeared from the SPBs during anaphase. It is likely that GFP-CulA has a similar mitotic localization pattern as GFP-SkpA, but due to the faintness of the GFP-CulA signal, I was unable to demonstrate this definitively. As SkpA and CulA are both components of the SCF complex, it is no surprise that they show similar localization patterns, as described above. However, I found that GFP-SkpA also displayed a unique localization pattern.

I discovered that GFP-SkpA localized to the very extreme of the hyphal tip, or apex, a localization pattern that I did not observe with GFP-CulA. The localization of GFP-SkpA at the apex is consistent with localization to the Spitzenkörper, a structure found at the tips of fungal hyphae that is an organizing center for hyphal growth. It is made up of secretory vesicles, which contain components necessary for tip growth, as well as cytoskeletal elements and various other proteins (Taheri-Talesh *et al.*, 2008). GFP-SkpA could also be seen as rapidly moving dots and larger spots in the cytoplasm, often near the hyphal tip. Surprisingly, although GFP-CulA does not localize at the apex of hyphal tips, I did observe GFP-CulA dots and spots *near* the hyphal tip, similarly to GFP-SkpA. These dots and larger spots near the hyphal tip are consistent with vesicles and endosomes, respectively.

In *S. cerevisiae*, Skp1 was shown to interact with a F-box protein called Rcy1, which localized to areas of polarized growth and was required for the recycling of the v-SNARE Snc1. Loss of Skp1 resulted in recycling defects, indicating that a Skp1/Rcy1 complex played a role in

the recycling of plasma membrane proteins (Galan *et al.*, 2001). In *A. nidulans*, the Skp1 homolog SkpA (my work) and the Rcy1 homolog RcyA (Herrero *et al.*, 2014; Taheri-Talesh *et al.*, 2008) display similar localization patterns in the cytoplasm and at the Spitzenkörper. However, deletion of *rcyA* did not affect the accumulation of SynA at the hyphal tip (Herrero *et al.*, 2014), which strongly indicates that RcyA does not have a major function in the recycling of SynA in *A. nidulans*. It is, thus, unclear what the function(s) of RcyA and SkpA are at the Spitzenkörper. However, I can speculate that RcyA and SkpA arrive at the Spitzenkörper via secretory vesicles. As CulA does not localize at the Spitzenkörper, one possibility is that CulA accumulates at the Golgi and/or endosomes but does not accumulate in secretory vesicles and, thus, does not localize at the apex. Co-localization studies with CulA and SkpA with proteins that are known to localize to specific compartments of the *A. nidulans* secretory pathway will clarify what compartments CulA and SkpA localize to and should help reveal their function(s) at those locations.

I have also studied the terminal phenotypes of both *culA*Δ and *skpA*Δ germlings and determined that the SCF complex plays a crucial role in suppressing septation near the growing hyphal tip. Deletion of either *culA* or *skpA* resulted in a large percentage of tip cells with a single nucleus, which is a very unusual phenotype. Multinuclear tip cells are thought to facilitate rapid tip growth [discussed in (Horio and Oakley, 2005)]. However, the mechanism by which septation is inhibited near the growing hyphal tip is unknown. These data, coupled with the localization patterns of CulA and SkpA, raises an intriguing theory that the SCF complex is a component of a mechanism by which cells mark the apical tip to prevent septum formation from occurring near the growing tip. As the SCF complex is an E3 ubiquitin ligase, this could potentially occur through tip biased targeting of protein(s) for destruction that are required for septal initiation.

My initial interest in studying the SCF complex was that Cdh1 is targeted for destruction via SCF complexes in other organisms and I was interested in identifying regulators of CdhA in *A. nidulans.* I found that deletion of *culA* led to a significant increase in the abundance of CdhA in all nuclei in *A. nidulans*, regardless of the cell cycle stage. Thus, the SCF complex in *A. nidulans* plays a central role in targeting CdhA for destruction as anticipated. Furthermore, I discovered that the deletion of *culA*, but not *skpA*, recapitulated an unusual *mipA*D159 phenotype (Chapter 6). A subset of nuclei in *culA*Δ germlings failed to accumulate NimE$^{\text{Cyclin B}}$ and NimX$^{\text{Cdk1}}$ (two separate experiments), likely due to constitutive APC/C-CdhA activity. Although it initially appeared odd that *skpA*Δ germlings would not display a similar phenotype, as both CulA and SkpA are a part of the SCF complex, I believe there is a fairly simple explanation. Deletion of *skpA* resulted in fewer nuclei, a higher frequency of septa, and a higher frequency of uninuclear tip cells than observed in *culA*Δ germlings. These more severe phenotypes could potentially be due to SkpA's unknown function(s) at the Spitzenkörper. In *mipA*D159 cells, the percentage of NimE$^{\text{Cyclin B}}$ negative nuclei increases with additional rounds of nuclear division. As *skpA*Δ germlings do not undergo as many nuclear divisions as *culA*Δ germlings, this could be one reason why we observe few NimE$^{\text{Cyclin B}}$ negative nuclei. Furthermore, I can only score S/G_2 tip cells with 2 or more nuclei for this experiment, and *skpA*Δ germlings have many uninuclear tip cells. I speculate that the additional function(s) of SkpA mask some of the phenotypes (such as NimE$^{\text{Cyclin B}}$ negative nuclei) observed in *culA*Δ germlings.

Finally, I also identified an interesting genetic interaction between CulA and γ-tubulin. The C-terminal fusion of GFP to CulA (*culA*-GFP) caused a slight loss of function, particularly at lower temperatures. Strains carrying both *culA*-GFP and the *mipA*D159 allele showed strong, synthetic growth inhibition. This synthetic genetic interaction indicates that the SCF complex and γ-tubulin

have a common function that is essential for growth. One obvious common function is the inactivation of CdhA. An ongoing experiment is the generation of *culA*-GFP, *cdhA*Δ, *mipA*D159 strains in order to determine if CdhA is the cause of the synthetic growth inhibition. My preliminary data demonstrate that these strains display a similar pattern of growth to the *culA*-GFP, *mipA*D159 strains, suggesting that most or all of the growth inhibition is independent of CdhA activity.

Taking all of my data on cell cycle-related cyclins and components of the SCF complex together, I believe that the SCF complex is the stronger candidate by which γ-tubulin regulates the cell cycle in both a CdhA-dependent and CdhA-independent manner. It is, however, difficult to speculate on the connection between γ-tubulin and the SCF complex as the SCF complex has numerous targets during the cell cycle. I think it is unlikely that γ-tubulin regulates CulA or SkpA directly, as my data show that the deletion of either of these two proteins causes hyperseptation, which is not a phenotype observed in the *mipA* mutants. Instead, I speculate that γ-tubulin interacts with one or more F-box proteins and that this interaction is required for their localization and/or function. Specific F-box proteins have been implicated in Cdh1 destruction at G_1/S (Fukushima *et al.*, 2013), topoisomerase IIα-dependent DNA decatenation (Kratz *et al.*, 2016), activation of the spindle assembly checkpoint (Guardavaccaro *et al.*, 2008), regulation of centrosome number (Pagan and Pagano, 2011), etc. Thus, mis-regulation of F-box protein(s) in *mipA* mutants is a possible source of the aberrant cell cycle phenotypes we observe.

Of particular interest, the same F-box protein (β-TrCP) that regulates Cdh1 at the G_1/S transition in mammalian cells was shown to promote activation of the SAC. SCF-β-TrCP was shown to target REST, a transcription factor that negatively regulates the expression of Mad2, for destruction in G_2 (Guardavaccaro *et al.*, 2008). Guardavaccaro *et al.* (2008) revealed that the

expression of a stable version of REST, which was unable to bind β-TrCP, prevented sufficient expression of *mad2* and led to several phenotypes including premature sister chromatid separation, chromosomal mis-segregation during anaphase, aneuploidy, and faster mitotic slippage in the presence of a spindle inhibitor. As these are all phenotypes observed in *mipA*D159 and other *mipA* mutants, it is interesting to speculate that a F-box protein in *A. nidulans* may play a similar role in regulating proper mitotic progression and progression into S-phase. There are, however, numerous F-box proteins in *A. nidulans* with homology to human β-TrCP: AN2861 (4e-48), AN6217 (2e-45), AN5593/Fbx23 (2e-45), and AN6359/SconB (1e-44) just to name a few. Future experiments could determine whether any F-box proteins interact with *A. nidulans* CdhA and SAC components and, if specific F-box proteins are identified, whether those directly interact with γ-tubulin. If γ-tubulin does not directly interact with any F-box proteins, then one potential explanation is that γ-tubulin regulates a target or targets of the SCF complex and, perhaps, γ-tubulin and the SCF complex work in parallel pathways to regulate the cell cycle.

References

Abenza, J.F., Pantazopoulou, A., Rodriguez, J.M., Galindo, A., and Penalva, M.A. (2009). Long-distance movement of *Aspergillus nidulans* early endosomes on microtubule tracks. Traffic *10*, 57-75.

Aher, A., and Akhmanova, A. (2018). Tipping microtubule dynamics, one protofilament at a time. Curr. Opin. Cell Biol. *50*, 86-93.

Akhmanova, A., and Steinmetz, M.O. (2015). Control of microtubule organization and dynamics: two ends in the limelight. Nat. Rev. Mol. Cell Biol. *16*, 711-726.

Barlow, A.L., Macleod, A., Noppen, S., Sanderson, J., and Guerin, C.J. (2010). Colocalization analysis in fluorescence micrographs: verification of a more accurate calculation of pearson's correlation coefficient. Microscopy and Microanalysis *16*, 710-724.

Bathe, F., Kempf, C., Osmani, S.A., Osmani, A.H., Hettinger, S., Wohlmann, E., and Fischer, R. (2010). Functional characterization of a new member of the Cdk9 family in *Aspergillus nidulans*. Eukaryot. Cell *9*, 1901-1912.

Bergen, L.G., and Morris, N.R. (1983). Kinetics of the nuclear division cycle of *Aspergillus nidulans*. J. Bacteriol. *156*, 155-160.

Bergen, L.G., Upshall, A., and Morris, N.R. (1984). S-phase, G2, and nuclear division mutants of *Aspergillus nidulans*. J. Bacteriol. *159*, 114-119.

Bok, J.W., Hoffmeister, D., Maggio-Hall, L.A., Murillo, R., Glasner, J.D., and Keller, N.P. (2006). Genomic mining for *Aspergillus* natural products. Chem. Biol. *13*, 31-37.

Campbell, R.E., Tour, O., Palmer, A.E., Steinbach, P.A., Baird, G.S., Zacharias, D.A., and Tsien, R.Y. (2002). A monomeric red fluorescent protein. Proc Natl Acad Sci U S A *99*, 7877-7882.

Cao, L., Chen, F., Yang, X., Xu, W., Xie, J., and Yu, L. (2014). Phylogenetic analysis of CDK and cyclin proteins in premetazoan lineages. BMC Evol. Biol. *14*, 10.

Cao, Y.N., Zheng, L.L., Wang, D., Liang, X.X., Gao, F., and Zhou, X.L. (2018). Recent advances in microtubule-stabilizing agents. Eur J Med Chem *143*, 806-828.

Chaaban, S., and Brouhard, G.J. (2017). A microtubule bestiary: structural diversity in tubulin polymers. Mol Biol Cell *28*, 2924-2931.

Chen, S.H., Chen, S., Tokarev, A.A., Liu, F., Jedd, G., and Segev, N. (2005). Ypt31/32 GTPases and their novel F-box effector protein Rcy1 regulate protein recycling. Mol Biol Cell *16*, 178-192.

Chen, S.H., Shah, A.H., and Segev, N. (2011). Ypt31/32 GTPases and their F-Box effector Rcy1 regulate ubiquitination of recycling proteins. Cell Logist *1*, 21-31.

Choudhury, R., Bonacci, T., Arceci, A., Lahiri, D., Mills, C.A., Kernan, J.L., Branigan, T.B., DeCaprio, J.A., Burke, D.J., and Emanuele, M.J. (2016). APC/C and SCF(cyclin F) Constitute a Reciprocal Feedback Circuit Controlling S-Phase Entry. Cell Rep *16*, 3359-3372.

Clutterbuck, A.J. (1970). Synchronous nuclear division and septation in *Aspergillus nidulans*. J Gen Microbiol *60*, 133-135.

Costes, S.V., Daelemans, D., Cho, E.H., Dobbin, Z., Pavlakis, G., and Lockett, S. (2004). Automatic and quantitative measurement of protein-protein colocalization in live cells. Biophys. J. *86*, 3993-4003.

Cuschieri, L., Nguyen, T., and Vogel, J. (2007). Control at the cell center: the role of spindle poles in cytoskeletal organization and cell cycle regulation. Cell Cycle *6*, 2788-2794.

Davidson, G., Shen, J., Huang, Y.L., Su, Y., Karaulanov, E., Bartscherer, K., Hassler, C., Stannek, P., Boutros, M., and Niehrs, C. (2009). Cell cycle control of wnt receptor activation. Dev. Cell *17*, 788-799.

De Souza, C.P., Hashmi, S.B., Nayak, T., Oakley, B., and Osmani, S.A. (2009). Mlp1 acts as a mitotic scaffold to spatially regulate spindle assembly checkpoint proteins in *Aspergillus nidulans*. Molecular Biology of the Cell *20*, 2146-2159.

De Souza, C.P., Hashmi, S.B., Osmani, A.H., Andrews, P., Ringelberg, C.S., Dunlap, J.C., and Osmani, S.A. (2013). Functional analysis of the *Aspergillus nidulans* kinome. PLoS One *8*, e58008.

De Souza, C.P., Hashmi, S.B., Osmani, A.H., and Osmani, S.A. (2014). Application of a new dual localization-affinity purification tag reveals novel aspects of protein kinase biology in *Aspergillus nidulans*. PLoS One *9*, e90911.

De Souza, C.P., Osmani, A.H., Hashmi, S.B., and Osmani, S.A. (2004). Partial nuclear pore complex disassembly during closed mitosis in *Aspergillus nidulans*. Curr. Biol. *14*, 1973-1984.

de Vries, R.P., Riley, R., Wiebenga, A., Aguilar-Osorio, G., Amillis, S., Uchima, C.A., Anderluh, G., Asadollahi, M., Askin, M., Barry, K.*, et al.* (2017). Comparative genomics reveals high biological diversity and specific adaptations in the industrially and medically important fungal genus *Aspergillus*. Genome Biology *18*, 28.

Dohn, J.W., Jr., Grubbs, A.W., Oakley, C.E., and Oakley, B.R. (2018). New multi-marker strains and complementing genes for *Aspergillus nidulans* molecular biology. Fungal Genet. Biol. *111*, 1-6.

Dunne, P.W., and Oakley, B.R. (1988). Mitotic gene conversion, reciprocal recombination and gene replacement at the benA, beta-tubulin, locus of *Aspergillus nidulans*. Mol. Gen. Genet. *213*, 339-345.

Dyer, P.S., and O'Gorman, C.M. (2011). A fungal sexual revolution: *Aspergillus* and *Penicillium* show the way. Curr. Opin. Microbiol. *14*, 649-654.

Dyer, P.S., and O'Gorman, C.M. (2012). Sexual development and cryptic sexuality in fungi: insights from *Aspergillus* species. FEMS Microbiol. Rev. *36*, 165-192.

Edgerton, H., Paolillo, V., and Oakley, B.R. (2015). Spatial regulation of the spindle assembly checkpoint and anaphase-promoting complex in *Aspergillus nidulans*. Mol. Microbiol. *95*, 442-457.

Edgerton-Morgan, H., and Oakley, B.R. (2012). γ-Tubulin plays a key role in inactivating APC/C(Cdh1) at the G(1)-S boundary. J Cell Biol *198*, 785-791.

Farache, D., Emorine, L., Haren, L., and Merdes, A. (2018). Assembly and regulation of gamma-tubulin complexes. Open Biol *8*.

Fernandez-Abalos, J.M., Fox, H., Pitt, C., Wells, B., and Doonan, J.H. (1998). Plant-adapted green fluorescent protein is a versatile vital reporter for gene expression, protein localization and mitosis in the filamentous fungus, *Aspergillus nidulans*. Mol. Microbiol. *27*, 121-130.

Fiddy, C., and Trinci, A.P. (1976). Mitosis, septation, branching and the duplication cycle in *Aspergillus nidulans*. J Gen Microbiol *97*, 169-184.

Findeisen, P., Muhlhausen, S., Dempewolf, S., Hertzog, J., Zietlow, A., Carlomagno, T., and Kollmar, M. (2014). Six subgroups and extensive recent duplications characterize the evolution of the eukaryotic tubulin protein family. Genome Biol Evol *6*, 2274-2288.

Freed, E., Lacey, K.R., Huie, P., Lyapina, S.A., Deshaies, R.J., Stearns, T., and Jackson, P.K. (1999). Components of an SCF ubiquitin ligase localize to the centrosome and regulate the centrosome duplication cycle. Genes Dev. *13*, 2242-2257.

Frescas, D., and Pagano, M. (2008). Deregulated proteolysis by the F-box proteins SKP2 and beta-TrCP: tipping the scales of cancer. Nat. Rev. Cancer *8*, 438-449.

Fukushima, H., Ogura, K., Wan, L., Lu, Y., Li, V., Gao, D., Liu, P., Lau, A.W., Wu, T., Kirschner, M.W.*, et al.* (2013). SCF-mediated Cdh1 degradation defines a negative feedback system that coordinates cell-cycle progression. Cell Rep *4*, 803-816.

Furukawa, M., Zhang, Y., McCarville, J., Ohta, T., and Xiong, Y. (2000). The CUL1 C-terminal sequence and ROC1 are required for efficient nuclear accumulation, NEDD8 modification, and ubiquitin ligase activity of CUL1. Mol. Cell. Biol. *20*, 8185-8197.

Galagan, J.E., Calvo, S.E., Cuomo, C., Ma, L.J., Wortman, J.R., Batzoglou, S., Lee, S.I., Basturkmen, M., Spevak, C.C., Clutterbuck, J.*, et al.* (2005). Sequencing of *Aspergillus nidulans* and comparative analysis with *A. fumigatus* and *A. oryzae*. Nature *438*, 1105-1115.

Galan, J.M., Wiederkehr, A., Seol, J.H., Haguenauer-Tsapis, R., Deshaies, R.J., Riezman, H., and Peter, M. (2001). Skp1p and the F-box protein Rcy1p form a non-SCF complex involved in recycling of the SNARE Snc1p in yeast. Mol. Cell. Biol. *21*, 3105-3117.

Guardavaccaro, D., Frescas, D., Dorrello, N.V., Peschiaroli, A., Multani, A.S., Cardozo, T., Lasorella, A., Iavarone, A., Chang, S., Hernando, E.*, et al.* (2008). Control of chromosome stability by the beta-TrCP-REST-Mad2 axis. Nature *452*, 365-369.

Guillet, V., Knibiehler, M., Gregory-Pauron, L., Remy, M.H., Chemin, C., Raynaud-Messina, B., Bon, C., Kollman, J.M., Agard, D.A., Merdes, A.*, et al.* (2011). Crystal structure of

gamma-tubulin complex protein GCP4 provides insight into microtubule nucleation. Nat. Struct. Mol. Biol. *18*, 915-919.

Haarhuis, J.H., Elbatsh, A.M., and Rowland, B.D. (2014). Cohesin and its regulation: on the logic of X-shaped chromosomes. Dev. Cell *31*, 7-18.

Harris, S.D. (2001). Septum formation in *Aspergillus nidulans*. Curr. Opin. Microbiol. *4*, 736-739.

Harris, S.D., Morrell, J.L., and Hamer, J.E. (1994). Identification and characterization of Aspergillus nidulans mutants defective in cytokinesis. Genetics *136*, 517-532.

Harris, S.D., Read, N.D., Roberson, R.W., Shaw, B., Seiler, S., Plamann, M., and Momany, M. (2005). Polarisome meets spitzenkorper: microscopy, genetics, and genomics converge. Eukaryot. Cell *4*, 225-229.

Herrero, S., Takeshita, N., and Fischer, R. (2014). F-box protein RcyA controls turnover of the kinesin-7 motor KipA in *Aspergillus nidulans*. Eukaryot. Cell *13*, 1085-1094.

Horio, T., and Oakley, B.R. (2003). Expression of *Arabidopsis* gamma-tubulin in fission yeast reveals conserved and novel functions of gamma-tubulin. Plant Physiol. *133*, 1926-1934.

Horio, T., and Oakley, B.R. (2005). The role of microtubules in rapid hyphal tip growth of *Aspergillus nidulans*. Mol Biol Cell *16*, 918-926.

Horio, T., Uzawa, S., Jung, M.K., Oakley, B.R., Tanaka, K., and Yanagida, M. (1991). The fission yeast gamma-tubulin is essential for mitosis and is localized at microtubule organizing centers. J. Cell Sci. *99 (Pt 4)*, 693-700.

Huang, G., Kaufman, A.J., Ramanathan, Y., and Singh, B. (2011). SCCRO (DCUN1D1) promotes nuclear translocation and assembly of the neddylation E3 complex. J. Biol. Chem. *286*, 10297-10304.

Hungerbuehler, A.K., Philippsen, P., and Gladfelter, A.S. (2007). Limited functional redundancy and oscillation of cyclins in multinucleated *Ashbya gossypii* fungal cells. Eukaryot. Cell *6*, 473-486.

Hwang, L.H., Lau, L.F., Smith, D.L., Mistrot, C.A., Hardwick, K.G., Hwang, E.S., Amon, A., and Murray, A.W. (1998). Budding yeast Cdc20: A target of the spindle checkpoint. Science *279*, 1041-1044.

Hydbring, P., Malumbres, M., and Sicinski, P. (2016). Non-canonical functions of cell cycle cyclins and cyclin-dependent kinases. Nat. Rev. Mol. Cell Biol. *17*, 280-292.

Jaspersen, S.L., Charles, J.F., and Morgan, D.O. (1999). Inhibitory phosphorylation of the APC regulator Hct1 is controlled by the kinase Cdc28 and the phosphatase Cdc14. Curr. Biol. *9*, 227-236.

Jimenez, J., Ricco, N., Grijota-Martinez, C., Fado, R., and Clotet, J. (2013). Redundancy or specificity? The role of the CDK Pho85 in cell cycle control. International Journal of Biochemistry and Molecular Biology *4*, 140-149.

Jung, M.K., May, G.S., and Oakley, B.R. (1998). Mitosis in wild-type and β-tubulin mutant strains of *Aspergillus nidulans*. Fungal Genet. Biol. *24*, 146-160.

Jung, M.K., Prigozhina, N., Oakley, C.E., Nogales, E., and Oakley, B.R. (2001). Alanine-scanning mutagenesis of Aspergillus gamma-tubulin yields diverse and novel phenotypes. Molecular biology of the cell *12*, 2119-2136.

Katoh, K., Rozewicki, J., and Yamada, K.D. (2017). MAFFT online service: multiple sequence alignment, interactive sequence choice and visualization. In Brief Bioinform.

Katsetos, C.D., and Draber, P. (2012). Tubulins as Therapeutic Targets in Cancer: from Bench to Bedside. Curr. Pharm. Des. *18*, 2778-2792.

Katsuki, M., Drummond, D.R., and Cross, R.A. (2014). Ectopic A-lattice seams destabilize microtubules. Nat Commun *5*, 3094.

Keck, J.M., Summers, M.K., Tedesco, D., Ekholm-Reed, S., Chuang, L.C., Jackson, P.K., and Reed, S.I. (2007). Cyclin E overexpression impairs progression through mitosis by inhibiting APC(Cdh1). J. Cell Biol. *178*, 371-385.

Kempf, C., Bathe, F., and Fischer, R. (2013). Evidence that two Pcl-like cyclins control Cdk9 activity during cell differentiation in *Aspergillus nidulans* asexual development. Eukaryot. Cell *12*, 23-36.

Khodjakov, A., and Rieder, C.L. (2001). Centrosomes enhance the fidelity of cytokinesis in vertebrates and are required for cell cycle progression. J. Cell Biol. *153*, 237-242.

Kilmartin, J.V. (2014). Lessons from yeast: the spindle pole body and the centrosome. Philos Trans R Soc Lond B Biol Sci *369*.

Kinoshita, K., Habermann, B., and Hyman, A.A. (2002). XMAP215: a key component of the dynamic microtubule cytoskeleton. Trends Cell Biol. *12*, 267-273.

Kollman, J.M., Merdes, A., Mourey, L., and Agard, D.A. (2011). Microtubule nucleation by gamma-tubulin complexes. Nat. Rev. Mol. Cell Biol. *12*, 709-721.

Konzack, S., Rischitor, P.E., Enke, C., and Fischer, R. (2005). The role of the kinesin motor KipA in microtubule organization and polarized growth of *Aspergillus nidulans*. Mol Biol Cell *16*, 497-506.

Kosetsu, K., Murata, T., Yamada, M., Nishina, M., Boruc, J., Hasebe, M., Van Damme, D., and Goshima, G. (2017). Cytoplasmic MTOCs control spindle orientation for asymmetric cell division in plants. Proc Natl Acad Sci U S A *114*, E8847-E8854.

Kramer, E.R., Scheuringer, N., Podtelejnikov, A.V., Mann, M., and Peters, J.M. (2000). Mitotic regulation of the APC activator proteins CDC20 and CDH1. Mol Biol Cell *11*, 1555-1569.

Kratz, A.S., Richter, K.T., Schlosser, Y.T., Schmitt, M., Shumilov, A., Delecluse, H.J., and Hoffmann, I. (2016). Fbxo28 promotes mitotic progression and regulates topoisomerase IIalpha-dependent DNA decatenation. Cell Cycle *15*, 3419-3431.

Lau, A.W., Inuzuka, H., Fukushima, H., Wan, L., Liu, P., Gao, D., Sun, Y., and Wei, W. (2013). Regulation of APC(Cdh1) E3 ligase activity by the Fbw7/cyclin E signaling axis contributes to the tumor suppressor function of Fbw7. Cell Res. *23*, 947-961.

Letunic, I., and Bork, P. (2016). Interactive tree of life (iTOL) v3: an online tool for the display and annotation of phylogenetic and other trees. Nucleic Acids Res. *44*, W242-245.

Li, S., Oakley, C.E., Chen, G., Han, X., Oakley, B.R., and Xiang, X. (2005). Cytoplasmic dynein's mitotic spindle pole localization requires a functional anaphase-promoting complex, gamma-tubulin, and NUDF/LIS1 in *Aspergillus nidulans*. Mol Biol Cell *16*, 3591-3605.

Lim, S., and Kaldis, P. (2013). Cdks, cyclins and CKIs: roles beyond cell cycle regulation. Development *140*, 3079-3093.

Liu, D., and Finley, R.L., Jr. (2010). Cyclin Y is a novel conserved cyclin essential for development in Drosophila. Genetics *184*, 1025-1035.

Lu, K.P., and Hunter, T. (1995). Evidence for a NIMA-like mitotic pathway in vertebrate cells. Cell *81*, 413-424.

Lukas, C., Sorensen, C.S., Kramer, E., Santoni-Rugiu, E., Lindeneg, C., Peters, J.M., Bartek, J., and Lukas, J. (1999). Accumulation of cyclin B1 requires E2F and cyclin-A-dependent rearrangement of the anaphase-promoting complex. Nature *401*, 815-818.

Ma, Z., Wu, Y., Jin, J., Yan, J., Kuang, S., Zhou, M., Zhang, Y., and Guo, A.Y. (2013). Phylogenetic analysis reveals the evolution and diversification of cyclins in eukaryotes. Mol Phylogenet Evol *66*, 1002-1010.

Malagon, F. (2013). RNase III is required for localization to the nucleoid of the 5' pre-rRNA leader and for optimal induction of rRNA synthesis in *E. coli*. RNA *19*, 1200-1207.

Mandelkow, E.M., Schultheiss, R., Rapp, R., Muller, M., and Mandelkow, E. (1986). On the surface lattice of microtubules: helix starts, protofilament number, seam, and handedness. J. Cell Biol. *102*, 1067-1073.

Manders, E.M.M., Verbeek, F.J., and Aten, J.A. (1993). Measurement of colocalization of objects in dual-color confocal images. Journal of Microscopy-Oxford *169*, 375-382.

Martin, M., and Akhmanova, A. (2018). Coming into Focus: Mechanisms of Microtubule Minus-End Organization. Trends Cell Biol.

Martin, M.A., Osmani, S.A., and Oakley, B.R. (1997). The role of γ-tubulin in mitotic spindle formation and cell cycle progression in *Aspergillus nidulans*. J. Cell Sci. *110 (Pt 5)*, 623-633.

Martin-Castellanos, C., Blanco, M.A., de Prada, J.M., and Moreno, S. (2000). The puc1 cyclin regulates the G1 phase of the fission yeast cell cycle in response to cell size. Molecular Biology of the Cell *11*, 543-554.

Maundrell, K. (1990). nmt1 of fission yeast. A highly transcribed gene completely repressed by thiamine. J. Biol. Chem. *265*, 10857-10864.

May, G.S., and Adams, T.H. (1997). The importance of fungi to man. Genome Res. *7*, 1041-1044.

Measday, V., Moore, L., Retnakaran, R., Lee, J., Donoviel, M., Neiman, A.M., and Andrews, B. (1997). A family of cyclin-like proteins that interact with the Pho85 cyclin-dependent kinase. Mol. Cell. Biol. *17*, 1212-1223.

Meyer, V., Andersen, M.R., Brakhage, A.A., Braus, G.H., Caddick, M.X., Cairns, T.C., de Vries, R.P., Haarmann, T., Hansen, K., Hertz-Fowler, C.*, et al.* (2016). Current challenges of research on filamentous fungi in relation to human welfare and a sustainable bio-economy: a white paper. Fungal Biology and Biotechnology *3*, 6.

Mikolcevic, P., Sigl, R., Rauch, V., Hess, M.W., Pfaller, K., Barisic, M., Pelliniemi, L.J., Boesl, M., and Geley, S. (2012). Cyclin-dependent kinase 16/PCTAIRE kinase 1 is activated by cyclin Y and is essential for spermatogenesis. Mol. Cell. Biol. *32*, 868-879.

Miller, M.A., Pfeiffer, W., and Schwartz, T. (2010). Creating the CIPRES Science Gateway for Inference of Large Phylogenetic Trees. In Proceedings of the Gateway Computing Environments Workshop (GCE) (New Orleans, LA), pp. 1-8.

Morris, N.R. (1975). Mitotic mutants of *Aspergillus nidulans*. Genet. Res. *26*, 237-254.

Mulder, K.C., Mulinari, F., Franco, O.L., Soares, M.S., Magalhaes, B.S., and Parachin, N.S. (2015). Lovastatin production: From molecular basis to industrial process optimization. Biotechnol. Adv. *33*, 648-665.

Murray, A.W., Solomon, M.J., and Kirschner, M.W. (1989). The role of cyclin synthesis and degradation in the control of maturation promoting factor activity. Nature *339*, 280-286.

Nalley, L., Tsiboe, F., Durand-Morat, A., Shew, A., and Thoma, G. (2016). Economic and environmental impact of rice blast pathogen (*Magnaporthe oryzae*) alleviation in the United States. PLoS One *11*, e0167295.

Nayak, T., Edgerton-Morgan, H., Horio, T., Xiong, Y., De Souza, C.P., Osmani, S.A., and Oakley, B.R. (2010). γ-tubulin regulates the anaphase-promoting complex/cyclosome during interphase. J. Cell Biol. *190*, 317-330.

Nayak, T., Szewczyk, E., Oakley, C.E., Osmani, A., Ukil, L., Murray, S.L., Hynes, M.J., Osmani, S.A., and Oakley, B.R. (2006). A versatile and efficient gene-targeting system for *Aspergillus nidulans*. Genetics *172*, 1557-1566.

Nigg, E.A., and Holland, A.J. (2018). Once and only once: mechanisms of centriole duplication and their deregulation in disease. Nat. Rev. Mol. Cell Biol.

Nigg, E.A., and Raff, J.W. (2009). Centrioles, centrosomes, and cilia in health and disease. Cell *139*, 663-678.

Nogales, E., Whittaker, M., Milligan, R.A., and Downing, K.H. (1999). High-resolution model of the microtubule. Cell *96*, 79-88.

O'Connell, M.J., Norbury, C., and Nurse, P. (1994). Premature chromatin condensation upon accumulation of NIMA. EMBO J. *13*, 4926-4937.

O'Connell, M.J., Osmani, A.H., Morris, N.R., and Osmani, S.A. (1992). An extra copy of $nimE^{cyclin\ B}$ elevates pre-MPF levels and partially suppresses mutation of $nimT^{cdc25}$ in *Aspergillus nidulans*. EMBO J. *11*, 2139-2149.

Oakley, B.R., and Akkari, Y.N. (1999). Gamma-tubulin at ten: progress and prospects. Cell Struct. Funct. *24*, 365-372.

Oakley, B.R., and Morris, N.R. (1983). A mutation in *Aspergillus nidulans* that blocks the transition from interphase to prophase. J. Cell Biol. *96*, 1155-1158.

Oakley, B.R., Oakley, C.E., Yoon, Y., and Jung, M.K. (1990). Gamma-tubulin is a component of the spindle pole body that is essential for microtubule function in *Aspergillus nidulans*. Cell *61*, 1289-1301.

Oakley, B.R., Paolillo, V., and Zheng, Y. (2015). γ-Tubulin complexes in microtubule nucleation and beyond. Mol Biol Cell *26*, 2957-2962.

Oakley, C.E., Edgerton-Morgan, H., and Oakley, B.R. (2012). Tools for manipulation of secondary metabolism pathways: rapid promoter replacements and gene deletions in *Aspergillus nidulans*. Methods Mol Biol *944*, 143-161.

Oakley, C.E., and Oakley, B.R. (1989). Identification of gamma-tubulin, a new member of the tubulin superfamily encoded by mipA gene of *Aspergillus nidulans*. Nature *338*, 662-664.

Oakley, C.E., Weil, C.F., Kretz, P.L., and Oakley, B.R. (1987). Cloning of the riboB locus of *Aspergillus nidulans*. Gene *53*, 293-298.

Oegema, K., Wiese, C., Martin, O.C., Milligan, R.A., Iwamatsu, A., Mitchison, T.J., and Zheng, Y. (1999). Characterization of two related *Drosophila* gamma-tubulin complexes that differ in their ability to nucleate microtubules. J. Cell Biol. *144*, 721-733.

Osmani, A.H., Davies, J., Liu, H.L., Nile, A., and Osmani, S.A. (2006a). Systematic deletion and mitotic localization of the nuclear pore complex proteins of *Aspergillus nidulans*. Mol Biol Cell *17*, 4946-4961.

Osmani, A.H., Oakley, B.R., and Osmani, S.A. (2006b). Identification and analysis of essential *Aspergillus nidulans* genes using the heterokaryon rescue technique. Nat Protoc *1*, 2517-2526.

Osmani, A.H., van Peij, N., Mischke, M., O'Connell, M.J., and Osmani, S.A. (1994). A single p34^{cdc2} protein kinase (encoded by *nimX*^{cdc2}) is required at G1 and G2 in *Aspergillus nidulans*. J. Cell Sci. *107 (Pt 6)*, 1519-1528.

Osmani, S.A., Engle, D.B., Doonan, J.H., and Morris, N.R. (1988). Spindle formation and chromatin condensation in cells blocked at interphase by mutation of a negative cell cycle control gene. Cell *52*, 241-251.

Osmani, S.A., and Goldman, G.H. (2008). The Aspergilli : genomics, medical aspects, biotechnology, and research methods (Boca Raton: Taylor & Francis).

Ovechkina, Y., Maddox, P., Oakley, C.E., Xiang, X., Osmani, S.A., Salmon, E.D., and Oakley, B.R. (2003). Spindle formation in *Aspergillus* is coupled to tubulin movement into the nucleus. Molecular Biology of the Cell *14*, 2192-2200.

Pagan, J., and Pagano, M. (2011). FBXW5 controls centrosome number. Nat. Cell Biol. *13*, 888-890.

Pagano, L., Caira, M., Candoni, A., Offidani, M., Fianchi, L., Martino, B., Pastore, D., Picardi, M., Bonini, A., Chierichini, A.*, et al.* (2006). The epidemiology of fungal infections in patients with hematologic malignancies: the SEIFEM-2004 study. Haematologica *91*, 1068-1075.

Pantazopoulou, A., and Penalva, M.A. (2009). Organization and dynamics of the *Aspergillus nidulans* Golgi during apical extension and mitosis. Mol Biol Cell *20*, 4335-4347.

Prigozhina, N.L., Oakley, C.E., Lewis, A.M., Nayak, T., Osmani, S.A., and Oakley, B.R. (2004). gamma-tubulin plays an essential role in the coordination of mitotic events. Mol Biol Cell *15*, 1374-1386.

Prigozhina, N.L., Walker, R.A., Oakley, C.E., and Oakley, B.R. (2001). Gamma-tubulin and the C-terminal motor domain kinesin-like protein, KLPA, function in the establishment of spindle bipolarity in *Aspergillus nidulans*. Mol Biol Cell *12*, 3161-3174.

Qiao, X., Zhang, L., Gamper, A.M., Fujita, T., and Wan, Y. (2010). APC/C-Cdh1: from cell cycle to cellular differentiation and genomic integrity. Cell Cycle *9*, 3904-3912.

Schier, N., and Fischer, R. (2002). The *Aspergillus nidulans* cyclin PclA accumulates in the nucleus and interacts with the central cell cycle regulator $NimX^{Cdc2}$. FEBS Lett. *523*, 143-146.

Schier, N., Liese, R., and Fischer, R. (2001). A Pcl-like cyclin of *Aspergillus nidulans* is transcriptionally activated by developmental regulators and is involved in sporulation. Mol. Cell. Biol. *21*, 4075-4088.

Schubert, M., Spiegel, H., Schillberg, S., and Nolke, G. (2018). *Aspergillus*-specific antibodies - Targets and applications. Biotechnol. Adv.

Shaner, N.C., Campbell, R.E., Steinbach, P.A., Giepmans, B.N., Palmer, A.E., and Tsien, R.Y. (2004). Improved monomeric red, orange and yellow fluorescent proteins derived from *Discosoma* sp. red fluorescent protein. Nat. Biotechnol. *22*, 1567-1572.

Sivakumar, S., and Gorbsky, G.J. (2015). Spatiotemporal regulation of the anaphase-promoting complex in mitosis. Nat. Rev. Mol. Cell Biol. *16*, 82-94.

Sorensen, C.S., Lukas, C., Kramer, E.R., Peters, J.M., Bartek, J., and Lukas, J. (2001). A conserved cyclin-binding domain determines functional interplay between anaphase-promoting complex-Cdh1 and cyclin A-Cdk2 during cell cycle progression. Mol. Cell. Biol. *21*, 3692-3703.

Stamatakis, A. (2014). RAxML version 8: a tool for phylogenetic analysis and post-analysis of large phylogenies. Bioinformatics *30*, 1312-1313.

Stefanini, I., Rizzetto, L., Rivero, D., Carbonell, S., Gut, M., Heath, S., Gut, I.G., Trabocchi, A., Guarna, A., Ben Ghazzi, N.*, et al.* (2018). Deciphering the mechanism of action of 089, a compound impairing the fungal cell cycle. Sci Rep *8*, 5964.

Steinberg, G., Penalva, M.A., Riquelme, M., Wosten, H.A., and Harris, S.D. (2017). Cell Biology of Hyphal Growth. Microbiol Spectr *5*.

Subach, O.M., Cranfill, P.J., Davidson, M.W., and Verkhusha, V.V. (2011). An enhanced monomeric blue fluorescent protein with the high chemical stability of the chromophore. PLoS One *6*, e28674.

Szewczyk, E., Nayak, T., Oakley, C.E., Edgerton, H., Xiong, Y., Taheri-Talesh, N., Osmani, S.A., and Oakley, B.R. (2006). Fusion PCR and gene targeting in *Aspergillus nidulans*. Nat Protoc *1*, 3111-3120.

Szewczyk, E., and Oakley, B.R. (2011). Microtubule dynamics in mitosis in *Aspergillus nidulans*. Fungal Genet. Biol. *48*, 998-999.

Taheri-Talesh, N., Horio, T., Araujo-Bazan, L., Dou, X., Espeso, E.A., Penalva, M.A., Osmani, S.A., and Oakley, B.R. (2008). The tip growth apparatus of *Aspergillus nidulans*. Mol Biol Cell *19*, 1439-1449.

Tamm, T. (2012). A thiamine-regulatable epitope-tagged protein expression system in fission yeast. Methods Mol Biol *824*, 417-432.

Teixeira, L.K., and Reed, S.I. (2013). Ubiquitin ligases and cell cycle control. Annu. Rev. Biochem. *82*, 387-414.

Todd, R.B., Davis, M.A., and Hynes, M.J. (2007). Genetic manipulation of *Aspergillus nidulans*: meiotic progeny for genetic analysis and strain construction. Nat Protoc *2*, 811-821.

Toews, M.W., Warmbold, J., Konzack, S., Rischitor, P., Veith, D., Vienken, K., Vinuesa, C., Wei, H., and Fischer, R. (2004). Establishment of mRFP1 as a fluorescent marker in *Aspergillus nidulans* and construction of expression vectors for high-throughput protein tagging using recombination in vitro (GATEWAY). Curr. Genet. *45*, 383-389.

Varanasi, N.L., Baskaran, I., Alangaden, G.J., Chandrasekar, P.H., and Manavathu, E.K. (2004). Novel effect of voriconazole on conidiation of *Aspergillus* species. Int. J. Antimicrob. Agents *23*, 72-79.

Vishniac, W., and Santer, M. (1957). The thiobacilli. Bacteriol Rev *21*, 195-213.

Visintin, R., Prinz, S., and Amon, A. (1997). CDC20 and CDH1: a family of substrate-specific activators of APC-dependent proteolysis. Science *278*, 460-463.

von Zeska Kress, M.R., Harting, R., Bayram, O., Christmann, M., Irmer, H., Valerius, O., Schinke, J., Goldman, G.H., and Braus, G.H. (2012). The COP9 signalosome counteracts the accumulation of cullin SCF ubiquitin E3 RING ligases during fungal development. Mol. Microbiol. *83*, 1162-1177.

Wang, H., Xu, Z., Gao, L., and Hao, B. (2009). A fungal phylogeny based on 82 complete genomes using the composition vector method. BMC Evol. Biol. *9*, 195.

Weil, C.F., Oakley, C.E., and Oakley, B.R. (1986). Isolation of *mip* (microtubule-interacting protein) mutations of *Aspergillus nidulans*. Mol. Cell. Biol. *6*, 2963-2968.

Weisenberg, R.C. (1972). Microtubule formation in vitro in solutions containing low calcium concentrations. Science *177*, 1104-1105.

Wertman, K.F., Drubin, D.G., and Botstein, D. (1992). Systematic mutational analysis of the yeast ACT1 gene. Genetics *132*, 337-350.

Wiese, C., and Zheng, Y. (2006). Microtubule nucleation: gamma-tubulin and beyond. J. Cell Sci. *119*, 4143-4153.

Wigge, P.A., Jensen, O.N., Holmes, S., Soues, S., Mann, M., and Kilmartin, J.V. (1998). Analysis of the *Saccharomyces* spindle pole by matrix-assisted laser desorption/ionization (MALDI) mass spectrometry. J. Cell Biol. *141*, 967-977.

Wolfe, K.H., and Shields, D.C. (1997). Molecular evidence for an ancient duplication of the entire yeast genome. Nature *387*, 708-713.

Wong, K.H., Todd, R.B., Oakley, B.R., Oakley, C.E., Hynes, M.J., and Davis, M.A. (2008). Sumoylation in *Aspergillus nidulans*: *sumO* inactivation, overexpression and live-cell imaging. Fungal Genet. Biol. *45*, 728-737.

Wong, R.W. (2010). An update on cohesin function as a 'molecular glue' on chromosomes and spindles. Cell Cycle *9*, 1754-1758.

Wu, D., Dou, X., Hashmi, S.B., and Osmani, S.A. (2004). The Pho80-like cyclin of *Aspergillus nidulans* regulates development independently of its role in phosphate acquisition. J. Biol. Chem. *279*, 37693-37703.

Xiong, Y., and Oakley, B.R. (2009). In vivo analysis of the functions of γ-tubulin-complex proteins. J. Cell Sci. *122*, 4218-4227.

Yang, L., Ukil, L., Osmani, A., Nahm, F., Davies, J., De Souza, C.P., Dou, X., Perez-Balaguer, A., and Osmani, S.A. (2004). Rapid production of gene replacement constructs and generation of a green fluorescent protein-tagged centromeric marker in *Aspergillus nidulans*. Eukaryot. Cell *3*, 1359-1362.

Ye, X.S., Fincher, R.R., Tang, A., Osmani, A.H., and Osmani, S.A. (1998). Regulation of the anaphase-promoting complex/cyclosome by bimAAPC3 and proteolysis of NIMA. Mol Biol Cell *9*, 3019-3030.

Yu, J.H., Hamari, Z., Han, K.H., Seo, J.A., Reyes-Dominguez, Y., and Scazzocchio, C. (2004). Double-joint PCR: a PCR-based molecular tool for gene manipulations in filamentous fungi. Fungal Genet. Biol. *41*, 973-981.

Yu, Z., Cai, M., Hu, W., Zhang, Y., Zhou, J., Zhou, X., and Zhang, Y. (2014). A cyclin-like protein, ClgA, regulates development in *Aspergillus nidulans*. Res. Microbiol. *165*, 462-467.

Zachariae, W., Schwab, M., Nasmyth, K., and Seufert, W. (1998). Control of cyclin ubiquitination by CDK-regulated binding of Hct1 to the anaphase promoting complex. Science *282*, 1721-1724.

Zarrin, M., Leeder, A.C., and Turner, G. (2005). A rapid method for promoter exchange in *Aspergillus nidulans* using recombinant PCR. Fungal Genet. Biol. *42*, 1-8.

Zhang, Y., Gao, X., Manck, R., Schmid, M., Osmani, A.H., Osmani, S.A., Takeshita, N., and Fischer, R. (2017). Microtubule-organizing centers of *Aspergillus nidulans* are anchored at septa by a disordered protein. Mol. Microbiol. *106*, 285-303.

Zi, Z., Zhang, Z., Li, Q., An, W., Zeng, L., Gao, D., Yang, Y., Zhu, X., Zeng, R., Shum, W.W., *et al.* (2015). CCNYL1, but not CCNY, cooperates with CDK16 to regulate spermatogenesis in mouse. PLoS Genet. *11*, e1005485.

Zur, A., and Brandeis, M. (2002). Timing of APC/C substrate degradation is determined by fzy/fzr specificity of destruction boxes. EMBO J. *21*, 4500-4510.